NASA Technical Memorandum 81169

Three-Dimensional Interactions and Vortical Flows With Emphasis on High Speeds

David J. Peake and Murray Tobak

March 1980

National Aeronautics and
Space Administration

NASA Technical Memorandum 81169

Three-Dimensional Interactions and Vortical Flows With Emphasis on High Speeds

David J. Peake
Murray Tobak, Ames Research Center, Moffett Field, California

An AGARDograph Compiled for the
AGARD Fluid Dynamics Panel

National Aeronautics and
Space Administration

Ames Research Center
Moffett Field, California 94035

THREE-DIMENSIONAL INTERACTIONS AND VORTICAL FLOWS WITH EMPHASIS ON HIGH SPEEDS

by

David J. Peake and Murray Tobak

Ames Research Center, NASA
Moffett Field, California 94035, U.S.A.

Editor: Robert H. Korkegi

Past Director of AGARD
Paris, France

DEDICATION

This AGARDograph is dedicated to the memory of Dietrich Küchemann, who for many years spearheaded the understanding of three-dimensional separated flows while Head of the Aerodynamics Department at RAE Farnborough. The wisdom, penetrating observations, and wide knowledge that this great scientist brought to bear in the fields of aeronautics and fluid mechanics are sadly missed. Dietrich will be remembered not only for his distinguished research, which remains with us in his lucid publications and books, but for his modesty, warmth, comradeship, and compassion for his fellow man. He conceived vortices to be the "sinews and muscles of fluid motion"; in our diagnosis of complex separated flows on flight vehicles, we trust that vortices have received just and full account.

ACKNOWLEDGMENT

One of us, David J. Peake, wishes to acknowledge the encouragement and support of the staff and L. H. Öhman, Head of High Speed Aerodynamics, NAE, Ottawa, and F. R. Thurston, Past Director of NAE, in the initiation of the AGARDograph. Collectively, we should like to thank the editor, R. H. Korkegi and J. Lloyd Jones, Past Chairman of the AGARD Fluid Dynamics Panel and Panel Members, for their patient and continuous support while the AGARDograph has been in preparation; and to G. T. Chapman and T. . Coakley and other members of the staff of NASA-Ames, who have provided constructive criticism, and produced the manuscript. Finally, a sincere word of thanks to all our friends and associates in Europe and in North America, without whose contributions the AGARDograph would never have commenced.

THREE-DIMENSIONAL INTERACTIONS AND VORTICAL FLOWS WITH EMPHASIS ON HIGH SPEEDS

David J. Peake and Murray Tobak

Ames Research Center, NASA, Moffett Field, California 94035, U.S.A.

SUMMARY

Diverse kinds of three-dimensional regions of separation in laminar and turbulent boundary layers are discussed that exist on lifting aerodynamic configurations immersed in flows from subsonic to hypersonic speeds. One of the common ingredients is that a three-dimensional boundary layer will detach from a surface along a swept separation line (adjacent to which the skin-friction lines converge rapidly) and will usually form a well organized coiled motion in all speed regimes. The scale of the vortical flow relative to the undisturbed boundary-layer thickness δ_0 changes, depending on the configuration and its attitude to the free stream. In axial corner and bluff protuberance flows, the coiled shear layer is immersed within δ_0. About slender bodies or sharp swept-back wings at angle of attack, the vortical flow is many times larger than δ_0, compressibility generally suppressing the scale. In hypersonic flow, high rates of heat transfer are encountered along lines of reattachment (adjacent to which the skin-friction lines diverge rapidly) that are associated with three-dimensional separation zones. The maximum rates of heat transfer – rates that may exceed the local stagnation point heating by factors of 10 or more – result from shock-on-shock interactions situated, not on the surface, but in the flow field in proximity to forward-facing parts of the airframe.

In all cases of three-dimensional flow separation, the assumption of continuous vector fields of skin-friction lines and external-flow streamlines, coupled with simple topology laws, provides a flow grammar whose elemental constituents are the singular points: nodes, foci, and saddles. Adopting these notions enables us to create sequences of plausible flow structures, to deduce mean flow characteristics, expose flow mechanisms, and to aid theory and experiment where lack of resolution in numerical calculations or wind-tunnel observations causes imprecision in diagnosing the three-dimensional flow features.

1. INTRODUCTION

The successful operation of the world's first slender-wing supersonic transport aircraft, "Concorde" (Figs. 1a and 1b), and the imminent launch of the hypersonic Space Shuttle, "Columbia" (Fig. 2), provide an impetus to comprehend inviscid-viscous interactions about flight vehicles of all types. In subsonic, transonic, and supersonic flows, weak interactions occur at low angles of attack where the essentially inviscid external flow[1] and the thin boundary layer may be treated individually for calculation purposes. When the interactions become strong, at higher angles of attack, they lead eventually to regions of three-dimensional (3D) separations and viscous vortical flows, so that the external and viscous flows may no longer be uncoupled. Customarily accompanying strong viscous-inviscid interactions and vortical flows on hypersonic configurations is substantial heat transfer to the surface in zones of flow reattachment.

The extensive interest in 3D flow separation is linked closely with wings of high leading-edge sweep and bodies of large fineness ratio that are typical of high-speed aircraft and missiles. Characteristically, these 3D regimes of boundary-layer separation can lead to comparatively steady streamwise vortices, unlike the more familiar so-called two-dimensional (2D) separation zones[2] with intermittent backflow and unsteadiness. The design aim must be to set up a structurally stable flow about the flight vehicle. In subscribing to this philosophy, we shall demonstrate that on the basis of simple topological reasoning, we may construct a rational sequence of plausible patterns of skin-friction lines and external streamlines about components of the vehicle as they undergo changes in angle of attack. The objective is to establish a lexicon of 3D vortical flow structures, verifiable in simple water-tunnel experiments, that may then be used as foundations to guide the diagnosis of the vortical flows that exist about the complete vehicle over extensive ranges of Mach number, Reynolds number, and vehicle attitude.

1.1 Flight Domains

Our discussion of 3D separated flows is introduced with the flight corridors for various vehicles (Poisson-Quinton 1968) in coordinates of altitude vs flight Mach number. These are shown in Fig. 3a. At the extreme, we see that we must cope with aerodynamic problems with vehicles flying up to about 100 km (300,000 ft) at speeds greater than 10,000 m/sec (30,000 ft/sec). Kinetic heating, which is the major problem of high-speed flight, arises from two processes: compression and shear in the boundary layer. The first is predominant at stagnation points and leads to very high local surface temperatures. To demonstrate this, the equilibrium stagnation temperatures behind the shock wave enshrouding the vehicle nose are plotted in Fig. 3a as dashed lines over the flight domains. We note that these temperatures reach about 150° C (300° F) for the "Concorde" cruising at about Mach 2, and higher than 7,000° C (13,000° F) for the "Apollo" capsule during its reentry phase. But temperatures less severe than these stagnation conditions, produced by viscous shear forces, are usually experienced over the remainder of the airframe. The "Columbia" must be provided with heat shielding, for example, to resist skin temperatures of more than 1,300° C (2,400° F) (see O'Lone 1976 and Fig. 3b). In addition, real gas effects become very important at hypersonic speeds. Two dash-dot lines are shown in Fig. 3a to the right of which the air contains more than 10% dissociated oxygen (O_2) and nitrogen (N_2), respectively.

The effects of viscosity also provide substantial problems in all speed regimes. The lower graph (Fig. 3c) displays the Reynolds number vs speed for some typical flight vehicles. Except in a few special cases, it is not possible to simulate these flight conditions in ground facilities. Large subsonic transport

---

[1]The flow region where turbulent and viscous stresses are insignificant.

[2]Even though the 2D separation zone may be essentially normal to the free-stream direction, the skin-friction lines usually form 3D cellular structures.

aircraft, "Concorde" and projected hypersonic airplanes, fly in a regime where all boundary layers are turbulent; the Space Shuttle will be involved with turbulent, transitional, and laminar boundary layers.

1.2 Aircraft Types

Three types of vehicles designed for long-range steady level flight exist. These may be characterized (Küchemann 1965) according to their ratio of semispan to overall length, s/ℓ, as we see in Fig. 3d. The classical aircraft with $s/\ell \sim 0.5$ is subsonic and possesses separate elements to provide the volume, lift, thrust, and control forces. Derived from the classical type is the swept-wing aircraft with a slightly smaller s/ℓ (~0.4), that operates at high subsonic and (sometimes) low supersonic speeds. The essential foundations of these two types are classical two-dimensional airfoil flows coupled with flows about bodies of revolution, on which Prandtl's boundary-layer approximations are valid for the prescribed attached viscous flows. With wings of high aspect ratio at high lift and at low speeds, the boundary layer detaches from the upper surface along a line that is nearly normal to the undisturbed stream; that is, the separation zone is largely two-dimensional. Such flow detachments are frequently sudden and usually result in a considerable loss of lift on the wing (*stalling*). Even on wings of high aspect ratio, however, there are regions where the separation lines are oblique to the flight direction, notably at the wing tips and in wing-body junctions. Under lifting conditions, the boundary layer on the lower surface of the wing rolls up to form two streamwise vortices just inboard of and above the tips. When fed additionally by the separated shear layer off the trailing edge, these form the trailing vortex system of the wing. The zones of separation in the wing-body junctions and their associated vortices often modify considerably the wing characteristics near maximum lift. Because of the often unpredictable experiences at low speeds with the stalling of wings of high aspect ratio, all flow separations have come to be regarded as undesirable. This is clearly too limited a view.

Much of the experimental and theoretical work on 3D separations has been concentrated on the sharp-edged slender wing about which the flow field is radically different from that about the large aspect ratio wing. This is the third aircraft type in Fig. 3d with a semispan to length ratio of about 0.25. The boundary layers growing outboard of the windward attachment line(s) on the lower surface separate at the leading edges and the consequent "free" shear layers are swept inboard of the leading edges and upward, coiling up to form two primary vortices (Fig. 4). These vortices, which have been shown to be fairly extensive regions of rotational flow with reduced total pressure, influence the upper surface-pressure distribution. They give rise to a substantial nonlinear contribution to lift that partially compensates for the extra drag due to the loss of the leading-edge suction force. The slender wing incorporates volume and lift integration. It may be compared (in Fig. 3d) with a fourth category, the first of a generation of hypersonic vehicles that integrates the propulsion system as well. The Shuttle Orbiter, shown in Fig. 3d, is not intended to fly for long periods under steady, level flight conditions. Its cross range of about 2,000 km (1,100 n. mi.) is also somewhat less than that of the first three classes of aircraft. It is included in this comparison with other slower, long-range designs because it is the only existing hypersonic vehicle with substantial payload capability (although boosted on takeoff, as shown in Fig. 2).

In the first three cases of straight, swept, and slender wings, the respective flow type is maintained throughout the flight range. The flows normal to the leading edge, being subsonic, may be described by elliptic differential equations. For the classical and swept shapes, the forces and moments generated are essentially linear functions of the vehicle attitude, so that small-perturbation or linearized analyses are the most frequently used calculation tools. The slender wing, on the other hand, develops large nonlinear forces.

The type of flow around the hypersonic vehicle will change with flight speed. The means for providing the lift, payload volume, and propulsion produce flows of the hyperbolic type with strong shock waves and expansions during the high-speed phase of the flight (Fig. 5). The 3D flow is interlaced with embedded discontinuities that enclose reacting and nonreacting regions, depending on the altitude and velocity along the flightpath. Changes from one flight regime to another must be gradual enough to be controllable. Frictional heating and transition effects will be especially important at elevated Mach numbers and altitudes, and surface pressure fluctuations, shear stresses, and temperatures must be known so that adequate shielding can be designed. Two kinds of shock boundary-layer interactions require our attention: (1) predominantly unswept shocks, which cause unsteady separations, and (2) highly swept shock waves associated with reasonably steady swept separation zones and coiled shear layers.

The regions of application for long-range aircraft in terms of slenderness ratio, s/ℓ, vs flight Mach number may be depicted as in the lower part of Fig. 3d (Küchemann 1965). Most existing types of aircraft, except for the Shuttle, lie to the left of the "sonic line," $\beta s/\ell = 1$, along which the leading edge of a slender or delta-wing vehicle is sonic. Below the horizontal line at $s/\ell \sim 0.2$, the span is too small to provide adequate lift at low speeds; as a result, present aircraft lie above this line. To the right of the sonic line, the hypersonic aircraft will possess a planform similar to a delta, with $s/\ell \sim 0.3$, but with the side edges situated outside the free-stream Mach cone from the nose. The aircraft must fly well at low speeds so that it can maneuver for a conventional landing and takeoff. The conflicting requirements for hypersonic and low-speed flight may perhaps be reconciled by designing the lower surface for hypersonic flight and the upper surface for low-speed flight (Squire 1971). Eggers, Petersen, and Cohen (1970) propose that a hydrogen-fueled turboramjet, hypersonic commercial transport cruising at Mach 6 could carry large payloads over long ranges and be economically competitive with subsonic and supersonic long-range transport aircraft.

We note that the potential utilization of the slender wing extends well into the hypersonic region. Present designs are limited by lifting requirements and lateral instability at low speeds. If we wish to design at s/ℓ ratios less than 0.2, Küchemann (1965) proposed that high-energy air could be injected at the 3D separation lines at the leading edges to increase the strength of the vortices emanating from the edges (and hence the lift) to provide improved low-speed performance.

The definition of slender implies that even though the flow at infinity may be above Mach 1, we are dealing with subsonic flows in the plane normal to the wing surface. For example, in the near-conical flow fields surrounding slender configurations at angle of attack, we shall see that some satisfactory analytical approaches have been developed to calculate the rolled-up shear layers from assumed 3D separation lines at sharp, swept leading edges, and on bodies by resorting to inviscid flow models (J. H. B. Smith 1966;

J. A. Weber et al. 1975: J. H. B. Smith 1978). In contrast, emphasis is also being placed on obtaining solutions to simplified forms of the Navier-Stokes equations using numerical procedures to compute the inviscid/viscous interactions in separation zones on relatively simple aerodynamic components. For example, separation in the cross-flow plane and in planes of conical-flow projection have been calculated on both blunt and pointed slender configurations in supersonic flow. These methods have employed "parabolic" and conical flow assumptions, respectively, to the Navier-Stokes equations with laminar viscous flows (Lubard and Rakich 1975; McRae 1976, 1977; and Vigneron, Rakich, and Tannehill 1978) and for turbulent flows with eddy viscosity models included (McRae and Hussaini 1978). Thin-layer approximations have been introduced into the Navier-Stokes equations by Pulliam and Steger (1978) to compute the laminar, transonic flow about a hemisphere-cylinder at angle of attack; and by Hung (1979) to compute the laminar, supersonic flow about a lifting cylinder-flare configuration. Kutler et al. (1978), making the same assumptions, have computed laminar flows about other component configurations, such as external corners. Internal corners have been treated by Hung and MacCormack (1977) and Shang and Hankey (1977) with laminar flows, and by Hung and MacCormack (1978), Shang, Hankey, and Petty (1978), and Horstman and Hung (1979) with turbulent flows (eddy viscosity models included). Previously, inviscid flow solutions with interacting shock waves in the cross-flow plane were obtained using "shock-capture" and "sharp-shock" techniques (Kutler 1974a,b).

Notwithstanding these impressive achievements, the ability to compute compressible separated flow regimes in three dimensions with their attendant vortical flows is far from attainment on a flight vehicle of general shape.

1.3 Design Aims

It emerges that flow separation in three dimensions is of vital significance to the entire spectrum of aerodynamic design as the swept 3D lines of attachment, separation, and reattachment form the skeleton structure around which the elements of the entire flow field can be assembled (Maskell 1955). The principles have evolved out of our experience with relatively straight wings of high aspect ratio at subsonic speeds and lead naturally to slender configurations of small aspect ratio (Maskell and Küchemann 1956). At moderate aspect ratios and sweep angles, the design problem is veiled in an apparent multiplicity of answers available to us (see Fig. 3d). Nevertheless, it is clear that in the area of recent military fighter design, the swept edge, in the form of a canard or a forward extension of the wing leading edge (LEX), has been accepted as instrumental in controlling the flow to produce high lift, especially for purposes of maneuvering (Fig. 6). We shall address the merits of controlled separations and the demerits of some uncontrolled separations (Küchemann 1955a, 1971; Peake 1978; Peake and Owen 1979) in later discussions of particular shapes of flight vehicle.

The "two-dimensional outlook," in which all flow separations are considered undesirable, must be discarded in favor of the realization that separations are inevitable somewhere on a body and that they may be used in a constructive and profitable manner. Three-dimensional separations bring order out of confusion by providing the basis for a flexible and systematic approach to the three-dimensional design problem (Maskell and Küchemann 1956). Once the lines of separation on a body are determined then, in principle, the structure of the mainstream flow containing the viscous vortices is also determined, because trailing or free viscous vortices spring from any lines of separation on a lifting body, and not just from a trailing edge, to impart the necessary average downward momentum to the fluid about the body.

The aerodynamic design of a lifting body, if it is to be successful throughout a range of flight conditions, must ensure that steady boundary conditions yield correspondingly steady flows to minimize buffet; that the lifting body should always be controllable throughout the flight envelope; and that there should be no unpleasant changes in force and moment characteristics. The goal to aim for is that flows should be dominated by free viscous vortices — with no large bubbles — and that the primary lines of separation should remain essentially fixed on the body throughout the flight range. This much wider than usual view of the aerodynamic design problem (Maskell and Küchemann 1956) should be contrasted with the restricted outlook that allows separation only at a trailing edge.

1.4 Catalog of Separated Flows

Inevitably, when the load-carrying, lifting, and propulsion components are integrated into an aircraft or missile configuration incorporating classical or swept-wing technology (Fig. 3d), the resulting interfering pressure fields produce separations that are often unanticipated, that are not fixed in location on the surface for all flight conditions, and that are, in this sense, uncontrolled. Examples of these usually unwanted 3D separated flows may be cataloged according to their causes (J. H. B. Smith 1975).

1. Flows over smooth walls in the presence of varying circumferential and lengthwise adverse pressure gradients. We include here those flows about bodies whose longitudinal axes in part or in whole are swept with respect to the oncoming stream, such as upswept rear fuselages or pointed and bluff-nosed missiles at angles of attack (Wickens 1964; Peake 1968, 1969; Atraghji 1967, 1968a,b; Grosche 1970; Peake, Rainbird, and Atraghji 1972; Kaye and Williams 1974).

2. Flows about protuberances attached to a wall where adverse pressure gradients are imposed abruptly. Antennae, bulbous wheel housings, cockpit canopies, pylons, boundary-layer diverters, and unfaired junctions of the wing and tail surfaces with the body are important examples (Meyer 1968; Peake, Rainbird, and Atraghji 1972; Gaudet and Winter 1973; Sedney and Kitchens 1975).

3. Flows about normal or inclined jets blowing from a wall. Control jets used for thrust-vector control cause substantial 3D separation of the local viscous flow in the region where the jet emerges from the vehicle surface (Hsia, Seifert, and Karamcheti 1964; Maurer 1966; Zakkay, Erdos, and Calarese 1968; Driftmyer 1974). In terms of upstream effect, the "solid blockage" caused by the jet is analogous to that of a protuberance.

4. Flows with shock waves present, sometimes associated with items (1) to (3). We shall pay particular attention to those separations produced in swept-shock/boundary-layer interactions (Korkegi 1971; Peake 1975; Peake and Rainbird 1975; Oskam, Bogdonoff, and Vas 1975; Oskam, Vas, and Bogdonoff 1975; Shang and Hankey

1977; Horstmann and Hung 1979), such as in corners, upon low aspect ratio wings, or at wing and fin-body junctions.

Although the effect of these uncontrolled separations on drag may not always be significant, high local heat transfer rates in reattachment zones (Korkegi 1971) and the induced interaction and potentially destabilizing effects of the vortex motions upon downstream control surfaces of a vehicle may be important (Nielsen 1978). In general, the uncontrolled flow separations have not been amenable to prediction and are not well understood. The disposition of the vortices and the scale of the separated flow domain, whether large (as in the case of body vortices from slender configurations at high angles of attack), or of the order of the oncoming boundary-layer thickness (as in the protuberance flow), will affect the magnitudes of locally induced suction pressures and, hence, the nonlinear increments to the body forces.

On hypersonic vehicles, in particular, aerodynamic ideals will be modified to varying degrees by the volume required for the payload, fuel, and propulsion systems. These requirements may cause substantial heating effects in flow reattachment zones resulting from shock/boundary-layer interactions and shock-on-shock impingement (Meyer and Vail 1967; Edney 1968; Tannehill, Holst, and Rakich 1976). On vehicles like the Space Shuttle, the location of impingement of the nose bow shock on the wing is important to the heat shield design. Provided the leading edges of the wing have large angles of sweepback, the bluff cross-sectional shape of the leading edge, incorporated for heating considerations, may still be "sharp," as far as fixing the region of the 3D separation is concerned.

Compressibility appears to alter the quantitative, but not the qualitative aspects of 3D separated flows. It has been found by experiment that the effect of increasing Mach number is to reduce the scale of the vortical motions with respect to the wing semispan on slender wings, and to increase the critical angle for the development of flow asymmetry of the rolled-up shear layers from bodies at high angles of attack (Moss and Isaacs 1964; Peake, Rainbird, and Atraghji 1972; Keener and G. T. Chapman 1974).

1.5 Scope of Review

This AGARDograph is the second concerned with the viscous-inviscid interactions that occur adjacent to the surfaces of aerodynamic vehicles in flows where compressibility and heat transfer effects are significant. The first volume (Hankey and Holden 1975) deals with the analytic modeling and experimental study of interactions between shock waves and laminar or turbulent boundary layers in axisymmetric or nominally two-dimensional flows. Such flows are relatively well understood when described in mean-flow terms; they are found, for example, in the hinge regions of aerodynamic flap controls of relatively large aspect ratio.

Notwithstanding the applicability and general success of the 2D methods reviewed by Hankey and Holden (1975) and discussed further by Peake and Rainbird (1976)[3], the above 2D methods may be used in only a restricted number of flow configurations, because nearly all practical viscous interaction problems are three-dimensional. In order to make a reasonable assessment of the skin friction and heat transfer at the surface, along with the overall pressures, forces, and moments on proposed high-speed aircraft and missiles — especially under conditions of pitch and yaw — we must develop rational design procedures (Küchemann 1969) in which the complexities of the inviscid and viscous 3D flow fields are modeled appropriately. Even with the continuation of the startling growth in our computer technology, it is not considered that the full three-dimensional, time-dependent Navier-Stokes equations incorporating subgrid scale turbulence modeling in complex flow fields will be solved in a routine manner for many years (but see the debatable optimism of D. R. Chapman, Mark, and Pirtle 1975; and D. R. Chapman 1979). To be able to do this requires an understanding of the basic physical principles involved (Küchemann 1969; Maskell 1961). The continuing objective is the prediction of the form of 3D separations at sharp edges and elsewhere on a general configuration, as essential constituents of an overall flow model that describes the enshrouding inviscid and viscous interacting flows. As we shall see, in only a limited number of circumstances, such as about cones and slender wings, do we comprehend the viscous and external flow fields; and these have developed from extensive initial calculation and experiment about corresponding configurations in incompressible flow (Peake, Rainbird, and Atraghji 1972; Rainbird et al. 1966). The slender wing, for example, is an impressive instance where the aerodynamic design aims were stated beforehand and then pursued in a rational manner (Küchemann 1969; Maskell 1961; Maskell and J. Weber 1959). In fact, we shall lean heavily upon the descriptions of 3D separated flows at low speeds, because regardless of the speed regime, we find that the topological features of the surface shear stress patterns are frequently the same. The dye flow experiments of Werlé (1973, 1974) and the oil-dot flow visualization technique of Meyer (1966) are exemplary in their definition of surface shear directions. In view of the paucity of viscous flow measurements on most complex 3D flow geometries, we shall rely on postulated topologies of both surface skin-friction lines and external stream patterns to provide a framework around which to build credible 3D flow models. The simple rules governing the behavior of singular points on the surface and in the stream form the substance of Sec. 2.

As a base of understanding for the controlled and uncontrolled flow-separation phenomena, we believe that it is useful to establish the flow fields about simple shapes that are elements of aircraft and missiles. The ensuing sections will, therefore, portray the flows about pointed and blunted slender wings and cones; cone-cylinders and other axisymmetric bodies; sharply swept wings; bluff protuberances; and in corners comprised of intersecting wedges. The means to implement the passive and active control of 3D separations will be included. We shall evidently be dealing with the complex interactions between shock waves and 3D boundary layers in many of these categories.

Examples of modern aerodynamic design will be discussed with particular reference to the slender wing and the Space Shuttle. Because appropriate emphasis will be placed on the high heat-transfer rates along reattachment regions on the vehicle surface, other important topics, such as the localized effects of hypersonic leading-edge interaction, supersonic wakes, and base flows, will not be included. Neither shall we make substantial comment on transition (except as affected by the appearance of organized vortex flows), the status of which is treated by Morkovin (1968); Tani (1969); Reshotko et al. (1975); and in AGARD CP-244 (1977)

---

[3] In their technical evaluation of the AGARD Fluid Dynamics Panel Symposium on "Flow Separation," the proceedings of which were published as AGARD CP-168 (1975).

on "Laminar - Turbulent Transition."* Attention will be concentrated on three-dimensional external flows about wetted surfaces where the undisturbed mean flow is relatively uniform and steady. Separations that develop are also three-dimensional and quasi-steady.

We have tried to compile an overview that is topical and to do this we have talked extensively with our friends and associates in the United Kingdom, in Europe, and in North America. We trust that our our interpretation of their work in this collated form will stimulate additional aimed research (Küchemann 1969) in aspects of three-dimensional flows that are of potential practical use. At the heart of this review is the conviction that separation is the prime ingredient of fluid motion determining the lift, drag, and thrust on flight vehicles. Separation, in reality, is almost always three dimensional and there are proved benefits to be gained in cultivating the three dimensionality (J. H. B. Smith 1975).

2. ATTACHMENT, SEPARATION, AND REATTACHMENT IN THREE-DIMENSIONAL FLOWS

2.1 Distinction Between Attached and Separated Flows

To begin this discussion, we shall try to make clear what we mean by a 3D separated flow and how it is to be distinguished from a 3D attached flow. This will also enable us to introduce some terminology that will be used consistently throughout the AGARDograph.

Let us first consider an attached flow and try to isolate those features that all attached flows should hold in common. To ensure that there will be wide acceptance of what we choose to call an attached flow, we take as our example the flow over a smooth slender body of revolution that is inclined at a small angle of attack to a uniform oncoming stream. A streamline in the oncoming flow attaches itself to the nose at a stagnation point, which we call a nodal singular point of attachment. It is the source of the continuous pattern of skin-friction lines that emerge from this point and envelop the body. Because of the favorable pressure gradient in the circumferential direction, the skin-friction lines emanating from the nodal point of attachment sweep around the sides of the body and tend to converge on either side of the particular skin-friction line running along the leeward ray. All of the skin-friction lines vanish into a single point near the aft end, out of which a single streamline departs into the external flow. This point, which can be considered a sink for the collection of skin-friction lines, we call a nodal point of separation. This actually completes the description of what we mean by an attached flow. Put simply, an attached flow may be defined as a flow containing two and only two singular points in the pattern of skin-friction lines; these are necessarily a nodal point of attachment and a nodal point of separation. Note, however, that an attached flow may feature skin-friction lines converging on either side of a particular line. Some researchers consider this to be a clear sign of flow separation and go on to label the particular line a "line of separation." In view of our example, however, which is clearly one of an attached flow, we are led to say that a skin-friction line emanating from a nodal point cannot be a line of separation, and that convergence of skin-friction lines on a particular line may be a necessary condition for separation, but it cannot be a sufficient condition.

Since, according to our definition, the class of attached flows is exhausted by those flows whose skin-friction line patterns contain two and only two nodal points, we shall say that all 3D flows whose skin-friction line patterns contain more than two nodal points are separated flows. The simplest possible separated flow is then one containing three nodal points, so that two must be of the same type. Suppose now that the angle of attack of the body is increased to the point where we have a flow whose skin-friction line pattern contains two nodal points of attachment and one nodal point of separation. The skin-friction lines emerging from each of the nodal points of attachment must be prevented from crossing; this is achieved by the insertion of a new singular point between them. We call this point a saddle point. Two skin-friction lines, one from each nodal point of attachment, enter the saddle point, and two skin-friction lines emerge. The two emerging lines act as barriers between the sets of lines emanating from each of the nodal points. Prevented from crossing, the skin-friction lines from each of the nodal points tend to converge on the lines acting as barriers. We call these particular lines, lines of separation, and their distinguishing feature is that they emerge from a saddle point. Note that we now have a pattern of skin-friction lines containing three nodal points and one saddle point, making a difference of two between nodal and saddle points. This relation — that nodal points exceed saddle points by two — is a topological rule that holds in general. It will figure often in the discussion to follow. Having the topological rule, we can make the distinction between attached and separated flows short and precise: The skin-friction line pattern for attached flow cannot contain any saddle points; the skin-friction line pattern for separated flow must contain at least one saddle point.

Taking a global view of the flow, the separation line is then the location along which the boundary layer detaches from the wall. There is then a particular surface in the flow that is "anchored" to the body along the separation line and prevents the converging boundary layers on each side of the separation line from coalescing. This surface is called a dividing surface and rolls up in its passage downstream. The saddle point in the pattern of skin-friction lines is also the source of the external streamlines that exist on the dividing surface. Note that on the body, beneath the core of the coiled-up dividing surface, there will be a line of inflexion points in the pattern of skin-friction lines interspersing the 3D separation line (on either side of which are converging skin-friction lines) and an associated reattachment line (on either side of which exist diverging skin-friction lines). This localized pattern of inflexion points in the body skin-friction line pattern is characteristic of the existence of a coiled-up dividing surface above it. Because it has a well-defined core, we shall invoke the popular terminology and call the flow in the vicinity of the coiled-up dividing surface a vortex.

Notwithstanding these definitions, it may be that the scale of resolution on the nose of a vehicle when separation exists (for example, at a relatively sharp apex) is such that the postulated combination of two nodes adjacent to a saddle point is not determinable. Even on a nose with a larger radius, we may only be able to identify a "source flow" in the pattern of skin-friction lines. Thus an important question arises: To what scale must we reduce our "window" of the flow so as not to omit the important kernels of its formation?

---

*See also the technical evaluation of this AGARD FDP Symposium by Morkovin (1978).

The problem cited above has caused difficulties, especially when experimental and analytical powers of resolution are imprecise, in synthesizing 3D flow fields from skin-friction line patterns alone. Nevertheless, in the ensuing sections, we shall attempt to demonstrate the usefulness of topological notions in providing a rational means for deciphering the intricacies of 3D separated flows, and as useful tools in constructing the characteristics of the external 3D flow fields in conjunction with the pattern of body skin-friction lines. (In a private communication, Legendre 1979 has pointed out that the groundwork for the topological notions, its language and its rules, were laid out in a series of fundamental mathematical papers by Poincaré (1878).

2.2 The Three-Dimensional Boundary Layer

The essential characteristic of a three-dimensional flow, which distinguishes it from the simpler two-dimensional and axisymmetric cases, is that pressure gradients exist in the transverse direction as well as along the external streamline direction. Although we can still assume that the pressure gradient is negligibly small through the thin, attached boundary layer along a normal to the surface, the transverse pressure gradient will cause the mean streamline curvature to increase toward the surface, in which direction there is increasing momentum-deficient flow. This skewing of the viscous flow, which is limited by the transverse components of shear stress that are caused to develop, is called "crossflow" or "secondary flow." Due to the crossflow (the response of the boundary layer to the transverse pressure gradients) the resultant directions of the mean-flow velocity vectors are nonplanar, as shown in Fig. 7. Near the outer edge of the boundary layer, the transverse gradient does not much alter the velocity vectors from the local external stream direction, but deeper in the layer, a substantial crossflow develops. The boundary conditions at the wall ($u = v = 0$) and at the edge of the viscous flow ($u = u_e$, $v = 0$) must be satisfied, of course.

Previous work has indicated that two systems of orthogonal coordinate axes are the most commonly used to resolve the three-dimensional boundary layer (see Cooke and Hall 1962; Nash and Patel 1972). The first is a system of natural or geodesic coordinates, so named because they are based on the geometry of the body. It is especially useful for bodies having developable surfaces, such as cones. The second system is one of streamline coordinates that is based on the geometry of the external flow. This is a system in which one family of coordinate curves is the projection of the external streamlines on the surface of the body; the other family consists of the orthogonal trajectories in the surface of the first family. These are shown in Fig. 7. The direction of the external streamline is known as the streamwise direction, ξ, and the transverse direction, n, is called the crossflow direction. With streamline coordinates, the velocity profiles resolve into u and v components, as shown in Fig. 7. If the maximum value of the crossflow velocity is small, small crossflow approximations can be made in the boundary-layer momentum equations, to decouple the calculation of the streamwise flow from the crossflow. As a separation line is approached, the development of "S"-shaped crossflow profiles occurs (see Rainbird 1968b). On very complex bodies, however, streamline coordinates can lead to very difficult differential geometry necessary to describe the metric coefficients (the stretching functions). Other orthogonal systems may then be more useful; see Myring (1970); Mangler and Murray (1975); Pulliam and Steger (1978). Unfortunately, a method to provide an optimized coordinate geometry to suit a general 3D flow problem has yet to be found.

Two additional mean-flow characteristics of three-dimensional boundary-layer profiles, when resolved in streamline coordinates, are illustrated in Fig. 8: the crossflow angle within the boundary layer and the polar velocity profile. Considerations of the boundary-layer equations in the viscous sublayer imply continuous skewing of the flow in this region, shown by curve (a). Only when the resultant pressure gradient is in the direction of the resultant wall shear stress (a condition not usually encountered in practice) can we assume collateral flow, curve (b); that is, where the crossflow velocity v is directly proportional to u close to the wall (Nash and Patel 1972). Infinitesimally close to the surface, the velocity vectors reach a limiting direction that differs by an angle ω_s (called the streamline divergence angle, Fig. 8) from the external stream direction. This streamline divergence angle will be small in the case of a boundary layer existing in a favorable pressure gradient, but may become very large when the pressure gradients become adverse. Moreover, there is no lag of growth in the crossflow with application of the transverse pressure gradient, but the reduction in crossflow lags the removal of the pressure gradient (Cooke and Hall 1962).

2.3 Historical Perspective of Limiting Streamlines and Skin-Friction Lines

If we consider the subject of three-dimensional viscous flows in its historical context, Sears (1948) utilized the concept of "limiting streamlines" in a paper discussing the laminar boundary layer on a yawed cylinder. Each streamline just above the surface is one of a continuous pattern. No matter how small the height of the streamline above the surface, the streamline will exist. If this height is allowed to approach zero, the streamline will become parallel to the surface, reflecting the more rapid decline towards zero of the fluid's normal velocity than its tangential velocity. The streamline is then identifiable as a limiting streamline: it possesses the same direction as a skin-friction line or a surface shear-stress trajectory. So long as the limiting streamline remains parallel to the surface, the pattern of limiting streamlines may be alternatively viewed as a "sheath" surrounding the body, whose projections onto the surface are the skin-friction lines. These limiting streamlines at the base of the boundary layer must not be confused with the streamlines of the external inviscid flow at the edge of the boundary layer; in general they will follow paths that are different in direction from the external streamlines.

Limiting streamlines typically originate at nodal points of attachment (e.g., on the nose of a body) and, after circumscribing the body surface, disappear into nodal points of separation. Since limiting streamlines springing from adjacent nodal points of attachment will tend to run into each other, there must exist between them a saddle point of either attachment or separation, emanating from which a single limiting streamline will act as a barrier between the streamlines from the adjacent nodal points and prevent them from crossing. If the adjacent limiting streamlines tend to converge on this line, the line will have the appearance of a line of separation; that is, a line near which adjacent limiting streamlines will tend to leave the surface. Sears (1948) included a sketch suggesting this behavior; however, he did not call the line in question a line of separation in his investigation of the laminar boundary layer on a yawed infinite wing. In subscribing to this work, Eichelbrenner (1954) and Eichelbrenner and Oudart (1955) proposed that a three-dimensional line of separation was the envelope of the converging adjacent limiting streamlines (conversely, from the line of attachment, limiting streamlines diverge).

It remained for Maskell (1955), in a paper remarkable for its clarity and descriptive power, to bring together a number of these notions and demonstrate how the limiting streamlines provide "a three-dimensional skeleton structure of the viscous flow." Maskell did not rely on boundary-layer concepts but based his discussion on the significance of separation in the flow as a whole. The hypotheses he proposed for synthesizing flow structures were clearly influenced by the results of experimental studies utilizing oil-streak flow-visualization techniques. If a flow-visualization indicator on a wind-tunnel model is very thin, it has been shown (see Maltby 1962) that the direction indicated by the streak passing through a point on the surface is very close to the direction of the skin-friction line through the point. Hence, insofar as it is true that a skin-friction line is the projection on the surface of a limiting streamline, the streak is likewise an indication of the direction of the corresponding limiting streamline. Maskell's hypotheses, together with the types of oil-streak flow-visualization techniques, yield a powerful means of diagnosing and synthesizing the qualitative features of three-dimensional viscous flows. Maskell conceived of two main types of separated flow structures: a bubble type (Fig. 9a) and a free-shear layer type (Fig. 9b).

Fluid accumulating at a three-dimensional separation line, which in general is set obliquely to the direction of the external and essentially inviscid flow field, leaves the separation line usually as a free-shear layer (Fig. 9b) and rolls up in the process of passing downstream. In both types of structure, Maskell hypothesized that a limiting streamline would join the separation streamline "tangentially" or would have a "cusp" on the separation streamline. The separation streamline therefore would be a "cusp locus" of limiting streamlines that join it from either side. Limiting streamlines from opposite sides that join the separation streamline at a single point were hypothesized to merge and to leave the surface as single streamlines along a "surface of separation."

Although the experimental evidence of oil-streak lines could be read to favor the picture of separation drawn by Maskell, the central idea that the line of separation was an envelope (see also S. Brown 1965) or a locus where limiting streamlines could attach themselves and merge together did not go unchallenged. An implicit criticism was contained in the results of Legendre (1956, 1965) and Oswatitsch (1957) who, independently, studied the mathematical behavior of the singular points associated with continuous vector fields. Their results, delineating the types and behavior of allowable elementary singular points, would not accommodate the complicated singular behavior called for by Maskell's picture of merging streamlines.

The issue was clarified and essentially resolved by Lighthill (1963) in an important and lucid review article. Lighthill abandoned the use of limiting streamlines to work instead with skin-friction lines and their associated surface vortex lines. Both of the latter systems of lines cover the surface completely, crossing each other everywhere at right angles. The advantages of working with skin-friction lines are twofold: first, they are defined uniquely everywhere on the surface, even in the vicinity of lines of separation, which are themselves skin-friction lines; and second, with skin-friction lines being defined uniquely everywhere on the surface, the pattern of skin-friction lines can be viewed as a continuous vector field. Hence, the allowable elementary singular points of the field can be delineated easily, as Lighthill showed, reproducing the previously cited results of Legendre (1956, 1965) and Oswatitsch (1957). Lighthill also noted that the number and types of singular points on the surface obey a topological rule (see also Davey 1961).

More recently, Legendre (1977), noting that controversy still existed over the interpretation of limiting streamlines in the vicinity of separation, recapitulated the simple mathematical basis for a limited number of elementary singular points. He observed that, so far as is currently known, all experimentally determined surface flow visualization patterns can be interpreted within the framework of a limited number of elementary singular points. There is, at present, no necessity to invoke more complicated singular behavior to cover the existing evidence.

Our own view supports that of Lighthill (1963) and Legendre (1977) – oil-streak flow-visualization surface patterns are best interpreted as being representative of skin-friction lines. Singular points in the patterns are consistent with the simplest possible hypotheses regarding the characteristics of continuous vector fields. Additionally, our view is that not only is it good scientific practice to hold only the simplest hypotheses consistent with the experimental evidence, but there are also advantages to be gained by such an economy. Recently, J. C. R. Hunt et al. (1978) have shown that the notions of elementary singular points and topological rules can be easily extended to apply to the flow above the surface on planes of symmetry, on projections of conical flows (J. H. B. Smith 1969), and on crossflow planes, etc. (see also Perry and Fairlie 1974). It is useful to consider the limited number of singular points and topological rules as components of an organizing principle – a flow grammar, whose finite number of elements can be combined in myriad ways to describe, understand, and connect together the properties common to all three-dimensional viscous flows.

2.4 Singular Points

Singular points in the pattern of skin-friction lines occur at isolated points on the surface where the surface vorticity and skin friction (orthogonal vector quantities tangential to the surface) become identically zero. Singular points are classifiable into two main types: nodes and saddle points. Nodes may be further subdivided into two subclasses: nodal points and foci (of attachment or separation).

A nodal point (Fig. 10a) is the point common to an infinite number of skin-friction lines. At that point, all of the skin-friction lines except one (labeled AA in Fig. 10a) are tangential to a single line BB. At a nodal point of attachment, all of the skin-friction lines are directed outward away from the node. At a nodal point of separation, all of the skin-friction lines are directed inward toward the node.

A focus (Fig. 10b) differs from a nodal point on Fig. 10a in that it has no common tangent line. An infinite number of skin-friction lines spiral around the singular point, either away from it (a focus of attachment) or into it (a focus of separation). Foci of attachment generally occur in the presence of rotation, either of the flow or of the surface, and will not figure in the present study.

At a saddle point (Fig. 10c), there are only two particular lines, CC and DD, that pass through the singular point. The directions on either side of the singular point are inward on one particular line and outward on the other particular line. All of the other skin-friction lines miss the singular point and take directions consistent with the directions of the adjacent particular lines. The particular lines act as barriers in the field of skin-friction lines, making one set of skin-friction lines inaccessible to an adjacent set.

For each of the patterns in Figs. 10a to 10c, the surface vortex lines form a system of lines orthogonal at every point to the system of skin-friction lines. Thus, it is always possible in principle to describe the flow in the vicinity of a singular point alternatively in terms of a pattern of skin-friction lines or a pattern of surface vortex lines.

Davey (1961) and Lighthill (1963) have noted that of all the possible patterns of skin-friction lines on the surface of a body only those whose singular points obey a topological rule are admissible: the number of nodes (nodal points or foci, or both) must exceed the number of saddle points by two. We shall demonstrate this rule and its recent extensions to the external flow field in a number of examples.

We should note that the 3D flow at a saddle point of attachment (Davey 1961) and the axisymmetric flow at a nodal point of attachment (Schlichting 1968) are available from exact solutions of the Navier-Stokes equations when arguments of "local similarity" are invoked. It appears that other singular points on the surface may also be given in numerical solutions of approximate forms of the Navier-Stokes equations.

2.5 Topography of Skin-Friction Lines

The singular points, acting either in isolation or in combination, fulfill certain characteristic functions that largely determine the distribution of skin-friction lines on the surface. The nodal point of attachment is typically a stagnation point on a forward-facing surface, such as the nose of a body, where the external flow from far upstream attaches itself to the surface. The nodal point of attachment thereby acts as a source of skin-friction lines that emerge from the point and spread out over the surface. Conversely, the nodal point of separation is typically a point on a rearward-facing surface, and acts as a sink where the skin-friction lines that have circumscribed the body surface may vanish.

The saddle point acts typically to separate the skin-friction lines issuing from or entering into adjacent nodes; for example, adjacent nodal points of attachment. An example of this function is illustrated in Fig. 11a (Lighthill 1963) and in the skin-friction line pattern on the cockpit windows of a Space Shuttle model (Fig. 11b; courtesy of L. Seegmiller, Ames Research Center). Skin-friction lines emerging from the nodal points of attachment are prevented from crossing by the presence of a particular skin-friction line emerging from the saddle point. This particular skin-friction line is called a line of separation. Skin-friction lines from either side tend to converge on the line of separation. Another graphic indicator of the line of separation is the behavior of the surface vortex lines. In the vicinity of a line of separation, the surface vortex lines become distorted, forming upstream-pointing loops with the peaks of the loops occurring on the line of separation.

Why limiting streamlines must leave the surface in the vicinity of a line of separation can be explained by a simple argument due to Lighthill (1963). In terms of general curvilinear coordinates orthogonal in the surface (ξ, η, ζ) with length parameters $h_1(\xi, \eta)$ and $h_2(\xi, \eta)$, the equation of the limiting streamline (or trajectory of the surface shear stress vector) becomes

$$\frac{h_1\, d\xi}{\tau_{SF}} = \frac{h_2\, d\eta}{\tau_{CF}} \qquad \text{at} \quad \zeta = 0$$

where

$$\tau_{SF} = \mu\left(\frac{\partial u}{\partial \zeta}\right)_{\zeta=0}$$

$$\tau_{CF} = \mu\left(\frac{\partial v}{\partial \zeta}\right)_{\zeta=0}$$

are the components of skin-friction parallel to the ξ and η axes, respectively. If, furthermore, (ξ, η, ζ) are arranged as streamline coordinates, then τ_{SF}, τ_{CF} are the respective streamwise and crossflow skin-friction components. Now if n is the distance between two adjacent limiting streamlines (see Fig. 12) and h is the height of a rectangular stream tube (being assumed small so that the local resultant velocity vectors are coplanar and form a linear profile) then the mass flux through the stream tube is

$$\dot{m} = \rho h n \bar{u}$$

where ρ is the density and $\bar{u}$ the mean velocity of the cross section. But the resultant skin friction at the wall is the resultant of τ_{SF} and τ_{CF}, or

$$\tau_w = \mu\left(\frac{\bar{u}}{h/2}\right)$$

so that

$$\bar{u} = \frac{\tau_w h}{2\mu}$$

Hence,

$$\dot{m} = \frac{h^2 n \tau_w}{2\nu} = \text{constant}$$

yielding

$$h = C\left(\frac{\nu}{n\tau_w}\right)^{1/2}; \qquad \nu = \mu/\rho$$

Thus h, the height of the limiting streamline above the surface, increases rapidly as the line of separation is approached. There are two reasons for the increase: first, the resultant skin friction τ_w approaches zero as the saddle point is approached; and second, n, the distance between adjacent limiting streamlines, falls rapidly as the limiting streamlines converge toward the line of separation. (The convergence of the limiting flow is a necessary condition for the occurrence of separation, but is not sufficient; see Sec. 2.1).

The converse of the line of separation is the line of attachment. Two lines of attachment are illustrated in Fig. 11a, emanating from each of the nodal points of attachment. Skin-friction lines tend to diverge from lines of attachment. Just as with the line of separation, a graphic indicator of the presence of a line of attachment is the behavior of the surface vortex lines. Surface vortex lines form downstream-pointing loops in the vicinity of a line of attachment with the peaks of the loops occurring on the line of attachment.

This section concludes with a discussion of the remaining type of singular point, the focus (of separation). The appearance of a focus on the surface invariably occurs in company with that of a saddle point. Together, they provide one mechanism through which surface vortex lines can, in effect, be extended into the fluid to form the familiar coiled "sheet" about a central vortical core. The word "sheet" is most properly reserved for the inviscid flow approximation to the viscous shear layer in the real flow that departs from the region of the three-dimensional-separation (skin-friction) line. Rather than use the word "sheet" we call the surface stemming from the line of separation a dividing surface (of separation).

Beginning at a saddle point on the wall, the dividing surface extends the function of the line of separation into the flow, acting as a barrier separating the set of limiting streamlines that have risen from near the surface on one side of the line of separation from the set arisen from the other side. The focus on the wall extends into the fluid as a concentrated vortex filament. The adjacent dividing surfaces (to which the focus on the wall is attached through saddle points) roll up with the same sense of rotation as the vortex filament. When one of these dividing surfaces extends downstream, it quickly draws the vortex filament into its core. In effect, then, the extension into the fluid of the focus on the wall serves as the vortical core about which the dividing surface coils.

This flow behavior was first hypothesized by Legendre (1965), who also noted (Legendre 1972) that an experimental confirmation existed in the results of earlier experiments that had been carried out by Werlé (1962). Figure 13a shows Legendre's original sketch of the skin-friction lines; Fig. 13b is a photograph that illustrates the experimental confirmation. The surface on which surface vortex lines extend into the fluid and coil around the extension of the focus (Fig. 13c) will be termed here a "horn-type dividing surface." On the other hand, it can happen that none of the adjacent dividing surfaces to which the focus is connected extends downstream. In this case the vortex filament emanating from the focus remains distinct ("tornado-like") and is seen as a separate entity on crossflow planes downstream of its origin on the surface.

A series of examples where the distinct vortex filament from the focus leaves the surface is shown on the wide range of aerodynamic configurations presented in Fig. 14. Figure 14a illustrates a focus of separation on the afterbody of an ellipsoid in a water tunnel at very low speed (Lahlou 1971). Figures 14b to 14d show foci of separation on lifting wings at angle of attack in laminar flow (Werlé 1974 and Legendre 1965) and in turbulent flow (courtesy of ARA Bedford and B. Elsenaar, NLR, Amsterdam). In each of the figures (Figs. 14b to 14d), the pressure gradient along the direction of the separation line is such as to cause a termination of the dividing surface (emanating from the separation line) into an eventual prominent focus. The buffet phenomenon is thought to be associated with this flow structure on the swept-wing examples, the spiraling vortex filament erupting from the surface with random motion. Finally, Figs. 14e and 14f illustrate foci of separation in supersonic flow on a cylinder-flare junction (courtesy of C. F. Coe, Ames Research Center) and on the booster of a Space Shuttle launch configuration (Dods and Cangie 1971). In the latter example, the adverse pressure gradient generated by the exhaust plumes of the booster evidently encourages termination of the dividing surfaces of separation on the fuselage just ahead of the exhaust nozzles.

In an interesting and potentially important additional interpretation of the focus, one begins by considering the pattern of lines orthogonal to that of the skin-friction lines; that is, the pattern of surface vortex lines. One immediately sees that a focus on the wall represents a common point marking the apparent termination of a set of surface vortex lines. If one imagines that each of these surface vortex lines is the bound part of a horseshoe vortex, then the extension into the fluid of the focus on the wall as a concentrated vortex filament is seen to represent the combination into one filament of the horseshoe-vortex legs from all of the bound vortices that have ended at the focus. One can envision the possibility of incorporating this description of the flow in the vicinity of a focus into an appropriate inviscid flow model. Lastly, although the combination focus/saddle point provides a way of forming coiled dividing surfaces around vortical cores, it does not seem to be the only way; it will be seen subsequently that the combination nodal-point/saddle-point also is capable of carrying out this function.

2.6 Merged Singular Points

The study of combinations of singular points leads to a question that has not yet received attention in the literature, namely: What is the nature of the flow in the vicinity of singular points when two or more isolated points tend to merge together? Although it is true in principle that merged singular points usually can be separated into their isolated elementary components by a sufficient magnification of the scale, it is also likely that many occasions will arise when the task of resolving details of the flow at the required

magnified scale is beyond the capacity of the experimental or analytical means available. Such occasions call for an alternative approach that will permit a deduction of the flow's nature on the basis of the observable evidence; that is, a deduction consistent with what would have been deduced on the basis of observations at the magnified scale, had sufficient means of resolution been available. It is suggested here that this approach will entail a study of singular points that have merged sufficiently closely so that, at the observable scale, they appear to be singular points of higher order.

To illustrate the nature of the results that are to be expected from this new and potentially important area of research, we present two examples that may be representative of the occasions most in need of a treatment of merged singular points. Figure 15a illustrates the merging of a saddle point of separation and a nodal point of attachment, such as might occur in the skin-friction line pattern of the flow before an obstacle standing on a wall. It will be noted that as the distance x_1 separating the saddle point and the nodal point tends towards zero, the skin-friction line pattern around the merged points combines features characteristic of the separate patterns around saddle points and nodal points. By way of speculation, we note that Fig. 15a admits of yet another interpretation that may prove useful in arriving at a suitable definition of the onset of separation in the flow before an obstacle. Let us imagine that the obstacle is first small enough so that no flow separation occurs, and that it is then enlarged incrementally until a stage is reached where the slightest further enlargement would bring about separation. It would seem that the skin-friction line pattern at that stage should contain a point such as the one illustrated on the right of Fig. 15a. This pattern would provide a suitable link between a skin-friction line topology prior to separation consisting of no singular points in the vicinity of the obstacle and a topology subsequent to the first appearance of separation consisting of two elementary singular points, the saddle point/nodal point combination illustrated on the left of Fig. 15a. Thus, a possible definition of the onset of separation might be based on the first appearance of the merged pair of singular points in the pattern of skin-friction lines.

The second example chosen for illustration may be representative of, for example, the separated flow in the vicinity of the stagnation point of a blunt-nose body at high angle of attack. It consists of three singular points in the pattern of skin-friction lines: two nodal points of attachment separated by a saddle point. The sketch on the left of Fig. 15b shows the skin-friction line pattern around the elementary singular points when separated by a distance x_1, and the right-hand sketch shows what happens as the separation distance x_1 tends toward zero.

It will be seen that the pattern of skin-friction lines around the merged singular points has the same general appearance as the pattern of lines around an elementary nodal point of attachment. Two of the lines emerging from the point ultimately act as lines of separation, all but two of the remaining lines converging on them from either side. Behavior of this type has been observed in a number of experimental studies on blunt bodies of revolution (Peake 1978, Han and Patel 1979) and has led some researchers to argue that flow separation can ensue out of an elementary node of attachment without the appearance of a saddle point in the pattern of skin-friction lines. A closer examination should reveal, however, that despite appearances, in the case of separated flow the behavior of the flow in the immediate vicinity of the stagnation point is not that appropriate to the flow about an elementary node.

2.7 Topography of Streamlines in Two-Dimensional Sections of Three-Dimensional Flows

After an unaccountably long time, it has become clear only within the last few years that the mathematical basis for the behavior of elementary singular points and for the topological rules that they obey is general enough to support a much wider regime of application than had been realized. The results reported by J. H. B. Smith (1969, 1975), Perry and Fairlie (1974), and J. C. R. Hunt et al. (1978) have made it evident that the rules governing skin-friction line behavior are easily adapted and extended to yield similar rules governing behavior of the flow itself. In particular, J. C. R. Hunt et al. (1978) have noted that if $\underline{v} = [u,(x, y, z_0), v(x, y, z_0), w(x, y, z_0)]$ is the mean velocity whose u, v components are measured in a plane $z = z_0 =$ constant, above a surface situated at $y = Y(x; z_0)$ (see Fig. 16), then the mean streamlines in the plane are solutions of the equation

$$\frac{dx}{u} = \frac{dy}{v}$$

which is a direct counterpart of the equation for skin-friction lines on the surface. J. C. R. Hunt et al. (1978) cautioned that for a general 3D flow the streamlines defined by the equation are no more than that — they are not necessarily the projections of the 3D streamlines onto the plane $z = z_0$, nor are they necessarily particle paths even in a steady flow. Only for special planes, such as for example, a streamwise plane of symmetry (where $w(x, y, z_0) = 0$) are the streamlines defined by the equation identifiable with particle path lines in the plane when the flow is steady, or with instantaneous streamlines when the flow is unsteady. In any case, since (u, v) (x, y) is a continuous vector field $\underline{V}(x, y)$, with only a finite number of singular points in the interior of the flow at which $\underline{V} = 0$, it follows that nodes and saddle points can be defined in the plane just as they were for skin-friction lines on the surface. Nodes and saddle points within the flow, excluding the boundary $y = Y(x; z_0)$, are labeled N and S, respectively, and are shown in their typical form in Fig. 16. The only new feature of the analysis that is required is the treatment of singular points on the boundary $y = Y(x; z_0)$. As introduced by J. C. R. Hunt et al. (1978) singular points there are defined as half-nodes N' and half-saddles S' (Fig. 16). With this simple amendment to the types of singular points allowable, all of the previous notions and descriptions relevant to the analysis of skin-friction lines carry over to the analysis of the flow within the plane.

In a parallel vein, J. C. R. Hunt et al. (1978) have recognized that, just as the singular points in the skin-friction lines on the surface obey a topological rule, so must the singular points in any of the sectional views of 3D flows obey topological rules. Although a very general rule applying to multiply connected bodies can be derived (J. C. R. Hunt et al. 1978), we shall list here for convenience only those special rules that will be useful in our subsequent studies of the flow past wings, bodies, and obstacles. In the five topological rules listed below, we assume that the body is simply connected and immersed in a flow that is uniform far upstream.

1. Skin-friction lines on a three-dimensional body (Davey 1961; Lighthill 1963);

$$\sum_N - \sum_S = 2$$

2. Skin-friction lines on a three-dimensional body B connected simply (without gaps) to a plane wall P that either extends to infinity both upstream and downstream or is the surface of a torus:

$$\left(\sum_N - \sum_S\right)_{P+B} = 0$$

3. Streamlines on a two-dimensional plane cutting a three-dimensional body:

$$\left(\sum_N + \tfrac{1}{2}\sum_{N'}\right) - \left(\sum_S + \tfrac{1}{2}\sum_{S'}\right) = -1$$

4. Streamlines on a vertical plane cutting a surface that extends to infinity both upstream and downstream:

$$\left(\sum_N + \tfrac{1}{2}\sum_{N'}\right) - \left(\sum_S + \tfrac{1}{2}\sum_{S'}\right) = 0$$

5. Streamlines on the projection onto a spherical surface of a conical flow past a three-dimensional body (J. H. B. Smith 1969):

$$\left(\sum_N + \tfrac{1}{2}\sum_{N'}\right) - \left(\sum_S + \tfrac{1}{2}\sum_{S'}\right) = 0$$

2.8 Selected Examples of Component Flows to Demonstrate Topography

A study of example cases will be undertaken in this section to demonstrate how the understanding of the behavior of singular points may facilitate hypothetical reasoning regarding the structure of flows about major components of the aircraft. Strict adherence to the topological rules that singular points must obey ensures at the same time that hypothetical flow patterns constructed on this basis remain within the realm of physical plausibility.

2.8.1 Slender Wings

The first example chosen for study is the flow about a slender delta wing at angle of attack. It is well known that the characteristic feature of this flow is the appearance of free shear layers that coil tightly around dividing surfaces of separation springing from the leading edges (see Figs. 4, 17, and 18). Figure 18 shows a typical pattern of skin-friction lines on the wing top surface, consistent with the existence of both primary and secondary separation lines, and the peak suction pressures in the crossflow plane resulting from the leading-edge (primary) vortices. However, the origin of the dividing surfaces and their detailed behavior in the vicinity of the apex remains conjectural. On the theoretical side, the difficulty is associated with the presence of sharp edges which violate ideas about analyticity; on the experimental side, the difficulty is associated simply with insufficient powers of visual or instrumental resolution.

Theoreticians have attacked the problem by focusing on a small region of the apex and magnifying the scale to a degree such that the edges there appear to be rounded enough to dispose of the question of analyticity. Then it is reasonable to assume that, just as for smooth round-nose bodies, the flow in the vicinity of the apex must be describable within the framework of rules governing the behavior of singular points. The assumption is not sufficiently exclusive to enable the determination of a unique flow pattern but only a limited number of physically plausible ones. Lighthill (1963) has proposed one such pattern, and Legendre (1972) has proposed yet another. These alternative patterns are illustrated in Fig. 19. As noted earlier, experimentally determined skin-friction patterns for the slender delta wing lack sufficient resolution near the apex to be of help in deciding which among alternative patterns is the operative one at a given angle of attack. Experimental results for the slender rectangular wing, on the other hand, do allow a clear and unambiguous resolution of the skin-friction lines near the leading edge. As will be seen, the flow over the slender rectangular wing is of great interest in itself. Additionally, it is reasonable to assume that this flow is similar in many respects, especially in the vicinity of edges, to that over the slender delta wing. If this assumption is adopted, results for the rectangular wing become available to help resolve the problem of the delta wing. The results reported by Wickens (1966) become particularly illuminating in this regard.

Figure 20 (from Wickens 1966) shows oil-flow patterns on the leeward surface of a slender rectangular wing at an angle of attack of 20°. Figure 21a is a deduction from Fig. 20 of the corresponding pattern of skin-friction lines on the leeward and windward surfaces. It will be noted that there are four foci, one nodal point of attachment, and five saddle points on the leeward surface and that the windward surface contains one nodal point of attachment. Assuming that all of the skin-friction lines except the particular ones on the centerline of the wing go into nodal points of separation, one at each tip of the wing trailing edge, while the particular lines on the centerline go into a saddle point at the trailing edge, we have eight nodes and six saddle points, giving a difference of two, in accordance with topological rule No. 1. Each of the five saddle points on the leeward surface separates the flows from adjacent pairs of nodes. Springing from the saddle points are dividing surfaces, the form of which we attempt to portray in Fig. 21b. On each side of the centerline, we suppose that the primary separation consists of the dividing surface which runs into the focus nearest the edge of the wing, taking the form of the "horn-type" dividing surface described previously (Legendre 1965).

Particularly noteworthy is the other focus-saddle-point combination near the centerline of the wing. For flow over a wing of infinite span (i.e., for 2D flow) the dividing surface springing from the saddle point on the centerline would extend indefinitely spanwise and, with the corresponding reattachment, would represent the so-called leading-edge separation bubble. If the span of the wing is reduced, the adverse spanwise pressure gradient would cause the dividing surface to turn downstream. With a further reduction in span, to the order of that depicted in Figs. 20 and 21, the downstream path of the dividing surface is blocked by an adverse streamwise pressure gradient. Its remaining recourse is to roll up around a focus, as portrayed in Fig. 21b. Emanating from the focus into the flow is an isolated vortex filament which passes downstream. This intricate flow structure may be cited as an example of how three-dimensionality can change the aspects of a relatively well known two-dimensional flow.

As the preceding discussion has suggested, we reason that the appearance of an isolated vortex filament emanating from a focus in the pattern of skin-friction lines evidences the last resort of a dividing surface that under easier circumstances would have extended downstream to form the site of a primary (or secondary) separation. This reasoning leads us to suppose that the flow structure depicted in Fig. 21, whether representative of a rectangular or delta wing, must have been preceded by a sequence of less complicated structures over intervals of angle of attack covering angles less than those in the range for which Fig. 21 is the appropriate structure. It should now be clear that by a less complicated structure we mean one with a smaller number of singular points in the pattern of skin-friction lines, and, in particular, one with a smaller number of foci.

All of the simpler structures that are possible, involving only a primary separation downstream of the nose region, can be easily delineated; the resulting sequences of flow structures constitute predictions, in a certain sense, that are amenable to experimental verification, at least for the rectangular wing. For example, if it is postulated that separated flow should begin without the appearance of foci in the pattern of skin-friction lines, then the surface patterns shown in Fig. 22 are a possible sequence of patterns that would lead to that of Fig. 21. In the vicinity of the apex, note that the initial pattern (Fig. 22a) is the one proposed by Lighthill (Fig. 19a), except that there is a change in the local curvature of the skin-friction lines leaving the nodes. Note also that the streamline flow on the plane running through the wing centerline contains one node (a focus) and four half saddles and so satisfies topological rule No. 3. Second in the postulated sequence should be a surface pattern containing a pair of foci. Of the two possible patterns, the first (Fig. 22b) is the one proposed by Legendre (Fig. 13a); the second (Fig. 22c) appears to combine features of Fig. 22a and 22b. The pattern with four foci (Fig. 22d) is a repetition of Fig. 21, and thus ends the sequence.

It is also possible to go forward from Fig. 21 and to postulate the flow structures over successive angle-of-attack ranges beyond the range in which Fig. 21 is the appropriate structure. We expect, for example, that over the next range a pair of secondary separations on the leeward surface should appear. This is accounted for, as Fig. 23 shows, by introducing another nodal point of attachment on either side of the one on the centerline. The adjacent nodal points must then be separated by the introduction of saddle points, and appropriate additions must also be made at the trailing edge to allow the skin-friction lines to disappear. The resulting topology has 12 nodes and 10 saddle points. Note also in Fig. 23 that the focus nearest the plane of symmetry, which terminates the nominally two-dimensional separated shear layer, is now also connected through a saddle point to the line of secondary separation. Thus, here, just as in the case of the primary separation, the vortex filament emerging from the focus is no longer isolated, but may act as the core of the horn-type dividing surface that extends the line of secondary separation into the flow.

An alternative pattern of skin-friction lines to that of Fig. 23 — one that contains a smaller number of singular points — can also be postulated. As shown in Fig. 24, the symmetry of the planform allows moving the additional nodes and saddle points over to the centerline and combining them there into a single additional node and saddle point. This again results in a pattern containing a secondary separation line, with now 11 nodes and 9 saddle points. Here, the vortex filament emerging from the focus nearest the plane of symmetry is again isolated and will eject into the flow normal to the surface.

The flow structures shown in Figs. 22 to 24 are physically plausible, particularly for the rectangular wing, in as much as the hypotheses postulated for flow separation were based on an experimental result for the rectangular wing. For the delta wing and other slender bodies, however, we note that a simpler hypothesis for primary, secondary, and tertiary separations has not been ruled out: namely, separations formed out of simple combinations of nodal points and saddle points of both separation and attachment may exist without the appearance of foci (see, e.g., Fig. 22a). Furthermore, it is possible that the idea of merging singular points, introduced earlier, will prove to be particularly useful here where there is physical evidence to suggest that the distance between a singular point and the apex may be allowed to approach zero.

Finally, one may draw the streamline patterns on crossflow planes that are consistent with the postulated patterns of skin-friction lines and, at the same time, are in accordance with topological rule No. 3. Figure 25 presents crossflow streamline patterns in a crossflow plane near the trailing edge. An unseparated flow is shown in Fig. 25a; flows with primary separations, consistent with Fig. 22, are shown in Fig. 25b and flows with secondary separations, consistent with Figs. 23 and 24, are shown in Fig. 25c. Figure 25d applies when the isolated vortices springing from foci on the surface (Figs. 21 and 22d) appear in the crossflow plane. Note that for nonslender bodies, the growth of the boundary layer may complicate the picture of velocity vectors close to the surface.

2.8.2 Symmetric Separated Flow About Slender Bodies

Since slender wings and bodies are topologically equivalent objects, it is reasonable to expect that everything said here about flow behavior over slender wings should find a counterpart in the behavior of flow over slender bodies. In contrast with the near-conical viscous flow field about the slender wing, the more general body flow exhibits substantial lengthwise effects, although the transverse (circumferential) pressure gradients still dominate. An example of such flow counterparts becomes evident by comparing one of the photographs of skin-friction line patterns reported by Hsieh (1977) (Fig. 26a) for flow over a hemisphere-cylinder at an angle of attack of 19° at Mach 1.4, with our deduction of the pattern shown in

Figs. 26b and 26c. The flow in the nose region would appear to be laminar. Here we find yet a simpler way of attaining a secondary separation (nine nodes, seven saddle points), combining a primary separation of the node-saddle-point type (Fig. 22a) and a secondary separation stemming from termination of the nominally two-dimensional separated shear layer (Fig. 23).

Again, as in Fig. 23, the vortex filament emerging from the focus nearest the plane of symmetry (see Hsieh and Wang 1976) acts as the core of the horn-type dividing surface that extends the line of secondary separation into the flow. (At Mach 1.0 and 1.2, in particular (Fig. 26a), an additional focus of corresponding rotation to that already described abbreviates yet another nominally 2D separation line near the intersection of the hemisphere with the cylinder.) Note also that we are postulating that the line of primary separation originates from a saddle point of attachment,[5] a singular point for which an illuminating theoretical treatment exists (Davey 1961). Also relevant here is a finite-difference computation of this hemisphere-cylinder flow, carried out by Pulliam and Steger (1978). If our interpretation of the experimental skin-friction line pattern is taken to be correct, it would appear that the computational results reproduce correctly the principal features of the primary and secondary separated flows as they are reflected in the skin-friction line patterns, except perhaps in the vicinity of the singular points on the leeward surface near the nose, the omissions there presumably being a consequence of locally insufficient grid resolution.

Patterns of skin-friction lines about blunted slender bodies at angle of attack in high Reynolds number turbulent flow provide little evidence of any foci of separation in the nose region. Rather, the experimental results imply simple node-saddle combinations to start both the primary and secondary separation lines. For example, an investigation of the subcritical flow about a 6:1 (major to minor axis ratio) ellipsoid at high Reynolds number was reported by Atraghji (1968b) and Peake, Rainbird, and Atraghji (1972), in which circumferential measurements of surface static pressure, surface impact pressure, and oil-dot flow visualization were made to identify the 3D viscous flow development. Figure 27 presents the skin-friction line pattern on the ellipsoid at Mach 0.74, and at a Reynolds number of 44×10^6, based on the 1.37 m (54-in.) length of the body. The boundary layers were turbulent. The skin-friction lines were deduced from oil-dot flow visualization records at angles of attack from 10° to 25°; for purposes of clarity, only a few of them are shown. As the angle of attack is increased, the circumferential adverse pressure gradient just past the flank ($\phi = 90°$, see Fig. 28) becomes more severe, causing a progressive thickening of the flow on the leeward side of the body; until at $\alpha = 25°$, there are two regions of converging skin-friction lines where we interpret that 3D separations are present. (This is not a very slender ellipsoid, but a corresponding situation would exist, of course, on a more slender ellipsoid at a reduced angle of attack). A similar postulate of the skin-friction line development on a blunt body of revolution was given in Thwaites (1960).

Figure 28 shows the calculated and the experimental isobar patterns (as well as some circumferential pressure distributions) on a distorted surface development at $\alpha = 25°$. Favorable circumferential pressure gradients are indicated by large open arrows and unfavorable gradients by shaded arrows. At this angle of attack, the circumferential pressure gradients completely swamp the axial gradients. From the calculated inviscid pressure distribution, we expect separation to occur somewhere to the leeward of the minimum pressure line; the experimental pressure distribution reflects this. The separation lines, where the convergence of the oil streaks is most noticeable, are shown here as chain-dotted lines, but both of these lines must stem from saddle points in the nose region. (As shown in Fig. 27, the skin-friction lines can all be traced back to emanate from the attachment region on the nose, but the resolution provided by the oil streaks does not allow us to determine the conjectured system of nodal attachment and saddle points[6] that inevitably exists.)

Figure 28 also shows the substantial suction peaks in the circumferential pressure distributions that have developed at $\alpha = 25°$, as a result of the windward boundary layer rolling up from the primary separation line S_1. The boundary layer growing from the leeward attachment line detaches from the surface along S_2. A cross section of this symmetric viscous flow development is sketched at the bottom of Fig. 27. It is of interest that the laminar flow about a similar ellipsoid at high angle of attack investigated by Werlé (1958) (top of Fig. 27) bears close similarity to the high Reynolds number turbulent flow. Han and Patel (1977, 1979) also provide surface flow visualization details of 3D separation on other spheroids in a water tunnel. Note that the view of the latter authors – that a separation line originates at the upstream stagnation point on the nose – may be reconciled with ours if on a close inspection the stagnation point is found to consist of a saddle point sandwiched between two closely spaced attachment nodes.

The details of the viscous flow development about the lee side of a body of revolution at angle of attack are similarly found on the underside of upswept afterbodies. Figure 29 displays the pattern of skin-friction lines on a 20° upswept rear fuselage at Mach 0.73 in high Reynolds number turbulent flow. The regions of primary and secondary separation are exactly analogous to the flows shown in Figs. 26 and 27. In turbulent flow, we require a very sharp change in surface curvature in the axial direction to provide adverse pressure gradients sufficiently steep to form a 2D separation line in the plane of symmetry. This separation line terminates in foci on a body as we explained in Figs. 26b and 26c, downstream of which there is a nodal point of attachment. A direct counterpart of such a flow formation is noted just downstream of the "knee" (Fig. 29) joining the fuselage forebody to the afterbody, with strong evidence of the nodal point of attachment depicted by the directions of the oil streaks.

2.8.3 Asymmetric Separated Flow About Slender Bodies

At even higher angles of attack than those already discussed, asymmetric vortex formations may occur in the leeward wake. The structure of the asymmetric flow over slender bodies is a topic of great current interest; despite intensive investigations, however, it remains imperfectly understood. Concepts involving, for example, "tearing of vortex sheets" (in our terminology, dividing surfaces) have been proposed to explain the appearance of new vortices in crossflow planes. These concepts, which entail something like the merging of streamlines, are once again tantamount to supposing very complicated singular behavior. We shall try to show that, on the contrary, hypotheses invoking the simplest possible singular behavior, when coupled with

---

[5]The two nodes and one saddle point of attachment have conceivably merged, as postulated in Sec. 2.6.

[6]Merged saddle points and attachment nodes.

some ideas borrowed from the "impulsive-flow analogy" (Allen and Perkins 1951a,b) yield flow structures consistent with the physical facts so far as they have been observed (see also Tobak and Peake 1979).

Consider a slender body moving in still air at constant velocity u in its axial direction and sinking with constant velocity v in a normal direction. Relative to the body, the mean flow is steady but, in the spirit of the impulsive-flow analogy, we choose to observe the flow in a space-fixed vertical plane $x = x_0$ as the body passes through it. Suppose that, at some instant, the flow in the plane around the cylindrical instantaneous cross section exhibits a primary separation that at that instant has shown the first sign of becoming asymmetric. Now consider a two-dimensional cylinder having the same cross section as the instantaneous cross section of the body in the fixed plane and sinking at the same rate v. Suppose that at some instant it is possible to find a flow over the cylinder that closely resembles the instantaneous flow in the fixed plane; that is, a flow that has the same number and types of singular points (two foci, one saddle point, and four half-saddles) corresponding to a primary separation (Fig. 25b) and that is incipiently asymmetric.

Observing that the crossflow Reynolds numbers (based on a characteristic dimension of the instantaneous cross section) are identical and that the instantaneous flows are closely similar, one can invoke the impulsive-flow analogy and argue that the flow in the fixed plane at subsequent time intervals, as successive cross sections of the body penetrate it, likewise will remain closely similar to flow over the cylinder at the same instants, so long as the cross section of the body changes only slowly. Thus, flows over the cylinder at successive instants translate into steady flows over the body at equivalent successive axial cross sections. For our purposes, we need not invoke the full analogy, but only an aspect of it that is much less demanding — we ask only that the succession of flow structures (i.e., the succession of topologies) in the fixed plane be the same as that for the cylinder. Note that we need not ask for an exact equivalence of flows nor an exact equivalence of intervals, but only an equivalent sequence of structures. This obviously holds whenever the impulsive-flow analogy holds, and probably also under much wider circumstances. Given this equivalence, the structural details of the wake behind the cylinder as the details change with increasing time are all that is needed to show us how new vortices appear in successive crossflow planes of the body.

Figure 30 illustrates a typical succession, starting with a flow having a primary separation that has just become asymmetric. (A recent experiment by Nishioka and Sato (1978) has shown very clearly that the originally symmetric flow with a primary separation becomes asymmetric as a result of a local instability in the vicinity of the enclosing saddle point, i.e., the "stagnation point" in the wake of the symmetric separated flow.) In Fig. 30a, the reattaching streamline is moving toward the dividing surface that runs into the upper focus. As it approaches, it causes an intense shear layer to develop in the vicinity of the dividing surface. The shear layer becomes locally unstable and rolls up to form a new focus separated from the remainder of the old one by a new saddle point. The new structure is illustrated in Fig. 30b. The reattaching streamline now moves toward the lower dividing surface and causes the formation there of a locally unstable shear layer, out of which is created another focus of opposite sense and an associated saddle point (Fig. 30c). The process continues cyclically in this way, adding successive foci and saddle points on alternate sides of the wake. In each succeeding structure, of course, the topology satisfies rule No. 3. (Additional details of the mechanism of vortex shedding are presented in Tobak and Peake 1979 and in Peake, Owen and Johnson 1980.)

When translated into the flow on successive crossflow planes of the body, the flow patterns depicted in Fig. 30 suggest that the following characteristics should be seen by an observer moving with the body. Starting with the crossflow plane containing the small initial asymmetry, one should, of course, see at least the first of the patterns illustrated in Fig. 30 and, if more than the first, in the same sequence. Figure 31 displays confirmation of this premise in the vapor-screen pictures of Jorgensen (1977), where we observe the forms of the crossflow vortex structures at three stations along a typical missile body at an angle of attack of 40°. It is evident that the impulsive flow structures shown in Figs. 30a and 30b are reproduced in the steady flow along the missile body. On the surface, skin-friction lines of primary separation should be continuous, although not necessarily rectilinear; their trajectories may exhibit considerable circumferential displacement. There should be a continuous line of attachment between the lines of separation that may (depending on the number of changes in the topology of the flow on crossflow planes) direct itself alternatively toward one and then the other line of separation without ever merging with either. As we have stressed, nowhere is there a necessity to argue that either skin-friction lines or crossflow streamlines must merge or become discontinuous.

Finally, we mention briefly another application of the impulsive-flow analogy that may prove particularly useful in the problem of assessing how the structure of the flow over the body changes as the governing parameters are varied over their operating ranges. In a later section we call attention to this question again; it is of obvious importance in design and it is the principal question in the theory of bifurcation.

We consider the steady flow in a crossflow plane at a fixed axial station of the body and, holding all other flow parameters constant, we ask how the topology of the steady flow in the fixed crossflow plane changes as the angle of attack is increased incrementally. Over the angle-of-attack range where invoking the impulsive-flow analogy can be justified, the answer is at hand: it can be shown that the sequence of topologies in the fixed crossflow plane that occurs as the angle of attack increases is the same as the sequence shown previously (Figs. 30 and 31) that occurs on crossflow planes at successive axial stations with the body at fixed angle of attack. This is true even though the crossflow Reynolds number of the analogous problem for the impulsively started cylinder must increase correspondingly with each increase of the body's angle of attack.

It turns out that after the impulsive start at each crossflow Reynolds number, there is a particular time at which the transient flow over the two-dimensional cylinder is comparable with the steady flow in the fixed plane on the three-dimensional body. Moreover, the flow topology at this time is one of a sequence that follows the same order as that which occurs with the passage of time at a fixed crossflow Reynolds number. Striking affirmation of this assertion is available in the results of an experimental study reported by Fellows and Carter (1969). They present a remarkable series of vapor-screen photographs showing the steady flow in a fixed crossflow plane of a very slender delta wing over a range of increasing angles of attack. The results are shown in Fig. 32, accompanied by sketches of our interpretation of the principal features of

the flows. It should be evident that the sequence is quite similar in principal features to the sequence of structures illustrated in our Fig. 30.

2.8.4 Obstacle Mounted on a Wall

The intriguing photographic frontispiece in Thwaites (1960) (see Fig. 33) showing the laminar, low-speed flow in the plane of symmetry before an obstacle on a wall, has no doubt challenged many researchers to fathom its intricacies. J. C. R. Hunt et al. (1978) have been particularly successful in demonstrating the usefulness of topological notions in this connection. Some researchers have understood that the photograph evidences a steady flow, although experiments by Schwind (1962), Peake and Galway (1965), and Peake, Galway, and Rainbird (1965) have clearly shown that the flow is unsteady and cyclic. Tobak and Peake (1979) have postulated a sequence of cyclic vortex structures about the obstacle in low-speed flow, one of which corresponds to Fig. 33. The sequence bears close resemblance to the commencement of vortex shedding in the impulsive flow-field development about a two-dimensional cylinder. But even though the low-speed external flow field is cyclic, it is true that the skin-friction line pattern remains invariant with time.

Figure 34a, taken from Peake, Galway, and Rainbird (1965), shows clearly the lines of primary and secondary separation that encircle the front face of the obstacle, from which primary and secondary dividing surfaces spring to form the legs of primary and secondary "horseshoe" vortices. More than two separation lines may be viewed, depending on the Reynolds number and the scale of the boundary layer relative to the obstacle cross section.

Under high Reynolds number conditions with turbulent boundary layers existing, it is likely that the external flow may have a toooology different from that in laminar flow and that it may be steady. For example, the skin-friction line pattern obtained by East and Hoxey (1968, 1969) (Fig. 34b) about a large protuberance in incompressible turbulent flow shows only one separation line and hence only one horseshoe vortex. In supersonic flow, there is a bifurcated shock structure ahead of the obstacle where the foot of the detached bow shock wave contacts the viscous flow. Nevertheless, the details of the skin-friction line development found by Sedney and Kitchens (1975) for a Mach 2.5 stream about an obstacle (shown in the top photograph of Fig. 35) are almost identical with the incompressible turbulent flow shown in Fig. 34b. Again, there appears to be only one horseshoe vortex, which has been made apparent in the lower photograph of Fig. 35 by a vapor-screen technique. The flow is from left to right. There is a saddle point of separation S on the axis of symmetry about 2 diameters ahead of the cylindrical obstacle, from which the 3D primary separation line emerges to pass around and downstream of the cylinder. Upstream and downstream skin-friction lines converge toward the 3D separation line from which a viscous horseshoe vortex grows within the depth of the undisturbed boundary layer. (We see that even though the scale of the separation relative to the undisturbed boundary-layer thickness is many times less than for the slender wing or slender body flows, the consequences are still severe.)

A streamline in the outer boundary layer attaches to the nodal point A in the plane of symmetry just ahead of the cylinder junction with the wall, from which an attachment line emerges and proceeds along the leading edge, and divergent skin-friction lines pass around the cylinder and downstream of it. One skin-friction line passes from the attachment node to the saddle point of separation. Others fan out from the attachment point in the plane of symmetry to eventually proceed toward the 3D separation line. Superimposed on the skin-friction pattern, we observe the bow shock wave B, and the rear leg (or Mach stem, M) of the bow shock bifurcation. Foci of separation are detected behind the obstacle. An enlargement of the skin-friction lines aft of the cylinder may be as sketched in Fig. 36. The focus V (in Fig. 35) will center the roll-up of the adjacent dividing surface that proceeds downstream. The focus closest to the cylinder will erupt as a spiral filament into the flow.[7] Note the close analogy between this streamline pattern and that sketched in Fig. 22d as one of the sequence of blunt-nose flows.

2.9 Bifurcation Theory

We have tried to show in some chosen examples how an understanding of singular points and topological rules may facilitate the drawing of reasonable hypotheses regarding the structure of flows about components of the aircraft. In some cases, application of these notions even allows a measure of prediction of flow sequences that the components might experience as the relevant parameters (angle of attack, Reynolds number, Mach number, etc.) are varied over the flight envelope. The notions that have proved useful rest on an exceedingly simple theoretical base. If we ask now how the theoretical base might be extended, particularly in the quantitative direction, we are led immediately to the main question – as the parameters of the problem are varied, can one map out in advance the boundaries separating regimes within which the mean flow structure (i.e., topology) remains fixed? The question brings to mind similar questions that have given rise to the mathematical theory of bifurcations (see, in particular, Joseph 1976; Benjamin 1978). The importance of the question may be judged if it is recalled that the design of the "Concorde" wing had as its principal aim the maintenance of one type of flow over the entire flight envelope.

The principal success of bifurcation theory in fluid mechanics has been the delineation of a succession of distinct and stable flow regimes (most markedly for rotating flows, i.e., the Taylor problem) that can occur following the initial loss of stability of laminar flow. Judging from the complexity of the mathematical machinery needed to achieve this success, one hesitates to attack the question that has been posed purely within the framework of bifurcation theory. However, the outlines of a mixture of theoretical and computational approaches may be envisioned as a result of some of the work currently being carried out successfully in the numerical computation of viscous flows over simple wings and bodies. The essential ingredient is a computational method capable of accurate solutions of the time-dependent equations of fluid motion, even though all that is sought is a steady-state mean solution that results after a sufficiently long passage of time. The use of accurate time-dependent flow computations is essential to ensure that all of the resulting steady-state solutions are stable. (The search for stable solutions by means of formal mathematical techniques is what makes the application of bifurcation theory so difficult.) Given such a computational method, and combining it with an explicit recognition of the behavior of singular points and

[7]The investigation into the low-speed flow about surface excrescences by Gregory and Walker (1951) yielded a not dissimilar flow structure behind an excrescence.

their topological rules, in principle one could find steady-state solutions over the ranges of the relevant parameters and simply pick out points in the space of parameters where the topology of adjacent solutions changes.

It can be anticipated that the establishment of boundary curves in accordance with the procedure just suggested would yield considerably more than a useful design tool, important as that is. By the way they have been defined, the boundary curves are intimately linked to the stability boundaries of the flow: every change from one topology to the next in effect signals that the flow corresponding to the first topology has become unstable. Hence, the boundary curves may turn out to define, or at least be linked to, the onset of buffet, stall, vortex breakdown, and similar indications of dramatically altered flow structure.

3. MODELING

3.1 Preliminary Comment

We generally accept that the Navier-Stokes momentum equations are axiomatic (Stewartson 1964) and that together with the continuity and thermal energy equations, they model the motion of a viscous, compressible, laminar or turbulent, heat-conducting fluid without chemical reactions, at points in space and time away from strong shock waves. In view of the nonlinearity of the equations, we are involved with a large number of possible solutions (due to random initial conditions) that we can obtain via numerical analysis — but these are solutions only in terms of averaged quantities over time and space (i.e., averaging due to finite mesh sizes used for resolution). Numerical solutions of the time-dependent Navier-Stokes equations, for a mesh point distribution sufficiently fine to represent turbulent motion, do not appear attainable in the near or distant future. In order to compute the various three-dimensional turbulent-flow structures possessing a substantial range of length and time scales, computational techniques themselves must be accurately time-dependent. Current finite difference procedures employing numerical artifices, such as damping from "artificial viscosity" inputs, for instance, may be inadequate because they introduce errors that may diverge in the development of the instantaneous flow field. Rubesin (1975) indicates that to define the three-dimensional boundary-layer flow upon an aircraft, the smallest significant scale demands mesh spacing 10^{-5} of the boundary-layer thickness leading to the order of 10^{17} mesh points overall. He remarks that the corresponding allowable time step in any given marching procedure is 1 μsec of real time. These potential requirements for computer storage and speeds, in order to solve the time-dependent Navier-Stokes equations, are in excess of projected computing machinery.

To bring the requirements for computer storage and speed within present capacities, we must resort to modeling the turbulence structures in 3D viscous flows and free shear layers springing from 3D separation lines. Current research in the United States is directed toward developing numerical procedures, turbulence transport models, and computer programs for obtaining solutions to the Reynolds averaged Navier-Stokes equations, usually involving parabolized or "thin-layer" approximations in 3D flows. As seen in Fig. 37, such solutions are feasible at present with subgrid scale turbulence modeling; however, for the practical computation of large turbulent eddies on even the simplest of aerodynamic components, these solutions require a thousandfold increase in the computational speed of present machinery.

An entertaining critique of computer simulation and accuracy limitations of numerical methods with regard to turbulence modeling is given in comments by Roache and Bradshaw (1975) in response to the essay of D. R. Chapman, Mark, and Pirtle (1975). Current computing power has far outstripped the availability of experimental data that are required to verify numerical results. "There are too many computers chasing too few facts" (P. Bradshaw 1972; private communication) and no super-computer will supply the correct physics. We agree with Roache (1975) that "the utility of closed-form solutions showing functional relationships is greater than a morass of numbers from a numerical experiment for one set of parameters." Hence, for a physical insight into practical flows in three dimensions, we still try to blend an external inviscid flow solution with an appropriate boundary-layer procedure, supplemented by special submodels of flow-separation phenomena, as well as attempting to exploit the conceptual simplicity of the full time-dependent Reynolds averaged Navier-Stokes equations (which still require subgrid turbulence models).

The correct physics has to be found from very careful experiments; "careful" is emphasized because there is always the risk of interference with the flow from pneumatic or hot wire probes (especially near the surface) or difficulties in beam alignment and vibration with nonintrusive "optical probes." The potential of the laser anemometer to obtain mean and fluctuating velocities (Owen and Johnson 1978a,b) coupled with holography and Raman scattering techniques (with lasers) to provide appropriate density and temperature measurements appear promising for the eventual revelation of three-dimensional flow fields.

3.2 Analytic Modeling of Three-Dimensional Separations

In the classical aircraft example of Fig. 3d, the aim of design has been to eliminate separation ahead of the trailing edge (Fig. 38) usually because substantial increases in drag and flow unsteadiness are introduced with essentially 2D separations on wings of high aspect ratio. With the increases in speed, lift, and angles of attack and yaw, demanded in the operation of lifting wings and bodies of smaller aspect ratio, extensive regions of three-dimensional separated flow are shed from many parts of the airframe (Figs. 4, 6, and 17) and new and tractable flow models are required. On wings with sharply swept leading edges, 3D separation occurs at the salient edges, being virtually independent of the oncoming boundary-layer properties at the high Reynolds numbers of interest to us. In the limit of infinite Reynolds number — or, for practical purposes, at high enough Reynolds numbers — the coiled viscous shear layer may be modeled approximately by an inviscid-flow vortex sheet. In other words, we adopt a viewpoint similar to that underlying the use of the Kutta-Joukowsky condition for determining flow at the trailing edge in inviscid wing theory (Legendre 1972). We say that viscosity causes the separation; the location is determined by the edge geometry, after which the flow may be modeled as an inviscid flow. The local behavior of a vortex sheet as it leaves the vicinity of a salient edge is tangential to either the top or underside of the edge, depending on the sign of the shed vorticity and on whether the external mean flow is directed inboard or outboard (Mangler and Smith 1970; Clapworthy and Mangler 1974).

In the region of the vortex external to the core, the axial velocity does not change substantially, and we may describe it to a satisfactory degree of approximation by ignoring diffusion (i.e., viscous) effects there (see Hall 1961). Diffusion is only important in the inner part of the vortex core where there are substantial velocity gradients. For a three-dimensional core growing in space, the swirling fluid is drawn into the core, acquiring a high axial velocity as it escapes along the axis (Küchemann and J. Weber 1965). Reynolds number does not appear to have a significant effect on the development of the large-scale structure of the flow, whereas the core center diminishes as Reynolds number increases. Conditions under which breakdown of the vortex core occurs have been reported by Hummel and Srinivasan (1967) and excellent detail in the crossflow during breakdown by Hummel (1965).

3.2.1 Sharp, Swept Leading Edge in Incompressible Flow

In numerical calculations of incompressible flows about swept edges there seems to be a qualified but free choice available as to whether the vortex sheet should be represented as collections of isolated vortices, as line vortices, or as a continuous sheet. Particular mathematical or numerical difficulties in the stability of the roll-up process, like those encountered by Sacks and Tickner (1966) and Sacks, Lundberg, and Hanson (1967), have been overcome by D. W. Moore (1974) and by Mokry and Rainbird (1975). In the two-dimensional, time-dependent problem of the roll-up of an initially plane vortex sheet, the latter authors discretized the sheet into suitable finite length elements; Fink and Soh (1974) used a similar approach in their "stepwise vorticity rediscretization" method.

The coiled vortex sheet model of Legendre (1952a,b) solved numerically by Mangler and J. H. B. Smith (1959) and later refined by J. H. B. Smith (1968), has provided good qualitative prediction of pressure distributions on slender wings of small aspect ratio in conical incompressible flow, as shown in Fig. 18. The real boundary condition — that nowhere should there be a pressure difference across the vortex sheet — was satisfied at a large number of points, while simultaneously imposing the requirement that at these same points the velocities on the sheet should be consistent with it being a stream surface in a three-dimensional flow. Assuming the streamwise growth to be conical, Mangler and J. Weber (1966) devised a new asymptotic shape to the core, wherein the vortex spiral became rolled more tightly and the shape more nearly circular, as the vortex center was approached.

The successful nonlinear analysis of J. H. B. Smith (1968) with the Kutta condition imposed at the swept salient edges has been extended to elliptic cones with strakes by Levinsky and Wei (1968). Similar analyses of delta wings with thickness (J. H. B. Smith 1971), with conical camber (Barsby 1972), and with yaw (Pullin 1972) have been reported. Nonconical slender wings with lengthwise camber plus curved leading edges, and those incorporating straight, thin cross sections, were investigated by J. H. B. Smith (1972) and R. W. Clark (1976), respectively. These and other examples to which this useful theory has been applied are discussed by J. H. B. Smith (1975).

The above models are limited to slender configurations, so that the considerable effects of the trailing edge are omitted. This deficiency has been offset in the more recent panel-type, influence-coefficient method of J. A. Weber et al. (1975), by which both conical and nonconical incompressible flows can be treated. The wing, the rolled-up vortex sheets (although treatment of the core regions is probably inadequate), and the wake are represented by "piecewise" continuous quadratic doublet distributions, and the Kutta condition is now assigned along the trailing as well as the leading edges. In Fig. 39, some results of these calculations are compared with results of the laminar flow low-speed delta wing experiments of Marsden, Simpson, and Rainbird (1958). These results include relatively large effects of the base, as we see in the pressure distributions of Fig. 39. The fall-off in loading toward the trailing edge is predicted satisfactorily. Gothic and arrow wings have also been treated successfully at $M_\infty = 0$. Compressibility corrections (Brune and Rubbert 1977) extend the range of applicability of the method of J. A. Weber et al. (1975) to high subsonic Mach numbers. Secondary separations on the wing surface (Fig. 18) are not included, however. Secondary separations of the laminar boundary layer (Fig. 39) cause much flatter suction peaks than with a turbulent boundary layer (see Fig. 18b). The workshop at Langley Research Center in May 1976 on "Vortex-Lattice Utilization" (NASA SP-405) debated the details of the numerical modeling of vortices from swept edges in essentially incompressible flow. Körner and Hirschel (1977) reviewed recent panel methods that were reported at Euromech 75 to solve inviscid linear subsonic and supersonic flow problems, wherein the inclusion of the attached boundary layer was coupled with the panel method in some examples, usually via an effective displacement surface or by normal blowing. Parker (1976) has provided a review of slender-wing theory and the effects of aspect ratio, thickness, and leading-edge shape on the pressure distribution and development of overall forces.

3.2.2 Sharp, Swept Leading Edge in Compressible Flow

There are few available physical models of supersonic mainstream flow in which leading-edge separation is still occurring from the subsonic swept edge (i.e., the Mach number normal to the leading edge is subsonic). Within the confines of slender body theory, C. E. Brown and Michael (1954) allowed the vorticity shed at each leading edge to collapse into a single line vortex, whereas Küchemann (1955b) considered the shed vorticity to be in the plane of the wing. Extensions to supersonic conical flow of the Brown and Michael method have been made by Nenni and Tung (1971), and of the Küchemann method by Squire (1963) and by Carafoli (1969).

3.2.3 Bodies

On bodies, the separation location is unknown a priori. We must attempt to calculate its position by 3D boundary-layer theory, which requires an appropriate external flow, or map its position from experimental surface oil-flow visualization. In the former, an iteration between the boundary layer and inviscid flow is required, with a guessed separation-line position, followed by subsequent correction of the inviscid pressure distribution. Once the separation line is supplied, an inviscid vortex sheet model of the separated flow can be invoked (in incompressible flow at least) on which the following boundary conditions will be adequate to determine it completely (J. H. B. Smith 1978). The sheet must leave the surface tangentially along the separation line. It is an open vortex sheet (as we have discussed already in reference to the slender wing) in the sense that fluid at the same total pressure wets the vortex sheet on either side. Both pressure and

velocity are continuous across the sheet, which is a stream surface. The velocity on the upstream side of the sheet provides the convective component to remove the vorticity from the surface.

On the downstream side of the sheet, replacing the Kutta condition for separation at a sharp edge is the requirement that the velocity be directed downstream tangentially to the separation line. On the upstream side of the separation line, the surface streamlines of the inviscid model are inclined to the separation line but are, of course, still tangential to the wall. The vortex sheet model may be used on simple shapes, such as pointed right-circular and elliptic cones, for which the separation lines are along generators and the coordinate geometry presents few difficulties. Angelucci (1971, 1973) has modeled the incompressible separated flow on bodies of revolution and of general cross section using arrays of line vortices, in preference to a vortex sheet. Although he demonstrates satisfactory agreement with experiment, he imposes a stagnation restriction on the crossflow as a boundary condition at the separation line itself.

On more complex configurations the solution eludes us, for boundary-layer calculations have not usually been successful in providing separation-line positions, particularly when separation starts some distance back from the nose. Moreover, we still do not have a suitable flow model for the breakaway dividing surface, under conditions where neither conical nor slender body flows exist, although the J. H. B. Smith (1978) model presumably should still be useful. The position of a 3D separation line may be interpreted in laminar and turbulent boundary-layer calculations as being where the local skin-friction lines become asymptotes to or simply converge toward the one skin-friction line identifiable as the separation line. The bending of the skin-friction lines increases considerably just prior to separation, and boundary-layer calculation methods break down where this occurs. Of course, the concepts of thin boundary-layer theory, although applicable upstream of and away from the 3D separation line, are inadequate at the separation line. Separation lines in laminar flow were constructed graphically by Peake and Galway (1965) and by Peake, Galway, and Rainbird (1965), and by numerical integration of the vector field of the wall shearing stresses by Shen (1967) and Shen and Jones (1967) in respective computations of flows about cylindrical and slender protuberances. Geissler (1975) supposed that when numerical instabilities developed in his laminar boundary-layer implicit finite difference method about an ellipsoid, a 3D separation line position could be inferred, although the inviscid pressure distribution was for attached flow.

In laminar, incompressible flow about simple bodies at angle of attack, where the effects of axial pressure gradients are negligible in comparison with the circumferential ones, we can demonstrate qualified agreement of calculated 3D separation lines with those of experiment. For instance, using small crossflow assumptions and streamline coordinates, Crabbe (1963, 1965) computed the separation line azimuthal angles on right-circular and elliptic cones to be just leading or just lagging the results from water-tunnel measurements (Rainbird, Crabbe, and Jurewicz 1963; Crabbe 1965). Such discrepancies as existed between theory and experiment were tentatively attributed to inaccuracies in the assumed pressure field, the modifications of the undisturbed pressures being attributed to interaction of the separated flow with the external flow. A corresponding analysis reported by Cooke (1965) showed the separation lines to be always ahead of the water-tunnel results of Rainbird, Crabbe, and Jurewicz (1963); the same physical result was found by Tsen and Arnaudon (1972) in their treatment of the compressible laminar boundary layer about cones at angle of attack in supersonic flow. Tsen and Arnaudon were able to show that although heat transfer did not change the location of separation significantly, a result in accord with the work of Cooke (1966) and Lin and Rubin (1973), heat transfer did affect the peak crossflow velocities.

Where axial as well as circumferential pressure gradients influence the separated flow development on other simple body shapes at angle of attack, such as prolate spheroids, Wang (1972, 1974a,b, 1975) and Geissler (1975) have reported numerical procedures to elucidate separation-line positions in laminar, incompressible flows. No comparisons with experiment were shown, however, to illustrate the accuracy of the calculations.

In turbulent, but still low-speed boundary layers, the prediction of separation has been attempted on infinite sheared wings – see the list in J. H. B. Smith (1975). Unfortunately, infinite sheared-wing flows are virtually impossible to reproduce in an experiment, for the viscous flows on the end-plate equivalent to the wing root will always contaminate the test boundary layer on the wing surface when at angle of attack. Notwithstanding these problems, Cumpsty and Head (1970) and Elsenaar, van den Berg, and Lindhout (1975) have provided substantial mean flow and, in the latter, normal as well as turbulent shear stress measurements, in flows approaching the 3D separation line. Virtually no other predictions of turbulent separation line position have been reported, except for the calculation by P. D. Smith (1973) of the secondary separation line on the top surface of a delta wing, the position of which agreed very closely with the experimentally obtained position of East (1974). It is of practical significance that Barsby (1973) calculated the vortex sheet springing tangentially from such a secondary separation line.

3.3 Numerical Modeling Based on Navier-Stokes Equations

So far we have seen that in devising tractable flow models, we have usually reduced the real flow to essentially a two-dimensional one (albeit in a crossflow plane) – although the solutions discussed above have some elements of three-dimensional flows – and then have proceeded with established analyses to provide numerical answers. Admitting the inherent difficulties in modeling 3D separated flows with physical realism, some recent research effort has been directed to solving the steady Navier-Stokes equations while accepting the cost of longer computation times.

3.3.1 Slender Cones

McRae (1976, 1977) has attempted to solve the laminar viscous flow field about a pointed, right-circular cone at high angle of attack, utilizing a simplified set of the Navier-Stokes equations (incorporating the conically symmetric flow approximation) along with MacCormack's (1969) finite difference time-dependent scheme. Based on a coordinate system, (r, θ, ϕ), fixed to the body with origin at the apex (see Fig. 40), a finite difference mesh was set up on the (θ, ϕ) spherical surface at a distance r from the cone apex. The calculation took place on this surface with viscous terms in the equations of motion scaled by the Reynolds number based on the spherical radius, r. The finite difference mesh was initialized with free-stream values of the flow everywhere, except at the surface, where zero velocities were input. The numerical

integration then proceeded in time, to the limit that produced a steady-state solution. The outer boundary condition for the integration was the free stream, so that the bow shock wave was captured and allowed for in the use of the conservation form of the governing equations.

Figure 41 illustrates the surface pressures and a crossflow (conical flow projection) velocity vector plot of a computed flow field about a 10° half-angle cone in a nominally Mach 8 free stream at $\alpha/\theta_c = 2.4$. The results are compared with the experimental data of Tracy (1963) with entirely laminar boundary-layer conditions, where a 3D separation was measured (using surface-flow visualization) at $\phi \doteq 150°$. The presence of a three-dimensional separation and rolled-up viscous shear layer is seen in McRae's (1976, 1977) calculated flow field. The utilization of a scalar eddy viscosity in this code (McRae and Hussaini 1978) has yielded results in good agreement with Rainbird's (1968a,b) high Reynolds number data on and above the cone surface (see Sec. 4.1).

Another approach toward calculating the entire supersonic flow field about a spherically blunted circular cone at angle of attack with 3D laminar separation (Figs. 42 and 43) has been reported by Lubard and Rakich (1975)[8] following the method of Lubard (1975) for a sharp cone (Fig. 44). The calculations are based on a single-layer system of three-dimensional parabolic equations that are approximations to the full, steady Navier-Stokes equations, valid from the body surface to the bow shock wave. This system, which includes the circumferential shear stress terms, is capable of predicting the flow within the separation zone on the lee side. The effects of viscous-inviscid interaction and entropy gradients due to both the curved bow shock and angle of attack are automatically included. Initial conditions of unseparated flow are assumed at the sphere-cone tangency plane[9] and are provided by using an inviscid time-dependent solution to which is added a viscous nonsimilar boundary-layer solution. The calculated results were compared with the experimental data of Cleary (1969) for a 15° angle of attack at Mach 10.6 and at a Reynolds number (based on the 23-in. slant length of the cone) of about 2.3×10^6. Figure 43 shows the calculated crossflow plane vector velocity distribution in the region close to the leeward generator at 14.8 nose radii downstream from the nose. The three-dimensional separation occurs at 155° to 160° in the crossflow plane at this axial station. The remaining graphs in Fig. 43 show that the experimental heating and pressure distributions on the leeward surface are in quite reasonable agreement with the calculation.

The sharp cone calculation of Lubard (1975) is for a Mach 16 laminar flow (Fig. 44). The forms of the S-shaped crossflow velocity profiles between the primary separation line ($\phi \sim 160°$) and the leeward meridian are analogous with the blunt cone calculation at Mach 10.6. Lubard (1975) also provided values of overall forces and moments which showed good agreement with the measurements of Pate (1974).

3.3.2 Slender Wings

The respective numerical methods of McRae (1976) and Rakich and Lubard (1975) have been used as bases for two new codes developed by Vigneron, Rakich, and Tannehill (1978) to compute the supersonic laminar flow field about a slender delta wing (with subsonic leading edges). In the first of these new codes, the flow is assumed conical and, as in McRae's code, the resulting Navier-Stokes equations are solved at a given Reynolds number with a time-marching explicit finite-difference algorithm. This approach has also been applied by Bluford (1972, 1979) to compute the flow about delta wings with supersonic leading edges. Rather than "capturing" the bow shock as did McRae (1976) and Bluford (1978, 1979), Vigneron, Rakich, and Tannehill (1978) claim fewer restrictions on body cross-sectional shape and distribution of finite-difference grid points if the shock wave is treated as a sharp discontinuity (see the comments of Kutler (1974b) on the merits of the individual shock-wave treatments). In the second code, by neglecting only the streamwise viscous derivatives, the parabolic mathematical form of the steady Navier-Stokes equations (with respect to the streamwise direction) is utilized. Whereas in the approach of Rakich and Lubard (1975), an implicit, iterative, finite-difference scheme was adopted, Vigneron, Rakich, and Tannehill (1978) present a new implicit, noniterative algorithm that improves computational efficiency and is not restricted to conical shapes. Results from both numerical techniques show close agreement with each other and with experiment. As an example, Fig. 45 displays the two calculated sets of comparative pressure contours and directions of velocity vectors in the crossflow plane about a 75° swept-back delta wing at an angle of attack of 10° in a Mach 1.95 flow; the proximity of the numerically and experimentally determined centers of the primary vortices (see the experiment of Monnerie and Werlé 1968) is very close.

3.3.3 Bodies of More General Shape

The numerical calculation of flows about blunted bodies other than cones has suffered from difficulties associated with the generation of appropriate grid meshes in the flow field. To help remedy this problem, Pulliam and Steger (1978) devised an automatic generation of highly warped spherical grids, using general coordinate transformations, that proceeds in the computation simultaneously with the flow field solver. The latter is an implicit finite-difference procedure suitable for computing unsteady 3D separated flows. The implicit approximate factorization technique that is employed permits small grid sizes for spatial accuracy and resolution of flow detail near the boundary, without imposing stringent limitations on stability.

The basic flow-field equations that are used are the compressible, time-dependent Navier-Stokes equations. In high Reynolds number flows, the viscous terms associated with the derivative in the direction normal to the wall are significantly larger than those along the body. Neglecting the latter in comparison with the former, sometimes called the "thin-layer" approximation, was one of the approximations in the development of boundary-layer theory; it is used in the steady, marching computation technique of Rakich and Lubard (1975) that has already been described. In the present formulation, the "thin-layer" approximation is used as well as retaining all of the unsteady and nonlinear inviscid flow terms in the equations of motion. In so doing, the solution can progress naturally from an arbitrary initial condition to an asymptotic steady state, permitting a flow field with viscous-inviscid interaction to develop as time progresses. (The conical-flow code of McRae (1976) utilizes the same logic). The method was applied to elucidate the details of the

---

[8]See also Rakich and Lubard (1975).

[9]Which may be unrealistic at high angles of attack.

laminar separated flow field about a hemisphere cylinder at an angle of attack of 19° in transonic flow (M_∞ = 1.2) with flow symmetry imposed about the windward and leeward meridian planes. Along most of the body, circumferential pressure gradients dominate, except in the region of the hemisphere-cylinder junction, where axial gradients are also strong.

Figure 46 presents some representative results of the calculation compared with one of the experimental results of Hsieh (1977). Overall features of the flow, such as surface pressures, 3D primary and secondary separation-line positions along the cylinder, and a 2D separation in the leeward plane of symmetry on the top of the nose region are predicted well. Neither the topology of the experimental skin-friction lines, nor the start of the individual separations, is captured satisfactorily, however. Figure 26 shows our conjectured view of the skin-friction line pattern on this hemisphere-cylinder example at M_∞ = 1.4 after examining the experimental oil-flow pattern. We believe that the primary separation line begins at a saddle point of attachment on the windward meridian and that the secondary separation line begins at a saddle point adjacent to a terminating focus of the nominally 2D separation line on the top of the nose. The rotation of the vortex filament erupting from the focus matches the rotation of the dividing surface from the secondary separation line and hence becomes affiliated with the secondary roll-up according to the model of Legendre (1965) (see Fig. 13). Note that as in the ellipsoid flow shown in Figs. 27 and 28, roll-up of the dividing surfaces from the primary and secondary separation lines (see the crossflow velocity vectors in Fig. 46) is detected only when the circumferential pressure gradients become sufficiently adverse. The separation lines must, however, begin at saddle points usually near the nose of the body.

A common flight vehicle configuration in which both axial and circumferential pressure gradients are very strong is the cylinder-flare at angle of attack in supersonic flow. The shock wave generated by the deflected surface of the flare interacts with the approaching attached boundary layer on the cylinder to form a massive zone of 3D separation around the entire periphery. The very evident feature of this flow, noted by Ericsson, Reding, and Guenther (1969, 1971), is the pair of large foci generated ahead of the cylinder-flare junction on the lee side, as shown in Fig. 47. This complex 3D flow separation stems from the cellular-focus flow development evident at zero angle of attack, which is clearly not 2D. A china-clay pattern at an angle of attack of 0° at Mach 1.2 is shown on the left-hand side of Fig. 47; on the right-hand side is a case at an angle of attack of 4° at Mach 1.2. A model of the flow at angle of attack, deduced by Ericsson, Reding, and Guenther (1969), is sketched on the bottom of Fig. 47.

Hung (1979) computed the flow about another cylinder-flare body at the same 4° angle of attack, but immersed in a Mach 2.8 stream, to compare with the experimental measurements of Robinson (1974). The computation used the "thin-layer" form of the Navier-Stokes equations and a system of transformed cylindrical coordinates. Since the deflection angle of the flare is 15°, the axial pressure distributions along generators from the windward to the leeward ray indicate a large, rapid increase in local static pressure on the wall in the shock-boundary-layer interaction region. Figure 48a shows the very good agreement between the pressures calculated by Hung (1979) and the ones determined experimentally by Robinson (1974). Note also the substantial effects of 3D separation when these results and the normal force distribution (Fig. 48b) are compared with the inviscid attached flow theory of Syvertson and Dennis (1957). Unfortunately, the presentation of the calculated limiting streamline velocity vectors in Fig. 48c and the oil-flow patterns in Fig. 47 lack resolution necessary to determine the intricacies of the separation lines and the associated singular points. With the results of the experiment and calculation in hand, we may again appeal to topological notions to synthesize both the skin-friction line pattern and the structure of the external flow; these are shown in Figs. 48d to 48h.

On the windward ray, there will be saddle points S_1 and S_2, associated with primary and secondary separations very close to the cylinder-flare junctions (Figs. 48f and 48g). The primary separation line from the windward ends in the large focus, F_1, on the cylinder that also terminates a horseshoe-shaped separation line starting from the saddle point S_3, situated just off the leeward meridian (Figs. 48e and 48f). Note that S_3 joins to a nodal point of separation N_S on the leeward ray. The secondary separation line from S_2 terminates in a smaller focus F_2 situated on the flare. The vortical filament from the larger focus is shed into the flow as shown on the model of Ericsson, Reding, and Guenther (1969) (Fig. 47). The filament from the smaller focus centers the adjacent rolled-up dividing surface that extends downstream from the saddle point S_4 on the flare. A cross section of all the rolled-up dividing surfaces is shown in Fig. 48h. The intriguing feature is that there is a vertical dividing surface, beginning on the leeward meridian at the nodal point of separation N_S, that continues all the way downstream to the end of the body. The streamlines in this dividing surface all emanate from a half-node of separation (see also Fig. 16) at the location of the saddle point S_5 in the pattern of skin-friction lines (Fig. 48f). Joined to this vertical dividing surface are the rolled-up dividing surfaces from the foci F_1. Finally, in Fig. 48d our proposed pattern of skin-friction lines is superimposed over the limiting streamline vector plot of Hung (1979), taking account of all the detail changes in local vector directions that his results display. This illustration is a clear demonstration of the usefulness of topological ideas in exposing the important details in the flow that have been given with insufficient resolution from experiment and from calculation.

3.3.4 Supersonic Flow Along Corners of Intersecting Wedges

Solutions of the complete Navier-Stokes equations for supersonic laminar flows in corners have been reported in respective papers by Hung and MacCormack (1977) and by Shang and Hankey (1977). The former authors looked at the supersonic laminar flow over a compression corner abutted to a sidewall in a free stream with a Mach number of 3. Shang and Hankey investigated a similar configuration at Mach 12.5, but without the flat plate ahead of the compression ramp. They found substantial agreement between their calculations of surface pressure, pitot pressure, and surface shear stress directions and the results of the experiment of Cooper and Hankey (1973). In particular, the rolled-up shear layer from the inboard of two 3D separation lines was especially clarified in both calculation and experiment. A high-energy or inviscid "finger" of flow was responsible for the high rate of heat transfer along the strongly divergent attachment line region between the two separation lines. Unfortunately, no experimental results are available for comparison with the more complex flow field addressed by Hung and MacCormack (1977). In the latter flow field a new algorithm developed by MacCormack (1976, 1977) has decreased the computation time to less than 1 hr; that is, a claimed decrease from that of an earlier code (MacCormack and Baldwin 1975) by an order of magnitude. Horstmann and Hung (1979) introduced a scalar eddy viscosity model into the code of Hung and

MacCormack (1977) and found good agreement with the swept shock turbulent boundary-layer experiments of Peake (1975) and Oskam, Vas, and Bogdonoff (1975). The details of these flows will be discussed more fully in Sec. 4.5.1.

3.3.5 Closing Comment

We have discussed (1) some intriguing and impressive results obtained from computations of the laminar flow fields about simple 3D aerodynamic components using approximate forms of the Navier-Stokes equations, and (2) the potential for obtaining satisfactory answers in turbulent flow once appropriate turbulence models can be found. Unfortunately, even these simple shapes must be surrounded with relatively coarse computational meshes; otherwise the available computer storage would be saturated, thus leading to a lack of resolution in the flow-field structure. Based on our study of the numerical calculations of Pulliam and Steger (1978) (hemisphere-cylinder at angle of attack) and of Hung (1979) (cylinder-flare at angle of attack), we arrive at an impasse. On the one hand, the singular points in the flow and on the body surface have simple, fundamental forms and their types, number, and placement practically characterize a real separated flow. On the other hand, it is just in the vicinity of those singular points that a finite difference scheme requires inordinately fine mesh spacing to capture their behavior. Even supposing that sufficient computer storage were available for the mesh to be tightened, computation costs would be increased, perhaps to an unacceptable degree.

As a way out, we suggest that it might be possible to make a useful advance in the computation of 3D separated flows if finite difference methods could be combined with a separate treatment (perhaps involving analytic or finite-element methods) of the singular points, thereby obtaining both an adequate resolution in the vicinity of the singular points and the avoidance of very fine meshes.

4. THREE-DIMENSIONAL SEPARATED FLOWS ABOUT SIMPLE COMPONENTS AND PRACTICAL FLIGHT VEHICLES

4.1 Pointed Cones

One promising approach to the design of hypersonic cruise aircraft is to consider lifting bodies whose shapes can be derived from parts of known flow fields (Küchemann 1965). In particular, conical flow fields have been studied in some detail, and J. G. Jones (1963) has given a method for deriving lifting surfaces from the flow field of a circular cone at zero angle of attack. Since boundary-layer interaction effects are especially important at hypersonic speeds, it is necessary to consider lifting surfaces with either constant or slightly falling pressure along the streamlines defining the surface and to avoid strong transverse pressure gradients which might lead to three-dimensional separation and high heat transfer along reattachment lines.[10] Neither the Jones lifting surfaces nor those derived from reversed Prandtl-Meyer flow (Townend 1963) satisfy this requirement. However, lifting surfaces derived from the flow field of cones at low angles of attack could be chosen to avoid serious viscous effects; Seddon and Spence (1968) discuss engine airframe integration by such methods. Hence, it is important to understand the practical limits (e.g., angle of attack) under which conical flow fields can be used without detriment in aerodynamic design.

In contrast with supersonic and hypersonic vehicles optimized for cruising at low angles of attack, the Space Shuttle concept designed for flight during reentry at very high angles of attack, and the requirement for antiballistic missiles and defensive weapons to perform rapid turning maneuvers, have posed difficult problems with uncontrolled 3D separated flows from the lee sides of bodies. Such coiled-up viscous vortical flows can adversely affect vehicle performance from the points of view of stability and heat transfer to the vehicle skin. The location and roll-up of the 3D separated flows from vehicle forebodies can influence the flight dynamics from asymmetries and their interaction with downstream control surfaces. The passage of these vortices into regions over the airframe where severe adverse pressure gradients exist may cause vortex breakdown and lateral stability problems. It has been found that heat transfer rates, especially on the leeward surfaces, may reach levels comparable with, or greater than, those along the windward generator. But first of all, let us review the fundamentals of conical flow.

A steady conical flow is one in which rays can be constructed from a point vertex such that the velocity is invariant in magnitude and direction along each ray, although it will change from ray to ray for a body at angle of attack (or yaw). The external flow past a finite conical body must be everywhere supersonic if the viscous and inviscid flow is to be virtually conical. In practice, however, it is found that the subsonic flow past a slender conical body is more-or-less conical downstream of the apex, extending to the zone where the effects of the base first intrude. It is clear that our present comprehension of the structure of coiled shear layers in both incompressible and compressible flows has stemmed largely from investigating these phenomena in nominally conical flow fields.

The terminology "conical flow streamlines" has sometimes caused confusion, for they are the intersections with a sphere (centered on the vertex) of stream surfaces that pass through the vertex (see Fig. 40). For convenience of illustration in two dimensions, the projection of these intersecting curves from the sphere onto a planar surface perpendicular to the cone axis is usually constructed to demonstrate the conical flow (including conical vortices) about a given body. Because we are dealing with the planar projections of stream surfaces and not the stream surfaces themselves, the axiom of continuity does not prevent conical streamlines from running together at singular points. (Note that in Sec. 2.7, topology rules nos. 5 and 3 distinguish respectively between the number of singular-points in a conical flow projection and in a crossflow plane.)

Within the confines of slender-body theory (R. T. Jones 1946 and Frankel 1955), J. H. B. Smith (1969) provides an elegant thesis on the structure of conical flow. Figures 49a to 49h portray some examples of inviscid conical streamlines about circular and elliptic cones at angle of attack. Here the "conical velocity," q, resolved from the magnitudes of v and w on the spherical surface of Fig. 40, is always subsonic. Moreover, if α is the angle of attack and θ_c the semi-angle of the vertex, the parameter

[10] Note that the desirability for separations to work favorably (i.e., when they are controlled) is not being contradicted. On configurations with no means of fixing, however, separation and reattachment zones will vary with angle of attack, Reynolds number, and Mach number, and may eventually become unsteady and asymmetrical on slender configurations at very high angles of attack.

$\bar{\alpha} = \alpha/\theta_c$ essentially controls the pressure gradient (there is no axial pressure gradient) and hence, the flow development at a given free-stream Mach number. Thus, θ_c may be removed as a governing parameter.

Figures 49a and 49b define the respective subsonic conical streamline patterns in a uniform stream and about a cone at zero angle of attack. When $0 < \bar{\alpha} < 0.5$, there is a half-saddle point on the windward generator and a half-nodal point on the top generator, shown in Fig. 49c. Since the body surface must be a surface of constant entropy wetted by streamlines that cross the nose shock wave in the windward plane of symmetry ($\phi = 0$), there must be a region of high vorticity near the cone surface, "the vortical layer" (Ferri 1950). All of the streamlines that cross the nose shock wave terminate at the nodal point at ($\phi = 180°$, $\vartheta = \theta_c$) where the entropy is multi-valued — the so-called "vortical singularity." At this position, the circumferential and radial components of velocity are identically zero. At $\bar{\alpha} = 0.5$, the singular point on the top of the circular cone is as shown in Fig. 49d. For $0.5 < \bar{\alpha} < 1$, the orientation of the nodal singular point turns through 90°. At $\bar{\alpha} > 1$, the half-node moves off the cone surface, becoming a full node along the leeward plane of symmetry, another half-saddle point remaining on the surface, as shown in Fig. 49e. In other words, the direction of the radial velocity changes from inward to outward at lift-off.

The form of the subsonic conical streamlines for an elliptic cone at zero angle of attack, but still in inviscid flow, is illustrated in Fig. 49f. At small angle of attack, the half-saddle points at the ends of the major axis move around to the windward side (Fig. 49g). At higher angles of attack, these two half-saddle points move closer to the windward plane of symmetry until they eventually coalesce; at the same time half-nodal singular points of the same kind as those seen on the circular cone (Fig. 49h) may appear on the leeward meridian. Note that in all of these proposed flow structures, topology rule No. 5 is obeyed.

We have paid particular attention to the form and meaning of the inviscid flow conical streamlines and the vortical singularity. We shall see, however, that although the effects of viscosity remain more or less confined within the bounds of conical flow they, and the eventual formation of transonic zones and shock waves at sufficiently high angles of attack or free-stream Mach number, apparently deter the appearance of the vortical singularity to much higher relative incidences than inviscid flow calculations would suggest.

Measurements by Nebbeling and Bannink (1976) of the conical streamlines about a 7.5° semi-apex angle cone in a Mach 2.94 free stream with turbulent boundary layers are shown in Figs. 50 to 52. Figure 50 shows the conical streamlines at a moderate relative incidence of $\bar{\alpha} = 1.65$. In the still subsonic conical flow (note that there are no shock waves in Fig. 50b), the conical streamlines external to the small region of separated viscous flow near the leeward generator continue to resemble the postulated inviscid flow in Fig. 49c even though the relative incidence was much lower in the latter calculation. The directions indicated by the arrows are the resultant velocity vectors (but not magnitudes) associated with the elevational (v) and circumferential (w) velocity components of the spherical coordinate system centered at the cone apex (shown in Fig. 40). When $\bar{\alpha}$ is increased to 2.31, Fig. 51 indicates that the component of Mach number normal to isobaric surfaces exceeds unity. Transonic crossflow and shock waves adjacent to the cone body now appear with a substantial region of viscous vortical flow from $\phi = 125°$ to the leeward meridian (see Figs. 51b to 51d). Nevertheless, the direction of the conical streamlines is still toward the leeward generator, and has not changed qualitatively from the $\bar{\alpha} = 1.65$ configuration shown in Fig. 50.

Increasing the relative incidence even more — to an $\bar{\alpha}$ of 3 — alters the conical flow streamline pattern substantially, as shown in Fig. 52. The nodal singular point (or vortical singularity) position above the leeward generator is near $Z/R = 3$ in the measured flow field of Fig. 52a, while a saddle singular point has also appeared at $Z/R = 1.9$. Note that the sum total of the measured singular points again satisfies topology law No. 5 for conical flow. This very high angle of attack flow field was discussed by Feldhuhn, Winklemann, and Pasiuk (1971). Debate on the "lift-off" of the inviscid vortical singularity has been offered by Holt (1954), Munson (1965), Melnik (1967), Barker and Bannink (1974), and by Fletcher (1975).[11] Clearly, the large-scale 3D separated flow on the leeward side of the cone that is shown in Fig. 52 differs from the inviscid flow pattern of subsonic slender-body conical streamlines proposed in Fig. 49e, and from the inviscid crossflow with internal shock waves in Fig. 53. Notwithstanding these shortcomings, our inviscid flow concepts are useful up to values of $\bar{\alpha} \sim 1$, beyond which viscous effects become increasingly important.

4.1.1 Methods of Calculating the Supersonic Conical, Inviscid, and Viscous Flow

Inviscid Flow — Considerable progress has been made using numerical methods to solve the nonasixymmetric inviscid supersonic flow about circular and elliptic cones — Stocker and Mauger (1962), Moretti (1965), Babenko et al. (1966), D. J. Jones (1968, 1969, 1970a,b, 1972), Klunker, South, and Davis (1971), and Camarero (1975). Provided the flow fields are "conically subsonic,"[12] it has been possible to find numerical solutions up to angles of attack where the vortical singularity lifts off the surface (i.e., to $\bar{\alpha}$ values of the order of 1.3 for circular cones). More recent computations have dealt with mixed flow field conditions that properly allow for "conically supersonic" regions (see Marconi and Salas 1973; Kutler 1974b; Fletcher 1974). Such extensions of inviscid flow calculations to higher relative incidence must be scrutinized carefully, since as we have seen, the effects of viscosity dominate the further development of the flow field above $\bar{\alpha} \sim 1$. For example, Fig. 51d illustrates the calculation of the mixed flow field about a 7.5° circular cone at relative incidence, $\bar{\alpha} = 2.31$ at $M_\infty = 2.94$, by the "shock-capturing" technique of Kutler (1974b). This inviscid procedure is inherently capable of predicting the location and strength of all flow discontinuities without knowledge of their presence. The discrete jumps are spread over several mesh intervals but can, nevertheless, be located precisely within that region. (This method contrasts with the "sharp-shock technique" of Marconi and Salas (1973), in which all known shock waves are treated as sharp discontinuities and the Rankine-Hugoniot equations are then applied across them.) We observe that although the calculated bow shock position in Fig. 51d is in reasonable agreement with the experimental

[11] It is not particularly revealing to view this "lift-off" feature for only supersonic mainstream flow. In the conical flow projection with which we are dealing, the half-node that exists at the leeward meridian sooner or later moves into the stream as a node — irrespective of whether the flow is inviscid, viscous and subsonic, or viscous and supersonic.

[12] Conically subsonic flows exist when the component of Mach number normal to rays is everywhere subsonic; otherwise, conically mixed (transonic) conditions are present.

measurement of Fig. 51c, the inviscid transonic crossflow domain "shocks-out" at $\phi = 150°$, much closer to the leeward generator than the $\phi = 125°$ noted in the experiment (see Fig. 51b). Again we infer that the large scale of the separated vortical flow dominates the leeward flow structure. We should be aware, however, that some nonlinear effects can be predicted using appropriate inviscid flow calculations. Schiff (1974), when utilizing the Euler equations of motion to compute the inviscid supersonic flow about conical bodies at angle of attack and in coning motion, reported nonlinear normal force developing at relative incidences greater than $\bar{\alpha} \sim 1.5$.

Nakao (1975) has attempted to take account of the viscous flow displacement effects on the lee side of the cone up to values of $\bar{\alpha} \sim 2$ by forming an equivalent conical body in the inviscid flow. The calculated surface pressure distributions on circular and elliptic cones, about which conically mixed flows exist, are claimed to be in good agreement with his own results and with the experimental laminar flow results of Tracy (1963). Zakkay, Economos, and Alzner (1974) also developed effective conical body shapes to represent the viscous-inviscid coupling with turbulent boundary layers up to high relative incidences. Fletcher and Holt (1976) pursued numerical solutions of the flow field about cones up to moderate relative incidences, in which interaction between the inviscid region and the laminar boundary layer on the body was allowed via a displacement effect. The solutions were invalid, however, near the leeward meridian.

Although flow separation about yawed circular cones represents one of the simplest cases in the general problem area of three-dimensional separation, progress has been slow in efforts to construct an inviscid flow model to describe the flow field at high angles of attack and to predict the vortex positions and nonlinear lift. The incompressible flow model of Bryson (1959) represents, in the simplest mathematical form, the effects of the separated flow by two straight vortex sheets emanating from arbitrarily specified positions on the body, each feeding a discrete vortex; it also imposes the condition of zero net force on the system. This gives unrealistic pressure distributions. A more adequate treatment, similar to that used by J. H. B. Smith (1966) for the equivalent delta-wing problem, is under consideration by J. H. B. Smith (1978), using calculated or experimentally determined separation positions at each relative incidence.

Boundary Layer — Methods for calculating the compressible laminar boundary layer on circular cones at small angle of attack were considered by F. K. Moore (1951) and Braun (1958). F. K. Moore (1952) also computed the flows in the plane of symmetry at large angle of attack, and Reshotko (1957) formulated an exact method to compute the laminar flow with heat transfer along the windward generator. Reasonable agreement between approximate integral methods and experimental laminar heat transfer data was also reported by Yen and Thyson (1963) and Chang et al. (1968). Cooke (1966) published an implicit finite difference method for calculating boundary layers on general conical surfaces. The method applies at large angles of attack, allows heat transfer and suction, and can predict separation. In applying his method to a circular cone of 7.5° semi-angle at moderate to high relative incidence ($\alpha/\sin\theta_c = 1$ and 2), Cooke used an inaccurate external flow field based on perturbation methods (Sims 1964) with a modification to ensure irrotationality. Other methods to calculate the laminar attached compressible boundary-layer flow from the windward meridian toward the line of primary separation, wherein the small crossflow assumption was invoked to uncouple the streamwise and crossflow momentum equations, have been documented by Chan (1966), Tsen (1967), Tsen and Arnaudon (1967), and Fannelop (1968). Attempts have been made by Mayne (1972), Popinski and Davis (1973), and by Popinski (1975) to account for the effects of the external streamlines of variable entropy, at relative incidences $\bar{\alpha} < 1$.

Of particular note is the experimental study by Chan (1969) of the laminar boundary layer on a 15° semi-angle cone at Mach 10.4, with a wall-to-stagnation temperature ratio of 0.23. The theoretical results for the inviscid and viscous flows were computed using the method of D. J. Jones (1968) and the small crossflow boundary-layer analysis of Tsen and Arnaudon (1967), respectively, with, of course, no coupling accounted for between the viscous and inviscid flow domains. The excellent agreement between theory and experiment up to values of $\bar{\alpha} = 1.2$ is illustrated in Fig. 54, supersonic crossflow occurring toward the limit of the angle of attack range. At $\bar{\alpha} \sim 0.8$, the pressure minimum shown in Fig. 54a starts to move away from the leeward generator ($\phi = 180°$), so that the boundary layer will meet a continuously steepening circumferential adverse pressure gradient as $\bar{\alpha}$ increases further. Relatively large recompressions beginning at around $\phi = 150°$ occur at $\bar{\alpha} = 1$ and 1.2, so that we would expect separation to occur in the crossflow plane soon thereafter. The heat-transfer measurements at these same relative incidences indicate the heat transfer minima have moved from the leeward generator to where we might infer the 3D separation lines to be located at $\phi \sim 165°$. The heat transfer at the leeward meridian, in fact, begins to increase rapidly for values of $\bar{\alpha} > 1$, consistent with an attachment line along that generator (Fig. 54c). We also note the same qualitative trend in change of both the circumferential pressure and heat-transfer distributions as $\bar{\alpha}$ increases. The resultant surface shear stress directions from the small crossflow theory agree well with oil-dot directions, as we see in Fig. 54d. Thus, we can confirm our earlier expectation that numerical methods for computing the conical inviscid flow field may be used with confidence (with the exception noted below) up to $\bar{\alpha} \sim 1$ as an external flow boundary condition, when allied with a suitable attached flow boundary-layer computation. The exception occurs very close to the leeward meridian where the rapid thickening of the viscous flow obviates the assumption of noncoupling between the inviscid and viscous domains.

Solutions to the three-dimensional, compressible, laminar boundary-layer equations have been obtained by Bordner and Davis (1971) for circular cones at relative incidences up to unity, when immersed in "inviscid" shear and axisymmetric wake flows.

Calculations of the compressible turbulent boundary layer about cones at angle of attack have been reported by Shaneorook and Sumner (1972), utilizing Head's (1960) entrainment concept; by Cousteix and Quemard (1972) and by Bontoux and Roux (1976), using mixing-length formulations; and by J. C. Adams (1972a,b). and Harris and Morris (1974), via eddy-viscosity approaches. The method of Harris and Morris begins computation through the laminar and transitional phases of the flow. Lin and Rubin (1975) have developed a two-layer model of the attached viscous-inviscid flow, using for the turbulent boundary-layer analysis either a mixing-length model or a two-equation kinetic-energy dissipation system to treat the problem of (Reynolds stress) closure. The turbulent flow in the plane of symmetry is discussed by Rubin and Bontoux (1975). All boundary-layer methods provide reasonable agreement with the high Reynolds number experiments of Rainbird (1968b).

Overall Viscous Flow Field – With the introduction of fast computers, such as the CDC 7600, a more or less complete picture of the flow field past cones at high angle of attack can be constructed by solving a simplified set of the Navier-Stokes equations (McRae 1976, 1977; Lubard 1975; Lubard and Rakich 1975). The physics of the flow would appear to be modeled correctly in laminar flow for the sharp (McRae and Lubard) and blunt (Lubard and Rakich) examples displayed in Figs. 41 to 44 and discussed in Sec. 3.3.1. The treatment of the flow about the nose in these calculations raises the question of how, if at all, the commencement of the separation lines is handled. For example, Lubard (1975) computed the laminar viscous separated flow about an essentially sharp 7° cone (of 0.003-in. nose radius) in a Mach 16.1 stream at a length Reynolds number, $R_{L_\infty} = 10^6$. The relative incidence, $\tilde{\alpha} = 1.43$, was chosen to permit comparison with some experiments on circular cones reported by Pate (1974). Because of the small nose radius involved with the "sharp" cone, the starting condition differed from the initial condition of Lubard and Rakich (1975) (for the blunt cone) in which the combined inviscid-flow/axisymmetric boundary layer was calculated around the nose. Now, a Navier-Stokes axisymmetric merged-layer zero angle-of-attack solution around a sphere, due to Victoria and Widhopf (1973), was rotated to provide a three-dimensional initial plane of data at the nose-sphere tangency plane, after which the approximate Navier-Stokes equations were used to continue the solution downstream. Although substantial adverse pressure gradients exist along generators, especially on the windward side of the cone – up to 10 to 20 nose radii downstream of the nose when the cone is pitched (Stetson 1971) – the circumferential gradient is favorable from the windward to the leeward generator. Hence, the starting condition that implies attached flow may or may not be satisfactory. The computation (Lubard 1975) indicated that a lee side primary separation first "appeared" at 300 nose radii downstream of the nose. Figure 44a gives the distribution of velocity vectors at the cone base station in a plane normal to the cone axis for $\tilde{\alpha} = 1.43$, on which the primary separation line, position ϕ_{s1}, may be interpreted in the range $155° < \phi_{s1} < 160°$. Integrated forces and moments from the calculations agreed tolerably well with tunnel measurements, as is shown in Fig. 44b, at this moderate angle of attack.

The invoking of the conical flow approximation does not permit a rationalization of any details of the flow near the nose in terms of singular points, because by definition the separation lines must proceed to a sharp apex. In spite of this philosophical difficulty, the utilization of the conical flow approximation produces quite realistic results in both laminar and turbulent flows. In the most recent of their published results, McRae and Hussaini (1978) computed the turbulent viscous flow over sharp cones in supersonic flow utilizing scalar eddy viscosity models. Although the eddy viscosity coefficients in the streamwise and crossflow senses require tuning to match precisely the experiments of Rainbird (1968a,b) in the regions close to the leeward meridian, very acceptable agreement between calculated and experimental surface pressures and directions of surface skin-friction lines can be obtained for engineering purposes for relatively large variations in the eddy viscosity coefficients[13] (Fig. 55).

4.1.2 Conical Three-Dimensional Flow Separations

Figure 56 (Crabbe 1965) shows the limiting streamlines of the laminar boundary layer on an elliptic cone at angle of attack in a water tunnel at a Reynolds number, based on cone length, of 2.7×10^5. The major axis of the elliptical cross section is vertical. Dye flow is here emerging from very small diameter orifices in the surface of the model. The coherent dye filaments seek the limiting streamline directions at the base of the 3D boundary layer. Remembering from Sec. 2.3 that the limiting streamlines provide a close representation of the skin-friction lines, we see in Fig. 56 that the limiting streamlines converge from both windward and leeward regions of the cone toward an asymptote – the primary separation line. On a conical surface, the condition for conical flow separation[14] is simple; namely, that the separation line should coincide with a generator. The condition along an attachment line is analogous, except that the direction of the skin-friction lines is now reversed as they diverge from the attachment line. The top picture of Fig. 57, with streaks from oil dots, and the results from a corresponding test with a titanium dioxide and oil mixture in Fig. 58, show the turbulent attachment line region along the leeward generator of a circular cone at a relative incidence of 2. Of course, these same features of skin-friction line divergence are also found along the windward generator, as shown in Fig. 60. The commencement of the primary and secondary separation lines in the region of the cone apex will follow one of the patterns discussed in Sec. 2.5, although the nodal and saddle singular points may be sufficiently close together to be considered as merged (Sec. 2.6).

The experimental results of Bannink and Nebbeling (1978) – Figs. 58 and 59a to 59f – illustrate beautifully the surface shear stress directions on an unwrapped surface (an applied thin plastic sheet) of a circular cone, to demonstrate the progressive development toward and beyond 3D separation of the thickening boundary layers on the leeward side of the body at a free-stream Mach number of 2.94 and up to high relative incidences. The development of the flow remains symmetrical about the plane of symmetry at this Mach number up to relative incidences of at least 2.5, subsequent to which, as Fig. 60 illustrates, wavy, nonconical separation line positions appear,[15] along with an asymmetric vortex development in the leeward separated flow field. The striations in the leeward wake showing in the Schlieren photograph are indicative of the sequence of vortex cores that are observable in the crossflow plane in Figs. 30, 31, and 32.

Flow separation occurs on sharp, circular cones at angles of attack typically greater than about three-fourths the nose semi-angle. In supersonic flow, in the absence of any axial pressure gradients, primary separation is seen in the lower photograph of Fig. 57 to be exactly along a generator. We detect the same overall features in the skin-friction line patterns in both low-speed and high-speed flows when Figs. 56,

---

[13] C_f and C_p in Fig. 55.

[14] In laminar flow, the resultant skin friction is proportional to $R_x^{1/2}$, where R_x is the Reynolds number based on wetted run. In high Reynolds number turbulent flows, the index power of the Reynolds number is close to unity. The skin-friction line direction, however, depends only on the ratio of crossflow to streamwise shear stress magnitudes, which in turn depend essentially on the ratio of crossflow to streamwise pressure gradients. Hence, even if there is an essential lack of conicity in the viscous flow development (boundary-layer thickness, shear stress, etc.), there is no such restriction on the skin-friction line direction.

[15] The oil flow provides a "filtered response" to any unsteadiness in the real flow.

57, and 58 are compared. Even in an incompressible flow, the conical nature of the skin-friction line at separation is preserved. This is because at relative incidences sufficient to cause separation, the circumferential pressure gradients are much larger than the axial gradients from the effects of thickness and the base. For the subsonic case as well then, the primary separation line lies essentially along a generator as illustrated in Fig. 56.

A sketch of the symmetrical external flow field past a cone at a large relative incidence with separation and embedded shocks at $\bar{\alpha} \sim 2.5$ is given in Fig. 61; the sketch corresponds with the Schlieren photograph and the symmetrical oil-flow display in Fig. 59d. In Fig. 61, A_1 is the windward attachment line and S_1 the separation line, where the primary boundary layer can no longer penetrate the circumferential adverse pressure gradient on the leeward side of the cone. It leaves the surface as a coiled free-shear layer of finite thickness and rolls up into the primary vortex V_1. The latter induces downflow of the inviscid fluid to provide an attachment line of divergent skin-friction lines along A_2 where the secondary boundary layer begins. It is this sudden enrichment of the downflow, once primary separation has commenced, that causes the heat transfer to increase in the region of the leeward meredian, as we saw in the laminar flow experiment of Chan (1969) in Fig. 54c. If the relative incidence is not much greater than unity, this secondary boundary layer will also separate at S_1, shown in Fig. 59b.

At higher relative incidences, typically nearer to 2, the result is as shown in Fig. 59c, with a secondary separation line, S_2, also apparent. Once the embedded shock waves appear in the crossflow, as sketched in Fig. 61, the steep circumferential adverse pressure gradients produce exceptionally well-defined primary and secondary lines of separation on the oil flow; they are visible in Figs. 59d to 59f. The secondary separation, S_2, gives rise to a weaker vortex V_2 of opposite sign to V_1, which is quite close to the cone surface. Additional downflow is induced to cause yet another attachment line at A_3 (see Fig. 59d). In principle, there appears no reason why the number of separation and attachment lines must end here. The resolution available from the oil-flow visualization does not permit us to diagnose additional separations between S_1 and S_2 at still larger relative incidences, but during the low-speed elliptic cone tests of Crabbe (1965), further lines with accompanying vortices were revealed in the water tunnel.

We note that the Mach-7 heat-transfer experiments in relatively high Reynolds number laminar viscous flow at $R_{L_\infty} = 21.6 \times 10^5$ by Guffroy et al. (1968), with a 9° semi-angle cone up to relative incidences of $\bar{\alpha} \sim 1.67$, demonstrated the same qualitative surface flow patterns overall, indicating primary and secondary separation lines that we have discussed in turbulent flow. But at lower Reynolds numbers, at $R_{L_\infty} = 4.9 \times 10^5$, Guffroy et al. (1968), as well as Tracy (1963) and other workers in laminar flow (e.g., Stetson 1971) have observed only primary separations. Tracy (1963), in fact, made extensive measurements of the hypersonic flow ($M_\infty = 8$) about a 10° semi-angle cone with laminar boundary layers ($R_{L_\infty} = 0.5$ to 4.2×10^5) up to moderately large relative incidence ($\bar{\alpha} = 2.4$). By slowly rolling his model, he was able to present continuous trace records of surface static pressure and heat transfer and measurements of the external flow field using a single fixed direction pitot tube. For angles of attack greater than about 12°, mixed (transonic) flow conditions prevailed, and the positions of the internal shock waves were clearly indicated by his surveys. It was noted that the leeward part of the nose shock wave and the outer parts of the internal shock waves were very weak, becoming tangential to a free-stream Mach cone with apex coincident with the cone apex. Also at angles of attack of 12° and above, boundary-layer separation was present. Tracy interpreted his pitot probe measurements as indicating a lobe[16] of vortical fluid above the leeward generator (Fig. 62a).

Similar results were obtained by Guffroy et al. (1968) at corresponding Reynolds numbers (see Fig. 62b). Stetson (1971) has also produced pitot surveys within laminar viscous flow above a 5.6° half-angle cone at Mach 14.2 at a length Reynolds number of almost 1×10^6. His results on separation line positions at moderate to high relative incidences are displayed in Fig. 63, in comparison with other measured laminar and turbulent results. The high Mach number, laminar cone flows appear to yield separation line positions that are closer to the leeward meridian than either the lower Mach number turbulent results, or the Mach zero laminar flow cases.

4.1.3 Rainbird's Measurements at High Reynolds Number

Rainbird (1968a,b) determined, in a series of well-instrumented experiments, both the turbulent viscous flow and the external flow field development about pointed circular cones at moderate to large relative incidences. Free-stream Mach numbers of 1.8 and 4.25 and high Reynolds numbers ($R_{L_\infty} = 3.4 \times 10^7$ to 6.8×10^7) were chosen to provide both conically subsonic flows and conically mixed (transonic) conditions with zero heat transfer. Typically, the viscous flow up to separation was measured on a 12.5° semi-angle cone; the external flow field was mapped above a 5° model. The cone surface quantities, such as static pressure, and shear stress magnitude and direction, were obtained on each model, chiefly at the 0.85 length station. The boundary-layer profiles were obtained using a three-tube servo-controlled yawmeter that emerged from the cone surface, while a pair of five-tube yawmeters, attached to the cone base, probed the external flow field. The cones were prepositioned in pitch and then rolled for the latter measurements.

The overall effects of viscosity on the normal force characteristics of the $\theta_c = 5°$ cone are given in Fig. 64, which shows both balance and integrated pressure results up to very large relative incidence (almost 6). The good agreement between these two sets of measurements, along with oil-flow visualization on the cone surface, established beyond doubt the conicity and symmetry of the flow up to $\bar{\alpha}$ values of 3 in the experiments of Rainbird (1968a,b). Figure 64 displays the substantial nonlinear lift that is generated above a relative incidence of about 1.5 from both viscous and inviscid means (Schiff 1974). Initially, the magnitude of this nonlinear lift increases more rapidly with $\bar{\alpha}$ at the higher Mach numbers. This is considered to be caused by the development of mixed flow conditions and internal shock waves generating separations with relatively stronger vortices.

---

[16] Symmetry demands that this lobe must contain at least two vortices.

4.1.4 Experimental Surface Pressure Distributions

The development of the surface pressure distributions with angle of attack can be followed from Figs. 65 and 66. At small relative incidences of $\bar{\alpha} < 0.6$, the surface pressure gradient is favorable (roughly proportional to $\sin\phi$), the external streamlines do not have an inflection point, and the boundary layer grows in a regular manner from the windward to the leeward generator. The flow is attached everywhere and only small crossflows are developed in the boundary layer. With increase of angle of attack the pressure gradient first becomes adverse near the leeward generator, and the point of minimum pressure moves rapidly around the cone surface, from $\phi = 180°$ to about $\phi = 130°$ for a relative incidence change from, say, 0.6 to 1.0. Note in Figs. 65a and 65b the excellent agreement up to $\bar{\alpha} \sim 1$ of the inviscid flow pressure distributions calculated by D. J. Jones (1969) and the experimental measurements, where the viscous/inviscid coupling is still small.

At the pressure minimum, the external streamlines have an inflection point (Fig. 67) beyond which the boundary layer encounters an adverse pressure gradient and thickens rapidly. The crossflow within the boundary layer (Fig. 68b) (as defined in Figs. 7 and 8) is first reduced and then reversed by the adverse pressure gradient until the skin-friction lines are turned along a generator of the cone ($\omega_s = 0$ at $\phi = \phi_{s1} = 168°$ for $\bar{\alpha} \sim 1$ in Fig. 65b). We observe in Fig. 68a, however, that the streamwise velocity distributions maintain reasonable fullness at all circumferential stations. At the same time, the boundary-layer thickness on the leeward generator is reduced (compare boundary-layer profiles at $\phi = 154.6°$ and $\phi = 180°$ in Fig. 68a) due to the draining away of low-energy fluid toward the pressure minima. The streamlines of this boundary layer growing away from the leeward generator pass beneath the separated primary boundary layer coming from the windward of the cone and form two symmetrically disposed lobes of vortical fluid on either side of the leeward generator (see Figs. 69a, 69b, and 70a). However, there is no sudden eruption of vortical fluid from the cone surface at $\bar{\alpha} \sim 1$ and, at high Reynolds numbers, these lobes are still thin compared, say, with the local cone radius.

We note that although the Mager (1952) representation of crossflow profiles in Fig. 68c bears poor resemblance to the measured profiles on the 12.5° cone, the calculated polar velocity profiles due to Shanebrook and Sumner (1971) in Fig. 68d, and to Cousteix and Quémard (1972) in Fig. 68e, are in good agreement with the measurements of Rainbird (1968a,b).

At still larger relative incidences of 2 or more (Figs. 66b and 66c), the adverse pressure gradient following the pressure minimum intensifies and the primary separation angle ϕ_{s1} occurs much earlier (Fig. 63). Between the circumferential angles for which ω_s is zero, Fig. 66 shows that there is a plateau of essentially constant pressure followed by a second pronounced pressure minimum and, finally, a recompression to zero pressure gradient at the leeward generator. We see in Figs. 69c, 69d, and 70b that under these conditions the scale of separated flow is more extensive and the shear layers roll up to form a pair of symmetrically disposed vortices close to the cone surface. The second pressure minima at $\phi = 180° \pm 14°$, produced by these vortices, also cause a marked thinning of the boundary layer and a very strong outflow away from the leeward generator (see the oil-flow features in Fig. 69d). Secondary separation of this leeward boundary layer also occurs in the neighborhood of $\phi = \phi_{s2} = 159°$ (Figs. 66b and 66c). The dividing surfaces are shown as "dash-dot" lines in Figs. 69 and 70. Many of these turbulent flow features are qualitatively similar to the laminar boundary-layer separation about circular cones at low speeds discussed by Rainbird, Crabbe, and Jurewicz (1963).

At the higher Mach number of $M_\infty = 4.25$, mixed flow conditions are present at $\bar{\alpha} = 2.1$ and 2.5, and the sharp pressure rise following the first pressure minimum is caused by embedded shock waves. The development of mixed flow conditions with internal shock waves usually causes (but not always) earlier separation, as can be seen in Fig. 63, where flow visualization measurements of ϕ_{s1} are given for the 5° and 12.5° cones. The primary separation line positions measured by Nebbeling and Bannink (1976) and Bannink and Nebbeling (1978) at Mach 2.94 and with a $\theta_c = 7.5°$ cone in turbulent flow (at a length Reynolds number $R_{L_\infty} \sim 7 \times 10^6$) follow the results of Rainbird (1968a,b) at his lowest Reynolds number. The laminar tests of Stetson (1971) and Guffroy et al. (1968) provide, as a result of density, temperature, or heat transfer effects, separation line positions closer to the leeward generator than we view for the turbulent boundary layer.

4.1.5 Surface Shear Stress and Direction

The surface shear stress directions (i.e., the directions of the skin-friction lines) were measured by streak-flow visualization from oil dots, an example of which is shown in Fig. 57. These results are given in Figs. 71a and 71b for various relative incidences at Mach 1.8 and 4.25. Data measured at two lengthwise positions, $x/L = 0.65$ and 0.85, are presented at the largest relative incidence $\bar{\alpha} = 2.5°$; within the scatter, they show no systematic influence of lengthwise location. For all conically subsonic cases, the skin-friction line directions are reduced smoothly to zero (separation) by the adverse pressure gradient but, with embedded shocks present, separation is produced extremely rapidly. Where the skin-friction line direction ω_s is at a maximum (negative) value close to the leeward meridian, there is an inflexion point in the pattern of skin-friction lines immediately beneath the core of the primary vortex. This location may also be read from Figs. 69c and 70b.

The magnitudes of the local skin-friction coefficient, determined from Preston (surface pitot) tubes, are shown in Figs. 72a and 72b for Mach 1.8 and 4.25, respectively. We note that the Preston tubes were aligned against the surface skin-friction lines for each circumferential angle, and that a two-dimensional boundary-layer calibration of these tubes was assumed to apply.

For a relative incidence of about unity, the magnitude of the local skin-friction coefficient decreases smoothly to a minimum but finite value at separation, and increases again to a value at the leeward generator that is close to the zero incidence skin-friction coefficient. At $\bar{\alpha} = 2.1$, there are minimum, but finite values, at both primary and secondary separation lines along with very high values near the leeward generator due to the strong outflow. (The measurement of skin friction and direction in subsonic flow on a cone utilizing yawed pairs of hot wires buried in the surface repeated the trends found in supersonic flow (see Peake, Owen, and Higuchi (1973)).)

Note that although the actual surface shear stress ($\tau_w = C_{fe} 0.7 \rho_e M_e^2$) on the leeward generator exceeds that along the windward generator for $M_\infty = 1.80$, the reverse is true for $M_\infty = 4.25$, due to the low density on the leeward side in this latter case. In fact,

$$(\tau_w)_{\phi=180^\circ} = 1.11(\tau_w)_{\phi=0^\circ} \quad \text{for } M_\infty = 1.8,\ \bar{\alpha} = 2.12$$

while

$$(\tau_w)_{\phi=180^\circ} = 0.65(\tau_w)_{\phi=0^\circ} \quad \text{for } M_\infty = 4.25,\ \bar{\alpha} = 2.10$$

In closing this commentary on cone surface conditions, we again refer the reader to Fig. 55 that illustrates the reasonable agreement obtained between the scalar eddy viscosity Navier-Stokes solution of McRae and Hussaini (1978) and Rainbird's (1968a,b) measurements of surface pressure and skin-friction direction.

4.1.6 External Flow on the Leeward Side of the Cone

Pitot pressure contours (i.e., lines of constant values of the ratio of local pitot pressure divided by pitot pressure of the undisturbed uniform stream) were constructed from surveys made at various probe heights while rolling the cone at a fixed angle of attack setting. These contours are shown in Figs. 69 and 70 for Mach 1.8 and 4.25. The pitot pressures were corrected for the measured local flow angularities.

At moderate relative incidence, $\bar{\alpha} = 1.01$ and 1.26, the contours show the lobes of vortical fluid accumulating near the leeward generator, the maximum thickness occurring at a larger ϕ value than from where the windward boundary layer has separated ($\omega_x = 0$). At the larger relative incidences, the centerline of the separating shear layer (i.e., the dividing surface, indicated by the dash-dot line) can be seen starting from the primary separation angle ϕ_{S1} and merging into the well-defined, but rather extensive, vortex core. The boundary layer near the leeward generator and beneath the vortex core was too thin to be penetrated by the yawmeter probes, but the lobe of the vortical fluid from it can be seen, for $\bar{\alpha} = 2.5$, just beyond the secondary separation angle, ϕ_{S2}. We note that fluid of high total pressure flows down toward the leeward generator (providing the region of divergent flow from the attachment line) and outward under the vortex core. For the conically mixed $M_\infty = 4.25$, $\bar{\alpha} = 2.49$ case shown in Fig. 70, the position of the internal shock wave is also indicated.

Figure 73 provides an example of the circumferential distribution of the transverse components of Mach number and flow direction at a height above the cone surface equal to 0.2 times the local cone radius, and slightly above the center of the vortex core. Rapid changes of these quantities through the separated shear layer (indicated as SSL on the figure) and near the vortex core, VC, are shown, together with the strong downflow near the leeward generator. It is interesting to compare the vortex core heights with those given for low-speed flow with laminar separation in Rainbird et al. (1963). From Figure 74 we see that the vortex cores occur at very nearly the same circumferential position, but are nearer the cone surface at a given $\bar{\alpha}$ for the higher Mach number turbulent boundary-layer results. This is partly due to the much later (larger ϕ) separation positions in turbulent flow.

The structure of the external flow that emerges from the high Reynolds number measurements of Rainbird (1968a,b) and the somewhat lower Reynolds number tests of Nebbeling and Bannink (1976) at large relative incidence, with its well-defined symmetrical vortices and high skin-friction coefficient near the leeward generator (Fig. 61), contrasts strongly with Tracy's (1963) measurements taken at much lower Reynolds numbers ($R_{L_\infty} = 0.5 \times 10^5$ to 4.2×10^5) with laminar boundary layers. His results indicate a massive lobe of vortical fluid on the leeward side at $\bar{\alpha} = 2.4$ (shown in Fig. 62a), with the maximum thickness of the displacement surface occurring at the leeward meridian. The effects of Reynolds number are dominant here. Figure 62b shows the external flow field as mapped by Guffroy et al. (1968) in laminar flow at $\bar{\alpha} = 2.22$ at a Reynolds number corresponding to that used by Tracy (1963). Although the separated shear layer itself is very much in evidence, the detail of the flow structure between the surface and the shear layer near the leeward generator is still imprecise; indeed, it is more reminiscent of Tracy's lobular regime. Increasing the length Reynolds number by a factor of 4 at the same $\bar{\alpha} = 2.22$ in Fig. 62c decreases the height of the shear layer above the leeward surface, but there may then be both primary and secondary separations present.

4.1.7 Summary of Results for Flow About Sharp Cones

For relative incidences up to $\bar{\alpha} \sim 1$, where there is virtually no 3D separation, numerical solutions of the inviscid supersonic flow about circular cones provide good agreement with experiment.

At high Reynolds numbers, the development of the viscous flow and separation about circular cones with increasing relative incidence is a continuous and essentially conical process, involving the formation of symmetrically disposed lobes of vortical fluid ($0.8 < \bar{\alpha} <$ about 1.5) which develop into vortices and remain comparatively close to the cone surface on either side of, and near, the leeward generator.

Once primary and secondary separations have developed in turbulent flow under conically mixed (transonic) crossplane conditions, the primary separation line position becomes virtually invariant at $\phi_{S1} = 123^\circ$ for all relative incidences above 2. Curiously, secondary separations have not usually been witnessed in supersonic laminar flow at low Reynolds numbers.

The construction of an inviscid flow model with free vortex sheets, analogous to the corresponding slender delta-wing case, is needed to describe the laminar or turbulent flow at large relative incidence ($\bar{\alpha} >$ about 1.5). Otherwise, we must resort to solutions of the Navier-Stokes equations for which satisfactory results are obtainable for laminar flow. Solutions for turbulent flow with eddy viscosity models are also obtainable but are less satisfactory due to the lack of appropriate experimental information to set up the modeling of the subgrid scale turbulence.

The concentration on cone flows has been deliberate since we know a great deal about them, and since many of the flow phenomena seen on flight vehicles at angle of attack are dominated by nose effects. The

swept separations on other configurations will be seen to be analogous in many respects to the conical flows discussed in this section.

4.2 Blunt Cones

A blunt nose or leading edge is usually required on a hypersonic vehicle for survival during the reentry phase of flight, although improved materials and better design estimates have enabled very slender shapes and small bluntness ratios (the ratio of nose radius to base radius) to be used successfully. Blunt conical shapes are used in nonlifting reentry applications; slender blunt cones provide usable lift-to-drag ratios for lifting reentry flight. As the bluntness ratio is increased, the viscous-inviscid interaction in the nose region becomes increasingly important in its effect along the body; at a given angle of attack, decreasing the cone half-angle also increases the severity of the interactions on the lee side. Ablation of the surface material, due to mass transfer enhancing the displacement effects, augments the interaction. Fannelop and Waldman (1968) note that the primary effect of ablation is to reduce viscous drag, the lift remaining almost unchanged relative to the nonablating case. A physical flow model of ablation was outlined by Canning et al. (1968) to explain the crosshatching and other observed patterns on biconic, concave, and convex ablating models in a Mach 7 airstream with maximum local Reynolds numbers, based on model length, approaching 10×10^6. An interesting hypothesis that related the crosshatching to the kind of vortex structures that we are discussing was proposed by Tobak (1970). He suggested that the crosshatching was the result of spatially periodic variations in surface pressure in both the spanwise and longitudinal directions and that the source of the pressure variations was the presence in the boundary layer of an array of regularly spaced counterrotating longitudinal vortices that originated from surface irregularities near the leading edge.

Blunting the apex of a circular cone causes substantial perturbation to the conicity of the combined viscous and inviscid flow fields. The effects are felt over a considerable number of nose radii downstream. If we take the axial position where the line of minimum pressure on the leeward side first returns to alignment with a conical ray as an indicator of flow conicity, Fig. 75 shows that increasing the angle of attack actually diminishes the downstream effect of the nose on the leeward side. Notwithstanding, at $\bar{\alpha}$ values as high as 3, the influence of the nose is still apparent up to more than 30 nose radii downstream at $M_\infty = 14.2$.

The effects of bluntness and relative incidence were included in a normal force correlation proposed originally by Whitfield and Wolny (1963) (and used later by George and Whitfield 1968) at angles of attack up to 90°, in airstreams at Mach 7 and above, as:

$$\frac{C_N}{\theta_c} \sim \left(1 + \frac{\alpha}{\theta_c}\right)^2 \left[1 - \left(\frac{RN}{RB}\right)^2\right]$$

where RN is the nose radius and RB is the base radius. The above relationship indicates that both a high relative incidence and a large ratio of nose-to-base radius for a given value of θ_c will dominate the overall nonlinear lifting performance of a blunt cone. By inference then, these normalized parameters will also govern the pressure (and the heat transfer) distributions on the body. To maintain a given normal force as bluntness is increased, relative incidence must also be increased.

4.2.1 Experimental Surface Pressure Distributions

Stetson (1971) reported measuring the longitudinal and circumferential static pressure distributions on the surfaces of two $\theta_c = 5.6°$ cones, of 30% and 10% bluntness, the respective cone lengths equalling about 25 and 94 nose radii. The laminar flow on each cone was studied in a Mach 14.2 airstream at a length Reynolds number of $R_{L_\infty} \sim 0.4 \times 10^6$. At moderate to high relative incidences, say up to $\bar{\alpha} \sim 2$, the longitudinal pressure distributions measured along the cone surface generators (ϕ = constant) initially indicate highly favorable pressure gradients due to the massive expansion of the flow from the stagnation point region behind the bow shock (Fig. 76). These lengthwise gradients then turn adverse downstream of $x/RN \sim 6$ on the windward side of the cone, the maximum steepness being situated at $\phi = 0°$, along the windward generator. Under these circumstances, of course, the cone boundary layer will develop under a favorable circumferential pressure gradient all the way from the windward generator as far as two symmetrical minimum pressure positions off the leeward plane of symmetry, as we see in Fig. 77. Thereafter, the circumferential pressure continues to increase toward the leeward generator (except near the cone base where a slight trough occurs on the leeward meridian). At the relative incidence of 1.79, we can determine from Fig. 78 that the leeward circumferential pressure gradient in the nose region turns adverse at the axial station somewhere between $2.4 < x/RN < 10.3$, where we would expect a noticeable effect of separated flow to begin.

4.2.2 Skin-Friction Line Patterns and Heat Flux Distributions in Laminar Flow

Figures 79 and 80 show respective low and high Reynolds number results of experimental surface oil-flow visualization on blunt cones at angle of attack in hypersonic flow (Stetson 1971; Cérésuela, Kretzschmer, and Rehbach 1968). Figure 81a is a postulated pattern of skin-friction lines which appears in accord with the low Reynolds number oil pattern displayed in Fig. 79a. This pattern is the first in the sequence of plausible flow patterns on a blunt apex that was shown in Fig. 22a, where the primary separation line starts from a saddle point in the nose region. Reducing the bluntness from 30% (Fig. 79a) to 10% (Fig. 79b) erases the experimental detail resolution in the nose region, but confirms the existence of the primary separation line. The enhanced Reynolds number flow shown in Figs. 80a and 80b at a relative incidence corresponding to Stetson's flows in Fig. 79, demonstrates a like pattern of only primary separation. Once the angle of attack increases to a relative incidence of 4, however (Figs. 80c and 80d), both primary and secondary separation lines appear. The resolution available from the streaking oil dots does not allow a categorical interpretation of how the secondary separation line forms, but it could start from another saddle point on the leeward meridian (Fig. 81b) or from a saddle point off-axis that is joined to a focus (Fig. 81c). The vortical filament from the focus will center the roll-up of the dividing surface from the secondary separation line as we saw in the hemisphere-cylinder, transonic flow case in Fig. 26.

The heat-flux distributions measured by Cérésuela, Kretzschmer, and Rehbach (1968) on the 56% blunt cone are plotted in Fig. 82, in both the circumferential and axial directions. In totally laminar flow, we would expect these heat flux distributions to follow the pressure distributions, if Reynolds analogy holds.

A comparison of Stetson's pressure distributions on his 30% blunt cone in Fig. 76 indeed shows close agreement with the trend of the French heat flux measurements, the "peaky" performance along the windward and leeward generators being associated with recompression effects downstream of the nose overexpansion. Note that these broad peaks are obviously <u>not</u> associated with the conjectured nodal points of attachment in Figs. 81b and 81c; neither are they thought representative of boundary-layer transition behavior with such a large bluntness ratio (see Cleary 1969). Also in this laminar flow field, the heat transfer effects on the leeward side, even in the presence of primary and secondary separations, are relatively minor in comparison with those on the windward side. Cleary (1969) notes that similarity theory is generally suitable for estimating laminar heating rates on blunt cones up to $\bar{\alpha}$ values of at least 2. He suggests that, under these conditions, the effects of crossflow in the boundary layer on the heating rates are relatively small. As far as calculations are concerned for the external flow field, Cérésuela, Kratzschmer, and Rehbach (1968) showed that numerical solutions of the inviscid flow field (see Fig. 80) gave good prediction of the bow shock wave position up to $\bar{\alpha} \sim 4$, but as before (for the pointed bodies) produced poor results of leeward surface pressure distributions above $\bar{\alpha} \sim 1$.

4.2.3 Calculation of Viscous Flow

From the theoretical standpoint, the attached laminar boundary layer about blunt cones has been dealt with successfully, up to relative incidences of unity, by Fannelop and Waldman (1968) and Nomura (1976), who invoked the assumptions of small crossflow. In an attempt to obviate these small crossflow assumptions, Der (1969) used an inviscid pressure field (from modified Newtonian theory) allied with an explicit finite difference approach. This inviscid pressure field, unfortunately, does not provide an adverse circumferential pressure gradient and cannot, therefore, predict crossflow separation. Mayne (1977) has computed the laminar viscous shock layer on a blunt bi-conic body at low angles of attack.

As we saw with the sharp cones, the viscous-inviscid interactions on the leeward side of the blunt cone cannot be treated adequately with noncoupling of the viscous and inviscid flow domains. Thus, the 3D Navier-Stokes blunt cone solutions of Lubard and Rakich (1975), the results from which were displayed in Fig. 43 and discussed in Sec. 3.3.1, have provided the most appropriate solution to date of the viscous, separated laminar flow at moderate to high angles of attack.

4.2.4 Boundary-Layer Transition

Boundary-layer transition on bodies at angle of attack has a powerful influence on the leeward inviscid-viscous interaction and on the heat transfer to the leeward surface in the presence of separated flow. As a general rule, the transition zone moves rearward along the windward meridian and forward along the leeward meridian as angle of attack is increased; but neither a full description nor a complete understanding of the details of the transition front between these end points is available. Once the transition region is determined at zero angle of attack, the deviation from symmetry in the transition zone with increasing angle of attack is a function only of relative incidence (Reda 1977).

The several processes of transition (see Morkovin 1968, 1978) are sensitive to a great number of environmental factors and model conditions. These processes, namely the reception of the boundary layer to various kinds of disturbances ("receptivity"), the amplification of competing linear instabilities, and the ensuing nonlinear processes, are all extremely complex phenomena. At sufficiently low Reynolds numbers, the region of transitional or incipient turbulent flow is often characterized by the appearance of regular arrays of vortices within the boundary layer with axes slightly skewed from the direction of the external stream. The development of these arrays of nearly streamwise vortices has been associated with instability of the crossflow within the 3D boundary layer (see, e.g., Tobak 1973), but their subsequent progress through regions of adverse pressure gradient remains much of a mystery. What happens, for instance, as these vortices approach a line of 3D separation? Do they break down rapidly as a result of secondary instabilities and proceed to turbulence instantaneously? At high enough Reynolds numbers and depending on the perturbation environment, bypasses to the normal amplification processes may take place, so that the vortices may not be observed. Of course, there is always the question of whether the longitudinal vortices are associated just with the instability of the 3D boundary layer or whether they are also related to the development of the entropy layer. The former is the more likely, since the longitudinal vortices have also been observed in subsonic flow (see Maltby 1962). Also, we must not forget the contributions of 3D roughness elements, in association with vortex stretching due to axial and circumferential pressure gradients, in the production of turbulent spots and wedges (Morkovin 1968). It is clear that we must learn the manner in which disturbances in the free stream and other disturbances enter and amplify within the viscous flow and determine their spectra, since certain regions of the spectrum have a direct influence on transition and others do not (Reshotko 1977). To complicate matters further, the effects of transition may be dissimilar on the same model, when tested in different wind-tunnel facilities or flight (Dougherty and Fisher 1980).

In this review, we wish to comment briefly on the effects of transition from selected references as they pertain to the development of 3D separations and associated heat transfer on blunt bodies at angle of attack. We begin by demonstrating the effects of bluntness on skin-friction line direction at Mach 6.05, in some experiments performed by McElderry (1974) with $\theta_c = 6°$, 10% blunt and sharp cones at Reynolds numbers based on cone length from typically 2×10^6 to 16×10^6. Relative incidences of up to 2 were investigated, with extensive regions of laminar, transitional and turbulent boundary layers existing on the cones. Figure 83 presents some of McElderry's results along the $\phi = 90°$ generator, plotted as angle $\omega_s°$ (with respect to the generator direction) at relative incidences of 1.0, 1.5, and 2.0. The results for the blunt cone with laminar and turbulent flow are depicted with shaded symbols and joined with dashed and full lines, respectively. First, we note from Fig. 83 that increasing the angle of attack does not change the position of the transition zone along the flank of the sharp cone, but on the blunt cone, moves the transition zone forward toward the nose. At a given angle of attack, however, bluntning delays the onset of transition (see also Cleary 1969). Second, the skin-friction line direction on the blunt cone reduces by about 30° through the transition region. This is because the turbulent boundary layer is more resistive to skewing in the circumferential pressure gradient than its laminar counterpart. (The results on the sharp cone are insufficient to determine any changes in ω_s through transition.) Third, the effects of the 10% bluntness are not apparent in the laminar flow downstream of $x/L \sim 0.4$ where, in Fig. 83, we see that the values of ω_s on both blunt and sharp cones overplot to within the scatter of the measurements. From these comparisons,

it is evident that the nose blunting is the overriding influence affecting transition location and hence, by implication, will have a large effect on the leeward separated flow development.

From a practical point of view, it would appear that high heating rates materialize along the leeward side once there are shock waves in the crossflow causing primary and secondary separations in transitional or turbulent flow. Figure 84 displays an oil-flow pattern of Zakkay et al. (1972), indicating well-defined regions of primary and secondary separation in the Mach 6 transitional flow about a $\theta_c = 10°$ blunt cone at $\bar{\alpha} \sim 2$. Note the large difference at the same relative incidence between the form of the heating distribution along the leeward ray in the flow of Zakkay et al. (1972), shown in Fig. 84, when compared with the laminar-flow distribution shown in Fig. 82. The sudden turnaround and rapid increase in heat-transfer shown in Fig. 84 are ascribed to the onset of transition (see Cleary 1969). The heat-transfer rate continues to increase along the cone until a plateau is reached at a value approximately three times higher than that along the windward meridian. Eventually, the onset of transition also occurs along the windward meridian, at a distance of 6 nose radii farther downstream than the onset along the leeward ray. The entire transition zone is hence skewed with respect to the axis of the cone. A conjectured skin-friction line pattern appropriate to the oil-flow result of Zakkay et al. (1972) is shown in Fig. 81b. We perceive that the region of high heating on the leeward meridian, indicated on the oil-flow pattern photograph, could be attributable to the flow at the attachment node situated upstream of, but adjacent to, the saddle point of the secondary separation line. This saddle point could well be at the onset of transition, suggesting a possible link between transition and secondary separation processes in this case.

Reynolds number is a crucial regulator of the peak heating to the leeward meridian on shuttle nose configurations as Whitehead et al. (1972) revealed; Figs. 85 and 86 are from their paper. Figure 85 displays the leeward heating to a conceptual shuttle model immersed in a Mach 6 stream at Reynolds numbers based on the body length from 0.7×10^6 to 3.3×10^6. At all Reynolds numbers shown in Fig. 85, divergent skin-friction lines ("feather-like" patterns) were said to exist along the leeward generator, so that the secondary boundary layer developing from this leeward attachment line continued to drain into the thickening lobes of vortical fluid on either side of the plane of symmetry. The heat transfer distribution at $R_{L_\infty} = 0.7 \times 10^6$ and 1.2×10^6 resembles qualitatively that which was measured in a completely laminar boundary layer by Cérésuela, Kretzschmer, and Rehbach (1968) (see Fig. 82e) and which was relatively insignificant in comparison with the windward heating. When the Reynolds number R_{L_∞} increases to above 2.2×10^6, transition would appear to occur near $x/L = 0.4$, or else a nodal point of reattachment provides the peak in heating. Despite this (still) low Reynolds number at the 20° angle of attack, the flow events around the lee-side nose region make transition the more likely explanation producing this heat transfer signature (see Cleary 1969) especially since the skin-friction lines do not undergo radical changes. Furthermore, Widhopf and Hall (1972) have measured transition on the nose-cap of blunted cones to show similar heat-transfer distributions. It is known, for instance, that during the transition process, a peak in heat transfer (or wall temperature) above the adjacent laminar and turbulent values occurs where the rate of "turbulent bursts" is presumed to be at a maximum in the transition zone – see Owen (1970); Peake et al. (1977). That such a peak was not plotted in Fig. 84 in the heat-transfer measurements of Zakkay et al. (1972) could be due to its occurrence between measuring points. The additional peaks in leeward heating at the very high relative incidences shown in Fig. 86 might be caused by relaminarization, followed by renewed transition, since the axial pressure gradient is favorable along almost all of the leeward generator. However, such diagnoses would be aided by circumferential skin-friction and heat-transfer measurements, plus fine resolution oil-streak flow visualization. The heating off the plane of symmetry may be equally as important as the leeward flow, since other attachment lines will exist once primary, secondary, and perhaps other 3D separations have developed.

In contrast with these transitional flows, we observe from the measurements of Widhopf (1971a) in Fig. 87, where a $\theta_c = 9°$, 40% blunt cone was tested in a Mach 10.6 stream at $R_{L_\infty} = 26 \times 10^6$, that the fully turbulent heat transfer data at relative incidences up to 2.22 show no surprises; they follow in qualitative terms the laminar (very) blunt cone results of Cérésuela, Kretzschmer, and Rehbach (1968). Useful heat transfer correlations for blunt cones at angles of attack up to $\bar{\alpha} \sim 2.2$ were also obtained by Widhopf (1971b). A calculation of the zero-angle-of-attack heat-transfer distribution, together with a detailed surface-pressure distribution, allowed a rapid evaluation of the turbulent or laminar heat-transfer rates anywhere on the body of the blunted cone up to $\bar{\alpha} \sim 2$.

Further commentary on blunt-nose vehicles of the Shuttle type will be deferred to Sec. 4.9.

4.2.5 Turbulent Flow Field on the Leeward Side

The leeward flow field about the blunt cone exhibits a different flow structure from that about a sharp cone at the same relative incidence in hypersonic flow. To demonstrate these differences, McElderry (1974) measured pitot pressures in the leeward turbulent separated flows about $\theta_c = 6°$, 10% blunt- and sharp-cone models at Mach 6. Figure 88 presents some of these results at a relative incidence, $\bar{\alpha} = 2$, plotted as contours of constant fractions of the free-stream pitot pressure existing ahead of the cone shock waves. It is clear that the overall pattern of pitot contours about the blunt cone (Fig. 88a) differs from the recognizable primary and secondary vortex structures existing on the sharp cone (Fig. 88b) by the additional zone of low energy that straddles the leeward plane of symmetry about 1 cone radius above the leeward meridian. If we postulate that the flow structures for the blunt and sharp cones are as shown in Figs. 89a and 89b, we see immediately that the pair of isolated top vortices above the blunt model could be those originating from foci on the nose. Such a flow is analogous to the inboard surface foci shown in Fig. 24, for example, and the inboard vortices shown in cross section about the slender wing on Fig. 25d, providing yet one more possible flow structure in addition to those in Figs. 81a to 81c. Some lack of resolution in the pitot measurements has perhaps prevented the discovery of these nose vortices in Fig. 88a, but from considerations of symmetry, we believe that two vortices must exist as shown in Fig. 89a. The small regions of high total pressure between the nose vortices and the primary vortices correspond in location with the saddle points (Fig. 89a) where there is zero velocity in the crossflow plane. In our discussion of the patterns of skin-friction lines on the blunt cone examples in this section, we see that we have utilized most of the possibilities of blunt nose flows conjectured in Figs. 22-24. We also cannot rule out the possibility that the flow in Fig. 89a is a counterpart to that shown at $M_\infty = 1.0$ and 1.2 for the hemisphere-cylinder (Fig. 26a). Finally, we might comment that the external lobular shape of the leeward turbulent flow about the blunt cone in

hypersonic flow is curiously not dissimilar to that found by Tracy (1963) for the hypersonic laminar flow field about a sharp cone (Fig. 62a). The existence of shock waves in the same particular locations in the leeward flow field in the respective turbulent and laminar cases shown in Figs. 88a and 62a should also be noted.

4.3 Long Slender Bodies

4.3.1 Introductory Comment

The body of a typical missile or rocket consists of a low-drag nose shape attached to a circular cylindrical afterbody. The afterbody is about 10 body diameters in length and has stabilizing fins or a flare mounted close to the base end. Such long bodies are very prone to flow separation once they depart from a zero angle of attack flight condition. To oversimplify the picture, we may regard the long cylinder as a cone of essentially zero included angle and so for any small angle of attack, the relative incidence is very large and separation is inevitable somewhere down the body. The typical separated flow regimes encountered on the leeward side with increasing angle of attack are (1) a symmetrical vortex wake about the meridian plane; (2) a relatively steady asymmetric vortex wake; and (3) an unsteady diffuse vortex wake. These regimes are illustrated (Figs. 90a-90c) in side elevation in the water-tunnel experiments of Fiechter (1966) for a tangent-ogive cylinder up to angles of attack of about 60°.

4.3.2 Steady Symmetric Separations

On very long, pointed or blunt-nosed slender configurations, separation first occurs symmetrically with a pair of vortices trailing back along the body. Figure 91 illustrates such body separations in side elevation on a blunted cone-cylinder-flare model at a low relative incidence in a Mach 4 airstream. The separations and vortex wake are recognizable in the photograph at about 1-2 body diameters behind the cone-cylinder junction and proceed downstream on the leeward side of the body in a well ordered and structured fashion (see Fig. 90a). These symmetric vortices are virtually identical in form in the crossflow plane at corresponding relative incidences, provided the crossflow is subsonic. By way of example, Fig. 92a shows the crossflow about an ogive-cylinder at 20° angle of attack at $M_\infty \sim 0$, made visible with dye and aluminum particles in a water-tunnel study by Werlé (1974). The close analogy between this low-speed case and a Mach 2 wind-tunnel result for another ogive-cylinder at 26° angle of attack (O'Hare and Jones 1973) is revealed in Fig. 92b. The figure shows a composite of laser vapor-screen photographs for various crossflow planes along the body, assembled in an isometric view. Both primary and secondary vortices are observable.

Careful measurements of the crossflow velocity vectors and contours of constant pitot-pressure deficit in low-speed symmetrical flow were made by Grosche (1970), as shown in Figs. 93a and 93b. The pitot contours display evidence of both the primary and secondary separations that were seen on the cone in Fig. 69. Note in Fig. 93c that when a wing is added to the body at the same angle of attack, there is a substantial shift in the position of the body vortices due to the larger induced effects of the controlled flow separations at the edges of the swept wing. Some preliminary measurements of the 3D velocity components within the nominally symmetrical leeward wake were made by Owen and Johnson (1978b), using a laser velocimeter.

Some painstaking experiments on missile configurations at angle of attack were made by Boersen (1975) to elucidate the fine details of the skin-friction line patterns. Figure 94 shows some of his results. Figure 94a displays the primary separation line in turbulent flow along a $\theta_c = 20°$ blunted cone-cylinder (without flare or fins) at a low relative incidence of 0.6, $R_{L_\infty} \sim 10 \times 10^6$, and at Mach 2.3. There is a strong resemblance between this flow and that about the ellipsoid discussed in Sec. 2.8.2 (Figs. 27 and 28). The flow is symmetrical about the meridian plane but notice, on the unwrapped surface of the cylinder, in Fig. 94b, the gradual convergence of the skin-friction lines emanating from the clearly defined windward attachment line zone, followed by the very abrupt turning into the primary separation line, S_1. The induced downflow between the primary vortices (Fig. 92a) causes a rapid divergence along the leeward generator, A_1, toward the apparent beginning of a secondary separation region, S_2. This behavior is particularly noticeable in Fig. 94c where the length Reynolds number has increased by a factor of 3 over the flow shown in Fig. 94b. Naturally, if we maintain our hypothesis of demanding patterns of continuous skin-friction lines associated with a limited number of singular points, the attachment and separation lines that are very evident in these elegant flow visualization studies of Boersen (1975) must emanate from (merged) nodal and saddle singular points on the surface at the nose. Only when the local circumferential pressure gradients become sufficiently adverse do we see the rapid turning of skin-friction lines to form asymptotes to the particular skin-friction lines that are the primary and secondary separation lines.

Changing the forebody to a $\theta_c = 20°$ sharp cone (see Fig. 95a) at the same relative incidence of 0.6 (Boersen 1975) produces no substantial change to either the flow symmetry or to the commencement of the 3D separated region, but a tertiary and even a fourth separation line are now observed on the downstream part of the cylinder. Circumferential pressure distributions at the axial stations identified in Fig. 95a are plotted in Fig. 95b, where increasing Reynolds number is demonstrated to typically enhance the magnitude of the suction pressures. Note that the windward generator is on the right-hand side of the figure, and circumferential angle increases toward the left, the reverse notation to that used, for example, for the cone in Fig. 66. At station 1, the circumferential pressures are still dominated by the apparent attached viscous flow leaving the pointed conical forebody and no observable separation has developed just downstream of the cone-cylinder junction even though the circumferential pressure gradient is adverse between $120° < \phi < 180°$. Except near the cone-cylinder junction, the axial pressure gradients are negligible. Beyond the minimum pressure point at stations 2 - 5, however, close to $\phi \sim 90°$, the circumferential adverse pressure gradient has steepened sufficiently to provoke primary separation[17] near the flank. At station 3, the pressure distribution is reminiscent of the cone flow in Fig. 66, with the primary and secondary separations[17] present (compare also the oil flows in Fig. 95c and Fig. 58). At subsequent stations downstream along the cylindrical afterbody, further very sharp changes in the curvature of the pressure distributions are detected, consistent with possible embedded shock waves at positions c and d in

[17]Note that for consistency with the topological notions advanced in Sec. 2, the particular skin-friction lines that become observable as separation lines downstream on the body will commence at (merged) singular points at the cone apex consisting of nodes and saddles in proximity.

Fig. 95c, and the associated development of additional separation lines[17] at e and g. A tentative sketch of the crossflow is provided in Fig. 95c, which differs in some respects from that proposed by Boersen (1975). Ragsdale (1972) has provided some flow-field measurements around a tangent-ogive cylinder at higher Mach numbers (3.5 and 4.0) that compare in features with the lower Mach number measurements of Boersen (1975).

These body separations have an important effect on the vehicle's static and dynamic stability. At small relative incidences, where the separation is steady and symmetrical with respect to the angle-of-attack plane, the ensuing body vortices produce a nonlinear contribution to the overall normal force and pitching moment. If the fin system is not symmetrically orientated with respect to the angle-of-attack plane, however, a cross-coupling side force, yawing moment, and rolling moment can arise even at small angles of attack.

Flows such as these were studied extensively in the 1950s, particularly at NACA (Jorgensen and Perkins 1958) and at NASA, by Jernell (1968) (cone cylinders and ogive cylinders, $0° < \alpha < 180°$) and by Jorgensen and Nelson (1974, 1975) (cylinders with assorted nose shapes and bodies of elliptical cross section). A summary of these latter experiments and force predictions from crossflow methods is given in Jorgensen (1977). A good understanding, in an overall sense, has been obtained on the development of both forces and moments. An estimate, in incompressible flow, of the overall forces and moments acting on a slender body of revolution without fins was offered in Küchemann (1973) summarizing an analysis done 20 years earlier. Vortex sheets, as plane vertical surfaces, were assumed to exist all along the cylinder and the vorticity vector in the sheet was assumed to lie in a direction halfway between the direction of the free stream and the body axis. Results of typical calculations utilizing this very simple symmetric model are shown (Fig. 96) to be in quite reasonable agreement with experimental results. To demonstrate the effects of nose shape, a series of tests at high Reynolds number was reported by Peake, Rainbird, and Atraghji (1972) who summarized the experiments of Atraghji (1967, 1968a) on the characteristics of a family of 16 pointed conical and tangent-ogives attached to cylindrical afterbodies (see Fig. 97). Each nose could be fitted to a cylindrical afterbody length of either 6 or 12 body diameters, but there were no stabilizing fins attached. Forces and circumferential pressures were measured and the oil dots applied to the surface of the models yielded the patterns of skin-friction lines. At low angles of attack (typically up to $\alpha \sim 3°$) where there was attached flow, the slope of the normal force/angle-of-attack plot, C_{N_α}, increased with Mach number and semi-nose angle, θ_c (see Fig. 98). The effect of overall slenderness ratio, L/D, was less clear, although at $M_\infty = 0.5$ the trend was established of an increasing C_{N_α} with L/D. Calculations using slender body theory (Ward 1955), the USAF "Datcom" data sheets (Hoak 1965), and the method due to Öhman (1964) were also performed. As a general rule, the theories appear to underpredict C_{N_α} at a given semi-nose angle and slenderness ratio.

In the range of angle of attack (characteristically $\alpha = 3°$ to 11°) for the series of nose shapes tested, three-dimensional leeward flow separation is symmetric. The induced suction pressures from the rolled-up shear layers generate a large nonlinear normal force component, but no side force. With the normal force represented by a quadratic in α:

$$C_N = K + b_1\alpha + d_1\alpha^2$$

where K only removes the experimental uncertainty in the true measurement, Fig. 99 illustrates the increase in coefficients b_1 and d_1 with both Mach number and slenderness ratio, with a significant variation in d_1 at a given Mach number and slenderness ratio attributable to the semi-nose angle, θ_c. The more slender ogives listed in Fig. 97 (07, 09, and 011) would appear to generate a larger nonlinear lift throughout the Mach number range and for both afterbody lengths.

As we have seen, rational calculations of the symmetrical separated flow field about long slender bodies at angle of attack are few. Development of a "Navier-Stokes" computational technique similar to that used by Pulliam and Steger (1978) to determine the separated flow about a long blunt body at moderate angle of attack (see Sec. 3.3.3) should be encouraged, to attain finer resolution of the flow-field details in the vortex wake and on the surface.

4.3.3 Steady Asymmetrical Separations

At relative incidences of long slender bodies higher than those just discussed, say for values typically more than 2, separations and body vortices become asymmetric but still relatively steady in space. The result is that large side forces, yawing moments, and rolling moments are developed, especially on fin-stabilized vehicles (see Fidler and Bateman 1975).

The onset of asymmetry and the initial direction of the side force are responsive to small changes in geometry at the nose, Reynolds number, and Mach number, up to angles of attack where conditions in the leeward crossflow become transonic. As speed increases further, the significant side forces disappear (Peake, Rainbird, and Atraghji 1972). The asymmetries occur in both laminar and turbulent flows so that transition is presumably not an essential ingredient causing asymmetry. Notwithstanding, the implication from recent tests by Lamont (1979) with a tangent-ogive cylinder at angle of attack, at Reynolds numbers encompassing laminar, transitional, and turbulent boundary-layer separation, is that the vortex wake is less structured in the transition domain, leading to reduced side and normal forces at a given subsonic Mach number. In the fully laminar or turbulent regions, on the other hand, where the organization of the flow field is well defined, the respective magnitudes of the side force are larger and are closely matched. It is likely that the levels of vorticity and acoustic disturbance in most wind tunnels will also affect the initial occurrence of asymmetries (B. L. Hunt and Dexter 1978).

A rational explanation for the development of asymmetry in the flow may be related to the stability of the velocity profiles in the vicinity of the saddle singular point that exists in the stream above the body vortices (see Figs. 25b-25d). In the example of the flow about a circular cylinder situated perpendicular to an oncoming stream, Nishioka and Sato (1978) determined asymmetric instabilities to amplify initially in

[17]See footnote on Page 31.

the region of the saddle point, to herald the commencement of asymmetric but well-structured wake flow. Thus, for a body of general shape at high angle of attack, we may conjecture that flow perturbations will impose fluctuations on the saddle-point flow that will accentuate the instability mechanism. Evidence points to extremely small surface irregularities in the surface curvature at the nose as governing the initial direction of the asymmetry in the vortex flow field. This is understandable in view of the fact that a given body at angle of attack under identical flow conditions will provide a repeatable side force direction at a prescribed roll orientation; and near-mirror images of the side-force/angle-of-attack performance for roll angles ±90° (see Peake, Owen, and Higuchi 1978). Despite this knowledge, unforeseen geometrical imperfections lying within production tolerances on a typical flight vehicle may alter the asymmetric vortex flow development sufficiently to provide unpredictable stability problems (Titiriga, Skow, and Moore 1978). We do not yet understand the influence of geometrical imperfections on the fluid mechanics, nor how the nominally small disturbances of the fluid flow at these imperfections can amplify so considerably. A small flat, for instance, machined in turn on each side of the nose was effective in completely switching the sign and amplitude of the yawing moment (Ericsson and Reding 1978).

It would appear that at forebody relative incidences where asymmetry of the vortex wake commences, we are always dealing not only with separation of the primary boundary layers that develop on each side from the windward generator, but with secondary separations of the leeward boundary layer in addition. The onset of asymmetry would seem to be characterized initially by a rapid, local movement circumferentially of one (or both) secondary separation lines followed, as angle of attack is increased further, by circumferential movement of the primary separation lines (Rainbird et al. 1966; Peake, Rainbird, and Atraghji 1972). The asymmetric skin-friction line pattern on the conical surface development shown in Fig. 60 illustrates this latter flow situation, with "wobbly" primary and secondary separation line traces existing all along the cone (Bannink and Nebbeling 1978). There, the free-stream Mach number is 2.94 and the relative incidence is 4.5. At lower free-stream Mach numbers, however, the asymmetric separation lines have been found to be conical (Peake, Owen, and Johnson 1980).

The asymmetric vortex wake usually develops from asymmetric separation line positions on the body, but the latter does not appear to be a necessary condition for the former to occur. An appraisal (Keener and G. T. Chapman 1977) of some earlier, low-subsonic speed tests of Shanks (1963) in which forces and moments were measured on very slender, flat-plate, delta wings (sweep angles from 70° to 84°) at angle of attack, indicates that even though the separation lines were fixed at the sharp leading edges, asymmetry in the leading-edge vortices, as determined by the onset of significant rolling moment, occurred when the angle of attack was about three to four times the wing semi-nose angle. This angle of attack for asymmetry is splendidly illustrated on the vapor-screen pictures (Fig. 32) about another very slender delta wing immersed in a Mach 2.8 flow (Fellows and Carter 1969). Nonetheless, the sharp edges have a beneficial effect in delaying the onset of asymmetry to higher relative incidences than those obtained with smooth pointed forebodies or forebody-cylinder configurations (Peake, Rainbird, and Atraghji 1972; Keener and G. T. Chapman 1974; Keener, G. T. Chapman, and Kruse 1976).

Hence, we have the alternative descriptions of (1) leeward asymmetries in primary and secondary separation line positions coupled with asymmetric vortex flow (e.g., Fig. 60), or (2) symmetric fixed primary separation line positions (but asymmetries, no doubt, in secondary separation position, (Fig. 32) still yielding asymmetric vortex flow at suitably high angles of attack. The reasons for such flow behavior are evidently complex and perplexing. Nevertheless, the amplification of perturbations to produce an instability at the saddle point (Nishioka and Sato 1978), and to which we alluded previously, would seem to cover the descriptions presented.

Because the development of the turbulent flow structures in the three-dimensional swept separation zones and in the tightly coiled free-shear layers is virtually unexplored, the modeling of the leeward flow asymmetries poses severe problems. Recourse has been made, for rough predictions of the flows about missile shapes, to inviscid flow approximations of the leeward region, utilizing arrays of line vortices (see the review by Nielsen (1978) of nonlinearities in missile behavior at high angles of attack). Alternatively, the impulsively started flow analogy proposed many years ago by H. J. Allen and Perkins (1951b) has frequently been applied (Deffenbaugh and Koerner 1977) as we have intimated in Sec. 2.8.3. In this hypothesis, we may remember, the development of the crossflow with distance along an inclined body of revolution is likened to the growth with time of the two-dimensional flow past the corresponding circular cylinder impulsively started from rest. Useful engineering formulae have certainly resulted utilizing the analogy. Nevertheless, given the complexities of the three-dimensional boundary-layer growth, separation, and vortex development about slender bodies at angle of attack, it is intriguing that the impulsive-flow analogy can provide more than just qualitative details of the flow. We have already seen, however, in the discussion in Sec. 2.8.3, that if we restrict ourselves to invoking the impulsive-flow analogy to provide only the overall flow structure, the topologies of the 2D unsteady and the 3D steady cases appear virtually analogous (Tobak and Peake 1979). If we demand stricter correspondence between the 2D unsteady and 3D steady cases, there are issues for debate. For instance, the growth of the unsteady 2D vortex differs essentially from that of the steady 3D vortex in space. Küchemann and J. Weber (1965) point out that, in three dimensions, fluid entering the core of the vortex can be discharged axially, whereas in two dimensions no such escape is available. Thus, the 2D core must expand continuously outward with time to accommodate all of the fluid entering the vortex. Küchemann and J. Weber show further that there is only one case in inviscid flow where the two kinds of vortex are formally identical: where the steady, three-dimensional flow is conical (so that slenderness assumptions can be invoked); and where the unsteady flow is permitted to grow linearly with time. Hence, if the development of the real viscous wake (in 2D with time, and in 3D with distance along the body) can be represented by these respective but special inviscid approximations to vortex growth, then the impulsive-flow analogy should be a suitable artifice under conditions of high Reynolds number. To date, Lamont and B. L. Hunt (1976, 1977) have probably extracted the limits of usefulness of the 2D unsteady analogue as it is presently understood to describe the nature of "out-of-plane" forces on a pointed body of revolution at high angles of attack.

For the missile at sufficiently high angle of attack, the asymmetric vortex flow is coupled with asymmetries in primary (and secondary) separation line positions. An example is shown in Fig. 100 where the asymmetric primary separation line positions on the port and starboard of a 5.8° cone-cylinder and a 13.9° ogive-cylinder, at Mach 0.6 and at identical 18° angles of attack, are plotted. The boundary layers are turbulent. This figure demonstrates the important influence of nose shape on the asymmetry of the flow. We detect that on the very slender conical nose, at its relative incidence of just over 3, there is substantial

flow asymmetry all along the body (solid lines in Fig. 100). In contrast, because the less slender ogival nose is at a relative incidence of about only 1.3, the commencement of separation there shows only slight asymmetry, with less difference in separation line positions from side to side (dashed lines in Fig. 100).

The direction of the side force changes with angle of attack but is repeatable for the same model geometry in a given test. If the forebody is indexed with respect to the afterbody, the magnitude of the side force may well be altered (Keener and G. T. Chapman 1974). The real effect of Reynolds number on the onset of asymmetry remains conjectural, however, since changing the density of the tunnel airstream in a given experiment frequently alters the disturbance level.

Figure 101 illustrates the magnitude of the mean side force coefficient C_Y with respect to the normal force coefficient C_N, as model angle of attack is increased, for the selection of nose shapes shown in Fig. 97 with the 12D afterbody length. Unsteady fluctuations in side force coefficient, with peak-to-peak amplitudes as high as ± 0.3 at $\alpha = 25°$ were measured, superimposed upon the mean C_Y levels. For angles of attack up to about 27°, increasing either the semi-nose angle or the Mach number reduced the amplitude of the side force. In fact, at $M_\infty = 2$ when $\theta_C > 10°$, and for all configurations at $M_\infty = 3.5$, no measurable side force was obtained. Reference should be made to the paper by Reding and Ericsson (1977), who discussed the maximum vortex-induced side forces obtainable on slender bodies. Figure 102 presents the critical angle for flow asymmetry (judged by the side force exceeding, say, 5% of the normal force) plotted against the semi-nose angle θ_C. As before, we confirm that the onset of flow asymmetry is delayed by increasing θ_C and Mach number. But the effect of the longer afterbody is to provoke asymmetry at a lower angle of attack.

Oil-dot flow visualization permitted the locations of the 3D separation lines to be measured. In Fig. 103a, the circumferential positions of the primary separation lines are plotted along the body for the most slender cone-cylinder configuration at $M_\infty = 0.5$ (C5-12D in Fig. 97) at $\alpha = 25°$. There, one of the asymmetric separation lines shows very large, but characteristic, excursions along the cylinder afterbody with respect to the meridian plane. The random nature of the starting direction of the asymmetry on the forebody at these high relative incidences can be determined from Figs. 103a and 100. On the former, the separation lines, for this particular nose hardware and angle of attack, just happen to begin symmetrically disposed near the sharp apex, but diverge rapidly thereafter. On the latter illustration, the separation lines are asymmetrically disposed all along the body. In contrast note, in Figs. 103b, 94, and 95, the monotonic movement of the symmetric separation line positions towards the leeward meridian as the nose is approached from the base.

Some circumferential pressure distributions representative of the steady asymmetric vortex flow field at $\alpha = 25°$ and $M_\infty = 0.5$, along the conical nose and cylindrical afterbody of C5-12D, are plotted in Fig. 104, the measurement stations also being shown in Fig. 103. The heavy line represents the shape of the body. Asymmetries in the pressure distributions about the meridional plane begin at the nose, but vary in degree with distance down the body. The large suction peaks in the range of circumferential angle $135° < \phi < 180°$ are those induced by the vortices emanating from the primary separation lines shown in Fig. 103. Secondary and even additional separation lines are indicated on the downstream part of the afterbody by the many changes in the sign of the circumferential pressure gradient (compare with Fig. 95b).

4.3.4 Unsteadiness in the Asymmetrical Separations

In the recent experiments of Peake, Owen, and Johnson (1980), it was revealed during the viewing of the leeward crossflow about a circular cone with vapor-screen flow visualization (Fig. 105) that as the angle of attack was increased and the asymmetry progressively developed, the secondary vortices began to fluctuate with increasing unsteadiness, until one of the primary vortices (the port side in this case) virtually rolled over the other (Figs. 105a and 105b). Such behavior was characteristic at both subsonic and supersonic free-stream Mach numbers, appearing to be consistent with the substantial root-mean-square fluctuations in velocity in regions of maximum velocity gradient in the leeward flow that were measured by Owen and Johnson (1978a,b). As angle of attack increased to still higher values, the shear layer feeding the vortex farthest from the surface continued to stretch with great unsteadiness (Fig. 105c), eventually appearing to roll-up halfway along its length while maintaining continuity with the original vortex. Figures 105d and 105e illustrate the mechanism repeating for the starboard side vortex. The intricate mechanism that starts the asymmetric flow field development, once an asymmetric disturbance is allowed to amplify (Nishioka and Sato 1978), has been postulated at length by Tobak and Peake (1979).

Keener, G. T. Chapman, and Kruse (1976) attempted to draw some tentative boundaries based on angle of attack and fineness ratio between the various flow regimes that appear on the leeward side of ogive-cylinder bodies in subsonic flow. Figure 106 illustrates these zones at Mach 0.6 for nominally turbulent viscous flows. We observe that three angle-of-attack boundaries are plotted as functions of overall fineness ratio, thus separating the angle of attack range of 0° to 90° into the three regions of different vortex formations that were introduced in Sec. 4.3.1 and in Fig. 90. Recall that the regions are (1) regions of symmetrical steady vortices, typically up to angles of attack of about 1.5 times the semi-nose angle in subsonic flow; (2) regions of quasi-steady asymmetric vortex flows; and (3) at very high angles of attack, a "two-dimensional unsteady wake-like" flow. In Fig. 102, we detected in the high Reynolds number data of Peake, Rainbird, and Atraghji (1972) that the angle of attack at which the onset of asymmetric side-force development occurred was particularly sensitive to semi-nose angle, and less dependent on afterbody length. The data in Fig. 102 have been plotted again in Fig 106. Along a given vertical bar representing fixed nose and afterbody fineness ratios, we see again the dependency of onset angle on semi-nose angle. The higher Reynolds number data of Peake, Rainbird, and Atraghji indicate the onset of asymmetry at lower angles of attack than the data presented by Keener, G. T. Chapman, and Kruse (1976).

4.3.5 Form of the Leeward Vortex Wake

At angles of attack prior to the onset of asymmetries in the leeward flow, the free shear layer rolls up smoothly from the vicinity of the separation line, and passes downstream as a well organized coiled motion (e.g., Fig. 92). In the Schlieren photographs of the symmetrical leeward separation in supersonic flow about the circular cone (Fig. 59c) and about the blunted cone-cylinder (Fig. 91) we observe no irregularities in the passage downstream of the straight vortex-core regions. The additional separation lines that we viewed

on the downstream part of the cylinder in Fig. 95a, but again symmetrically disposed with respect to the pitching plane, are thought to give rise to other shear layers whose cores are very close to the surface of the cylinder (Fig. 95c).

Once the separation lines are no longer symmetrical with respect to the pitching plane, the Schlieren photograph of the cone flow in Fig. 60 shows striations in the leeward wake. Thomson and Morrison (1971) reported analogous Schlieren results about cone-cylinders in supersonic flow consistent with very large changes in local density in the flow. The start of the striations is not clear (presumably being very close to the apex), but they bend as they leave the body, to pass downstream at an angle approximately midway between the angle of the body axis and the free-stream velocity vector. (The water-tunnel picture of Fig. 90b also shows sharp kinks in the vortex core positions.) These striations may be indicative (1) of an instability and consequent change in form of each of the shear layers feeding the primary vortices at consecutive left-and-right stations along the body (Figs. 30-32, 105), or (2) of the layers from the secondary and additional separation lines now rolling up away from the body surface also to pass downstream. Thomson and Morrison (1971) follow the former explanation, citing wake traverses in their support.

No comment has been made in the literature for slender body flows as to the possibility that the striations may be shock waves in the crossflow, or that the shear layer itself may become "multibranched" (Küchemann 1972). For example, Fig. 107 shows some observations of Maltby of the flow about a long flat plate, initially at angle of attack (Fig. 107a), and then under conditions of slight yaw in addition (Fig. 107b). Maltby (see Küchemann 1972) associated the "double branching" of the port-side vortex shown in Fig. 107b with the "intersection" of the leeward attachment line and the port-side primary separation line. The hypothesis of continuous skin-friction lines, of course, disallows such an "intersection" unless it is a singular point. Figure 107 sketches a conjectured saddle-point/focus formation on the wing edge that does indeed permit the attachment line to "meet," but never touch the primary separation line at close quarters. The vortical filament from the focus will now center the roll-up from the "new" primary separation line as it extends downstream along the edge from the saddle point (see Fig. 13). If secondary separations are present also, the movement of the reattachment line between the primary and secondary separation lines (A_2 in Fig. 108 and in Fig. 94, for instance) toward the primary separation line may also provide the mechanism for a corresponding development in the shape of the dividing surfaces leaving slender bodies. A sketch of the hypothesis is provided in Fig. 108.

Finally, we should note that a similar mechanism may be associated with an instability of the dividing surface itself, coupled with fluctuations in the flow adjacent to the separation line. Figure 109 depicts a flow of this kind from observations by Pierce (1961). It appears that a small-scale array of "double-branched cores" can be superimposed upon a larger scale motion which itself has a large core region.

As these comments may suggest, a picture is gradually emerging, albeit still imprecise, of the nature of the asymmetric, steady and unsteady leeward flows about slender bodies at angle of attack. Much still remains to be done in understanding these flows, particularly with regard to defining the effects of transition, Reynolds number, and compressibility.

4.3.6 Control of the Orientation of the Forebody Vortex Flow Field

Investigations have shown that as the development of the asymmetry is particularly sensitive to surface imperfections at the nose, potential means of controlling the forebody flow could be via deployment of a single small strake or by spinning the nose (Neihouse, Klinar, and Scher 1960). Keener and G. T. Chapman (1974) displayed the effectiveness of symmetrical strakes placed at the nose of a forebody alone to reduce the asymmetrical forces and moments. Flattening of the forebody in the yaw plane provides the same result (Titiriga, Skow, and Moore 1978). On the other hand, since we know that missiles having long cylindrical afterbodies will eventually develop asymmetrical flows regardless of nose conditions, we might be led to expect that such local treatment at the nose would probably not influence the downstream flow substantially. Notwithstanding, Rao (1978, 1979) has demonstrated that utilizing helical separation trips about the forebody (Fig. 110a) to disrupt the normal development of separation has been effective in alleviating side forces and yawing moments on short missile and fuselage shapes at high angles of attack (Figs. 110b-110d). It is considered (Rao) that the helical trips upset the well-organized motion of the leeward vortices to cause a relatively rapid diffusion of vorticity; some evidence of this phenomenon is presented in the water-tunnel picture (Fig. 111) of a slender fighter aircraft at high angle of attack.[18] In the wind-tunnel results displayed in Figs. 110c and 110b, however, we note that the reduction of side force produced by the helical trips is recovered as normal force, implying that there is a well-ordered flow structure rather than a diffuse one. W. H. Clark, Peoples, and Briggs (1972) utilized other roughness devices such as grit or vortex generators at the nose of missile shapes to alleviate the development of asymmetric forces and moments. Unfortunately, the mounting of "add-on" excrescences to the airframe is usually detrimental to the cruise-drag performance of a vehicle, and may provide problems with stability if not tailored with extreme care. Clearly, strakes or large trips may only be used on aircraft or on "bank-to-turn" missiles where there are fixed planes of symmetry. Moreover, large strakes attached to the forebody are less than enthusiastically accepted by radar engineers, when the strakes transform substantially the nominal round symmetry of the forebody cross section.

In view of the deficiencies of many of these passive devices at limiting the side force without other performance penalties, studies have been undertaken by Skow, Moore, and Lorincz (1979) and by Peake and Owen (1979) in which a novel blowing scheme controlled and fixed the orientation of the forebody vortices at high angles of attack. These authors investigated ogival- and conical-shaped forebodies, respectively. Small amounts of air were injected normally or tangentially to the forebody surface very close to the nose, but on one side of the leeward meridian beneath the vortex farthest from the wall. Normal injection was found to be more effective than tangential injection (Peake and Owen 1979). By a process of fluid amplification (typically changes in side force coefficient could be accommodated up to about 40 times the blowing momentum coefficient) the injected air was completely effective in biasing the asymmetry, as is shown in the laser vapor-screen photographs in Fig. 112. The camera was situated behind the slightly blunted conical

[18] An alternative view is that this phenomenon could be associated with breakdown of the laminar vortices into turbulence by the trip.

forebody and we take a pilot's view of the flow field.[19] The jet orifice in the forebody's surface was chosen to be located on a leeward generator between the positions of the primary and secondary separation lines in the symmetric flow field, just prior to asymmetry commencing. The jet was located back from the nose at 12% of the forebody length; the laser vapor screen and circumferential pressures were measured at the 87% length station.

Thus the pilot's view of the flow is one of the jet penetrating the forebody flow field and pluming backwards toward him above the forebody vortices along the entire length of the cone. Figures 112a to 112g illustrate the development of the combined jet/forebody turbulent vortex flow field in a Mach 0.6 airstream at a relative incidence of 3.3 (cone semi-angle, $\theta_c = 5°$) as the jet momentum is progressively increased. The sequence begins in Fig. 112a with a very low rate of jet momentum having only a small effect on the forebody asymmetric flow. From the orientation of the vortices, the largest suctions are generated on the port side beneath the vortex closest to the surface, generating a side force in that direction. The jet is situated on the starboard side of the leeward ray beneath the highest vortex as shown in the inset sketch. With increasing jet momentum (Figs. 112b and 112c) the high vortex is brought closer to the surface until both vortex positions and pressures are symmetrical with respect to the meridian plane (see Fig. 112d). The amplitude of the side force is now reduced to zero. With still further increase of jet momentum, the side-force direction is reversed and increases in the opposite sense, as shown in Figs. 112e-112g. A distinctively organized and stablé flow structure emerges with skewed contrarotating vortices in the jet positioned above the forebody flow and no shedding. A postulate of the combined jet and forebody vortex flow structure is shown in Fig. 113, with the enclosing saddle point (see Fig. 89) moved to a location above the jet vortices, far from the surface. Hence the introduction of jet air, in terms of its effect in the crossflow plane far from the injection point, is to develop a completely controllable flow structure, providing a side-force direction and magnitude dependent only on the jet momentum at a given angle of attack. Such a system could be used to inhibit spin departures on fighter aircraft (Skow, Moore, and Lorincz 1979) or as a direct side-force control.

4.4 Bluff Protuberances

We introduced in Sec. 2.8.4 and in Figs. 33-35 the important class of three-dimensional viscous flows in which the initially two-dimensional or axisymmetric boundary layer suddenly meets a steep, adverse pressure gradient due to the blockage effect of a protuberance. The adverse nature of the pressure field relaxes as the flow proceeds around the obstruction, whether or not the obstruction is partially or wholly immersed within the boundary layer. Relative to the local external stream direction, the boundary-layer flow first skews outward in the adverse pressure field and then inward upon encountering the favorable region. If the protuberance is sufficiently bluff, a three-dimensional separation region exists close to and about the junction of the protuberance with the surface. There are two main areas toward which the physics of this flow field may be directed: the practical flight vehicle configurations to be addressed below; and about roughness elements providing horseshoe vortices as instigators of boundary-layer transition (Gregory and Walker 1951). These are the turbulent wedges, the stationary equivalent of turbulent spots (see Cantwell, Coles, and Dimotakis 1978).

Typical examples of bluff surface protuberances include wing leading edges at wing-root fuselage junctions, the foreparts of bulbous wheel housings and boundary-layer diverters. As an example, East and Hoxey (1968) have commented on the low-speed, boundary-layer effects in an "idealized" wing-body junction formed by an obstruction with a nose 30.5 cm (1 ft) in radius whose base was immersed in a turbulent boundary layer 14 cm (5.5 in.) deep, and hence, of similar thickness to a boundary layer on a full-scale aircraft. Even though the shear layer resulting from the primary separation line about the base of the cylinder (Fig. 34) was seen to roll-up within the depth of the undisturbed boundary layer (this observation was made previously in laminar flow studies by Rainbird et al. (1966); Peake and Galway (1965); Peake, Galway, and Rainbird (1965)), it appears that the surface static pressure distribution and local mainstream were distorted to an extent to indicate that these effects would be significant (Küchemann 1970) in a practical wing-body junction. In this section, we shall attempt an outline of the flow about bluff protuberances which, when streamlined, become satisfactory diversion systems for viscous flows. J. C. R. Hunt et al. (1978) provide a detailed discussion of the flow around various 3D surface obstacles in terms of the singular points of the wall shear stress and mean streamline patterns. The frontispiece in Thwaites (1960) (Fig. 33), showing coiled shear-layer motions under low-speed conditions about the base of a circular cylinder joined to a wall, is an impressive illustration of the complexities with which we are faced in studying such 3D separated flows (see Tobak and Peake 1979). Nevertheless, the skin-friction line patterns on the wall surrounding the protuberance appear qualitatively the same irrespective of Mach number and Reynolds number (compare Figs. 34 and 35).

The incompressible laminar boundary layer on a flat plate flowing around a protuberance of either circular or Rankine oval section was investigated experimentally and analytically by Peake and Galway (1965) and Peake, Galway, and Rainbird (1965). It was shown that the initial line of 3D separation about the cylinder — the primary separation line — could be predicted to agree reasonably well with experiment. In addition, these experiments in a water tunnel facilitated an understanding of many of the complex flow phenomena downstream of the primary separation region in the zones of secondary separation and roll-up of the dividing surfaces.

The model that was used for the water-tunnel experiments (Fig. 114) was subsequently sting-mounted in a high Reynolds number wind-tunnel environment, to compare the location of the 3D separation lines in subsonic turbulent flow with those measured in laminar flow for both circular and oval section protuberances. The flat plate had a span of 25 cm (9.8 in.) and a chord of 36 cm (14 in.) with the cylinder axis set 25 cm (10 in.) from the leading edge. In addition, a range of circular cylinders, of length-to-diameter ratio L/D between 4.5 and 18, and diameter-to-undisturbed momentum deficit thickness of the boundary layer D/θ_c between 40 and 200, was tested. The Reynolds number based on cylinder diameter spanned the range $0.2 \times 10^6 < R_D < 2.4 \times 10^6$ at Mach 0.2 and 0.3. As expected, the separation of the turbulent boundary layer was closer to the cylinder than in the laminar case, as exemplified by the flows about the 2:1 and 4:1 oval cylinders shown in Fig. 115.

[19]Note the initial orientation of forebody vortices in Fig. 112 on the cone with slight bluntness is of opposite hand to the orientation on the sharp cone in Fig. 105.

Figure 116a displays the tracings of the turbulent primary and secondary separation line positions about the circular cylinders plotted to a base of unit cylinder diameter, for various ratios of D/θ_c at $M_\infty = 0.2$ and for long cylinders (compared with the boundary-layer thickness) of $L/D = 9$. With decrease of D/θ_c (i.e., decreasing D with respect to the same initial boundary layer in the experiment) the primary and secondary separation line positions move in an upstream direction away from the cylinder (Fig. 116b). If the ratio D/θ_c is assumed to be the appropriate normalizing parameter, then this result can also be interpreted in terms of holding D constant and increasing the boundary-layer momentum thickness θ_c. In this light, a thicker, more momentum-deficient flow will obviously separate sooner, thus providing the trend shown in Figs. 116a and 116b. Westkaemper (1968), in his measurements in supersonic flow about circular section protuberances, reported that for cylinder L/D ratios greater than unity, the distance of the saddle singular point, Δ/D, from the cylinder leading edge was virtually independent of L/D, D/θ_c, M_∞ and R_D, equalling $\Delta/D = 2.65$. We note that this simple correlation places the primary separation line well upstream of the subsonic measurements of Peake, Rainbird, and Atraghji (1972), displayed in Fig. 116, as a result of the strong adverse pressure gradients and upstream influence of the bow shock wave interacting with the approaching boundary layer (see Fig. 35). The subsequent work of Sedney and Kitchens (1975, 1976), however, disagreed with the correlation of Westkaemper (1968); Sedney and Kitchens found a strong effect of protuberance height, L/D, and free-stream (supersonic) Mach number on separation distance, Δ/D. Some examples of the Sedney and Kitchens (1976) results, demonstrating these findings, are plotted in Figs. 117 and 118. In contrast, the effect of increasing Reynolds number on separation distance was found to be relatively weak once boundary layers were turbulent (see Fig. 117); this is to be expected, since the interaction is pressure dominated.

The importance of these 3D separations about protuberances in supersonic and hypersonic flow is illustrated by the high heat-transfer rates that are sometimes sufficient to burn through the skin of the flight vehicle (Korkegi 1971). Piping, antennae, and other projecting fittings, which may or may not protrude through the boundary layer, are often located on the outer skins of rockets. These protrusions, along with blunt leading edges of fins, cause local 3D separations of the flow with attendant high rates of heat transfer in regions where flow reattachment occurs (any divergent region of skin-friction lines emanating from a nodal point of attachment such as A in the top photograph of Fig. 35). For example, Burbank, Newlander, and Collins (1962) measured heat-transfer rates almost seven times the undisturbed flat plate boundary-layer values about cylinders normal to surfaces. Other studies with blunt fins and cylinders mounted on flat surfaces have provided the basic flow patterns in terms of the surface skin-friction line patterns, the upstream extent of interaction and surface pressures (Dolling, Cosad, and Bogdonoff 1978; Sedney and Kitchens 1976, 1975; Winkelmann 1970; Couch 1969; Mashburn 1969; Branstetter 1968; Young, Kaufman, and Korkegi 1968; Meyer 1968; Westkaemper 1968, 1967; Price and Stallings 1967; Thomas 1967), and the effect of sweep, plus surface and leading-edge heating rates (Bushnell 1965; Beckwith 1964; Hiers and Loubsky 1967; Surber 1965; Bloom and Pallone 1957).

The preceding comments in this section provide a framework within which to discuss the study of Meyer (1968), where the heat-transfer measurements about a rectangular protuberance on a rocket in flight were compared with high Reynolds number wind-tunnel measurements on a half-scale model. In support of the flight measurements of temperature and heat transfer, oil-flow visualization and surface pressures were obtained on the wind-tunnel model under conditions roughly corresponding with the flight data. The flight vehicle was a Bristol Aerospace of Canada, Black Brant III sounding rocket of 25 cm (10 in.) diameter fitted with a 5.4° semi-angle nose cone. The altitude attained in the tests was about 114 km (71 miles). Figure 119 shows the Reynolds number-Mach number history of the rocket flight, together with the wind-tunnel test points. It is clear that, although the wind-tunnel Reynolds numbers were somewhat below those obtained during the rocket flight, they were nonetheless high and should have provided a reasonable simulation. The undisturbed wall temperature conditions were, however, different: essentially an adiabatic wall for the wind-tunnel measurements and a moderately cold wall for the rocket measurements. The simulation was still considered reasonable as the differing wall temperature datum conditions should have had a relatively small effect on the flow development at these Mach numbers.

Figure 120a shows the geometry of the protuberance panel that was fitted into the side of the cylindrical section just downstream of the rocket nose cone, and the locations of the thermocouples on this panel. The material thickness of 3 mm (0.125 in.) was estimated to limit surface temperatures to less than 1,100° C (2,000° F). Instantaneous measurements of temperature during the flight were determined from the thermocouple voltages. Local heat transfers were calculated from the measured temperatures by treating every element of the panel skin as a calorimeter and assuming that there were no temperature differences across its thickness. The effects of heat conduction along the skin and radiation from it (particularly to the cold interior structure) were included. Data from the rocket instrumentation were passed to the ground station via telemetry.

Figure 120b shows the wind-tunnel model on which surface oil-flow visualization and pressure measurements were made, and gives the layout of the pressure measuring holes at locations corresponding closely with the flight thermocouples. In addition to the protuberance, static pressure holes were distributed in a row along a generator at 90° to the plane containing the centerline of the protuberance; a pitot rake for measuring the undisturbed boundary-layer profile and thickness was located on a generator diametrically opposite. The lengths of the pitot tubes were designed so they would be ahead of the position of the separation line about the base of the rake. Measurements were made in the wind tunnel at zero angle of attack at test Mach numbers of 2.00, 3.00, and 4.25 corresponding with the Reynolds numbers shown in Fig. 119. Measurements of the undisturbed pressure distribution on the cylindrical section of the wind-tunnel model showed the protuberance position to be downstream and essentially clear of the interaction effects between the corner expansion and the boundary layer at the cone-cylinder junction, except at Mach 4.25. The undisturbed turbulent boundary-layer profiles, in terms of local Mach number vs distance from the surface and at an axial station just upstream of the protuberance location, are shown in Fig. 121. The protuberance height (Fig. 120b) was nominally twice that of the oncoming boundary-layer thickness at all wind-tunnel test conditions. Figures 122a-122c show the wind-tunnel oil-flow patterns on the skin of the rocket and rectangular protuberance, all of which are qualitatively the same at the three supersonic Mach numbers (and slightly changing Reynolds numbers). These skin-friction line patterns on the rocket skin are analogous with the circular protuberance results of Sedney and Kitchens (1975) that are displayed in Fig. 35. For completeness, a sketch is included in Fig. 123 which provides a view of the separated flow along the axis of symmetry of

the protuberance that we have constructed from the oil-flow patterns. Note especially the reattachments at positions 1 to 5 where high heating rates will be expected. This centerline topology should be compared with the low-speed case proposed by J. C. R. Hunt et al. (1978), where in this plane, of course, all separation and attachment points will occur as half-saddles (see Sec. 2.7).

The distributions of static pressure coefficient C_p measured in the wind tunnel on the surface of the protuberance along its centerline and locally upstream and downstream, are presented in Fig. 124. Plotting in this manner, with distance along the surface normalized by the protuberance height L, results in a rough collapse of the data. The locations of the two reattachments numbered 1 and 2 in Fig. 123 are confirmed by pressure peaks, but the remaining mooted reattachment points occur presumably between the pressure holes on the model. With increasing free-stream Mach number from 2 to 4.25 we detect, in Fig. 124, that the normalized distance of the saddle points of primary separation (shown as $S_{2.0}$, $S_{3.0}$, and $S_{4.25}$) move upstream in accordance with the results of Sedney and Kitchens (1975, 1976), which are shown in Fig. 118.

The temperatures and heat-transfer rates measured in flight along the centerline of the protuberance are shown in Figs. 125 and 126 up to about 20 sec after the launch of the rocket. Temperature "hot spots" and maximum heat-transfer rates occur at the positions just ahead of the protuberance and front face corresponding with the positions of peak pressure measured in the wind tunnel. Figure 126 gives the normalized heat transfer H/HQ along the centerline of the protuberance; it is noted that except for the time of 4.7 sec these data correlate fairly well and follow closely the distributions of the surface pressure given in Fig. 124. The heat transfer on the surface ahead of the protuberance may be compared with heat-transfer data given in Burbank, Newlander, and Collins (1962) for the surface ahead of a circular cylinder standing normal to a flat plate. The data given here do not appear to have as smooth a monotonic increase as those obtained for the region ahead of the cylinder, although the maximum rates of heating are similar. Korkegi (1971) debates the differences between typical protuberance centerline pressure distributions and those measured in two-dimensional flow.

The effect of sweeping the leading edge of the protuberance from 0° to 30° decreases the extent of the separation region; at larger sweep angles up to 75° the separation zone continues its reduction in conjunction with a decline in the pressure peaks (see Price and Stallings 1967). Topham (1965) has shown that attachment-line heating rates along the leading edge of swept cylinders with laminar, transitional, and turbulent boundary layers can be correlated in terms of a Reynolds number based on spanwise momentum thickness along the attachment line. Evidence of transition was found up to Mach numbers of 10. The protuberance flow field illustrates the impressive and high heat-transfer rates that are encountered along lines of reattachment, where there is substantial lateral draining of the viscous fluid. Concomitantly, high-energy air from the external stream is encouraged to sweep down to the surface by the induction effect of the dominant vortex from the primary or horseshoe-shaped separation line. The turbulent case is virtually independent of Reynolds number, although Mach number and protuberance height do affect the extent of the separation zone. There are currently no analytical means of predicting protuberance interaction characteristics at high Mach numbers.

In closing this section, we should note that upstream of a supersonic jet exhausting into a supersonic stream (the typical reaction control jet problem on a hypersonic vehicle) there develops a flow field not unlike that found about the blunt protuberance. Measurements in these jet flow fields have been reported, for example, by Lukasiewicz (1963); Maurer (1966); Glagolev, Zubkov, and Panov (1967); Zakkay, Erdos, and Calarese (1968); Werle et al. (1970); and Driftmeyer (1974).

4.5 Corner Flows Involving Swept-Shock/Boundary-Layer Interactions

The supersonic inviscid-viscous interacting flow in axial corners occurs in external junctions on supersonic flight vehicles and in the internal corners of supersonic rectangular propulsion intakes. When one or both surfaces in the corner are deflected relative to the free stream to obtain compression, there will be intersections of shock waves with shock waves, and between shock waves and viscous flows on each surface. Thus, even though the geometry is simple, the flow fields are extremely complex. We should note that even in the rectangular corner intersection aligned with the free stream without the presence of shock waves, there is substantial skewing of the three-dimensional merged viscous flows (Bloom, Rubin, and Cresci 1969).

Korkegi (1971) provided a thorough review of corner flow interaction experiments, and the reader is encouraged to study that document for a broad appreciation of the earlier investigations. Since that time, the major advances have been in the computational prediction of such flows by numerically solving the Navier-Stokes equations — in laminar flow by Hung and MacCormack (1977), Shang and Hankey (1977); and using eddy viscosity models in turbulent flow by Hung and MacCormack (1978), Shang, Hankey, and Petty (1978), and Horstman and Hung (1979). In addition, the mean-flow characteristics of the 3D turbulent skewed viscous flows in Mach 2 to 4 interactions have been measured by Peake (1975) and Oskam (1976). Cooper and Hankey (1976) have reported laminar measurements at Mach 12.5.

4.5.1 Axial Corner With Only One Surface Providing Compression

Historically, the investigation of turbulent axial corner flows began with a configuration in which only one surface applied compression, and in which the measurement of a few surface pressures (Stalker 1957, 1960) coupled with surface oil-flow visualization (Stanbrook 1961) was undertaken. In these early experiments, and in many subsequent tests, a swept-back shock wave was generated by a wedge standing normal to a flat test surface, the shock impinging upon the previously undisturbed boundary layer, causing it to skew in the direction of the shock wave (Lowrie 1965; McCabe 1966; Law 1975; Peake and Rainbird 1975; Oskam et al. 1975; Cousteix and Houdeville 1976).

In the swept shock wave/turbulent boundary-layer interaction, the flow in the plane normal to both the shock wave and the wall is frequently described as resembling a two-dimensional flow through a normal shock (see Miller and Redeker 1963). Figure 127 presents a schematic diagram of skin-friction lines beneath swept shocks after Green (1970). In Figure 127a, we show schematically the result of a weak shock/boundary-layer interaction where although the skin-friction lines are deflected substantially more than the inviscid streamlines, they do not converge and there is no 3D separation. The small sketch on the right-hand side is a

view along the shock wave, showing a pattern and interaction analogous to that for a weak normal shock wave in nominally 2D flow.

With increasing shock strength, from small to larger static pressure ratios, a stage is reached in the flow development where 3D separation just begins, and important qualitative flow changes start to occur. When the pressure rise is sufficiently strong to cause a rapid convergence of the skin-friction lines, the picture might be that shown in Fig. 127b. The view along the shock wave might provide us with an "open" or "closed" separation bubble,[20] with a consequent lambda foot to the shock and a vortical slip line passing downstream from the triple point of the shock intersection. In the left-hand sketch, the "open" or "closed" bubble[20] commences at the 3D separation line upstream of the inviscid shock wave position. Skin-friction lines emanating from a reattachment line region downstream of the shock pass through the projected line of the inviscid shock to run asymptotically with the separation line. The upstream skin-friction lines run with the separation line from ahead of the shock. The skin-friction line patterns in laminar flow are qualitatively similar to those in turbulent flows, but a sharp change in inclination of the 3D separation line is observed as a skewed impinging shock wave crosses a region of boundary-layer transition. The line in turbulent flow lies at a greater sweepback angle relative to the free-stream direction than in laminar flow (Korkegi 1972).

The oil-dot flow visualization pictures in Fig. 128 (Peake, Jones, and Rainbird 1970) show skin-friction line patterns at pressure ratios, once turbulent separation has just begun at $M_\infty = 2$ (Fig. 128a); and with a very strong separated flow development at $M_\infty = 4$ (Fig. 128b). The shear stress is finite along the separation line that begins at the saddle point very close to the wedge apex, and the skin-friction lines are generally in the direction of the shock wave (Figs. 127 and 128). In the immediate neighborhood of the junction of the shock generator with the wall, where the interaction is spreading quickly, the scale of the separation normal to the wall increases with distance outward along the shock, tending from a conical type flow to one of cylindrical similitude far away from the shock generator. The nominal flow conicity near the wedge allows us to represent the flow field in terms of the characteristics of conical flow or crossflow projections. We should understand that the details of the skin-friction lines around the intersection of the finite radius wedge nose with the plate will be as in the blunt protuberance flow in Fig. 35. We remember that the divergent reattachment line region begins at an attachment node on the plate situated very close to the leading edge of the cylinder. It is the continuation of this reattachment line downstream that is evident as a line from which adjacent skin-friction lines diverge close to the wedge-plate junction – see Fig. 128b.

Typical surface heating and surface pressure profiles normalized with respect to undisturbed values are shown in Fig. 129 (Scuderi 1978) corresponding with the separated flow cases illustrated in Figs. 127b and 128, for which the pressure ratio across the shock wave is typically greater than 1.5. We see that the free-stream flow is compressed through a compression fan as it approaches the shock wave. An initial pressure rise then occurs between the "extent of disturbance" and the shock wave position in the free stream (see Fig. 129). On the downstream side of the shock, a second higher pressure occurs, close to the wall of the wedge. The heat-transfer data follow the character of the pressure distribution. At pressure ratios across the shock of typically less than 1.5 (corresponding with Fig. 127a) both pressure and heating profiles rise smoothly from undisturbed values to maximum values near the wedge.

Some relatively simple correlations have been derived by Scuderi (1978) from the results of Neumann and Burke (1968); Token (1974); Peake and Rainbird (1975); Oskam et al. (1975); and Christophel et al. (1975), to provide a prediction base for both pressures and heating rates resulting from 3D shock wave, turbulent boundary-layer interactions. If x_0 is the distance of wetted run of undisturbed turbulent boundary layer to the leading edge of the wedge, and x_p the axial distance from the wedge leading edge to the point at which peak pressure p_p occurs, then the maximum heating h_p close to the wedge was expressed by Scuderi (1978) as:

$$\frac{h_p}{h_0} = \left[1.2\left(\frac{p_p}{p_\infty}\right)^{2.85} + 0.2\right]\left(1 + \frac{x_p}{x_0}\right)^{0.2}$$

The form of the equation reflects the dominance of the overall static-pressure ratio on the heating. Other correlations have been provided by Neumann and Hayes (1977) for fin/plate and fin/ogive-cylinder interactions. Hayes (1977) has provided an overview of recent work in the latter configuration when the body of revolution is at angle of attack and there are gaps between the fin and the body.

There has been continuous debate over many years regarding the concept of "incipient separation" in two-dimensional flows, and more recently, as to whether the concept is even meaningful in three-dimensional viscous flows (see Peake and Rainbird 1976). Some observers, for example, Stanbrook (1961) have noted the appearance of three inflection points in the streamwise wall static pressure distribution at incipient separation, as in 2D flow (Kuehn 1959) concurrent with the skin-friction lines running "parallel" with the shock wave at their maximum deflection. Others have proposed that incipient separation occurs when the skin-friction lines first converge toward an "envelope" (McCabe 1966); or when the upstream surface shear stress trajectories converge into one line that is parallel to the surface shear stress trajectories downstream of it (Lowrie 1965, using the criterion of Rogers and Hall 1960). According to our ideas of continuous skin-friction lines existing in association with a limited number of singular points, the asymptotic behavior must be the chosen form.

The length of the swept interaction in the streamwise sense depends on the pressure ratio across the shock wave, the nature of the disturbance causing it, and the upstream Mach number, Reynolds number, and oncoming boundary-layer thickness, δ_0. The latter has been commonly used as a scaling parameter for streamwise distance through the interaction, utilizing the inviscid shock wave position as origin. Equally well, the streamwise displacement thickness would also be suitable. The streamwise momentum thickness is also a characteristic parameter for scaling purposes, for it changes rapidly with distance through the interaction, but varies only slowly in regions of constant pressure upstream and downstream of the interaction. (In

[20] In the light of later evidence, the likelihood of a closed, swept separation bubble is considered remote.

contrast, we recollect from Sec. 4.4 that the location of the saddle point of separation upstream of the bluff protuberance in turbulent supersonic flow tends to scale with cylinder diameter rather than with boundary-layer parameters.) Korkegi (1973) found that a simple correlation exists for incipient turbulent boundary-layer separation due to a skewed shock wave. He took the incipient separation data of McCabe (1966) and Lowrie (1965) along with the corresponding shock wave angles, Mach numbers, and pressure rises, and concluded that the flow-deflection angle at incipient separation θ_{wi}, was inversely proportional to the upstream mainstream Mach number, where

$$\theta_{wi} = \frac{0.3}{M_\infty}$$

Korkegi also proposed that incipient separation occurred at an approximate constant pressure rise, $p_i/p_\infty = 1.5$, and independently of Mach number, at least over the range of $2 < M_\infty < 3.4$. (We note that such behavior is contrary to that for two-dimensional turbulent boundary-layer separation, where θ_{wi} and p_i/p_∞ both increase with increase of M_∞.) By comparison, Goldberg (1973) has reported that the angle for 3D incipient separation at $M_\infty = 5.9$ is virtually insensitive to Reynolds number based on boundary-layer thickness in the range $10^5 < R_{\delta_3} < 10^6$, and is about 9°. This result, however, is not consistent with an extrapolation of Korkegi's correlation.

Figure 130 illustrates the crossflow in a swept shock-wave/laminar boundary-layer interaction at $M_\infty = 6$, by means of vapor-screen flow visualization (D. S. Rao 1978: private communication). The photographs indicate the gradual thickening of the viscous flow through incipient separation to a strongly separated structure. Incipient separation is simply the condition at which the overall pressure ratio across the swept shock wave causes the flow to leave the surface; the wedge angles for incipient separation from various experiments are shown beneath the photographs along with the correlation of Korkegi (1973). At the wedge deflection angle of 12° in Fig. 130, there is a clear indication of a flattened vortex structure, with a rolled-up and stable free shear layer passing downstream toward the observer.

Figure 131 is an enlargement of one of the vapor-screen pictures of D. S. Rao (1978: private communication), showing his labeling of the flow field. (Note the reflection of the rolled-up shear layer in the floor beneath.) Bertram and Henderson (1969) have reported similar pictures using electron-beam flow visualization in axial corners with both surfaces producing compression. One should note the resemblance of the axial corner flow with the flattened vortex structure illustrated by Sedney and Kitchens (1975) about the blunt protuberance in Fig. 35.

The swept-shock/laminar boundary-layer interaction flow model in Fig. 132 is a schematic representation (due to D. S. Rao 1978: private communication) of that shown on the vapor-screen flow visualization photograph of Fig. 131. This figure is introduced to provide conceptually a reason for the high peak of surface heat transfer very close to the wedge-plate intersection (Fig. 129). Cooper and Hankey (1974) and Rao conceive that the vortical layer ("jet") emanating from the triple-point of the lambda foot of the shock wave moves toward the surface and impinges on the surface where the skin-friction lines diverge rapidly (the reattachment line in Fig. 127b). The induction effect of the coiled free shear layer will encourage, of course, (virtual) free-stream air to be diverted toward the surface and provide high heating. It is also possible that the vortical layer from the triple point meets the wedge surface at the location where the wedge boundary layer is shown to be very thin in Fig. 132. Notwithstanding, the inviscid flow computations of the external flow shock-wave patterns (see Sec. 4.5.3) appear to support the former conjecture.

The mean flow details in the viscous flow field of the swept-shock/turbulent boundary-layer interaction have been provided by Peake and Rainbird (1975) and Peake (1975) at free-stream Mach numbers 2 and 4, and by Oskam, Bogdonoff, and Vas (1975); Oskam, Vas, and Bogdonoff (1975, 1976); and Oskam (1976) at Mach 3. Horstman and Hung (1979) have examined these experimental results and compared them with calculations employing time-dependent, compressible Navier-Stokes equations, with Reynolds mass-averaged variables. Bulk viscosity and the specific turbulent energy in the normal stress terms are omitted, so that the equations are complementary with laminar flow, except for the addition of the Reynolds stress tensor and the Reynolds heat flux. The former was expressed in terms of the product of an isotropic eddy viscosity and mean velocity gradient and a turbulent Prandtl number was used for the latter. The equations and details of the numerical analysis are provided in Hung and MacCormack (1977, 1978).

Figure 133 presents a comparison between the calculations of Horstman and Hung (1979) and the Mach 3, 10° wedge flow of Oskam (1976). The coordinate system is shown in Fig. 129. This is a 3D separated flow, where, as shown in Fig. 133, streamlines originating near the surface at $0.05\ \delta_0$ converge and lift off the surface, as we would expect from the discussion in Sec. 2.3 (and see Fig. 12). Figures 134 and 135 show the very good agreement that exists between the computed and measured streamwise and crossflow velocity profiles. Figures 136 and 137 show the computed and measured wall pressures, skin friction, heat transfer in the x and y directions, and limiting streamline angles. For each parameter, the computations predict the experimental points to a remarkable degree. Similar measurements by Peake (1975) at Mach 2 and for a wedge deflection of 8° are also predicted closely.

Horstman and Hung (1979) also computed the very strong viscous-inviscid interaction case of Peake (1975), in which experimental measurements were made with a wedge angle of 16° at Mach 4, the skin-friction line directions of which are shown in Fig. 128b. Here the converging of the skin-friction lines is ahead of the projection on the surface of the shock wave in the inviscid flow, and there is a massive eruption of streamlines away from the surface at the 3D separation line, as the calculations show in Fig. 138. The computed resultant velocity vectors of the limiting streamlines are shown in Fig. 139, with the 3D separation line and inviscid shock-wave positions marked. Close to the inviscid shock line, we can detect inflexions in the limiting streamline directions along a ray from the nose of the shock generator; the inflexions are characteristic of a vortex core existing above the surface (see the case of the slender wing flow in Fig. 18). Evidence of the rotational flow is given in Horstman and Hung (1979), but the reader is cautioned to be aware of the different values of component velocities perceived depending on the plane of projection. Figure 140, for instance, shows the velocity components resolved normal to the direction of the vortex core (at 26° to the free-stream direction in Fig. 139); but presented in a cut perpendicular to the undisturbed stream at

$x'/\delta_0 = 9$. Because this is not a conical flow projection, we do not see a crossflow separation profile at the 3D separation line position at $y/\delta_0 = 9.7$ (actually off the figure). Since the velocities are perpendicular to the core, however, the identity of the vortex from the 3D separation line is established. Even for this very strong interaction case, the computation of Horstman and Hung (1979) provided quite satisfactory prediction of surface conditions and velocity profiles (Figs. 141 and 142).

In summary, the turbulent mean flow in an axial corner with one surface of compression has been satisfactorily diagnosed by experiment and predicted by a Navier-Stokes calculation incorporating the simplest of eddy viscosity models (Horstman and Hung 1979). The boundary-layer method of Nash and Scruggs (1978), on the other hand, provided less satisfactory agreement with the data of Peake (1975) (especially skin-friction line directions) for an unseparated case at a wedge angle of $\theta = 8°$ at Mach 2. In contrast, an integral boundary-layer scheme of Cousteix and Houdeville (1976) yielded quite reasonable agreement with their own Mach 2.3 test results for a $\theta = 6°$ wedge deflection. On balance, it would appear that adequate simulation of the inviscid-viscous interaction, especially when the shock wave is strong, requires a solution based on the Navier-Stokes equations. Fortunately, the mean-flow details can be reproduced with a high degree of accuracy by employing the simplest of turbulence models.[21]

4.5.2 Secondary Separation in Axial Corner with One Compression Surface

Korkegi (1976) draws attention to the close degree of qualitative agreement obtained in nominally conical laminar and turbulent corner interactions. Laminar data (e.g., Watson and Weinstein 1970; Cooper and Hankey 1974; Charwatt and Redekeopp 1967) show extensive regions of 3D separation that are comparable in extent with turbulent flows at very large wedge angles (Freeman and Korkegi 1975; Law 1975; Neumann and Token 1974). For very strong skewed shock interactions with turbulent boundary layers, a second line of oil accumulation is obtained indicative of secondary separation, as shown in Fig. 143a from Law (1975). The striking resemblance to the skin-friction lines on the leeward side of the circular cone that was discussed in Sec. 4.1 should be noted. The details in Fig. 143a for a turbulent flow at Mach 6 with wedge angle of 20° are virtually identical with the laminar flow at Mach 12.5 with wedge angle of 15° reported by Cooper and Hankey (1974) (shown in Fig. 143b). In both illustrations, a reattachment line associated with the primary vortex is very close to the corner formed by the vertical wedge and the plate. There is also a second reattachment line between the two separation lines, as we saw on the cone flow in Figs. 59e and 59f. Figure 144 provides the pitot pressure contours in the laminar Mach 12.5 flow of Cooper and Hankey (1974), displaying the positions of peak shear and heating close to the wedge at the reattachment line A_1 (see Fig. 143). The vortex from the primary separation line would appear responsible for the "low" region with the secondary separation providing a smaller coiled flow of opposite rotation, tucked beneath the primary flow (just as on the cone). Heat-transfer rates, which we have discussed already, are highest along reattachment lines; they exhibit two peaks in the cases of the extensive 3D laminar and turbulent separation, consistent with the observations of two reattachment line regions in Figs. 143 and 144. The spanwise pressure distributions for these large-deflection laminar and turbulent cases also show qualitative agreement (Korkegi 1976).

Shang and Hankey (1977) have provided impressive results from a computation to compare with the laminar data of Cooper and Hankey (1974), using the unsteady compressible 3D Navier-Stokes equations in conservative form. The equations of state, Sutherland's viscosity law, and an assigned Prandtl number closed the system of equations. The lower illustration in Fig. 143 is the computed resultant magnitude of surface shear stress, plotted as its cube root, to prevent substantial overlapping of the vectors. We see evidence that all of the essential features of the oil-flow visualization in terms of convergence and divergence of skin-friction lines are duplicated in the computation. Especially notable is the high shear stress close to the corner where the maximum peaks in surface pressure (Fig. 145a) and heat-transfer rate (Fig. 145b) are found at position A_1, Fig. 143. We notice, in addition, in Fig. 145b, the high total temperatures near the plate surface in the flow at this location. In Fig. 145c, the conical crossflow velocity component is projected onto the y-z plane. The crossflow velocities make a sharp turn toward the corner intersection as they pass through the shock wave generated by the wedge. Beneath the triple point, the crossflow turns 180°, indicating a vortex center, as shown in Fig. 145d. A thin boundary layer is shown on the wedge surface flowing toward the corner. The initial development of the S-shaped crossflow profile farthest from the corner specifies the primary separation line position at approximately $y = 18$ cm (7 in.) (Fig. 145c). The resolution available on the latter illustration prevents us from identifying the relatively small region of secondary separated flow. Figures 145c and 145d indicate that the crossflow well away from the surface enters the corner region beneath the triple point, bringing with it a high level of energy to the region of A_1. The graph of Fig. 145d defines the supersonic zones of the flow field, showing it to be subsonic beneath the triple-point region. However, there is an area of embedded supersonic crossflow just above the plate and about 2.5 cm (1 in.) from the corner. Shang and Hankey (1977) surmise that it is the existence of this supersonic region, followed by a compression shock wave, that produces the secondary separation and vortex. Thus, it is evident that the hypersonic laminar corner flow with secondary separation can be predicted very successfully by the Navier-Stokes computation of Shang and Hankey (1977). These authors have recently extended their method to incorporate an eddy viscosity model to predict turbulent corner interactions (Shang, Hankey, and Petty 1978).

4.5.3 Axial Corner Comprised of Two Intersecting Wedges

The classic laminar flow experimental investigation by Charwat and Redekeopp (1967) in the Mach range of 2.5 to 4, established the salient features of the inviscid flow and intersecting shock waves, although no corner vortices were reported. The basic shock wave structures, essentially conical in nature, that were synthesized by Charwat and Redekeopp (1967) from extensive pitot pressure measurements, are shown isometrically in Fig. 146. The shock waves generated by each wedge are joined by the third shock wave, bordering Zone I and the free-stream flow. Slip surfaces pass from the ends of this third shock towards the corner. Additional shock legs proceed to the surface — a curved shock between Zones II and III, and a spread of the corner disturbance outside of the inner shocks (Zone III) beyond which the flow is nominally two-dimensional, Zone IV. Subsequent investigations in supersonic and in hypersonic flow have revealed essentially the same flow features (Cresci et al. 1969; Watson and Weinstein 1970; West and Korkegi 1972; Nangia 1974; Freeman

[21] See also Shang, Hankey, and Petty (1978, 1979).

Korkegi 1975). Bertram and Henderson (1969), with their sweeping electron-beam flow visualization technique, and Kipke and Hummel (1975), produced strong evidence of corner vortices.

Use of the shock-capturing technique in inviscid flow calculations (Kutler 1973, 1974a,b; Shankar, Anderson, and Kutler 1975; Kutler et al. 1975) provides a reasonable description of the wave structures. For example, Fig. 147a shows a calculation of contours of constant density (Shankar, Anderson, and Kutler 1975) in a transverse plane of one of the corner flows for which measurements by Charwat and Redekeopp (1967) exist. We see that the dominant laminar viscous flow displaces the wave structure outward, when compared with the inviscid flow numerical results. Differences in detail are also shown between the shock-wave shapes from the experiment and calculation, and in the surface pressure distributions shown in Fig. 147b. The experimental results of Nangia (1974), on the other hand, were for turbulent flow, and the experimental shock positions in Fig. 148a show closer agreement with results of inviscid flow calculations. The "effective thickening" of the body by the turbulent flow is obviously less than in laminar flow and accounts for the improvement between the experimental results and the inviscid theory results. Good correspondence is also obtained between the surface pressures (Fig. 145b). Other very interesting comparisons are shown in the calculations of Kutler et al. (1975) and the experiments of Nangia (1974), when the intersecting surfaces are at different wedge angles, when one of the surfaces causes an expansion flow, and when the leading edge of one wedge is swept back.

In spite of the relatively good prediction of the shock-wave structures, the corner problem must still be viewed as an inviscid-viscous interacting flow problem, for as we have seen in Secs. 4.5.1 and 4.5.2, we are dealing with 3D swept separations and ensuing vortical flows. In fact, Charwat and Redekeopp (1967) remark that at the foot of the shock leg between Zones III and IV (see Fig. 146), a line of oil accumulation was observed, signifying a swept 3D separation line. Figure 149, from Bertram and Henderson (1969), features representative oil-flow, heat-transfer, and surface-pressure data from laminar flow experiments with intersecting wedges of equal compression angles. Measurements from Langley Research Center at Mach 20 are shown on the top in Fig. 149; the Mach 3 results of Charwat and Redekeopp are shown below.

On the oil-flow pattern at Mach 20, we detect two lines of converging skin-friction lines representative of two separation lines, providing primary and secondary separations as discussed in the previous section. Two lines representing the locus of inflections in the skin-friction line patterns are indicative of the existence of both primary and secondary vortices. The pitot-pressure traverses by Charwat and Redekeopp (1967) also indicate primary and secondary separations. Both pressure distributions exhibit a sharp rise and a plateau associated with the inner shock structure, following a more gentle rise over Zone III (Fig. 146). The heat-transfer distributions exhibit a marked trough at the primary separation line position, followed by a rapid rise to two peaks, corresponding with the two divergent reattachment line locations on the oil-flow pattern. The drop in heat transfer at the wedge intersection, which is also shown by Stainback and Weinstein (1967) and Cresci (1966), is attributed by Korkegi (1971) to the mutual interaction and thickening of the combining shear flows.

Although the above discussion deals with 90° corners, studies have been made with corner angles varying from 60° to 270° (Cresci 1966; Stainback and Weinstein 1967; Watson and Weinstein 1970; Kipke 1973; Kipke and Hummel 1975). With decreasing corner angle, higher pressures and heat rates develop, accompanied by an outward displacement of the inner shock wave. The complete analytical definition of the strong viscous-inviscid interaction in corners with two compression surfaces will presumably be accomplished in due course via Navier-Stokes computations.

4.5.4 Waves From a Supersonic Inlet Interacting With Flows on Adjacent Surfaces

The half-cone or quarter-cone inlet mounted adjacent to a fuselage sidewall and wing/fuselage intersection may cause a substantial problem of swept shock wave/turbulent boundary-layer interaction, particularly at off-design conditions. The intake is usually raised from the fuselage surface to permit both bleeding and diversion of the oncoming viscous flows (Faro 1965).

Figure 150 shows an oil-flow pattern taken by Culley (1972a,b) about a $\theta_c = 25°$ half-cone intake at Mach 1.6 and at a Reynolds number of 6×10^6, based on the wetted run to the intake capture face of 5 cm (2 in.) diameter. The inlet was operating at design shock cone position and at maximum mass flow (with some spillage, as seen on the Schlieren photograph). Even though auxiliary ram (bleed) intakes were located in the plane of the cowl lip to ingest the turbulent fuselage boundary layer, there was clearly a substantial diversion of the fuselage boundary layer upstream of the bleed ducts. The fuselage flow was three-dimensionally separated by intersection with the intake pressure field, the separation line coinciding approximately with the projection of the cone shock on the fuselage wall. Thus it would appear that the most deficient portion of the fuselage boundary layer is spilled as vortices into the airplane flow field.

As an initial step in predicting this flow field, a calculation of the partial cone flow itself about the same $\theta_c = 25°$ half-cone at Mach 1.6 was performed (Peake, Jones, and Rainbird 1970) but without a reflection plane. The pressure field that would be impressed upon the fuselage is approximately that existing between the shock wave and the half-cone, as shown in Fig. 151. The maximum overall pressure ratio between the shock and the cone is greater than 1.5, so that, as we saw in Sec. 4.5.1, 3D separation would be expected.

Culley (1972b, 1975) also showed that with a quarter axisymmetric intake model, the use of a splitter plate to isolate the airframe boundary layer from the adverse influence of the intake could involve a multishock viscous compression and 3D separation of the fuselage boundary layer upstream of the splitter plate (Fig. 152) that was not influenced by variations in the intake mass flow.

Other serious swept-shock/boundary-layer interaction problems in propulsion layouts may be encountered beneath supersonic wing planforms when designers attempt to take advantage of "favorable interference" effects (Swan 1965; Sigalla and Hallstaff 1967) from compressions about engine nacelles and boundary-layer diverters.

Figure 153a shows the oil-dot flow pattern on the undersurface of a lifting 70° delta wing at $C_L = 0.08$ in a free-stream flow of $M_\infty = 2.75$ at a Reynolds number, based on the maximum wing chord, of 24×10^6 (Peake and Rainbird 1973). The four nacelle arrangement is typical in position and scale of a supersonic transport layout. The two uppermost intakes were operating at design mass flow with cone shock on lip. One will note a small region of three-dimensional separation caused by the wedge-shaped pylons (diverters) and cowl pressure field in Fig. 153b, where the propulsion nacelles have been removed to facilitate inspection of the oil flow. The lower pair of intakes was throttled internally to about 70% design mass flow, forcing the throat normal shock outside of the cowl lip. The result of operating subcritically is to cause a massive three-dimensional separation of the starboard under-wing boundary layer and high local heat-transfer rates in the reattachment regions downstream of the separation. Figure 153c exhibits a postulated pattern of singular points and skin-friction lines in the vicinity where the adjacent separation lines interfere with each other. The interference appears to result in the formation of a nodal point of separation (like that shown on the cylinder flare in Fig. 48e) interspersed between the two saddle points immediately ahead of each wedge-shaped diverter. A sketch of the streamlines in the streamwise plane of symmetry passing through the node of separation is also given in Fig. 153c. The accompanying changes in lift are shown in Fig. 154. At a cruise lift coefficient of 0.08, occurring at an angle of attack of about 3° for this symmetrical wing, there is a 20% increase in lift from the throttling of the 4 intakes to 70% of the design mass flow; the corresponding increase in drag for subcritical operation is illustrated in Fig. 155. At off-design Mach numbers, the shock/boundary-layer interactions and resulting 3D separations may be even more severe in their effects on drag.

From these cursory glimpses at two examples of propulsion inlets, we see that the intersecting wedge corner flow studies provide us with a substantial basis for diagnosing the flow features in other complex geometries.

4.6 Shock-on-Shock Interactions

The most serious surface heating problem encountered in hypersonic vehicle design is the result of shock-on-shock interactions in proximity to the vehicle skin. Extremely high heat-transfer rates, many times ordinary stagnation-point values, may occur in relatively small regions on the vehicle surface accompanied by high pressure peaks that complicate the design of the thermal protective skin (Keyes and Hains 1973; Hains and Keyes 1972). Unlike an ordinary stagnation point, the location of the region of peak heating is not well defined and the interaction region will move about on the body depending on Mach number, altitude, and vehicle attitude. Figure 156, for example, shows practical examples of shock-impingement heating (Edney 1968); Fig. 157 reveals the shock-wave shapes and aerodynamic interference heating about a model of the Space Shuttle Orbiter matched to its external hydrogen-oxygen tank, from a test combining Schlieren and phase-change coating techniques (Creel and J. L. Hunt 1972). Probably the first in-flight confirmation of the severity of shock impingement heating was the damage to the ventral fin of the NASA X-15A-2 rocket-driven airplane during a high-altitude flight at Mach 6.7. The unswept ventral fin supported a ramjet test model (Fig. 158a) that came adrift from the airplane during flight as a result of the catastrophic shock-impingement heating damage (Figs. 158b and 158c).

Leading-edge sweep was found early to have a marked influence on shock-impingement heating. For highly swept cylinders or fins, near 45° or more, no local increases in heating are observed (Beckwith 1964; Bushnell 1965; Hiers and Loubsky 1967; Gulbran et al. 1967) and leading-edge heating rates are found to be reasonably well predicted by simple infinite swept cylinder theories using local flow conditions. For upswept or moderately swept cylinders, high local heating is noted at the leading edge in the vicinity of the intersection of the external shock with the cylinder bow wave (Hiers and Loubsky 1967; Newlander 1961; Gulbran et al. 1967; Bushnell 1968). Heat peaks as high as 10 times stagnation values had been observed in the earlier work, as shown in Fig. 159. The very localized nature of the heat peak due to shock impingement is illustrated by the relatively narrow "burn through" on the fin in Fig. 158.

The apparent anomaly in leading-edge heating between unswept or moderately swept configurations and highly swept ones is, however, easily explained (Korkegi 1971). The heat peak has been associated with the impingement of a "jet-type" shear layer originating at the intersection of the external shock and bow shock of the blunt fin. For high sweep angles the shear layer does not impinge on the leading edge, but rather flows tangentially to it and, therefore, no heat peak is observed. This explanation is basically correct; however, the flow structure for low-sweep angles is considerably more complex than that of a simple shear layer, as will be discussed further on. Although early investigators identified the problem of shock impingement and contributed much needed data on local heat rates, it was not until the extensive and pioneering study of Edney (1968), who obtained exceptionally high-quality Schlieren photographs, that an understanding of the interference flow field was gained. Edney categorized shock interference patterns into the six types that are shown in Fig. 160a (Hains and Keyes 1972). In the sketch of each type, A is the impinging shock wave, B is the bow shock wave around the body, and C is the interference region on the body where peak heating and peak pressures are found. Shock-wave/boundary-layer interactions are found in Types I, II, and V, and shear-layer attachment is observed in Type III. Type VI interaction is characterized by an expansion-fan/boundary-layer interaction that lowers the heat transfer. The Type IV interaction produces intense heat-transfer rates and pressure peaks from the impingement of the "jet-type" shear layer on the body surface. Correlations of peak heating resulting from Types I, II, III, and V are presented in Keyes and Morris (1972). Some typical levels of peak heating are marked in Fig. 160a also. The quantity Q_{ref} is the stagnation point heating without interference, but with identical free-stream conditions. The regions where interference heating may be found on a Shuttle plus Booster during ascent are also given in Fig. 160a. Interference heating can occur on the wing and tail surfaces, in the gap region between the vehicles, on the nose of the Orbiter, and on deflected control flaps. Figure 160b shows where the respective interference types would be located on a hemisphere.

Figure 161 (Hains and Keyes 1972) illustrates the interfering shock patterns on the mated Shuttle and Booster during ascent. At low supersonic Mach numbers, the bow shock wave encases the entire configuration and there is no interference. As the vehicle accelerates to hypersonic Mach numbers, Type V or VI interference can be recognized on the upper surface of the Orbiter, with associated heat transfer rates up to five times stagnation values. As Mach number increases still further, the interaction moves to the nose region of the Orbiter and Type IV and III patterns develop. It is here that the largest heat-transfer rates

will develop, up to at least 20 times the stagnation point condition. (In Type III flow, the surface heat transfer in the attachment region depends strongly on whether the shear layer is turbulent; Birch and Keyes 1972.) Real gas effects will probably enhance this value. Still further increases in flight Mach number lead to Type II and then to a Type I pattern. We note that the bow shock waves may reflect back and forth several times in the gap region between the vehicles, producing hot spots at many locations along the fuselages. Detailed heating measurements for off-centerline shock interference on hemispheres and fins were presented in Keyes (1973).

Clearly, the flight trajectory has an important effect on the heat transfer. Hains and Keyes (1972) calculated the peak heat-transfer amplification for Type IV interference on a typical Shuttle ascent trajectory (assuming the ratio of specific heats $\gamma = 1.4$) up to 76 km (250,000 ft). Figure 162 indicates that Type IV interference could not develop below an altitude of 38 km (125,000 ft). Notwithstanding, depending on the number of local wave reflections in the "jet flow" to the surface, enormous peak heat-transfer amplifications -- between 20 and 37 times the stagnation point rate -- were computed, corresponding with the "jet bow shock" located in Region 7 or 8 (see Fig. 163). Figure 164 illustrates shock-on-shock interactions about the mated configuration at Mach 20.

Because the experiments of Edney (1968) are classic in their definition of the shock-on-shock structures, let us conclude this section with a discussion due to Korkegi (1971) on the effect of varying the sweep angle of a cylindrical leading-edge fin on a flow interference pattern at Mach 4.6, and with a wedge deflection angle of 5° (Fig. 165). The three types of interference flow fields associated with positive sweep (namely Types IV, V, and VI) that are the most likely to be encountered on vehicle wings and vertical control surfaces (see Fig. 164) are shown in Fig. 165 (after Edney 1968).

Figure 165a shows a typical interference structure for an unswept configuration, with a break in the bow shock and a supersonic jet in the otherwise subsonic shock layer, which impinges on the leading edge. The supersonic jet, which includes embedded shocks, is bounded by shear layers and its exact structure is dependent on the bow-shock detachment distance in relation to viscous effects, that is, on some Reynolds number. Because the shock layer flow is subsonic, the structure of the bow shock in the neighborhood of its intersection with the external shock is not readily predictable. Thus, this type of interaction, which results in the highest heat rates, is the most complex and least understood of any encountered in practical applications. Figure 165b shows a moderately swept configuration for which the shock-layer flow is slightly supersonic. The jet has thinned considerably and a shear layer originates at the intersection of the bow wave with an embedded shock, behind which the flow is locally subsonic. Edney (1968) points out that the jet and shear layer may strike the leading edge far downstream of the impingement point, where, because of diffusion, their influence on heat rates will be considerably less than for the unswept case. The embedded shock impinging on the leading edge may cause a local separation and boundary-layer transition. In Fig. 165c, resembling a highly swept edge, the shock-layer flow is entirely supersonic and the shear layer misses the surface; hence, high heat rates do not arise. It is for this configuration that simple infinite swept cylinder theories have been found to adequately predict heat rates when local flow conditions are used (Beckwith 1964; Hiers and Loubsky 1967; Bushnell 1968).

Summarizing, shock-on-shock interactions close to the vehicle skin can result in the largest heating rates against which the designer must protect the vehicle -- rates as high as 20 times (or more) the local stagnation point heat-transfer rate. The Type IV interaction classified by Edney (1968), with its impinging jet flow, is the most complex and, unfortunately, provides the highest heat transfers (and associated peak pressures). Calculations in two dimensions based on the Navier-Stokes equations and using a time-dependent, finite-difference method, have been attempted by Tannehill, Holst, and Rakich (1976). Their results indicate that in principle all six types of Edney's classifications can be computed. In inviscid flow, in another application, Kutler and Sakell (1975) computed the unsteady three-dimensional flow field resulting from the interaction of a plane shock wave with a cone-shaped vehicle traveling supersonically.

4.7 Supersonic and Hypersonic Delta Wings

The regions of application of various aircraft types in terms of slenderness ratio vs flight Mach number were illustrated in Fig. 3d. There it was indicated that delta wings (and possibly wave-riders) were potential shapes for vehicles flying at supersonic and hypersonic Mach numbers. Consequently, there has been a substantial effort to diagnose the flows over delta wings with supersonic leading edges (i.e., when the component of Mach number, M_N, normal to the leading edge exceeds 1) to parallel the clear understanding that we already possess of flows over slender configurations with subsonic leading edges (such as the "Concorde"). Wilde and Cormery (1970) and Leyman and Markham (1974), in fact, provide retrospective but very useful accounts of the aerodynamic derivation of the "Concorde" wing, and an overall philosophy of predicting the aerodynamic characteristics of supersonic transport aircraft. A survey of lee-side flow phenomena on supersonic and hypersonic delta planforms has been provided by Dunavant, Narayan, and Walberg (1976).

In general, the flow over a delta wing at angle of attack changes from one dominated by leading-edge separation when $M_N < 1$, to a flow that is characterized, when $M_N > 1$, by a Prandtl-Meyer expansion inboard of the bow shock and an attached flow at the leading edge. These two flow fields over flat-topped, sharply swept delta wings are illustrated in Fig. 166. In the case of the subsonic leading edge in Fig. 166a, the particular feature at moderate to high angles of attack is the existence of a secondary separation and dividing surface that rolls up beneath the primary vortex (see also Fig. 18). The boundary layer growing from A_2 toward this secondary separation, S_2, is relatively thin. In the flow about the supersonic leading edge shown in Fig. 166b, there is an attached boundary layer beneath the expansion fan from the leading edge (Fig. 167). This region of Prandtl-Meyer attached flow eventually terminates at an embedded shock wave that causes the formation of a swept 3D separation line, well inboard from the leading edge (Cross 1968). The dividing surface coils up from this inboard separation line, but stays within the depth of the viscous layer, whose edge is at a height of about 1 wing semispan above the leeward surface (see the Mach 12 vapor-screen crossflow picture in Fig. 168). The regimes of leading-edge separation and Prandtl-Meyer attached flow (followed by shock-induced separation) can also be distinguished on the basis of spanwise vortex position vs angle of attack, α_N. Figure 169 illustrates that the core positions for the flow with leading-edge separation are situated, in general, much closer to the wing tip than are the shock-induced vortex cores.

Among parameters also affecting the occurrence of leading-edge separation or shock-induced separation, is wing thickness. Figure 170a illustrates these two differing leading-edge conditions about "thin" wings where the maximum thickness-to-chord ratio is typically $\lesssim 0.2$. Note the opposite directions of the skin-friction lines near the leading edge – toward the edge for separation at the leading edge, and away from the edge for separation inboard. For thick wings with supersonic leading edges and with thickness-to-chord ratios $\gtrsim 0.3$, Szodruch (1977) and Narayan (1978) have postulated some changes to the basic shock-induced separation patterns that are dependent on angle of attack and order of the viscous interaction parameter[22] χ, as we see in Fig. 170b. How and when these changes in flow structure occur will be discussed in the following paragraphs.

The parameters of wing sweep, free-stream Mach number, and angle of attack may be effectively collapsed into the component of Mach number normal to the leading edge M_N, and the angle of attack in the same plane α_N; see the inset sketch at the top of Fig. 171. In the $\alpha_N - M_N$ plane, Stanbrook and Squire (1964) gave broad limits for the occurrence of either the subsonic or supersonic leading-edge flow regimes for thin, sharp wings;[23] the boundary curve in the $\alpha_N - M_N$ plane has come to be known as the "Stanbrook-Squire Boundary" as we see in the main illustration of Fig. 171. The experiments of Szodruch (1977) (which were partly summarized in Szodruch and Ganzer 1979) revealed, however, that for a thick delta wing, shock-induced separation (region 5 in Fig. 171) occurred at much higher values of Mach number M_N than given by the right-hand side of the Stanbrook-Squire Boundary; furthermore, the additional separated-flow regimes schematically drawn in Fig. 170b could be represented on the $\alpha_N - M_N$ diagram in Fig. 171 as regions 4 and 6. Again, the width and extent of these new boundaries cannot yet be defined precisely. In the view of Szodruch (1977), the flow in region 4 is characterized by a swept separation bubble beginning at or close to the leading edge, whereas Rao and Whitehead (1972) labeled this flow as one with "embedded vortices." Szodruch (1977) also added two more regions in Fig. 171, those numbered 1 and 3. In region 1, with the wing at very high angle of attack and $M_N < 1$, a local transonic condition in the crossflow was thought to occur such that a small horizontal normal shock existed above the leeward meridian just beneath the primary vortex pair. Region 3, encompassing leading-edge separation at low angles of attack, extended the Stanbrook-Squire Boundary to higher values of M_N for the thick-wing case. The influence of chord Reynolds number on the flow types and boundaries may be significant (Szodruch 1978) and typical cuts at M_N = constant and α_N = constant in Fig. 171 are displayed in Figs. 172 and 173 to illustrate the sensitivity of flow type to a two-order-change in Reynolds number. The cut in Fig. 172 has been chosen at $M_N \sim 2.5$. We note that the shock-induced separation region 5 changes to region 6 with leading-edge separation (plus shock) at ever-decreasing Reynolds number as α_N becomes very large. If α_N is now maintained at a nominally constant value of 28° (Fig. 171), increasing the Reynolds number to about 10^7 virtually destroys the separation-with-shock region 4 as we see in Fig. 173. Thus, to accommodate these substantial effects of Reynolds number on the $\alpha_N - M_N$ diagram, the boundary zones in Fig. 171 must deliberately be left broad.

We shall now make use of the $\alpha_N - M_N$ diagram plotted again in Fig. 174 as a suitable panorama on which to present some chosen experimental results of the different regimes of separated flow measured by Maltby (1962), Thomann (1963), Cross (1968), Monnerie and Werlé (1968), Rao and Whitehead (1972), Szodruch (1977), and Narayan (1978). This display simply shows the $\alpha_N - M_N$ range of test conditions of these investigators with a tabulation of Reynolds numbers based on maximum chord of the delta wing models. It is clear that with the exception of the high Reynolds number test of Rao and Whitehead (1972), we are dealing with flows in which laminar-turbulent transition will play an important role. Figure 174 shows that the ranges of test Mach number used by Monnerie and Werlé (1968) and by Szodruch (1977) span the Stanbrook-Squire Boundary from regions 1 and 2 to region 4; Maltby (1962) (and Richards 1976) worked within the rough confines of the Stanbrook-Squire Boundary. The Mach 12 experiment of Cross (1968) is definitely in the regime of laminar flow where expansion and shock/boundary-layer interactions are dominant (regions 5 to 6).

Let us now discuss briefly the structure of the flow in the various regimes illustrated in Figs. 170 and 171, beginning with the subsonic leading-edge flows to the left-hand side of the Stanbrook-Squire Boundary. Figures 175 and 176 show, respectively, the flow visualization results of Monnerie and Werlé (1968) at free-stream Mach numbers of 0 and 1.95 at the same angle of attack of 25° for identical models of 75° sweepback angle. The skin-friction line patterns show clear evidence of nearly conical flow; the dominant primary vortices from the leading-edge separations may be inferred from the bubble flow visualization in the water tunnel and from the pitot-pressure contours measured in the wind tunnel. Evidence of a secondary separation is also indicated in Figs. 175 and 176. In addition, there is also a third line of oil coalescence on the Mach 1.95 skin-friction line pattern (counting also the line along the sharp leading edge) which causes one to speculate on perhaps yet a small tertiary vortex flow existing in addition to the primary and secondary flows. The small centerline shock in the flow region 1 is that showing in Fig. 176 on the lee-side of the vehicle. The side elevation Schlieren photograph in Fig. 176 certainly indicates evidence of a shock very close to the surface, with what appears to be the primary vortex existing well above it. The divergent attachment line region is along the leeward meridian in both the incompressible and compressible flow regimes.

Moving now to the right in Fig. 174 "into" the Stanbrook-Squire Boundary, we next view in Fig. 177 the Mach 3 experimental result of Thomann (1963) for his 76° swept-back delta-wing model. The test point shown is for a relatively low angle of attack of 6.5°. At the bottom of Fig. 177, we observe the leeward skin-friction line pattern that Thomann obtained; it provides some striking contrasts with the high angle-of-attack results of Monnerie and Werlé (1968) in Fig. 176. The pattern in Fig. 177 does not display an attachment line along the leeward meridian, but rather indicates a noticeable region of divergence at a distance of 40% of the semispan from the wing centerline. At this location, the peak Stanton number was measured, which is clear evidence of an attachment line. Between this attachment line and the wing edge, there is a point where the recovery factor of the wall temperature distribution is at a minimum, thus indicating a line of secondary separation. Note the asymptotic behavior of the skin-friction lines toward the separation line at the wing edge, and toward the secondary separation line farther inboard. The path of the primary vortex core will exist above the locus of inflexion points in the skin-friction line pattern at about the 50% semispan position, where we observe the peak in suction pressure induced by the primary vortex. The induced suction peak from the secondary vortex is not observable near the wing edge, because

[22] $\chi = M^3\sqrt{R_{L_\infty}}$.

[23] Rounded edges were also investigated.

of the difficulty of installing a large number of pressure orifices in the thin-edge region. By way of verification of the low angle-of-attack flow field with a (very) subsonic leading edge, we present in Fig. 178 some water-tunnel pictures from Werlé (1958) that especially illustrate the parallel behavior of the skin-friction lines along the leeward meridian. A postulate of the flow field is also provided beneath the water-tunnel photographs.

Some vapor-screen pictures of leading-edge separation taken by Maltby (1962) at various angles of attack in a Mach 1.75 airstream with a wing of 65° sweepback angle are shown next in Fig. 179. This range of angle of attack is seen in Fig. 174 to be also "within" the confines of the Stanbrook-Squire Boundary. The flat plate delta wing was actually attached to a body; evidence of both nose and junction vortices is quite distinct at higher angles of attack. There is also evidence of a (weak) shock wave existing on top of the primary vortex structure. The effect of adding leading-edge camber is, by reducing α_N, to reduce the overall height of the primary vortex core position above the wing and also to flatten the vortex structure as can be determined by comparing Fig. 180 with Fig. 179.

We noted in Sec. 4.2.4 that one of the several processes of transition is frequently characterized by the appearance of arrays of vortices with axes slightly skewed from the local external flow direction when the body is at low angle of attack. In Fig. 180, with the cambered slender wing at 1° angle of attack, we see a row of near-circular, small black patches behind the inner part of the wing; with increasing angle of attack, the row of patches disappears. Maltby (1962) considers that these patches represent a row of streamwise vortices in the boundary layer that are caused by an instability of the three-dimensional shear flow in the region of the cambered, swept leading edge (see Squire et al. 1963). It has also been inferred by McDevitt and Mellenthin (1969) that these vortices exist on cones at high Mach number; some of their representative results are shown in Figs. 181a and 181b. Figure 181a illustrates an oil-film study on a 10° half-angle cone at 5° angle of attack with a transitional attached boundary layer immersed in a Mach 7.4 airstream. In the laminar region of the flow near the cone apex and on the windward side, the delicate pattern of the skin-friction lines has a distinctively different appearance and direction from that farther back on the lee side, an enlargement of which is shown in Fig. 181b. McDevitt and Mellenthin (1969) as well as other researchers (e.g., Ginoux 1967) claim that this regular pattern of leeward streak lines (separation lines?) is indicative of the existence of streamwise vortices entrained within the boundary layer. Clearly, the presence of the vortices substantially alters the appearance and the direction of the local skin-friction line pattern reflecting the interaction between the vortices and the mean crossflow. At a higher relative incidence than the experimental result of McDevitt and Mellenthin (1969), Fig. 182 (Rao 1978: personal communication) shows the existence of these vortices in a vapor-screen experiment in conjunction with analogous oil-streak lines on another cone example. Here, primary separation has developed on the cone leeside; and it is interesting to speculate whether the pattern progresses from these arrays of boundary-layer vortices at low angle of attack to a smaller discrete number of vortices with increasing angle of attack, to merge finally with the primary separation.

Returning to Fig. 174, we should now like to draw attention to the Mach 6 (and 6.8) delta-wing flow fields investigated by Rao and Whitehead (1972) at low angles of attack (5° and 10°), the sample experimental points for which are shown to be in Zone 4 . The leeward flow is characterized as having attached flow at the leading edge but with arrays of vortices "embedded" within the viscous flow, commencing some distance downstream of the apex, that eventually become two main vortex structures. This flow, in our view, is once again consistent with the transitional flow containing the streamwise vortices observed by Maltby (1962), McDevitt and Mellenthin (1969) and by D. S. Rao (1978: personal communication). Rao and Whitehead (1972) prepared a composite of the surface pattern from their results, coupled with vapor-screen flow visualization at several stations down the model. In the range of their tests, attached leading-edge flow was indicated as shown in Fig. 170b but it was considered that there was insufficient definition to determine whether an inboard separation line existed. The locus of identifiable inflexion points on the skin-friction lines, of course, is symptomatic of a vortex core existing above it.

From Fig. 183, Rao and Whitehead (1972) postulated a closely spaced symmetric pair of contrarotating vortices such that the common induced flow in the plane of symmetry was directed toward the wing. A characteristic pattern of divergent skin-friction lines ("feather-like" traces) was observed on the surface. After a short run, the "feather" was observed to split symmetrically into separate trails (see also Fig. 170b). Notably, at increased angles of attack, Rao and Whitehead (1972) recorded that the "feather pattern" was preserved over a relatively longer chord length of the model before splitting. We note that this Mach 6, low angle-of-attack behavior of the skin-friction lines of the aft lee-side center region is not unlike that found at the lower Mach number of 3 in Fig. 177 (Thomann 1963). The spanwise leeward heating distributions in the transitional flow measured at low angles of attack by Rao and Whitehead (1972) are also not unlike those that would be expected with a 3D separation line existing at the location where the value of Stanton number is lowest (Fig. 184), and with an attachment line region situated just outboard of the centerline, where the highest value of the Stanton number is measured. The vortex model conceived by Rao and Whitehead (1972) to explain their flow at low angle of attack is presented in Fig. 185a. It is based on a "two layer" model of the hypersonic laminar boundary layer. This consists of an inner layer of low-momentum flow changing rapidly to near-inviscid conditions in the outer layer. The wall layer skews very rapidly because of the increasing (spanwise) adverse pressure gradient toward the center of the wing, while the outer streamlines follow the inviscid flow through the compression (Fig. 185b). At the "interface" of the two layers, a lateral shear is considered to develop, producing an embedded sheet of streamwise vorticity that forms an array of streamwise vortices near the apex and eventually rolls up into two main vortices further downstream. The symmetrical vortex pair will then drain fluid from the region of the leeward meridian by induction.

As we have seen, the "embedded" array of vortices has been inferred at moderate (Mach 6) hypersonic Mach numbers, at relatively small angles of attack, and at sufficiently large Reynolds numbers that the viscous interaction parameter is small (see Fig. 170b and Narayan 1978). With an increase in angle of attack and elevation of the free-stream Mach number to 10, all measurements have been made at low Reynolds numbers because of facility limitations. Hence, the flow conditions have ostensibly been laminar with no inference of "embedded vortices" (Cross 1968; Narayan 1978). Narayan (1978) made measurements on an 80° swept-back delta wing at Mach 10 along the locus joining the half-circle symbols ◐ on the α_N - M_N chart shown in

Fig. 174. At angle of attack, he found only inboard separated (Zone 5 in Fig. 174) and leading-edge separated flows (Zone 6 in Fig. 174), but Reynolds number had a strong influence on the boundary between these flow regimes.

Figure 186 shows the spanwise heat transfer variations for a range of angle-of-attack settings from 0° to 22°. In these flows, Narayan (1978) concluded from his oil-flow patterns that no embedded vortices existed. The character of the spanwise heat-transfer distributions changes from one with minimum values on the meridian in attached flow to one with a peak on the meridian and minimum heat-transfer rates at the locations of the separation lines between the meridian and the leading edge, for α = 5° to 22°. At α = 22°, the primary separation is at the leading edge with an apparent secondary separation line existing at the heat-transfer minima.

In the flow examples cited for thick wings, we have seen that the boundary regions drawn on the α_N - M_N diagram provide us with a map of where, in broad terms, the leeward flow regions change as either α_N or M_N alters. The Stanbrook-Squire Boundary clearly delineates the change from a leading-edge separated-flow type to one with varying degrees of shock-induced separation in the crossflow; that is, from regions 2 to 4 and 5 in Fig. 171. Less precisely determinable, on the other hand, are the remaining boundaries in Fig. 171. We may illustrate this imprecision by reference to the last example of our selection of delta-wing flows, namely, the Mach 4 and 7 examples of Monnerie and Werlé (1968) (see Fig. 174). Here at the same angle of attack of 10°, the normal Mach number M_N is, respectively, about 1.2 and 2.2. Figures 187a and 187b show the pitot contours in these flows, the kinks indicating the locations of shock waves above the leeward separation zones. Although we might expect the Mach 4 flow field of Monnerie and Werlé (1968) (the ▲ in Fig. 174) to exhibit similar features to the attached leading-edge flow field of Rao and Whitehead (1972) (because it is nominally located in Zone 4), Fig. 187a clearly shows it to have a separated flow at the leading edge so that it is more properly located in Zone 6 . Thus, the "extension for thick wings" boundary (see Fig. 174) at high angles of attack, α_N, should not be interpreted too literally. Finally, the Mach 7, leading-edge-attached flow example of Monnerie and Werlé (1968), on the other hand, does provide evidence that the separation line is located inboard from the leading edge (see Fig. 174) and hence a flow representative of Zone 5.

On the theoretical side, the thin shock-layer concept of Messiter (1963) has been extended and modified by many researchers (e.g., Roe 1972; Squire 1974). Stollery and Richards (1976) have provided a mini-review of shock-layer theory to illustrate its usefulness and some of its shortcomings. Hefner and Whitehead (1972) have shown that the windward surface-pressure distributions for 60° swept deltas at Mach 6 with attached leading-edge shock waves may be predicted in both magnitude and trend of measured pressures by the method of lines (Klunker, South, and Davis 1972). Better agreement occurs at higher angles of attack where windward viscous effects are nominally small. Some numerical computations with approximate forms of the Navier-Stokes equations have been attempted recently to elucidate the leeward flow characteristics (Vigneron, Rakich, and Tannehill 1978; Bluford 1978; see Sec. 3.3.2). No analysis is currently available to predict the complex viscous-inviscid leeward flow regimes with transition and heating on slender wings with supersonic leading edges.

4.8 Delta Wing With Half-Cone

The isolated delta wing provides only a very small volume, so that it is of practical importance to determine the effect of adding a central body. One choice, in order to maintain conical flow, consists of a half-cone placed on the flat surface of a delta wing so that the apex of the half-cone is coincident with that of the delta. Good lift-to-drag ratios are suggested by Eggers (1960) when the vehicle shown in Fig. 188 derives its lifting effectiveness from a favorable interference of the cone pressure field with the delta-wing undersurface (Meyer and Vail 1967). Viscous and theoretical cross sections of the essentially conical flow about the vehicle of Fig. 188a under conditions of high Mach number and moderate angle of attack are shown in Figs. 188b and 188c. As angle of attack is increased, the intersection B of the wing and cone shocks in the inviscid flow moves outboard until, at large angles of attack, the leading-edge shock wave detaches and a single detached shock surrounds the underside of the vehicle. With laminar boundary layers present, in particular, flow separation will be likely due to the adverse pressure gradient that the shock BC presents to the boundary layer growing on the wing. A particular example of the separated 3D viscous flow that may occur is illustrated in Fig. 188b, which bears close resemblance to the hypersonic corner flow results obtained by Cooper and Hankey (1974) and shown in Fig. 144. Along flow reattachment lines, high heat-transfer rates will be likely, as we have seen already. In general, attempts to take advantage of favorable interference may often result in 3D separated flows, as we discussed in Sec. 4.5.4.

The inviscid flow theory of Mandl (1964) provided the shock-wave patterns shown in Fig. 188c. Portnoy (1968) has calculated the lift and drag due to angle of attack in both subsonic and supersonic flow if the flow is attached. Kutler and Lomax (1971) have also shown calculations of supersonic flow fields about similar bodies using a shock-capturing, finite difference approach. An adaptation of the Navier-Stokes corner-flow computation of Shang and Hankey (1977) would clearly be valuable in providing the real flow field details.

Figures 189a and 189b from Meyer and Vail (1967) show surface shear-stress directions on the windward of the vehicle with the model at 15° angle of attack, corresponding with the interpretation of the viscous flow shown in Fig. 188b. The boundary layers were laminar. Figure 190 gives the measured spanwise heat-transfer and surface-pressure distributions as well as the locations of the 3D separation lines and the reattachment lines. Note that S is the distance measured around the surface from the windward generator to the wing tip position. Here again, we note that spikes in the heat-transfer distribution occur along the reattachment lines and that flow separation is associated with minima in the heat-transfer distribution. Small peaks in the pressure distributions are measured at the reattachment lines. Meyer and Vail (1967) found that the length of the streak from carefully applied, and very uniform oil dots, was qualitatively related to the surface shear stress at hypersonic flow conditions. Hence, a comparison was made between the streak lengths and the measured heat-transfer distribution, as we see in Fig. 191. The curve of the streak-length distribution was matched to the curve of the heat-transfer distribution at the points labeled A and B. The agreement is seen to be quite remarkable; provided the shear stress is high enough to cause the oil dot to flow, the streak-length distribution clearly provides a very satisfactory indication of the magnitude of the resultant surface shear stress. Referring once again to Fig. 188b, we see that the slip

surface from the shock-on-shock intersection adjacent to the junction between the cone and the wing will probably proceed toward the corner. The resultant very high heat transfer on the wing surface may well be the reattachment line of this shear layer (see Sec. 4.5.1 and 4.6). Dunavant (1964) has also provided heat-transfer data on a similar half-cone delta model and Bertram and Henderson (1969) have published a short review of the flow around such bodies.

4.9 Shuttle Orbiter

The aerodynamic design of the Space Shuttle Orbiter has been described in great detail by Bornemann and Surber (1978) with special emphasis devoted to the criteria used in establishing the external configuration from the requirements of vehicle trim, control, performance, and aerodynamic heating. The Shuttle wing is of double-delta planform with leading-edge sweep angles of 81° and 45°. The upper limit of the sensible atmosphere begins at about 120 km (75 mi), and from there down to about 70 km (44 mi), rarefied gas flows are encountered by the Orbiter as it reenters the atmosphere. Aerodynamic design problems in this region involve the effectiveness of the reaction control jets and their influence on the Orbiter flow field, in addition to the viscous interaction effects associated with low Reynolds number, high Mach number flows. During this reentry phase, where lift, drag, and pitching moment essentially govern the entry trajectory, range and heating rates, the angle of attack of the Orbiter changes from about 40° to 30°, while a nominal 60° angle of bank is maintained (see Fig. 192). With further reduction in altitude, the control jets are deactivated as the aerodynamic controls increase in effectiveness. This transition begins at about Mach 5 and is completed at about Mach 1.5, during which time an additional change in angle of attack and bank is demanded (Fig. 192). The aerodynamics at high angle of attack are hence of crucial importance in all regimes of Orbiter flight (see also Marvin et al. 1972). The high aerodynamic heating rates on the lee side of the vehicle were broached in Sec. 4.2 when we considered the flow about blunt cones, and the heating interference effects due to shock-on-shock interactions were debated in Sec. 4.6. The enormous heating rates due to shear-layer "jet-type" impingement (e.g., on wing and fin leading edges) from intersecting shock waves were shown in Figs. 157, 161, and 162 to be especially high during the boost phase of the ascent trajectory. The leeward flow pattern over the wing of the Shuttle at high Mach number will be the shock-induced type (region 5) or leading-edge separation with shock type of region 5 (see Fig. 171). We shall now consider the respective windward and leeward flow fields in successive sections.

4.9.1 Windward

The heating and streamline patterns about the windward of the Shuttle Orbiter have been calculated by Rakich and Lanfranco (1976) using exact inviscid flow field analysis following Rakich and Park (1973), Rizzi and Bailey (1975), and Rakich, Bailey, and Park (1975) together with a 2D boundary-layer method (DeJarnette and Hamilton 1973, 1975) and quasi-3D theories (Fannelop 1968). It was clear that because of the large size of the Shuttle Orbiter and the high-altitude-entry trajectory, finite-rate (i.e., nonequilibrium) chemical reactions had to be considered in flow-field simulations above an altitude of 40 km (25 mi). The Shuttle will experience peak heating shortly after it reenters the Earth's atmosphere, where viscous conditions are laminar (see the isotherms in Fig. 3b). Once the Orbiter has descended to about 80 km (50 mi), under conditions of no appreciable deceleration (Fig. 192), we note from Fig. 193a that there should be no significant viscous displacement effects on the inviscid flow field. Even though these effects are small, however, the changing edge conditions due to boundary-layer growth must be taken into account, due to entrainment of hot gas that passed through the bow shock wave (entropy swallowing). Figure 193b shows that the windward surface heating on the Orbiter computed by Rakich and Lanfranco (1976) agrees quite closely with wind-tunnel test results conducted at 30° angle of attack at Mach 7.3 ($R_{L_\infty} = 1.7 \times 10^6$). The reference heating, q_0 on Fig. 193b, is the value calculated for a sphere equal to the nose radius of the vehicle. Correlations for 3D effects at the stagnation point (i.e., effect of angle of attack on location) are shown by Rakich and Lanfranco (1976) to be small. Figure 193c shows the windward centerline heating in flight, and suggests that the effect of finite-rate chemical reactions becomes negligible some distance downstream from the nose. Since the nonequilibrium effects appeared small, the windward spanwise heating distributions are plotted in Fig. 193d for the equilibrium flight conditions, but including entropy-swallowing effects. Three axial stations are shown with an unexplained fall-off in heating as the windward meridian is approached. The calculated windward "inviscid surface" streamlines from the method of Rakich and Lanfranco (1976) corresponded quite well with the skin-friction line patterns obtained in wind-tunnel tests (Fig. 193e).

4.9.2 Computation of Overall Inviscid Flow Field

The left-hand side of Fig. 194 displays, by electron-beam illumination, the Mach 20 flow field about a model of the Shuttle Orbiter at 30° angle of attack in the 22-in. helium tunnel at Langley Research Center (Woods and Arrington 1972). In the view that one has "through" the quasi-transparent shock envelopes, one can also detect the oil-streak pattern on the model surface (which is shown to better advantage on the right-hand side of the figure). The intersection of the bow shock wave with the wing leading-edge shock is clearly demonstrated.

Computing 3D inviscid flows about supersonic and hypersonic configurations by means of "shock-capturing" techniques was comprehensively reviewed by Kutler (1974b). The "shock-capturing" technique is inherently capable of predicting the location and strength of all flow discontinuities and their interactions without knowledge of their presence. This method contrasts with an alternative method of calculation, the "sharp-shock" technique (Marconi and Salas 1973; Marconi, Yaeger, and Hamilton 1975) in which all known shock waves are treated as sharp discontinuities by predicting their motion and applying the Rankine-Hugoniot equations across them. The shock-capturing technique is easy to apply (Kutler 1974b) and gives good detail of external shock wave shapes. The flow discontinuities, rather than appearing as discrete jumps, are spread over several mesh intervals, but can be located precisely within those regions. In applying the shock-capturing technique, Kutler writes the (hyperbolic) unsteady or steady Euler equations that govern inviscid flow, in conservation form; the equations are then integrated, using a finite-difference scheme with appropriate boundary conditions applied at the extremities of the computational domain. We have already commented upon the success of predicting the inviscid flow shock patterns in the external corner flows discussed in Sec. 4.5.3. A comparison of characteristics and shock capturing methods with application to the Shuttle was made by Rakich and Kutler (1972). They concluded that of the two methods, the shock-capturing method was faster, calculated secondary shocks better, and treated difficult flows more readily. Notwithstanding, it was also felt (Rakich and

Kutler 1972) that the shock-capturing technique would benefit by employing "sharp shock" (i.e., the Rankine-Hugoniot) relations across the bow shock wave. Evidently, both the "shock-capture" and "sharp-shock" approaches have their merits; however, according to Chaussee, Holtz, and Kutler (1975), the shock-capture calculation appears to give more plausible predictions of the cross-sectional shock-shapes about the Orbiter. Figure 195 illustrates the comparison between the shock-capture calculations of Chaussee, Holtz, and Kutler, and measurements made of shock shape and surface pressures at Mach 7.3 and 30° angle of attack. The comparisons are remarkably close considering the nature of the lee-side 3D viscous flows that we saw in Fig. 194. The differences between perfect and real gas effects in multishocked 3D supersonic flow fields have been shown to have minor influence on the shape of the enshrouding shock waves (Kutler, Reinhardt, and Warming 1975).

4.9.3 Viscous-Inviscid Overall Flow Field

The skin-friction line patterns on a model of a conceptual delta-wing Orbiter at 20° angle of attack and tested in a Mach 6, $R_{L_\infty} = 5 \times 10^6$ flow, are shown in Fig. 196 (Hefner 1972). This pattern is closely identifiable in form with the pattern obtained by Woods and Arrington at $M_\infty = 20$ (Fig. 194). Therefore, the following discussion will be relevant to both Mach numbers. The flow from the windward attachment line expands around the blunt leading edge to remain attached on the leeward surface for a finite distance before leaving the surface at the 3D swept separation line induced by the inboard embedded shock wave that we discussed in Fig. 166b. Hence, the flow is one of the "shock-induced type" shown in region 5 of Fig. 171, and rolls up to form a substantial vortex — section B-B on Fig. 196. There is an attachment line region of very strong divergence of the skin-friction lines midway up the fuselage, as a consequence of the induced effect of this primary vortex structure on the wing. The shear stress and heat transfer along this region are correspondingly high; the latter is shown in Fig. 197 for $\alpha = 20°$ and 40°. At section A-A in Fig. 196, near the nose, the flow continues farther around the body before it separates at what we may term a primary separation for the body flow, that passes down the body through section B-B. Again the effect of the coiling dividing surface from this second primary separation line is to encourage a rapid draining outboard of the fluid passing along the leeward meridional attachment line, with free-stream air induced to flow very close to this region. High shear stresses and consequent high heating are again obtained. Note the secondary separations associated with both the wing flow and the body (nose) flow.

Spanwise heating distributions are shown in Fig. 198, where within the spatial resolution of the experimental measurements for the 20° angle-of-attack case (illustrated by shaded symbols), we can associate the peaks and troughs with the 3D strong reattachment and primary (wing and body) separation lines, respectively (see especially Fig. 198c). The heating along the leeward surface meridian in the axial sense at various angles of attack is shown in Fig. 199; there is an increase in the number of peaks as angle of attack increased (compare with the blunt cone flow discussed in Sec. 4.2.4). A satisfactory and complete explanation of the fluid mechanics along the leeward meridian is still awaited. The heating peaks in the nose region apparently increase as Reynolds number is increased (Hefner 1972). Figure 200 shows vapor-screen pictures at various stations along the body with a curious "handle" existing immediately above the leeward meridian. This "handle" may contain the vortices emanating from the primary separation line of the body flow, the shear layers feeding the vortices being stretched substantially (see the postulate of the crossflow in Fig. 196b). On the other hand, the vapor-screen pictures may be indicating an analogous flow on the body lee side to that for the blunt cone displayed in Figs. 88a and 89a, where additional vortices from foci on the lee-side surface pass downstream close to the meridian plane, but above the primary vortices. Unfortunately, the detail available in the oil-streak pattern in Fig. 196a does not permit the choosing between the two alternatives.

The side oblique view of the model representing the present Shuttle Orbiter in Fig. 201 shows an oil-flow pattern at Mach 20 and an angle of attack of 30° (Stone and Mulfinger 1974) very similar to that described for Hefner's model (see also Fig. 194, due to Woods and Arrington 1972). The length Reynolds number for the flow condition in Fig. 201 is 1×10^6, close to the full-scale value in flight at Mach 20. For comparison, Fig. 202 displays the Orbiter immersed in a transonic flow at zero angle of attack, with a very strong swept wing shock/boundary-layer interaction existing close to midchord position.

The 3D separated flows about the Shuttle Orbiter are clearly very complex throughout its flight envelope. Reference should again be made to Bornemann and Surber (1978) for a very thorough discussion of the control aspects of the vehicle resulting from these separated flows from Mach 20 to 0.

4.10 Transonic Swept-Wing Separated Flows and Their Control

We have seen that when the separation lines can be fixed by salient edges (sharply swept leading edges, for instance, Fig. 1b) we have an example of "controlled flow separation" (Fig. 4). Throughout the range of flight conditions, the flow field is virtually invariant in form, being dominated by the dividing surfaces leaving the separation lines to form well-organized and comparatively steady vortex motions. These leading-edge vortices can, in turn, be controlled by additional active means, to induce more lift: first, to prevent vortex breakdown, by blowing in a spanwise direction along the axis of the vortex, as discussed by Dixon (1969, 1972) and others (Cornish 1970; Bradley and Wray 1974; Campbell 1975) (see Fig. 203); second, by blowing normal to the leading edge, either to enhance the primary vortex (Barsby 1971; Spillman and Goodridge 1972), or to control secondary separations (Alexander 1963). Clearly, other examples of swept edges, such as strakes or leading-edge extensions (Fig. 6) and vortex generators (Fig. 204), themselves provide controlled flow separations, but in the latter case, the generated vortex motions are used to promote mixing of high-energy air with recalcitrant viscous flow downstream of the flow separation device (Pearcey 1961).

On a swept wing in transonic flow, buffet is a direct result of vortex formation and subsequent vortex breakdown, whether from part-span free shear layers, from forward-shock/rear-shock interactions, or from leading-edge separations. A spiral focus is formed on the wing, leading to a tightly wound vortex filament springing normally from the surface. Buffet intensity is low until a significant area of the wing is affected by the focus (Benepe 1969). Under these conditions, we may speculate that the location of a large spiral focus on a solid surface may indeed not hold to one spot, so that its movement may be the cause of the flow unsteadiness. In a recent publication, Legendre (1979) discusses the formation of foci on swept wings and their changing patterns with increasing angle of attack. In Fig. 14c, we saw a swept wing in buffet, with a large focus evident on each wing top surface, caused by strong shock-induced separation. This flow is unsteady. Bore (1972) shows an analogous flow in Fig. 205a, which when "treated" with vortex generators, succeeded in controlling the spread of shock-induced separation at Mach 0.88 (Fig. 205b). The effect of

two wing fences in combination with the vortex generators improved the roll steadiness (Figs. 205c and 205d), each fence effectively blocking inboard spanwise movement of the leading-edge dividing surface by acting as a partial reflection plate, thus providing a favorable pressure gradient in the outboard direction across the fence (Küchemann 1973). Similar effects can be achieved with discontinuities in the leading edge, such as notches or sudden leading-edge extensions.

The large leading-edge extension or strake offers one significant advantage in that induced lift produced by the vortices from the sharp edges can be used to extend the combat maneuvering capabilities of a military aircraft, particularly in transonic flow. Figure 206 shows the improvement in lift boundary, steadiness in rolling moment performance, and root-mean-square wing-root bending moment as a result of adding a strake to a wing similar to that shown in Fig. 205 (Moss 1978). Figure 207 shows the contours of constant pitot pressure measured behind another straked configuration and the very large inboard influence of the strake vortex as angle of attack increases. Figure 208 shows an interpretation by Moss (1978) of oil-flow visualization patterns on the strake and swept wing with a swept separation line running back from the strake across the wing. Küchemann (1971) has proposed that the vortex avoids the necessity for the formation of the usual forward branch of the wing shock pattern by providing a "soft" boundary for the flow turning inboard over the leading edge, instead of the "stiff" boundary given by the fuselage side.

Figures 209 and 210 provide oil-flow patterns of two other straked configurations (E. R. Beeman 1977: personal communication) in subsonic flow. The former has fuselage boundary-layer diversion slots at the strake-fuselage intersection that maintain a "clean" and near-zero angle-of-attack flow into the inlet beneath the strake up to high angles of attack. Flow through the slots is entrained into the strake vortices, as shown in Fig. 211. Note the exceptionally well-behaved attached flow over the wing in Fig. 209, and the vortex breakdown in Fig. 211. For a configuration such as this, which utilizes vortex lift, the interaction between the strake and nose vortices and the two vertical tails, when the aircraft is yawed, sets the lateral-directional characteristics. Apparently, a single, vertical tail is not compatible with vortex lift, unless special attention is paid to the nose. Figure 210 shows a fighter aircraft configuration that has a single vertical tail. It is at high angle of attack, with leading and trailing-edge flaps deflected. Note the substantial differences between Figs. 209 and 210 in the surface pattern downstream of the kink at the wing-strake intersection. Fiddes and Smith (1979) predict a large lateral velocity near the kink in the leading edge, which changes the direction of the local onset velocity and provides a higher effective sweep to the outer wing. Other means of controlling 3D swept-shock-induced separations (e.g., by blowing) are discussed in Peake (1978).

5. CONCLUDING REMARKS

We have described the structure of 3D separated flows about various types of flight vehicle and aerodynamic components immersed in flows equivalent to flight domains from Mach 0 to 20 and encompassing the viscous flow regimes from laminar to turbulent. Typical vehicle configurations displayed have been slender shapes, such as pointed and blunt cones, missiles, delta wings, the "Concorde," and the Shuttle Orbiter. Important component flows have been those about bluff protuberances, in axial corners, and through shock-on-shock interactions.

By holding strictly to the notions of continuous vector fields of skin-friction lines and external streamlines in association with a restricted number of singular points (nodes, saddles, and foci) on the surface and in particular projections of the flow (the crossflow plane, for example), we have a language to classify rationally and unambiguously the 3D separated flow field about any useful aerodynamic configuration. Sequences of structures of ascending elaboration of saddles, nodes, and foci can be assembled, which are then available to guide experiments when observation is imprecise, or to check the veracity of numerical calculations. We have shown, moreover, that in cross-sectional projections of diverse 3D separated flows, the mechanisms become familiar, occurring repeatedly from flow to flow. As an approach to design, we may postulate sequences, starting with the simplest number of singular points on the surface and in the flow, for a vehicle at low angle of attack, and increasing in complexity as angle of attack becomes large. The philosophy of design, especially at high angles of attack when the leeward vortical flows have a tendency to become asymmetric, must be one of controlling the locations of the 3D separations on the vehicle, such as at sharp edges, or by active control from blowing, for example. The design aims, in summary, are that we require steady boundary conditions to provide steady flows, and symmetric boundary conditions to yield symmetric flows. We further demand that as flow regimes change with increasing angle of attack there should be no discontinuous jumps to give uncontrollable forces and moments.

This glossary of diverse 3D separated flows has demonstrated that when a 3D boundary layer detaches from the surface it will, almost without exception, leave along a swept separation line, rolling up in the process into a well-organized nominally steady vortical motion. The underlying mechanism appears to be independent of both Reynolds number and Mach number, although under laminar conditions the flow features are normally more exaggerated. Hence, the overall details of many flows of practical interest can be determined in a water-tunnel facility in which aircraft and missile designers can make changes to configurations quickly and very cheaply. Some airplane and missile companies are currently doing this.

In hypersonic flow, the consequences of 3D swept separations are enhanced heating rates along adjacent reattachment line regions of high shear stress. Maximum heating rates are obtained, however, as a consequence of shock-on-shock interference from which, under the worst circumstances, a shear-layer "jet-type" flow may emerge to impinge locally on the vehicle skin. Under these conditions, heat-transfer rates more than 20 times the local stagnation-point heat-transfer rate have been measured. Such heating may clearly lead to catastrophic structural failure if inadequate attention is given to heat shielding.

Although we have demonstrated a satisfactory understanding in general of the structures of 3D separated flows, we are only able to compute them about a limited number of simple aerodynamic components. Numerical techniques invoking either inviscid approximations to model the coiling shear layers, or approximate forms of the Navier-Stokes equations, have been successful and should be encouraged further. But the physics of the turbulence in 3D separated flow regimes has not yet been investigated to any great extent, and an appeal to well-planned experiments with nonintrusive instrumentation must be made in this regard. To restrict the avenues of possible research, and as a suitable starting point, it might be useful to

concentrate on measuring the fluctuating flow quantities in the vicinity of the singular points to determine if there is any identifiable, and perhaps universal, turbulence field associated with each type of singular point.

We deem it useful to end this review by specifying the issues that have been raised, from both experiments and calculations, in the study of singular points. First, there is the question of scale effects. Many large-scale flow phenomena involve a small-scale organized substructure (e.g., arrays of longitudinal vortices on the scale of the thickness of the transitional boundary layer or vortex-shedding on the scale of a shear-layer thickness). In some cases, this organized substructure (or a part of it) is capable of determining the outcome of the evolution of the large-scale structure; in other cases, it is not. Is it possible, then, to formulate a principle that will distinguish between the vital and the unimportant organized substructures? Can one devise an averaging technique that will preserve the essential structures and smear out the remaining ones? A clarification of these queries should also shed light on similar problems involved in turbulence modeling. The utilization of meshes in finite difference calculations obviously provides a process of averaging but more work is needed to understand the ramifications of altering mesh intervals. Moreover, we need to incorporate an adequate treatment of the essential singular points in numerical calculation schemes either by refining the mesh size about the singular points or by including some analytical representation of the flow about the singular points within the numerical scheme.

Second, the rules underlying the placement, number, and types of singular points in terms of the governing flow parameters and body geometry need elaboration. This is particularly true in the nose region where nodal points of attachment and saddle points will tend to merge.

Third, the mechanisms by which stationary flow structures change their topology from one level of complexity to the next (i.e., as they bifurcate) need to be exposed. For example, studies are needed to provide the links between bifurcation phenomena and the large-scale structural changes in the flow that are characteristic of buffet, stall, and vortex breakdown.

REFERENCES

Adams, J. C., "Finite-Difference Analysis of the Three-Dimensional Turbulent Boundary Layer on a Sharp Cone at Angle of Attack in a Supersonic Flow," AIAA Paper 72-186, Jan. 1972a.

Adams, J. C., "Analysis of the Three-Dimensional Compressible Turbulent Boundary Layer on a Sharp Cone at Incidence in Supersonic and Hypersonic Flow," AEDC TR 72-66, June 1972b.

Alexander, A. J., "Experiments on Delta Wing Using Leading-Edge Blowing to Remove the Secondary Separation," Coll. of Aero., Cranfield, Report 161, 1963.

Allen, H. J. and Perkins, E. W., "Characteristics of Flow Over Inclined Bodies of Revolution," NACA RM A50 L07, Mar. 1951a.

Allen, H. J. and Perkins, E. W., "A Study of Effects of Viscosity on Flow Over Slender Inclined Bodies of Revolution," NACA Report 1048, 1951b.

Angelucci, S. B., "A Multivortex Method for Axisymmetric Bodies at Angle of Attack," J. Aircraft, Vol. 8, No. 12, 1971, pp. 959-966.

Angelucci, S. B., "Multivortex Model for Bodies of Arbitrary Cross-Sectional Shapes," AIAA Paper 73-104, 1973.

Atraghji, E. G., "The Influence of Mach Number, Reynolds Number, Semi-Nose Angle and Roll Rate on the Development of the Forces and Moments Over a Series of Long Slender Bodies of Revolution at Incidence," Nat. Res. Coun. of Canada, NAE 5x 5/0020, Mar. 1967.

Atraghji, E. G., "Pressure Distribution Over a Family of Inclined Long Slender Bodies of Revolution at M_∞ = 0.5, 2.0 and 3.5," Nat. Res. Coun. of Canada, NAE 5 x 5/0029, Aug. 1968a.

Atraghji, E. G., "Surface Visualization, Surface Pressure and Surface Preston Tube Pitot Pressure Measurements over a 6:1 Ellipsoid at Incidence, at Mach 0.3 and 0.74," Nat. Res. Coun. of Canada, NAE 5 x 5/0032, 1968b.

Babenko, K. I., Voskresenski, G. P., Lyubimov, A. N., and Rusanov, V. V., "Three-Dimensional Flow of an Ideal Gas Past Smooth Bodies," NASA TT F-380, Apr. 1966.

Bakker, P. G. and Bannink, W. J., "Conical Stagnation Points in the Supersonic Flow Around Slender Circular Cones at Incidence," Delft U. of Tech., The Netherlands, Dept. of Aero. Eng., Report VTH-184, Nov. 1974.

Bannink, W. J. and Nebbeling, C., "An Experimental Investigation of the Expansion Flow Field over a Delta Wing at Supersonic Speed," Delft U. of Tech., The Netherlands, VTH-167, Sept. 1971.

Bannink, W. J. and Nebbeling, C., "Measurements of the Supersonic Flow Field Past a Slender Cone at High Angles of Attack," AGARD CP-247, Oct. 1978.

Barsby, J. E., "Calculations of the Effect of Blowing from the Leading-Edges of a Slender Delta Wing," RAE Tech. Report 71077; ARC R and M 3692, 1971.

Barsby, J. E., "Flow Past Conically-Cambered Slender Delta Wings with Leading-Edge Separation," RAE Tech. Report 72174, ARC R and M 3749, 1972.

Barsby, J. E., "Separated Flow Past a Slender Delta Wing at Low Incidence," Aeronaut. Quart., Vol. 24, No. 2, 1973, pp. 120-128.

Beckwith, I. E., "Experimental Investigation of Heat Transfer and Pressures on a Swept Cylinder in the Vicinity of its Intersection with a Wedge and Flat Plate at Mach Number 4.15 and High Reynolds Numbers," NASA TN D-2020, 1964.

Benepe, D. B., "Aerodynamic Buffet," FZM-5384, General Dynamics, Fort Worth, Texas, June 1969. (Presented at U. of Tennessee Space Inst., June 1969, in Special Topics in Transonic Aerodynamics — New Developments).

Benjamin, T. B., "Bifurcation Phenomena in Steady Flows of a Viscous Fluid. I, Theory. II, Experiments." Proc. Roy. Soc. London, Ser. A., Vol. 359, 1978, pp. 1-43.

Bertram, M. H. and Henderson, A., "Some Recent Research with Viscous Interacting Flow in Hypersonic Streams," ARL 75-0212, 1969, pp. 7-30.

Birch, S. F. and Keyes, J. W., "Transition in Compressible Free Shear Layers," J. Spacecraft & Rockets, Vol. 9, No. 8, Aug. 1972, pp. 623-624.

Bloom, M. H. and Pallone, A., "Heat Transfer to Surfaces in the Neighborhood of Protuberances in Hypersonic Flow," WADC TN 57-95, USAF, Wright-Patterson ADC, Aug. 1957.

Bloom, M. H., Rubin, S. G., and Cresci, R. J., "Three-Dimensional Viscous Interactions," ARL 75-0212, 1969, pp. 493-522.

Bluford, G. S., "Navier-Stokes Solution of the Supersonic and Hypersonic Flow Field Around Planar Delta Wings," AIAA Paper 78-1136, 1978.

Bluford, G. S., "Numerical Solution of the Supersonic and Hypersonic Viscous Flow Around Thin Delta Wings," AIAA J., Vol. 17, No. 9, Sept. 1979, pp. 942-949.

Boersen, S., "Reynolds Number Effects on Pressure and Normal Force Distributions Along Conically Pointed Circular Cylinder at Mach Number of 2.3," NLR TR 75124U, Sept. 1975.

Bontoux, P. and Roux, B., "Compressible Turbulent Boundary Layer on a Yawed Cone," AIAA J., Vol. 14, No. 5, May 1976, pp. 545-546.

Bordner, G. L. and Davis, R. T., "Compressible Three-Dimensional Laminar Boundary Layers on Cones at Incidence to Shear and Axisymmetric Wake Flows," ARL 71-0262, Nov. 1971.

Bore, C., "Post-Stall Aerodynamics of the Harrier GR1," AGARD CP-102, Apr. 1972.

Bornemann, W. E. and Surber, T. E., "Aerodynamic Design of the Space Shuttle Orbiter," AGARD CP-247, Sept. 1978.

Bradley, R. G. and Wray, W. O., "A Conceptual Study of Leading-Edge-Vortex Enhancement by Blowing," J. Aircraft, Vol. 11, No. 1, Jan. 1974, pp. 33-38.

Branstetter, C. B., "The Drag of Circular Cylinders Mounted on a Flat Plate in M = 1.91 Flow," DRL-TR-68-17, U. of Texas, Aug. 1968.

Braun, W. K., "Turbulent Boundary Layer on a Yawed Cone in a Supersonic Stream," NACA TN-4208, 1956.

Brown, C. E. and Michael, W. H., "On Slender Delta Wings with Leading-Edge Separation," J. Aeron. Sci., Vol. 21, 1954, pp. 690-4, 706.

Brown, S., "Singularities Associated with Separating Boundary Layers," Roy. Soc. London Phil. Trans., Series A., Vol. 257, 1965, pp. 409-444.

Brune, G. W. and Rubbert, P. E., "Boundary-Value Problem of Configurations with Compressible Free Vortex Flow," AIAA J., Vol 15, No. 10, Oct. 1977, pp. 1521-1523.

Bryson, A. E., "Symmetric Vortex Separation on Circular Cylinders and Cones," J. App. Mech., Vol. 26, 1959, pp. 643-648.

Burbank, P. B., Newlander, R. A., and Collins, I. M., "Heat Transfer and Pressure Measurements on a Flat Plate Surface and Heat Transfer Measurements on Attached Protuberances in a Supersonic Turbulent Boundary Layer at Mach Numbers of 2.65, 3.51 and 4.44," NASA TN D-1372, Dec. 1962.

Bushnell, D. M., "Interference Heating on a Swept Cylinder in the Region of its Intersection with a Wedge in Hypersonic Flow," NASA TN D-3094, 1965.

Bushnell, D. M., "Effects of Shock Impingement and Other Factors on Leading-Edge Heat Transfer," NASA TN D-4543, Apr. 1968.

Camarero, R., "A Numerical Method for the Solution of Three-Dimensional Supersonic Flows," CASI Trans., Vol. 8, No. 2, Sept. 1975, pp. 35-43.

Campbell, J. F., "Augmentation of Vortex Lift by Spanwise Blowing," AIAA Paper 75-993, Aug. 1975.

Canning, T. N., Tauber, M. E., Wilkins, M. E., and Chapman, G. T., "Orderly Three-Dimensional Processes in Turbulent Boundary Layers on Ablating Bodies," AGARD CP-30, May 1968.

Cantwell, B. J., Coles, D. E., and Dimotakis, P. E., "Structure and Entrainment in the Plane of Symmetry of a Turbulent Spot," J. Fluid Mech., Vol. 87, Pt. 4, 1978, pp. 641-672.

Carafoli, E., "Wing Theory in Supersonic Flow," Pergamon, Oxford, 1969.

Cérésuela, R., Kretzschmer, G., and Rehbach, C., "Étude Théorique et Expérimentale de l'Écoulement Hypersonique autour d'un Corps Émoussé en Incidence," AGARD CP-30, May 1968.

Chan, Y. Y., "An Approximate Method for Three-Dimensional Compressible Laminar Boundary Layers with Small Cross-Flow," Nat. Res. Coun. of Canada Aero. Rept. LR-455, June 1966.

Chan, Y. Y., "An Experimental Study of a Yawed Circular Cone in Hypersonic Flows," AIAA J., Vol. 7, No. 10, Oct. 1969, pp. 2035-2037.

Chang, P. K., Smith, R. A., Casarella, M. J., and Oh, Y. H., "Analysis of Laminar Flow and Heat Transfer on a Hypersonic Cone at High Angle of Attack," Mech. Eng. Dept., Catholic U. of America, Washington, D.C., TR 2, Aug. 1968.

Chapman, D. R., "Computational Aerodynamics Development and Outlook," Dryden Lectureship in Research, AIAA Paper 79-0129, Jan. 1979.

Chapman, J. R., Mark, H., and Pirtle, M. W., "Computers Versus Wind Tunnels for Aerodynamic Flow Simulations," Astronaut. & Aeronaut., Vol. 13, No. 4, Apr. 1975, pp. 22-29, 35.

Charwat, A. F. and Redekeopp, L. G., "Supersonic Interference Flow Along the Corner of Intersecting Wedges," AIAA J., Vol. 5, No. 3, Mar. 1967.

Chaussee, D. S., Holtz, T., and Kutler, P., "Inviscid Supersonic/Hypersonic Body Flow Fields and Aerodynamics from Shock-Capturing Technique Calculations," AIAA Paper 75-837, June 1975; also J. Spacecraft & Rockets, Vol. 13, No. 6, June 1976, pp. 325-331.

Christophel, R. G., Rockwell, W. A., and Neumann, R. D., "Tabulated Mach 6, 3D Shock Wave – Turbulent Boundary Layer Interaction Heat Transfer-Data," AFFDL-TM-74-212-FXG Supplement, Feb. 1975.

Clapworthy, G. J., and Mangler, K. W., "The Behaviour of a Conical Vortex Sheet on a Slender Wing Near the Leading-Edge," RAE Tech. Report 74150, 1974.

Clark, R. W., "Non-Conical Flow Past Slender Wings with Leading-Edge Vortex Sheets," RAE Tech. Report 76037, Mar. 1976.

Clark, W. H., Peoples, J. R., and Briggs, M. M., "Occurrence and Inhibition of Large Yawing Moments During High Incidence Flight of Slender Missile Configurations," AIAA Paper 72-968, Sept. 1972.

Cleary, J. W., "Effects of Angle of Attack and Bluntness on Laminar Heating Rate Distribution on a 15° Cone at Mach Number of 10.6," NASA TN D-5450, Oct. 1969.

Cooke, J. C., "The Laminar Boundary Layer on an Inclined Cone," AGARDograph 97, Part 2, May 1965, pp. 909-931.

Cooke, J. C., "Supersonic Laminar Boundary Layers on Cones," RAE Tech. Report 66347; also ARC CP 1063, 1966.

Cooke, J. C. and Hall, M. G., "Boundary Layers in Three-Dimensions," Progress in Aeronautical Sciences, Vol. 2, 1962, pp. 222-282.

Cooper, J. R. and Hankey, W. L., "Flowfield Measurements in an Asymmetric Axial Corner at M = 12.5," AIAA J., Vol. 12, No. 10, Oct. 1974, pp. 1353-1357; also AIAA Paper 73-676, Jan. 1973.

Cornish, J. J., "High Lift Applications of Spanwise Blowing," ICAS Paper 70-09, Sept. 1970.

Couch, L. M., "Flow Field Measurements Downstream of Two Protuberances on a Flat Plate Submerged in a Turbulent Boundary Layer at Mach 2.49 and 4.44," NASA TN D-5297, July 1969.

Cousteix, J. and Quémard, C., "Velocity Profiles and Wall Shear Stress of Three-Dimensional Turbulent Boundary Layers," ONERA TP 1134, 1972.

Cousteix, J. and Houdeville, R., "Épaissement et Séparation d'une Couche Limite Turbulente Soumise en Intéraction avec un Choc Oblique," La Recherche Aérospatiale, No. 1, Jan./Feb. 1976, pp. 1-11.

Crabbe, R. S., "An Application of Cooke's Method to the Laminar, Incompressible Boundary Layer on a Right Circular Cone at Incidence," Nat. Res. Coun. of Canada Aero. Report LR-391, Dec. 1963.

Crabbe, R. S., "Flow Separation About Elliptic Cones at Incidence," Nat. Res. Coun. of Canada Aero. Report LR-436, Aug. 1965.

Creel, T. R. and Hunt, J. L., "Photographing Flow Fields and Heat Transfer Patterns in Color Simultaneously," Astronaut. & Aeronaut., Apr. 1972, pp. 54-55.

Cresci, R. J., "Hypersonic Flow Along Two Intersecting Planes," Proc. 1966 Heat Transfer and Fluid Mech. Inst., Stanford U. Press, Stanford, Calif., pp. 357-365.

Cresci, R. J., Rubin, S. G., Nardo, C. T., and Lin, T. C., "Hypersonic Interaction Along a Rectangular Corner," AIAA J., Vol. 7, No. 12, Dec. 1969, pp. 2241-2246.

Cross, E. J., "Experimental and Analytical Investigation of the Expansion Flow Field Over a Delta Wing at Hypersonic Speeds," ARL 68-0027, Feb. 1968.

Culley, M., "A Side-Mounted Supersonic Intake and the Problem of Three-Dimensional Boundary-Layer Separation," ARL ME 137, Australia, June 1972a.

Culley, M., "Viscous Interaction in Integrated Supersonic Intakes," First International Symposium on Air Breathing Engines, Marseilles, France, June 1972b.

Culley, M., "A Brief Examination of the Flow External to a F-111 Intake at Mach 1.6," ARL/ME 357, Australia, July 1975.

Cumpsty, N. A. and Head, M. R., "The Calculation of Three-Dimensional Turbulent Boundary Layers. Part IV: Comparison of Measurements with Calculations on the Rear of a Swept Wing," Aeronaut. Quart., Vol. 21, 1970, pp. 121-132.

Davey, A., "Boundary-Layer Flow at a Saddle Point of Attachment," J. Fluid Mech., Vol. 10, 1961, pp. 593-610.

Deffenbaugh, F. D. and Koerner, W. G., "Asymmetric Vortex Wake Development on Missiles at High Angles of Attack," J. Spacecraft & Rockets, Vol. 14, No. 3, Mar. 1977, pp. 155-162.

Der, J., "A Study of General Three-Dimensional Boundary-Layer Problems by an Exact Numerical Method," AIAA Paper 69-138, Jan. 1969.

Dixon, C. J., "Lift Augmentation by Lateral Blowing Over a Lifting Surface," AIAA Paper 69-193, Feb. 1969.

Dixon, C. J., "Lift and Control Augmentation by Spanwise Blowing over Trailing-Edge Flaps and Control Surfaces," AIAA Paper 72-781, Aug. 1972.

Dods, J. B. and Cangie, C. D., "Flow Visualization Studies of Three Space Shuttle Launch Configurations at Mach Numbers from 0.8 to 2.0," NASA TM X-62,074, Sept. 1971.

Dolling, D. C., Cosad, C. D., and Bogdonoff, S. M., "Three-Dimensional Shock Wave Turbulent Boundary-Layer Interactions — A Parametric Study of Blunt Fin-Induced Flows," AIAA Paper 78-159, Jan. 1978.

Dougherty, N. S. and Fisher, D. F., "Boundary-Layer Transition on a 10-Degree Cone: Wind-Tunnel/Flight Data Correlation," AIAA Paper 80-0154, Jan. 1980.

Driftmyer, R. T., "Thick, Two-Dimensional, Turbulent Boundary Layers Separated by Steps and Slot Jets," AIAA J., Vol. 12, No. 1, Jan. 1974, pp. 21-27.

Drougge, G. and Larson, P. O., "Pressure Measurements and Flow Investigations on Delta Wings at Supersonic Speeds," FFA Report 57, The Aeronautical Research Institute of Sweden, Stockholm, Sweden, 1956.

Dunavant, J. C., "Heat Transfer to a Delta Wing-Half-Cone Combination at Mach Numbers of 7 and 10," NASA TN D-2799, Mar. 1964.

Dunavant, J. C., Narayan, K. Y., and Walberg, G. D., "A Survey of Leeside Flow and Heat Transfer on Delta Planform Configurations," AIAA Paper 76-118, 1976.

East, L. F., "Measurements of the Three-Dimensional Turbulent Boundary Layer Induced on the Surface of a Slender Delta Wing by the Leading-Edge Vortex," RAE TR 73141, ARC 35269, 1974.

East, L. F. and Hoxey, R. P., "Boundary Layer Effects in an Idealized Wing-Body Junction at Low Speed," RAE TR 68161, July 1968.

East, L. F. and Hoxey, R. P., "Low-Speed Three-Dimensional Turbulent Boundary-Layer Data, Part 1," RAE TR 69041, Mar. 1969.

Edney, B. E., "Anomalous Heat Transfer and Pressure Distributions on Blunt Bodies at Hypersonic Speeds in the Presence of an Impinging Shock," FFA Report 115, The Aeronautical Research Institute of Sweden, Stockholm, Sweden, Feb. 1968.

Eggers, A. J., "Some Considerations of Aircraft Configurations Suitable for Long-Range Hypersonic Flight," Hypersonic Flow, Butterworth and Co., (Canada) Ltd., Toronto, Jan. 1960, pp. 369-390.

Eggers, A. J., Petersen, R. H., and Cohen, N. B., "Hypersonic Aircraft Technology and Applications," Astronaut. & Aeronaut., June 1970, pp. 30-41.

Eichelbrenner, E. A., "Observations on a Criterion for Three-Dimensional Laminar Boundary-Layer Separation," Rech. Aéron., No. 40, July-Aug. 1954, pp. 3-5; also NRC (Canada) TT-962, 1961.

Eichelbrenner, E. A. and Oudart, A., "Three-Dimensional Laminar Boundary-Layer Separation," Rech. Aéron., No. 47, 1955, pp. 11-14; also NRC (Canada) TT-963, 1961.

Elsenaar, A., van den Berg, B., Lindhout, J. P. F., "Three-Dimensional Separation of an Incompressible Turbulent Boundary Layer on an Infinite Swept Wing," AGARD CP-168, Nov. 1975.

Erickson, G. E., "Water Tunnel Flow Visualization: Insight into Complex Three-Dimensional Flow Fields," AIAA Paper 79-1530, July 1979.

Ericsson, L. E., Reding, J. P., and Guenther, R. A., "Effects of Shock-Induced Separation," Lockheed Missiles and Space Co., Sunnyvale, Calif., L-87-69-1, July 1969.

Ericsson, L. E., Reding, J. P., and Guenther, R. A., "Analytic Difficulties in Predicting Dynamic Effects of Separated Flow," J. Spacecraft & Rockets, Vol. 8, No. 8, Aug. 1971, pp. 872-878.

Ericsson, L. E. and Reding, J. P., "Unsteady Aerodynamic Flow Field Analysis of the Space Shuttle Configuration. Part I. Orbiter Aerodynamics," Lockheed Missiles and Space Co., Sunnyvale, Calif., LMSC-D057194, Apr. 1976.

Ericsson, L. E. and Reding, J. P., "Coupling Between Boundary-Layer Transition and Vehicle Motion," Working Group Meeting on High Angle of Attack Missile Aerodynamics, NASA-Langley Research Center, Mar. 1978.

Fannelop, T. K., "A Method of Solving the Three-Dimensional Laminar Boundary Layer Equations with Application to the Lifting Re-Entry Body," AIAA J., Vol. 6, No. 6, June 1968, pp. 1075-1084.

Fannelop, T. K. and Waldman, G. D., "Displacement Interaction and Flow Separation on Cones at Incidence to a Hypersonic Stream," AGARD CP-30, May 1968.

Faro, I. D. V., "Supersonic Inlets," AGARDograph 102, May 1965, pp. 121-123.

Feldhuhn, R. H., Winkelmann, A. E., and Pasiuk, L., "An Experimental Investigation of the Flowfield Around a Yawed Cone," AIAA J., Vol. 9, No. 6, June 1971, pp. 1074-1081.

Fellows, K. A. and Carter, E. C., "Results and Analysis of Pressure Measurements on Two Isolated Slender Wings and Slender Wing-Body Combinations at Supersonic Speeds. Vol. 1. Analysis," ARA Report 12, Nov. 1969.

Ferri, A., "Supersonic Flow Around Circular Cones at Angles of Attack," NACA TN-2236, Nov. 1950.

Fiddes, S. P. and Smith, J. H. B., "Strake-Induced Separation from the Leading-Edges of Wings of Moderate Sweep," AGARD CP-247, Oct. 1979.

Fidler, J. E. and Bateman, M. C., "Asymmetric Vortex Effects on Missile Configurations," AIAA Paper 75-209, Jan. 1975.

Fiechter, M., "Über Wirbelsysteme an schlanken Rotationskörpern und ihren Einfluss auf die aerodynamischen Beiwerte," Deutsch-Französisches Forschungs-Institut Saint-Louis," Report 10/66, 1966.

Fink, P. T. and Soh, W. H., "Calculation of Vortex Sheets in Unsteady Flow and Applications in Ship Hydrodynamics," Proc. of 10th Symposium on Naval Hydrodynamics, M.I.T., Cambridge, Mass., June 1974.

Fletcher, C. A. J., "Supersonic Flow About Cones at Large Angles of Attack," Coll. of Eng., U. of California, Berkeley, Report FM-74-8, May 1974.

Fletcher, C. A. J., "Vortical Singularity Behind a Highly Yawed Cone," AIAA J., Vol. 13, No. 8, Aug. 1975, pp. 1073-1078.

Fletcher, C. A. J. and Holt, M., "Supersonic Viscous Flow Over Cones at Large Angles of Attack," J. Fluid Mech., Vol. 74, Part 3, 1976, pp. 561-591.

Frankel, L. E., "Supersonic Flow Past Slender Bodies of Elliptic Cross-Section," ARC R and M 2954, 1955.

Freeman, L. M. and Korkegi, R. H., "Experiments on the Interaction with a Turbulent Boundary-Layer of a Skewed Shock Wave of Variable Strength at Mach 2.5," ARL 75-0182, June 1975.

Gaudet, L. and Winter, K. G., "Measurements of the Drag of Some Characteristic Aircraft Excrescences Immersed in Turbulent Boundary Layers," AGARD CP-124, 1973.

Geissler, W., "Calculation of the Three-Dimensional Laminar Boundary Layer Around Bodies of Revolution at Incidence and With Separation," AGARD CP-168, May 1975.

George, O. L. and Whitfield, J. D., "An Extended Correlation of Hypersonic Conical Normal Force Data to Large Incidence," AIAA J., Vol. 6, No. 9, Sept. 1968, pp. 1771-1772.

Ginoux, J. J., "Instabilité de la Couche Limite sur Ailes en Flèche," Zeitschrift für Flugwissenschaften, 15 Jahrgang, Heft 8/9, Aug./Sept. 1967, pp. 302-305.

Glagolev, A. I., Zubkov, A. I , and Panov, Y. A., "Supersonic Flow Over an Obstacle in the Form of a Gas Jet on a Plate," USSR Acad. of Sci., Bull., Fluid and Gas Mechanics, No. 3, 1967, pp. 97-102.

Goldberg, T. J., "Three-Dimensional Separation for Interaction of Shock Waves with Turbulent Boundary Layers," AIAA J., Vol. 11, No. 1, Nov. 1973, pp. 1573-1575.

Green, J. E., "Interactions Between Shock Waves and Turbulent Boundary Layers," Progress in Aerospace Sciences, Vol. 11, Pergamon Press at Oxford, 1970, pp. 235-340.

Gregory, N. and Walker, W. S., "The Effect on Transition of Isolated Surface Excrescences in the Boundary Layer," ARC R and M 2779, 1951.

Grosche, F. R., "Wind Tunnel Investigation of the Vortex System Near an Inclined Body of Revolution With and Without Wings," AGARD CP-71, Sept. 1970.

Guffroy, D., Roux, B., Marcillat, J., Brun, R., and Valensi, J., "Étude Théorique et Expérimentale de la Couche Limite autour d'un Cône Circulaire Placé en Incidence dans un Courant Hypersonique," AGARD CP 30, May 1968.

Gulbran, C. E., Redeker, E., Miller, D. S., and Strack, S. L., "Heating in Regions of Interfering Flow Fields. Part II. Leading-Edge Shock Impingement," AFFDLM TR 65-49, Jan. 1967.

Hains, F. D. and Keyes, J. W., "Shock Interference Heating in Hypersonic Flows," AIAA J., Vol. 10, No. 11, Nov. 1972, pp. 1441-1447.

Hall, M. G., "A Theory for the Core of a Leading-Edge Vortex," J. Fluid Mech., Vol. 11, Pt. 2, Sept. 1961, pp. 209-228.

Han, T. and Patel, V. C., "Flow-Visualization of Three-Dimensional Boundary-Layer Separation on Bodies of Revolution at Incidence," Iowa Inst. of Hydraulic Research, IIHR Report 205, June 1977.

Han, T. and Patel, V. C., "Flow Separation on a Spheroid at Incidence," J. Fluid Mech., Vol. 92, Pt. 4, 1979, pp. 643-657.

Hankey, W. L. and Holden, M. S., "Two-Dimensional Shock Wave Boundary-Layer Interactions in High Speed Flows," AGARDograph 203, June 1975.

Harris, J. E. and Morris, D. J., "Solution of the Three-Dimensional Compressible, Laminar and Turbulent Boundary-Layer Equations with Comparisons to Experimental Data," 4th Int. Con. on Numerical Methods in Fluid Dynamics, Boulder, Colo., June 1974.

Hayes, J. R., "An Overview of the Test Program and Representative Data Taken on the Modular Missile Configuration," AFFDL-TM-77-90-FXG, Oct. 1977.

Head, M. R., "Entrainment in the Turbulent Boundary Layer," ARC R and M 3152, 1960.

Hefner, J. N., "Lee-Surface Heating and Flow Phenomena on Space Shuttle Orbiters at Large Angles of Attack and Hypersonic Speeds," NASA TN D-7088, Nov. 1972.

Hefner, J. N. and Whitehead, A. H., "Surface-Flow, Pressure and Heat Transfer Studies of Two Conical Delta Wings at a Mach Number of 6," NASA TM X-2668, Dec. 1972.

Hiers, R. S. and Loubsky, W. J., "Effects of Shock-Wave Impingement on the Heat Transfer on a Cylindrical Leading Edge," NASA TN D-3859, Feb. 1967.

Hoak, D. E., "Body Lift in the Non-Linear Angle-of-Attack Range," Sec. 4.2.12, October 1960 (revised, Nov. 1965). USAF Stability and Control Datcom, Flight Control Div., Air Force Flight Dynamics Lab., Wright-Patterson Air Force Base, Ohio.

Holt, M., "A Vortical Singularity in Conical Flow," Quart. J. Mech. & Appl. Math., Vol. 7, 1954, pp. 438-455.

Horstman, C. C. and Hung, C. M., "Computation of Three-Dimensional Turbulent Separated Flows at Supersonic Speeds," AIAA Paper 79-2, Jan. 1979.

Hsia, H. T. S., Seifert, H. S., and Karamcheti, K., "Shocks Induced by Secondary Fluid Injection," AIAA Paper 64-111, Jan. 1964.

Hsieh, T., "An Investigation of Separated Flows About a Hemisphere-Cylinder at Incidence in the Mach Number Range from 0.6 to 1.5," AIAA Paper 77-179, Jan. 1977.

Hsieh, T., and Wang, K. C., "Concentrated Vortex on the Nose of an Inclined Body of Revolution, AIAA J., Vol. 14, No. 5, 1976, pp. 698-700.

Hummel, D., "Untersuchungen über das Aufplatzen der Wirbel an schlanken Delta-flügeln," Z. Flugwiss, Vol. 13, Pt. 5, 1965.

Hummel, D. and Srinivasan, P. S., "Vortex Breakdown Effects on the Low-Speed Aerodynamic Characteristics of Slender Delta Wings in Symmetrical Flow," J. Roy. Aeronaut. Soc., Vol. 71, No. 676, Apr. 1967, pp. 319-322.

Hung, C. M., "Numerical Solution of Supersonic Laminar Flow Over an Inclined Body of Revolution," AIAA Paper 79-1547, July 1979.

Hung, C. M. and MacCormack, R. W., "Numerical Solution of Supersonic Laminar Flow Over a Three-Dimensional Compression Corner," AIAA Paper 77-694, June 1977.

Hung, C. M. and MacCormack, R. W., "Numerical Solution of Three-Dimensional Shock Wave and Turbulent Boundary Layer Interaction," AIAA Paper 78-161, Jan. 1978.

Hunt, B. L. and Dexter, P. C., "Pressures on a Slender Body at High Angle of Attack in a Very Low Turbulence Level Airstream," AGARD CP-247, Oct. 1978.

Hunt, J. C. R., Abell, C. J., Peterka, J. A., and Woo, H., "Kinematical Studies of the Flows Around Free or Surface-Mounted Obstacles; Applying Topology to Flow Visualization," J. Fluid Mech., Vol. 86, Part 1, 1978, pp. 179-200.

deJarnette, F. R. and Hamilton, H. H., "Inviscid Surface Streamlines and Heat Transfer on Shuttle-Type Configurations," J. Spacecraft & Rockets, Vol. 10, No. 6, May 1973, pp. 314-321.

deJarnette, F. R. and Hamilton, H. H., "Aerodynamic Heating on 3D Bodies Including the Effects of Entropy-Layer Swallowing," J. Spacecraft & Rockets, Vol. 12, No. 1, Jan. 1975, pp. 5-12.

Jernell, L. S., "Aerodynamic Characteristics of Bodies of Revolution at Mach Numbers from 1.50 to 2.86 and Angles of Attack to 180°," NASA TM X-1658, Oct. 1968.

Jones, D. J., "Numerical Solutions of the Flow Field for Conical Bodies in a Supersonic Stream," CASI Trans., Vol. 3, No. 1, Mar. 1970, pp. 62-71; also Nat. Res. Coun. of Canada Aero. Report LR-507, July 1968.

Jones, D. J., "Tables of Inviscid Supersonic Flow About Circular Cones at Incidence, $\gamma = 1.4$," AGARDograph 137, Parts 1, 2, and 3, 1969.

Jones, D. J., "Effect of Specific Heat Ratio on Surface Pressure Coefficient for Lifting Cones," J. Spacecraft & Rockets, Vol. 7, No. 9, Sept. 1970a, pp. 1114-1146.

Jones, D. J., "Use of the Jones' Computer Programme to Determine the Flow Field for Conical Flow Situations. Part II. Eliptic Cones and Other Conical Bodies," Nat. Res. Coun. of Canada, NAE LTR-HA-1, Sept. 1970b.

Jones, D. J., "A Pressure Formula for an Inclined Circular Cone in Supersonic Flow, $\gamma = 1.4$," AIAA J., Vol. 10, No. 2, Feb. 1972, pp. 234-236.

Jones, J. G., "A Method for Designing Lifting Configurations for High Supersonic Speeds Using the Flow Fields of Non-Lifting Cones," RAE Report Aero. 2674, 1963.

Jones, R. T., "Properties of Low Aspect Ratio Pointed Wings at Speeds Below and Above the Speed of Sound," NACA Report 835, 1946.

Jorgensen, L. H., "Prediction of Static Aerodynamic Characteristics for Slender Bodies Alone and With Lifting Surfaces to Very High Angles of Attack," NASA TR R-474, Sept. 1977.

Jorgensen, L. H. and Perkins, E. W., "Investigations of Some Wake Vortex Characteristics of an Inclined Ogive-Cylinder Body at Mach Number 2," NACA Report 1371, 1958.

Jorgensen, L. H. and Nelson, E. R., "Experimental Aerodynamic Characteristics for a Cylindrical Body of Revolution with Various Noses at Angles of Attack from 0° to 58° and Mach Numbers from 0.6 to 2.0," NASA TM X-3128, Dec. 1974.

Jorgensen, L. H. and Nelson, E. R., "Experimental Aerodynamic Characteristics for Bodies of Elliptic Cross-Section at Angles of Attack from 0° to 58° and Mach Numbers from 0.6 to 2.0," NASA TM X-3129, Feb. 1975.

Joseph, D. D., "Stability of Fluid Motions I," Springer Tracts in Natural Philosophy, Vol. 27, Springer Verlag, New York, 1976.

Kaufman, L. G., Korkegi, R. H., and Morton, L. C., "Shock Impingement Caused by Boundary-Layer Separation Ahead of Blunt Fins," AIAA J., Vol. 11, No. 10, Oct. 1973, pp. 1363-1364.

Kaye, A. S. and Williams, M. J., "Pressure, Force and Cross-Flow Drag Distributions on Moderately Blunt Cone-Cylinder Bodies at Mach 7.5," Dept. of Supply, Australia, Report ARL/A. 142, Jan. 1974.

Keener, E. R. and Chapman, G. T., "Onset of Aerodynamic Side Forces at Zero Sideslip on Symmetric Forebodies at High Angles of Attack," AIAA Paper 74-770, Aug. 1974.

Keener, E. R., Chapman, G. T., and Kruse, R. L., "Effects of Mach Number and Afterbody Length on Onset of Asymmetric Forces on Bodies at Zero Sideslip and High Angles of Attack," AIAA Paper 76-66, Jan. 1976.

Keener, E. R. and Chapman, G. T., "Similarity in Vortex Asymmetries Over Slender Bodies and Wings," AIAA J., Vol. 15, No. 9, Sept. 1977, pp. 1370-1372.

Keyes, J. W., "Off-Center-Line Shock-Interference Heating Patterns on Basic Shapes in Hypersonic Flows," NASA TM X-2866, Dec. 1973.

Keyes, J. W. and Morris, D. J., "Correlations of Peak Heating in Shock Interference Regions at Hypersonic Speeds," J. Spacecraft & Rockets, Vol. 9, No. 8, Aug. 1972, pp. 621-623.

Keyes, J. W. and Hains, F. D., "Analytical and Experimental Studies of Shock Interference Heating in Hypersonic Flows," NASA TN D-7139, May 1973.

Kipke, K., "Untersuchungen an längsangeströmten Ecken im Hyperschallbereich," DGLR, Vortrags, No. 73-114, 1973.

Kipke, K. and Hummel, D., "Untersuchungen an längsangeströmten Eckenkonfigurationen im Hyperschallbereich," Z. Flugwiss. 23, Vol. 12, 1975, pp. 417-429.

Klunker, E. B., South, J. C., and Davis, R. M., "Calculation of Nonlinear Conical Flows by the Method of Lines," NASA TR R-374, Oct. 1971.

Klunker, E. B., South, J. C., and Davis, R. M., "Computer Program for Calculating Supersonic Flow on the Windward Side of Conical Delta Wings by the Method of Lines," NASA TM X-2438, 1972.

Korkegi, R. H., "Survey of Viscous Interactions Associated with High Mach Number Flight," AIAA J., Vol. 9, No. 5, May 1971, pp. 771-784.

Korkegi, R. H., "Effect of Transition on Three-Dimensional Shock-Wave Boundary-Layer Interaction," AIAA J., Vol. 10, No. 3, Mar. 1972, pp. 361-363.

Korkegi, R. H., "A Simple Correlation for Incipient Turbulent Boundary-Layer Separation Due to a Skewed Shock Wave," AIAA J., Vol. 11, No. 11, Nov. 1973, pp. 1578-1579.

Korkegi, R. H., "On the Structure of Three-Dimensional Shock-Induced Separated Flow Regions," AIAA Paper 76-165, Jan. 1976; also AIAA J., Vol. 14, No. 5, May 1976, pp. 597-600.

Körner, H. and Hirschel, E. H., "The Calculation of Flow Fields by Panel Methods — a Report on Euromech 75," J. Fluid Mech., Vol. 79, Part 1, 1977, pp. 181-189.

Küchemann, D., "Flow with Separations," RAE Tech. Memorandum Aero 453, Dec. 1955a.

Küchemann, D., "A Non-Linear Lifting-Surface Theory for Wings of Small Aspect Ratio with Edge Separations," RAE Aero. Report 2540, ARC 17769, 1955b.

Küchemann, D., "Hypersonic Aircraft and Their Aerodynamic Problems," Progress in Aeronautical Sciences, Vol. 6, Küchemann and Sterne, eds., Pergamon Press, 1965, pp. 271-353.

Küchemann, D., "Aerodynamic Design," Aeronaut. J., Vol. 73, No. 698, Feb. 1969, pp. 101-110.

Küchemann, D., "Some Remarks on the Interference Between a Swept Wing and a Fuselage," AGARD CP-71, Sept. 1970.

Küchemann, D., "On the Possibility of Designing Wings that Combine Vortex Flows with Classical Aerofoil Flows," Unpublished RAE Tech. Memorandum, 1971.

Küchemann, D., "The Aerodynamic Design of Aircraft — An Introduction. Part 1," RAE TM Aero 1421, May 1972; see also Pergamon Press, 1978.

Küchemann, D., "The Aerodynamic Design of Aircraft — An Introduction. Part 3," RAE Tech. Memo. Aero 1535, Aug. 1973; see also Pergamon Press, 1978.

Küchemann, D. and Weber, J., "Vortex Motions," ZAMM 45, 7/8, 1965, pp. 457-474.

Küchemann, D., "The Aerodynamic Design of Aircraft — An Introduction. Part 5," RAE Tech. Memo. Aero. 1622, February 1975, see also Pergamon Press, 1978.

Kuehn, D. M., "Experimental Investigation of the Pressure Rise Required for the Incipient Separation of Turbulent Boundary Layers in Two-Dimensional Supersonic Flow," NASA Memorandum 1-21-59A, Feb. 1959.

Kutler, P., "Numerical Solution for the Inviscid Supersonic Flow in the Corner Formed by Two Intersecting Wedges," AIAA Paper 73-675, July 1973.

Kutler, P., "Supersonic Flow in the Corner Formed by Two Intersecting Wedges," AIAA J., Vol. 12, No. 5, May 1974a, pp. 577-578.

Kutler, P., "Computation of Three-Dimensional, Inviscid Supersonic Flow," Lecture Notes in Physics, Springer-Verlag, New York, 1974b.

Kutler, P. and Lomax, H., "A Systematic Development of the Supersonic Flow Fields Over and Behind Wings and Wing-Body Configurations Using a Shock-Capturing Finite-Difference Approach," AIAA Paper 71-99, Jan. 1971.

Kutler, P. and Sakell, L., "Three-Dimensional, Shock-on-Shock Interaction Problem," AIAA Paper 75-49, Jan. 1975.

Kutler, P., Shankar, V., Anderson, D. A., and Sorenson, R. L.,"Internal and External Axial Corner Flows for Integrated Ram/Scramjet Nacelles. Part I," NASA SP-347, Mar. 1975.

Kutler, P., Reinhardt, W. A., and Warming, R. F., "Multishocked, Three-Dimensional Supersonic Flowfields with Real Gas Effects," AIAA J., Vol. 11, No. 5, May 1975, pp. 657-664.

Kutler, P., Pulliam, T. H., and Vigneron, Y. C., "Computation of the Viscous Supersonic Flow Over Symmetrical and Asymmetrical External Axial Corners," AIAA Paper 78-1135, July 1978.

Lahlou, O., "Flow About an Ellipsoid," Doctoral Thesis, Laval University, Québec City, Canada, 1971.

Lamont, P. J., "Pressure Distributions on an Ogive-Cylinder at High Angles of Attack with Laminar, Transitional or Turbulent Separation," Working Group Meeting on High Angle of Attack Missile Aerodynamics, AEDC, Tenn., Mar. 1979.

Lamont, P. J. and Hunt, B. L., Pressure and Force Distribution on a Sharp Nosed Circular Cylinder at Large Angles of Inclination to a Uniform Subsonic Stream," J. Fluid Mech., Vol. 76, Pt. 3, 1976, pp. 519-559.

Lamont, P. J. and Hunt, B. L., "Prediction of Aerodynamic Out-of-Plane Forces on Ogive-Nosed Circular Cylinders," J. Spacecraft & Rockets, Vol. 14, No. 1, Jan. 1977, pp. 38-44.

Law, C. H., "Three-Dimensional Shock Wave-Turbulent Boundary Layer Interactions at Mach 6," ARL 75-0191, June 1975.

Lee, G. H., "Note on the Flow Around Delta Wings with Sharp Leading-Edges," ARC R and M 3070, 1955.

Legendre, R., "Écoulement au Voisinage de la Pointe Avant d'une Aile à Forte Flèche aux Incidences Moyennes," Rech. Aéron. No. 30, 1952a, pp. 3-8; No. 31, 1953, pp. 3-6; No. 35, 1953, pp. 7-8.

Legendre, R., "Écoulement Autour de la Pointe Avant d'une Aile à Forte Flèche aux Incidences Moyennes," 8th Intern. Congress of Applied and Theoretical Mechanics, Istanbul, 1952b.

Legendre, R., "Séparation de l'Écoulement Laminaire Tridimensionnel," La Recherche Aéronautique, No. 54, Nov.-Dec. 1956, pp. 3-8.

Legendre, R., "Lignes de Courant d'un Écoulement Continu," Rech. Aérosp. No. 105, 1965, pp. 3-9.

Legendre, R., "La Condition de Joukowski en Écoulement Tridimensionnel," Rech. Aérosp., No. 5, 1972, pp. 241-248; also RAE Lib. Transl. 1709, 1973.

Legendre, R., "Lignes de Courant d'un Écoulement Permanent: Décollement et Separation," Rech. Aérosp., No. 1977-6, pp. 327-335.

Legendre, R., "Types de Décollements de l'Écoulement Transsonique autour d'une Aile en Flèche," ONERA TP 1979-75, 1979.

Levinsky, E. S. and Wei, M. H. Y., "Non-Linear Lift and Pressure Distribution on Slender Conical Bodies with Strakes at Low Speeds," NASA CR-1202, 1968.

Leyman, C. S. and Markham, T., "Prediction of Supersonic Aircraft Aerodynamic Characteristics," AGARD LS 67, 1974, pp. 5-1 to 5-52.

Lighthill, M. J., "Attachment and Separation in Three-Dimensional Flow," in Laminar Boundary Layers, Section II 2.6, L. Rosenhead, ed., Oxford Univ. Press, 1963, pp. 72-82.

Lin, T. C. and Rubin, S. G., "Viscous Flow Over a Cone at Incidence. Part 2: Boundary Layer," J. Fluid Mech., Vol. 59, Part 3, 1973, pp. 593-620.

Lin, T. C. and Rubin, S., "A Two-Layer Model for Coupled Three-Dimensional Viscous and Inviscid Flow Calculations," AIAA Paper 75-853, June 1975.

Lowrie, B. W., "Cross-Flows Produced by the Interaction of a Swept Shock Wave with a Turbulent Boundary Layer," Ph.D. Thesis, Univ. of Cambridge, Dec. 1965.

Lubard, S. C., "Laminar Separation on a Blunted Cone at High Angles of Attack," AGARD CP-168, May 1975.

Lubard, S. C. and Rakich, J. V., "Calculation of the Flow on a Blunted Cone at High Angle of Attack," AIAA Paper 75-149, Jan. 1975.

Lukasiewicz, J., "Some Studies in Supersonic and Hypersonic Aerodynamics at the von Karman Gas Dynamics Facility, AEDC," Presented at 6th BOWACA Symposium on Aeroballistics, Washington, D.C., 1963.

MacCormack, R. W., "The Effect of Viscosity in Hypervelocity Impact Cratering," AIAA Paper 69-354, 1969.

MacCormack, R. W., "An Efficient Numerical Method for Solving the Time-Dependent Compressible Navier-Stokes Equations at High Reynolds Number," NASA TM X-73,129, July 1976.

MacCormack, R. W., "An Efficient Explicit-Implicit Numerical Scheme for Solving the Compressible Navier-Stokes Equations," Presented at Meeting of the American Mathematical Society, New York, April 1977 (see also SIAM Proc., Vol. 11, 1978, pp. 130-155).

MacCormack, R. W. and Baldwin, B. S., "A Numerical Method for Solving the Navier-Stokes Equations and Application to Shock/Boundary-Layer Interactions," AIAA Paper 75-1, Jan. 1975.

McCabe, A., "The Three-Dimensional Interaction of a Shock Wave with a Turbulent Boundary Layer," Aeronaut. Quart., Vol. XVII, Aug. 1966, pp. 231-252.

McDevitt, J. B. and Mellenthin, J. A., "Upwash Patterns on Ablating and Non-Ablating Cones at Hypersonic Speeds," NASA TN D-5346, July, 1969.

McElderry, E. D., "An Experimental Study of Sharp and Blunt 6-Degree Cones at Large Incidence with a Turbulent Boundary Layer at Mach 6," AFFDL-TM-74-170, Sept 1974.

McRae, D. S., "A Numerical Study of Supersonic Viscous Cone Flow at High Angle of Attack," AIAA Paper 76-97, 1976.

McRae, D. S., "The Conically Symmetric Navier Stokes Equations: Numerical Solution for Hypersonic Cone Flow at High Angle of Attack," AFFDL-TR-76-139, Mar. 1977.

McRae, D. S. and Hussaini, M. Y., "Supersonic Viscous Flow Over Cones at Incidence," 6th Intl. Conf. on Numerical Methods in Fluid Dynamics, Tbilisi, USSR, June 1978.

Mager, A., "Generalization of Boundary-Layer Momentum Integral Equations to Three-Dimensional Flows Including Those of Rotating System," NACA Report 1067, 1952.

Maltby, R. L., "Flow Visualization in Wind Tunnels Using Indicators," AGARDograph 70, Apr. 1962.

Mandl, P., "A Theoretical Study of the Inviscid Hypersonic Flow About a Conical Flat-Top Wing-Body Combination," AIAA J., Vol. 2, No. 11, Nov. 1964.

Mangler, K. W. and Smith, J. H. B., "A Theory of the Flow Past a Slender Delta Wing with Leading-Edge Separation," Proc. Roy. Soc., Series A, No. 1265, May 1959, pp. 200-217.

Mangler, K. W. and Weber, J., "The Flow Field Near the Centre of a Rolled-Up Vortex Sheet," RAE TR 66324, 1966.

Mangler, K. W. and Smith, J. H. B., "Behavior of the Vortex Sheet at the Trailing Edge of a Lifting Wing," Aeronaut. J., Vol. 74, No. 719, 1970, pp. 906-8.

Mangler, K. W. and Murray, J. C., "Systems of Coordinates Suitable for the Numerical Calculation of Three-Dimensional Flow Fields," ARC CP 1325, 1975.

Marconi, F. and Salas, M., "Computation of Three-Dimensional Flows About Aircraft Configurations," Computers and Fluids, Vol. 1, Pergamon Press, 1973, pp. 185-195.

Marconi, F., Yaeger, L., and Hamilton, H. H., "Computation of High-Speed Inviscid Flows About Real Configurations," NASA SP-347, Mar. 1975.

Marsden, D. J., Simpson, R. W., and Rainbird, W. J., "The Flow Over Delta Wings at Low Speeds with Leading-Edge Separation," Coll. of Aero., Cranfield, Report 114, Feb. 1958.

Mashburn, J. H., "Turbulent Boundary Layer Separation Ahead of Cylindrical Protuberances in Supersonic Flow," AR-TR-69-17, U. of Texas, Aug. 1969.

Marvin, J. G., Seegmiller, H. L., Lockman, W. K., Mateer, G. G., Pappas, C. C., and DeRose, C. E., "Surface Flow Patterns and Aerodynamic Heating on Space Shuttle Vehicles," J. Spacecraft & Rockets, Vol. 9, No. 8, Aug. 1972, pp. 573-579.

Maskell, E. C., "Flow Separation in Three-Dimensions," RAE Aero. Report 2565, Nov. 1955.

Maskell, E. C., "On the Principles of Aerodynamic Design," Progress in Aeronautical Sciences, Vol. 1, No. 1, 1961, pp. 1-7.

Maskell, E. C. and Küchemann, D., "Controlled Separation in Aerodynamic Design," RAE TM 463, Mar. 1956.

Maskell, E. C. and Weber, J., "On the Aerodynamic Design of Slender Wings," J. Roy. Aeronaut. Soc., Vol. 63, Dec. 1959, pp. 709-721.

Maurer, F., "Three-Dimensional Effects in Shock-Separated Flow Regions Ahead of Lateral Control Jets Issuing from Slot Nozzle of Finite Length," AGARD CP-4, May 1966.

Mayne, A. W., "Analysis of Laminar Boundary Layers on Right Circular Cones at Angle of Attack, Including Streamline-Swallowing Effects," AEDC TR 72-134, Oct. 1972.

Mayne, A. W., Calculation of the Laminar Viscous Shock Layer on a Blunt Biconic Body at Incidence to Supersonic and Hypersonic Flow," AIAA Paper 77-88, Jan. 1977.

Melnik, R. E., "Vortical Singularities in Conical Flow," AIAA J., Vol. 5, Apr. 1967, pp. 631-637.

Messiter, A. F., "The Lift of Slender Delta Wings According to Newtonian Theory," AIAA J., Vol. 1, Apr. 1963, p. 794.

Meyer, R. F., "A Note on a Technique of Surface Flow Visualization," Nat. Res. Coun. of Canada Aero. Report LR-457, July 1966.

Meyer, R. F., "Rocket Experiments on the Heat Transfer to a Protuberance and to a Cavity," Nat. Res. Coun. of Canada Aero. Report LR-509, July 1968.

Meyer, R. F. and Vail, C. F., "An Experimental Study of the Hypersonic Flow About a Particular Half-Cone and Delta-Wing Lifting Configuration," Nat. Res. Coun. of Canada Aero. Report LR-475, Mar. 1967.

Michael, W. H., "Flow Studies on Flat Plate Delta Wings at Supersonic Speeds," NACA TN 3472, July 1955.

Miller, D. S. and Redeker, E., "Three-Dimensional Flow Separation," Bumblebee Aerodynamics Panel, Minutes of 48th Meeting at Defense Research Lab., U. of Texas, Nov. 1963.

Mokry, M. and Rainbird, W. J., "Calculation of Vortex Sheet Roll-Up in a Rectangular Wind Tunnel," J. of Aircraft, Vol. 12, No. 9, Sept. 1975, pp. 750-752.

Monnerie, B. and Werlé, H., "Étude de l'Écoulement Supersonique et Hypersonique autour d'une Aile Élancée en Incidence," AGARD CP-30, May 1968.

Moore, D. W., "A Numerical Study of the Roll-Up of a Finite Vortex Sheet," J. Fluid Mech., Vol. 63, No. 2, 1974, pp. 225-235.

Moore, F. K., "Laminar Boundary Layer on a Circular Cone in Supersonic Flow at a Small Angle of Attack," NACA TN-2521, Oct. 1951.

Moore, F. K., "Laminar Boundary Layer on a Cone in Supersonic Flow at Large Angle of Attack," NACA TN-2844, 1952.

Moretti, G., "Inviscid Flow Field Past a Pointed Cone at an Angle of Attack. Part I. Analysis," General Appl. Sci. Lab. Inc., Westbury, N.Y. Tech. Report 577, Dec. 1965.

Morkovin, M. V., "A Critical Evaluation of Transition," AFFDL TR 68-149, 1968.

Morkovin, M. V., "Technical Evaluation k. f the Fluid Dynamics Panel Symposium on Laminar-Turbulent Transition," AGARD-AR-122, June 1978.

Moss, G. F. and Isaacs, D., "8 ft x 8 ft Tunnel Tests on a Model of the De Havilland Blue Streak," ARC CP 734, 1964.

Moss, G. F., "Some UK Research Studies of the Use of Wing-Body Strakes on Combat Aircraft Configurations at High Angles of Attack," AGARD CP-247, Oct. 1978.

Munson, A. G., "The Vortical Layer on an Inclined Cone," J. Fluid Mech., Vol. 2^, 1965, pp. 625-643.

Murray, W. M. and Stallings, R. L., "Heat Transfer and Pressure Distributions on 60° and 70° Swept Delta Wings Having Turbulent Boundary Layers," NASA TN D-3644, Oct. 1966.

Myring, D., "An Integral Prediction Method for Three-Dimensional Turbulent Boundary Layers in Incompressible Flow," RAE TR 70147, Aug. 1970.

Nakao, S., "Supersonic Flow Past Conical Bodies at Large Angles of Attack," Tokyo University Inst. of Space and Aeronautics Sciences, Report 534, (Vol. 40, No. 14), Nov. 1975, pp. 369-420.

Nangia, R. K., "Three-Dimensional Wave Interactions in Supersonic Intakes," Second International Symposium on Air Breathing Engines, Sheffield, England, Mar. 1974.

Narayan, K. Y., "Lee-Side Flowfield and Heat Transfer of a Delta Wing at M_∞ = 10," AIAA J., Vol. 16, No. 2, Feb. 1978.

Nash, J. F. and Patel, V. C., "Three-Dimensional Turbulent Boundary Layers," SBC Technical Books, Atlanta, Ga., 1972.

Nash, J. F. and Scruggs, R. M., "Verification of a Three-Dimensional Turbulent Boundary-Layer Calculation Method," AFFDL-TR-78-15, Feb. 1978.

Nebbeling, C. and Bannink, W. J., "Experimental Investigation of the Supersonic Flow Field About a Slender Cone at High Incidences," Delft U. of Technology, The Netherlands, Dept. of Aerospace Eng. Report LR-233, Nov. 1976.

Neihouse, A. I., Klinar, W. J., and Scher, S. H., "Status of Spin Research for Recent Airplane Designs," NASA TR-R-57, 1960.

Nenni, J. P. and Tung, C., "A Second-Order Slender Wing Theory for Wings with Leading-Edge Separation in Supersonic Flow," NASA CR-1860, 1971.

Neumann, R. D. and Burke, G., "The Influence of Shock Wave-Boundary Layer Effects on the Design of Hypersonic Aircraft," AFFDL-TR-68-152, USAF Flight Dynamics Lab, 1968.

Neumann, R. D. and Token, K. H. "Prediction of Surface Phenomena Induced by Three-Dimensional Interactions on Planar Turbulent Boundary Layers," ICAS 74-058, Sept.-Oct. 1974.

Neumann, R. D. and Hayes, J. R., "Prediction Techniques for the Characteristics of the 3D Shock Wave Turbulent Boundary-Layer Interaction," AIAA Paper 77-46, Jan. 1977.

Newlander, R. A., "Effect of Shock Impingement on the Distribution of Heat Transfer Coefficients on a Right Circular Cylinder at Mach Numbers of 2.65, 3.51 and 4.44," NASA TN D-642, Jan. 1961.

Nielsen, J. N., "Non-Linearities in Missile Aerodynamics," AIAA Paper 78-20, Jan. 1978.

Nishioka, M. and Sato, H., "Mechanism of Determination of the Shedding Frequency of Vortices Behind a Cylinder at Low Reynolds Numbers," J. Fluid Mech., Vol. 89, Pt. 1, 1978, pp. 49-60.

Nomura, S., "Similar Boundary-Layer Analysis for Lee-Surface Heating on Yawed Blunted Cone," AIAA Paper 76-122, Jan. 1976.

Öhman, L. H., "A Surface Flow Solution and Stability Derivatives for Bodies of Revolution in Complex Supersonic Flow," Parts I and II, Nat. Res. Coun. of Canada Aero. Reports LR-419, 519, Nov. and Dec. 1964.

O'Hare, J. and Jones, J., "Flow Visualization Photography of a Yawed Tangent Ogive Cylinder at Mach 2," AEDC-TR-73-45, 1973.

O'Lone, R. G., "Thermal Tile Protection Ready to Roll," Aviation Week and Space Technology, Nov. 8, 1976, pp. 51-54.

Oskam, B., "Three-Dimensional Flow Fields Generated by the Interaction of a Swept Shock Wave with a Turbulent Boundary Layer," Report 1313, G.S Dynamics Lab., Princeton University, Dec. 1976.

Oskam, B., Bogdonoff, S. M., and Vas, I. E., "Study of Three-Dimensional Flow Fields Generated by the Interaction of a Skewed Shock Wave With a Turbulent Boundary Layer," AFFDL-TR-75-21, Feb. 1975.

Oskam, B., Vas, I. E., and Bogdonoff, S. M., "An Exploratory Study of a Three-Dimensional Shock Wave Boundary Layer Interaction at Mach 3," AGARD CP-168, May 1975.

Oskam, B., Vas, I. E., and Bogdonoff, S. M., "Oblique Shock Wave/Turbulent Boundary Layer Interactions in Three-Dimensions at Mach 3. Part I," AFFDL-TR-76-48, June 1976.

Oswatitsch, K., "Die Ablösungsbedingung von Grenzschichten," IUTAM Symposium on Boundary-Layer Research, Freiburg, 1957.

Owen, F. K., "Transition Experiments on a Flat Plate at Subsonic and Supersonic Speeds," AIAA J., Vol. 8, No. 3, Mar. 1970, pp. 518-523.

Owen, F. K. and Johnson, D. A., "Measurements of Unsteady Vortex Flow Fields," AIAA Paper 78-18, Jan. 1978a.

Owen, F. K. and Johnson, D. A., "Wake Vortex Measurements of Bodies at High Angle of Attack," AIAA Paper 78-23, Jan. 1978b.

Parker, A. G., "Aerodynamic Characteristics of Slender Wings and Sharp Leading Edges — A Review," J. Aircraft, Vol. 13, No. 3, Mar. 1976.

Pate, S. R., "Summary of Sharp Cone Static Force Measurements in AEDC VKF Tunnels A, B, C, F," Arnold Engineering Development Center, Tullahoma, Tenn., May 1974.

Peake, D. J. and Galway, R. D., "Three-Dimensional Separation of a Plane, Incompressible, Laminar Boundary Layer Produced by a Circular Cylinder Mounted Normal to a Flat Plate," AGARDograph 97, Pt. 2, pp. 1049-1080; also Nat. Res. Coun. of Canada Aero. Report LR-418, May 1965.

Peake, D. J., Galway, R. D., and Rainbird, W. J., "The Three-Dimensional Separation of a Plane, Incompressible, Laminar Boundary Layer Produced by a Rankine Oval Mounted Normal to a Flat Plate," Nat. Res. Coun. of Canada Aero. Report LR-446, Nov. 1965.

Peake, D. J., "The Flows About Upswept Rear Fuselages of Typical Cargo Aircraft," Nat. Res. Coun. of Canada, DME/NAE Quarterly Bulletin No. 1968(3), Oct. 1968.

Peake, D. J., "Three-Dimensional Flow Separations on Upswept Rear Fuselages," CASI J., Vol. 15, No. 10, Dec. 1969, pp. 399-408.

Peake, D. J., Jones, D. J., and Rainbird, W. J., "The Half-Cone Flow and Its Significance to Side-Mounted Intakes," AGARD CP-71, Sept. 1970.

Peake, D. J., Rainbird, W. J., and Atraghji, E. G., "Three-Dimensional Flow Separations on Aircraft and Missiles," AIAA J., Vol. 10, No. 5, May 1972, pp. 567-580.

Peake, D. J. and Rainbird, W. J., "The Drag Resulting from Three-Dimensional Separations Caused by Boundary-Layer Diverters and Nacelles in Subsonic and Supersonic Flow," AGARD CP-124, Apr. 1973.

Peake, D. J. and Rainbird, W. J., "The Three-Dimensional Separation of a Turbulent Boundary Layer by a Skewed Shock Wave, and Its Control by the Use of Tangential Air Injection," AGARD CP-168, May 1975.

Peake, D. J., "Three-Dimensional Swept Shock/Turbulent Boundary-Layer Separations with Control by Air Injection," Ph.D. Thesis, Carleton U., Ottawa, 1975; also Nat. Res. Coun. of Canada Aero. Report LR-592, July 1976.

Peake, D. J. and Rainbird, W. J., "Technical Evaluation Report on the Fluid Dynamics Panel Symposium on Flow Separation," AGARD-AR-98, Oct. 1976.

Peake, D. J., Bowker, A. J., Lockyear, S. J., and Ellis, F. E., "Non-Obtrusive Detection of Transition Region Using an Infra-Red Camera," AGARD CP-224, 1977.

Peake, D. J., "Phenomenological Aspects of Quasi-Stationary Controlled and Uncontrolled Three-Dimensional Flow Separations," AGARD LS 94, Feb. 1978.

Peake, D. J., Owen, F. K., and Higuchi, H., "Symmetrical and Asymmetrical Separations About a Yawed Cone, AGARD CP-247, Oct. 1978.

Peake, D. J. and Owen, F. K., "Control of Forebody Three-Dimensional Flow Separations," AGARD CP-262, May 1979.

Peake, D. J., Owen, F. K. and Johnson, D. A., "Control of Forebody Vortex Orientation to Alleviate Side Forces," AIAA Paper 80-0183, Jan. 1980.

Pearcey, H. H., "Shock-Induced Separation and Its Prevention by Design and Boundary-Layer Control," in Boundary Layer and Flow Control, Vol. 2, G. V. Lachmann ed., Pergamon Press, 1961, pp. 1166-1344.

Perry, A. E. and Fairlie, B. D., "Critical Points in Flow Patterns," Advances in Geophysics, Vol. 18B, Academic Press, 1974, pp. 299-315.

Pierce, D., "Photographic Evidence of the Formation and Growth of Vorticity Behind Plates, Accelerated from Rest in Still Air," J. Fluid Mech., Vol. 11, 1961.

Poincaré, H., "Oeuvres de Henri Poincaré, Tome 1," Gauthier-Villars et Cie, Paris 1928.

Poisson-Quinton, P., "From Wind Tunnel to Flight, the Role of the Laboratory in Aerospace Design," J. Aircraft, May-June 1968, pp. 193-214.

Popinski, Z., "Compressible Laminar Boundary Layers on Sharp Cone at Incidence with Entropy Swallowing," AIAA J., Vol. 13, No. 9, Sept. 1975, pp. 1135-1136.

Popinski, Z. and Davis, R. T., "Three-Dimensional Compressible Laminar Boundary Layers on Sharp and Blunt Circular Cones at Angle of Attack," NASA CR-112316, Jan. 1973.

Portnoy, H., "The Slender Wing with a Half Body of Revolution Mounted Beneath," Aeronaut. J., Vol. 72, No. 693, Sept. 1968, pp. 803-807.

Price, E. A. and Stallings, R. L., "Investigation of Turbulent Separated Flows in the Vicinity of Fin-Type Protuberances at Supersonic Mach Numbers," NASA TN D-3804, Feb. 1967.

Pulliam, T. H. and Steger, J. L., "On Implicit Finite-Difference Simulations of Three-Dimensional Flow," AIAA Paper 78-10, Jan. 1978.

Pullin, D. I., "Calculations of the Steady Conical Flow Past a Yawed Slender Delta Wing with Leading-Edge Separation," Imp. Coll., London, Aero. Report 72-17, 1972.

Ragsdale, W. C., "Flow Field Measurements Around an Ogive-Cylinder at Angles of Attack up to 15 Degrees for Mach Numbers 3.5 and 4," NOL TR 72-198, Aug. 1972.

Rainbird, W. J., "The External Flow Field About Yawed Circular Cones," AGARD CP-30, May 1968a.

Rainbird, W. J., "Turbulent Boundary-Layer Growth and Separation on a Yawed 12-1/2° Cone at Mach Numbers 1.8 and 4.25," AIAA J., Vol. 6, No. 12, Dec. 1968b, pp. 2410-2416.

Rainbird, W. J., Crabbe, R. S., and Jurewicz, L. S., "A Water Tunnel Investigation of the Flow Separation About Circular Cones at Incidence," Nat. Res. Coun. of Canada Aero. Report LR-385, Sept. 1963.

Rainbird, W. J., Crabbe, R. S., Peake, D. J., and Meyer, R. F., "Some Examples of Separation in Three-Dimensional Flows," CASI J., Vol. 12, No. 10, Dec. 1966, pp. 409-423.

Rakich, J. V. and Kutler, P., "Comparison of Characteristics and Shock-Capturing Methods with Application to the Space Shuttle Vehicle," AIAA Paper 72-191, Jan. 1972.

Rakich, J. V. and Park C., "Nonequilibrium Three-Dimensional Supersonic Flow Computations with Application to the Space Shuttle Orbiter Design," Proc. of Symposium on Application of Computers to Fluid Dynamic Analysis and Design, Polytechnic Inst. of Brooklyn Grad. Center, Long Island, N.Y., Jan. 1973.

Rakich, J. V., Bailey, H. E., and Park, C., "Computation of Nonequilibrium Three-Dimensional Inviscid Flow Over Blunt-Nosed Bodies Flying at Supersonic Speeds," AIAA Paper 75-835, 1975.

Rakich, J. V. and Lubard, S. C., "Numerical Computation of Viscous Flows on the Lee Side of Blunt Shapes Flying at Supersonic Speeds," NASA SP-347, Mar. 1975, pp. 531-542.

Rakich, J. V. and Lanfranco, M. J., "Numerical Computation of Space Shuttle Heating and Surface Streamlines," AIAA Paper 76-464, July 1976.

Rao, D. S. and Whitehead, A. H., "Lee-Side Vortices on Delta Wings at Hypersonic Speeds," AIAA J., Vol. 10, No. 11, Nov. 1972.

Rao, D. M., "Side-Force Alleviation on Slender, Pointed Forebodies at High Angles of Attack," AIAA Paper 78-1339, Aug. 1978. Also J. Aircraft, Vol. 16, No. 11, Nov. 1979, pp. 763-768.

Reda, D. C., "Comments on Session V of Symposium on Laminar-Turbulent Transition," AGARD CP-224, Oct. 1977.

Reding, J. P. and Ericsson, L. E., "Maximum Vortex-Induced Side Forces on Slender Bodies," AIAA Paper 77-1155, 1977.

Reinhardt, W. A., "Parallel Computation of Unsteady, Three-Dimensional, Chemically Reacting, Nonequilibrium Flow Using a Time-Split Finite-Volume Method on the Illiac IV," J. Phys. Chem., Vol. 81, No. 25, 1977, pp. 2427-2435.

Reshotko, E., "Laminar Boundary Layer with Heat Transfer on a Cone at Angle of Attack in a Supersonic Stream," NACA TN-4152, Dec. 1957.

Reshotko, E., "Round Table Discussion in Symposium on Laminar-Turbulent Transition," AGARD CP-224, Oct. 1977.

Reshotko, E. and other authors, "Recent Developments in Boundary-Layer Transition Research, AIAA J., Vol. 3, No. 3, Mar. 1975.

Richards, I. C., "Supersonic Flow Past a Slender Delta Wing: An Experimental Investigation Covering the Incidence Range $-5° \leq \alpha \leq 50°$," Aeronaut. Quart., Vol. XXVII, Pt. 2, May 1976, pp. 143-153.

Rizzi, A. and Bailey, H., "Reacting Nonequilibrium Flow Around the Space Shuttle Using a Time Split Method," NASA SP-347, 1975.

Roache, P. J. and Bradshaw, P., Letters in response to Chapman, Mark, and Pirtle (Astronaut. & Aeronaut., Vol. 13, No. 4, Apr. 1975, p. 35), Astronaut. & Aeronaut., Vol. 13, No. 9, Sept. 1975, pp. 4-6.

Robinson, M. L., "Boundary-Layer Effects in Supersonic Flow Over Cylinder-Flare Bodies," WRE Report 1238, Australia, July 1974.

Roe, P. L., "Thin Shock Layer Theory," AGARD LS 42, Vol. 1, 1972.

Rogers, E. W. E. and Hall, I. M., "An Introduction to the Flow About Plane Swept Back Wings at Transonic Speeds," J. Roy. Aeronaut. Soc., Vol. 64, 1960, p. 449.

Roux, B. and Bontoux, P., "Supersonic Turbulent Boundary Layer in the Symmetry Plane of a Cone at Incidence," AIAA J., Vol. 13, No. 6, June 1975, pp. 705-706

Rubesin, M., "Subgrid or Reynolds Stress Modeling for Three-Dimensional Turbulence Computations," Part 1. NASA SP-347, Mar. 1975, pp. 317-339.

Sacks, A. H. and Tickner, E. G., "An Exploratory Study of the Vortex Sheets Shed from the Leading-Edges of Slender Wings," NASA CR-73048, 1966.

Sacks, A. H., Lundberg, R. E., and Hanson, C. W., "A Theoretical Investigation of the Aerodynamics of Slender Wing-Body Combinations Exhibiting Leading-Edge Separation," NASA CR-719, 1967.

Schiff, L. B., "A Study of the Nonlinear Aerodynamics of Bodies in Nonplanar Motion," NASA TR R-421, Jan. 1974.

Schlichting, H., "Boundary-Layer Theory," McGraw-Hill, 1968, p. 91.

Schwind, R. G., "The Three-Dimensional Boundary Layer Near a Strut," MIT Gas Turbine Lab Report No. 67, May 1962.

Scuderi, L. F., "Expressions for Predicting 3D Shock Wave-Turbulent Boundary Layer Interaction Pressures and Heating Rates," AIAA Paper 78-162, Jan. 1978.

Sears, W. R., "The Boundary Layer of Yawed Cylinders," J. Aeronaut. Sci., Vol. 15, No. 1, Jan. 1948, pp. 49-52, (in Collected Papers of W. R. Sears through 1973, N. H. Kemp, ed., Valley Offset, N.Y.).

Seddon, J. and Spence, A., "The Use of Known Flow Fields as an Approach to the Design of High Speed Aircraft," AGARD CP-30, May 1968.

Sedney, R. and Kitchens, C. W., "The Structure of Three-Dimensional Separated Flows in Obstacle, Boundary-Layer Interactions," AGARD CP-168, May 1975.

Sedney, R. and Kitchens, C. W., "Measurement and Correlation of Separation Ahead of Protuberances in a Turbulent Boundary Layer," AIAA Paper 76-163, Jan. 1976.

Shanebrook, J. R. and Sumner, W. J., "Crossflow Profiles for Compressible Turbulent Boundary Layers," J. Aircraft, Vol. 8, No. 3, 1971, pp. 188-189.

Shanebrook, J. R. and Sumner, W. J., "Entrainment Equation for Three-Dimensional Compressible Turbulent Boundary Layers," AIAA J., Vol. 10, No. 5, May 1972, pp. 693-694.

Shang, J. S. and Hankey, W. L., "Numerical Solution of the Navier-Stokes Equations for a Three-Dimensional Corner," AIAA J., Vol. 15, No. 11, Nov. 1977, pp. 1575-1582.

Shang, J. S., Hankey, W. L., and Petty, J. S., "Three-Dimensional Supersonic Interacting Turbulent Flow Along a Corner," AIAA Paper 78-1210, July 1978; also AIAA J., Vol. 17, No. 7, July 1979, pp. 706-713.

Shankar, V., Anderson, D., and Kutler, P., "Numerical Solutions for Supersonic Corner Flow," J. Comput. Phys., Vol. 17, No. 2, Feb. 1975, pp. 160-180.

Shanks, R. E., "Low Subsonic Measurements of Static and Dynamic Stability Derivatives of Six Flat Plate Wings Having Leading-Edge Sweep Angles of 70° to 84°," NASA TN D-1822, 1963.

Shen, P. S., "Three-Dimensional Flow Separation of a Plane, Incompressible Laminar Boundary Layer Caused by a Half-Delta Wing on a Flat Plate," Nat. Res. Coun. of Canada Aero. Report LR-471, Feb. 1967.

Shen, P. S. and Jones, D. J., "Three-Dimensional Laminar Boundary-Layer Separation on a Flat Plate Due to a Flow Confrontation with a Half Cone at Incidence," Nat. Res. Coun. of Canada Aero. Report LR-485, June 1967.

Sigalla, A. and Hallstaff, T. H., "Aerodynamics of Powerplant Installation on Supersonic Aircraft," J. Aircraft, Vol. 4, No. 4, July-Aug. 1967, pp. 273-277.

Sims, J. L., "Tables of Supersonic Flow Around Right Circular Cones at Small Angle of Attack," NASA SP-3007, 1964.

Skow, A. M., Moore, W. A., and Lorincz, D. J., "A Novel Concept to Enhance Departure/Spin Recovery Characteristics of Fighter Aircraft Through Control of the Forebody Vortex Orientation," AGARD CP-262, May 1979.

Smith, J. H. B., "Improved Calculations of Leading-Edge Separation from Slender Delta Wings," RAE TR 66070, Mar. 1966; also Proc. Roy. Soc., Ser. A, Vol. 306, 1968, pp. 67-90.

Smith, J. H. B., "Remarks on the Structure of Conical Flow," RAE TR 69119, June 1969.

Smith, J. H. B., "Calculation of the Flow Over Thick, Conical Slender Wings with Leading-Edge Separation," RAE Tech. Report 71057; ARC R and M 3694, 1971.

Smith, J. H. B., "Similar Solutions for Slender Wings with Leading-Edge Separation," 13th International Congress of Theoretical Applied Mechanics, Moscow, 1972.

Smith, J. H. B., "A Review of Separation in Steady, Three-Dimensional Flow," AGARD CP-168, May 1975.

Smith, J. H. B., "Inviscid Fluid Models, Based on Rolled-Up Vortex Sheets, for Three-Dimensional Separation at High Reynolds Number," AGARD LS 94, Three-Dimensional and Unsteady Separation at High Reynolds Numbers, May 1978.

Smith, P. D., "An Integral Prediction Method for Three-Dimensional, Compressible, Turbulent Boundary Layers," RAE Tech. Report 72228, ARC R and M 3739, 1973.

Spillman, J. and Goodridge, M., "Flow Characteristics About a Delta Wing at 15° Incidence with and without Leading-Edge Blowing," Coll. of Aero., Cranfield, Report No. 9, 1972.

Squire, L. C., Jones, J. G., and Stanbrook, A., "An Experimental Investigation of the Characteristics of Some Plane and Cambered 65° Delta Wings at Mach Numbers from 0.7 to 2.0," ARC R and M 3305, 1963.

Squire, L. C., "The Estimation of the Non-Linear Lift of Delta Wings at Supersonic Speeds," J. Roy. Aeronaut. Soc., Vol. 67, 1963, pp. 476-480.

Squire, L. C., "Pressure Distribution and Flow Patterns at M = 4.0 on Some Delta Wings," ARC R and M 3373, 1964.

Squire, L. C., "Report on Euromech 20 - The Aerodynamics of Lifting Bodies at High Supersonic Speeds," Aeronaut. J., Vol. 75, No. 721, Jan. 1971, p. 18.

Squire, L. C., "Some Extensions of Thin Shock Layer Theory," Aeronaut. Quart., Vol. XXV, 1974, p. 1.

Stainback, P. C. and Weinstein, L. M., "Aerodynamic Heating in the Vicinity of Corners at Hypersonic Speeds," NASA TN D-4130, Nov. 1967.

Stalker, R. J., "The Pressure Rise at Shock-Induced Turbulent Boundary Layer Separation in Three-Dimensional Supersonic Flow," J. Aeronaut. Sci., Vol. 24, No. 7, July 1957, p. 547.

Stalker, R. J., "Sweepback Effects in Turbulent Boundary-Layer Shock-Wave Interaction," J. Aerospace Sci., Vol. 27, No. 5, May 1960, pp. 348-356.

Stanbrook, A., "An Experimental Study of the Glancing Interaction Between a Shock Wave and a Turbulent Boundary Layer," ARC CP 555, 1961.

Stanbrook, A. and Squire, L. C., "Possible Types of Flow at Swept Leading Edges," Aeronaut. Quart., Vol. XV, 1964, p. 72-82.

Stetson, K. F., "Experimental Results of Laminar Boundary-Layer Separation on a Slender Cone at Angle of Attack at M_∞ = 14.2," ARL 71-0127, Aug. 1971.

Stewartson, K., "The Theory of Laminar Boundary Layers in Compressible Fluids," Oxford Mathematical Monographs, Oxford U. Press, 1964, pp. 1-10.

Stocker, P. M. and Mauger, F. E., "Supersonic Flow Past Cones of General Cross-Section," J. Fluid Mech., Vol. 13, 1962, pp. 383-399.

Stollery, J. L. and Richards, I. C., "Supersonic Flow Past a Slender Delta Wing — An Experimental Study," ICAS 76-24, Oct. 1976.

Stone, C. R. and Mulfinger, R., "Hypersonic Stability and Control Characteristics of the Rockwell International 139-B Space Shuttle Orbiter," NASA TM X-71,968, July 1974.

Surber, T. E., "Heat Transfer in the Vicinity of Surface Protuberances," J. Spacecraft & Rockets, Vol. 2, No. 6, Nov. 1965, pp. 978-980.

Swan, W. C., "A Discussion of Selected Aerodynamic Problems on Integration of Propulsion Systems with the Airframe of Transport Aircraft," AGARDograph 103, Part I, Oct. 1965, pp. 23-68.

Syvertson, C. A. and Dennis, D. H., "A Second-Order Shock-Expansion Method Applicable to Bodies of Revolution Near Zero Lift," NACA Report 1328, 1957.

Szodruch, J., "Leeseiten-Strömung bei schlanken Deltaflügeln endlicher Dicke," Institut für Luft-und Raumfahrt Technische Universität, Berlin, ILR, Report 23, 1977.

Szodruch, J., "Reynolds Number Influence on Leeside Flow Fields," AIAA J., Vol. 16, No. 12, Dec. 1978, pp. 1306-1309.

Szodruch, J. and Peake, D. J., "The Leeward Flow Over Delta Wings at Supersonic Speeds," NASA TMX in preparation, Feb. 1980.

Szodruch, J. and Ganzer, U., "On the Lee-Side Flow Over Delta Wings at High Angle of Attack," AGARD CP-247, Oct. 1979.

Tani, I., "Boundary-Layer Transition," Annual Review of Fluid Mech., Vol. 1, 1969, pp. 169-196.

Tannehill, J. C., Holst, T. L., and Rakich, J., "Numerical Computation of Two-Dimensional Viscous Blunt Body Flows with an Impinging Shock," AIAA J., Vol. 14, No. 2, Feb. 1976, pp. 204-211.

Thomann, H., "Measurement of Heat Transfer, Recovery Temperature, and Pressure Distribution on Delta Wings at M = 3," FFA Report 93, The Aeronautical Research Institute, Stockholm, Sweden, 1963.

Thomas, J. P., "Flow Investigation About a Fin-Plate Model at a Mach Number of 11.26," ARL 67-0188, Sept. 1967.

Thomson, K. D. and Morrison, D. F., "The Spacing, Position and Strength of Vortices in the Wake of Slender Cylindrical Bodies at Large Incidences," J. Fluid Mech., Vol. 50, Pt. 4, 1971, pp. 751-583.

Thwaites, G., "Bodies at Moderate Incidence," Section IX 20 Incompressible Aerodynamics, Oxford at the Clarendon Press, 1960.

Tinling, B. E. and Allen, C. Q., "An Investigation of the Normal Force and Vortex-Wake Characteristics of an Ogive-Cylinder Body at Subsonic Speeds," NASA TN D-1297, 1962.

Titiriga, A., Skow, A. M., and Moore, W. A., "Forebody/Wing Vortex Interaction and Their Influence on Departure and Spin Resistance," AGARD CP-247, Oct. 1978.

Tobak, M., "Hypothesis for the Origin of Cross-Hatching," AIAA J., Vol. 8, No. 2, Feb. 1970, pp. 330-334.

Tobak, M., "On Local Inflexional Instability in Boundary-Layer Flows," J. Appl. Math. and Phys. (ZAMP), Vol. 24, 1973, pp. 330-354.

Tobak, M. and Peake, D. J., "Topology of Two-Dimensional and Three-Dimensional Separated Flows," AIAA Paper 79-1480, July 1979.

Token, K. H., "Heat Transfer Due to Shock Wave Turbulent Boundary Layer Interactions on High Speed Weapon Systems," AFFDL-TR-74-77, Apr. 1974.

Topham, D. R., "A Correlation of Leading-Edge Transition and Heat Transfer on Swept Cylinders in Supersonic Flow," J. Roy. Aeronaut. Soc., Vol. 69, No. 649, Jan. 1965, pp. 49-52.

Townend, L. H., "On Lifting Bodies Which Contain Two-Dimensional Supersonic Flows," RAE Report Aero 2675, 1963.

Tracy, R. R., "Hypersonic Flow Over a Yawed Circular Cone," GALCIT Memo. No. 69, Graduate Aeronautical Laboratories, Calif. Inst. of Tech., Pasadena, Calif., 1963.

Tsen, L. F., "Contribution à l'Étude de la Couche Limite Tridimensionnelle Laminaire Compressible avec Transfert de Chaleur," Publications Scientifiques et Techniques, No. 435, Ministère de l'Air France, Apr. 1967.

Tsen, L. F. and Arnaudon, J. F., "Couche Limite Laminaire Compressible sur une Surface Conique," Proc. of Canadian Congress of Applied Mechanics, Vol. 2, U. Laval, Québec, Canada, May 1967, pp. 20, 206-208.

Tsen, L. F. and Arnaudon, J. F., "Calcul par Iteration d'une Couche Limite Tridimensionelle et Comparison Expérimentale," Int. J. Heat Mass Transfer, Vol. 15, No. 7, 1972, pp. 1373-1394.

Victoria, K. J. and Widhopf, G. F., "Numerical Solution of the Unsteady Navier-Stokes Equations in Curvilinear Coordinates: The Hypersonic Blunt Body Merged Layer Problem," Lecture Notes in Physics, No. 19, Vol. III, Springer-Verlag, 1973.

Vigneron, Y. C., Rakich, J. V., and Tannehill, J. C., "Calculation of Supersonic Viscous Flow Over Delta Wings with Sharp Subsonic Leading Edges," AIAA Paper 78-1137, July 1978.

Voitenko, D. M., Zubkov, A. I., and Panov, Y. A., "Supersonic Gas Flow Past a Cylindrical Obstacle on a Plate," Mekhanika Zhidkosti i Gaza, Vol. 1, No. 1, 1966, pp. 121-125.

Wang, K. C., "Separation Patterns of Boundary Layer Over an Inclined Body of Revolution," AIAA J., Vol. 10, No. 8, Aug. 1972, pp. 1044-1050.

Wang, K. C., "Boundary Layer Over a Blunt Body at High Incidence with an Open Type of Separation," Proc. Roy. Soc. London, Ser. A, Vol. 340, 1974a, pp. 33-35.

Wang, K. C., "Boundary Layer Over a Blunt Body at Extremely High Incidence," Phys. Fluids, Vol. 17, No. 7, 1974b, pp. 1381-1385.

Wang, K. C., "Boundary Layer Over a Blunt Body at Low Incidence with Circumferential Reversed Flow," J. Fluid Mech., Vol. 72, Pt. 1, 1975, pp. 49-65.

Ward, G. N., "Linearised Theory of High Speed Flow," Chap. 9. Cambridge Univ. Press, England, 1955.

Watson, R. D. and Weinstein, L. M., "A Study of Hypersonic Corner Flow Interactions," AIAA Paper 70-227, 1970.

Weber, J. A., Brune, G. W., Johnson, F. T., Lu, P., and Rubbert, P. E., "Three-Dimensional Solution of Flows Over Wings with Leading-Edge Vortex Separation," AIAA Paper 75-866, June 1975.

Werlé, H., "Aperçu sur les Possibilités Expérimentales du Tunnel Hydrodynamique à Visualisation de l'O.N.E.R.A.," ONERA Tech. Not. 48, 1958.

Werlé, H., "Separation on Axisymmetrical Bodies at Low Speed," Rech. Aeron. No. 90, Sept.-Oct. 1962, pp 3-14.

Werlé, H., "Hydrodynamic Flow Visualization," Annual Review of Fluid Mechanics, Vol. 5, 1973, pp. 361-382.

Werlé, H., "La Tunnel Hydrodynamique au Service de la Recherche Aérospatiale," ONERA Publication No. 156, 1974.

Werle, M. J., Driftmyer, R. T., and Shaffer, D. G., "Supersonic Two-Dimensional Jet-Interaction Studies," NOL TR 70-242, Dec. 1970.

West, J. E. and Korkegi, R. H., "Supersonic Interaction in the Corner of Intersecting Wedges at High Reynolds Numbers," AIAA J., Vol. 10, No. 5, May 1972.

Westkaemper, J. C., "The Drag of Cylinders All or Partially Immersed in a Turbulent Supersonic Boundary Layer," DRL-549, U. of Texas, Mar. 1967.

Westkaemper, J. C., "Turbulent Boundary Layer Separation Ahead of Cylinders," AIAA J., Vol. 6, No. 7, July 1968, pp. 1352-1355.

Whitehead, A. H., Hefner, J. N., and Rao, D. M., "Lee-Surface Vortex Effects over Configurations in Hypersonic Flow," AIAA Paper 72-77, Jan. 1972.

Whitfield, J. D., Wolny, W., "Correlation of Hypersonic Static Stability Data From Blunt, Slender Cones," AIAA J., Vol. 1, No. 2, Feb. 1963, pp. 486-487.

Wickens, R. H., "Observations of the Vortex Wake of a Lifting Fuselage Similar to Those on Rear-Loading Transport Aircraft," Nat. Res. Coun. of Canada Aero. Report LR-395, Jan. 1964.

Wickens, R. H., "The Vortex Wake and Aerodynamic Load Distribution of Slender Rectangular Plates (The Effects of a 20-Degree Bend at Mid-Chord)," Nat. Res. Coun. of Canada Aero Report LR-458, July 1966.

Widhopf, G. F., "Turbulent Heat-Transfer Measurements on a Blunt Cone at Angle of Attack," AIAA J., Vol. 9, No. 8, Aug. 1971a.

Widhopf, G. F., "Heat-Transfer Correlations for Blunt Cones at Angle of Attack," J. Spacecraft & Rockets, Vol. 8, No. 9, Sept. 1971b.

Widhopf, G. F. and Hall, R., "Transitional and Turbulent Heat Transfer Measurements on a Yawed Blunt Conical Nosetip," AIAA J., Vol. 10, No. 10, Oct. 1972, pp. 1318-1325.

Wilde, M. G. and Cormery, G., "The Aerodynamic Derivation of the Concorde Wing," CASI J., Vol. 16, No. 5, May 1970, pp. 175-184.

Winkelmann, A. E., "Aerodynamic Interaction Phenomena Produced by a Fin Protuberance Partially Immersed in a Turbulent Boundary Layer at Mach 5," AGARD CP-71, Sept. 1970.

Woods, W. C. and Arrington, J. P., "Electron-Beam Flow Visualization – Applications in the Definition of Configuration Aerothermal Characteristics," AIAA Paper 72-1016, Sept. 1972.

Yen, S. and Thyson, M. A., "An Integral Method for Calculation of the Supersonic Laminar Boundary Layer with Heat Transfer on a Yawed Cone," AIAA J., Vol. 1, No. 3, Mar. 1963, p. 677.

Young, F. L., Kaufman, L. G., and Korkegi, R. H., "Experimental Investigation of Interactions Between Blunt Fin Shock Waves and Adjacent Boundary Layers at Mach Numbers 3 and 5," ARL 68-0214, Dec. 1968.

Zakkay, V., Erdos, J., and Calarese, W., "An Investigation of Three-Dimensional Jet Control Interaction on a Conical Body," AGARD CP-30, May 1968.

Zakkay, V., Calarese, W., and Wang, C. R., "A Theoretical and Experimental Investigation of the Hypersonic Turbulent Boundary Layer Subject to Normal and Longitudinal Pressure Gradients and Cross-Flow Along a Windward Plane of Symmetry," AIAA Paper 72-187, Jan. 1972.

Zakkay, V., Economos, C., and Alzner, E., "Leeside Flow Field Description Over Cones at Large Incidence," AFFDL-TR-74-19, July 1974.

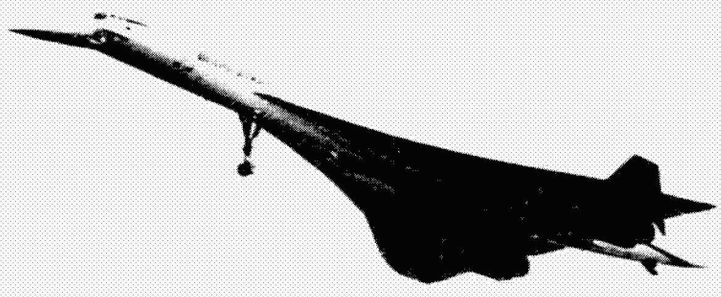

(a) ELEGANCE IN THE SKY
(COURTESY OF J.R. DIGNEY, NAE, OTTAWA)

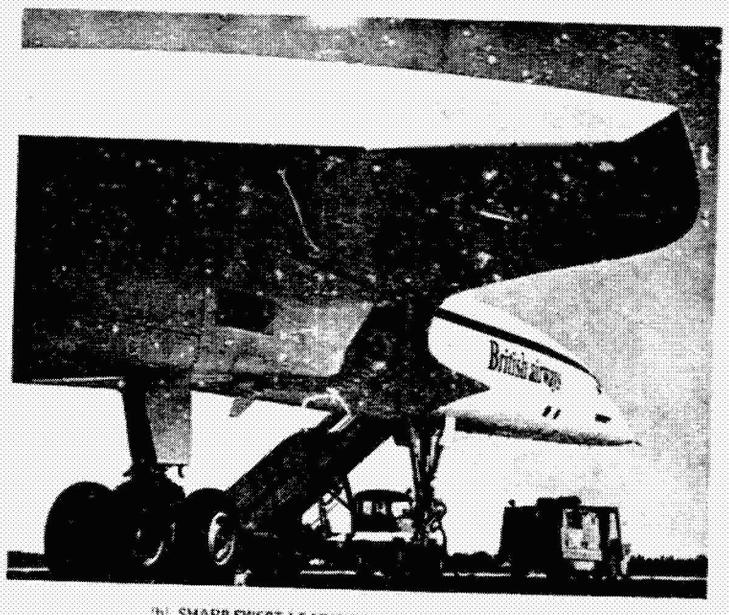

(b) SHARP SWEPT LEADING EDGE OF "CONCORDE"

Fig. 1 "Concorde."

Fig. 2 Space Shuttle "Columbia" (courtesy of Rockwell International).

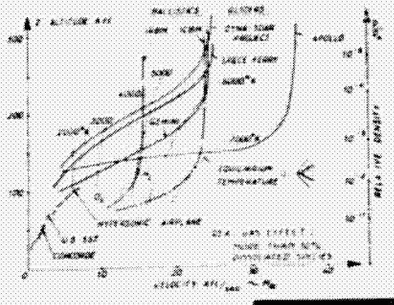

(a) Flight corridors for typical high speed vehicles, with indications of the equilibrium stagnation temperature and the onset of air dissociation encountered at high speed (Poisson-Quinton 1968)

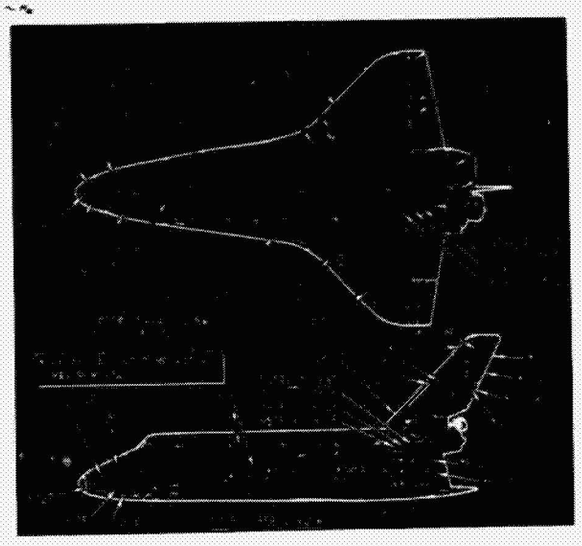

(b) Isotherms on shuttle orbiter expected during re-entry or ascent (O'Leone 1976)

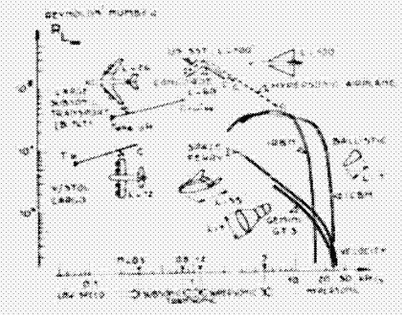

(c) Flight speed regimes and Reynolds numbers for various vehicles (Poisson-Quinton 1968)

Fig. 3 Flight domains.

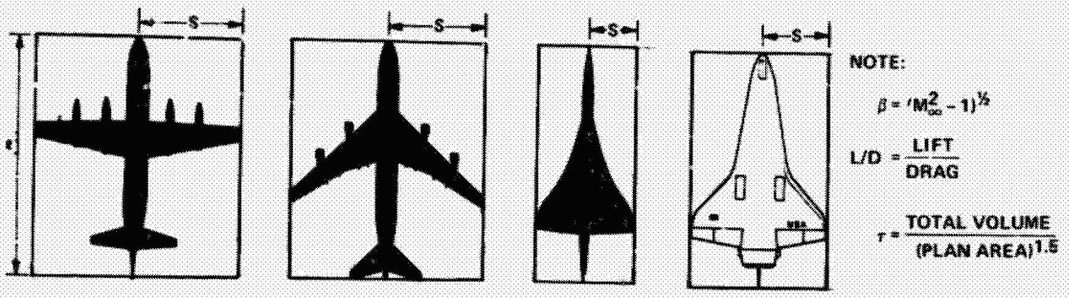

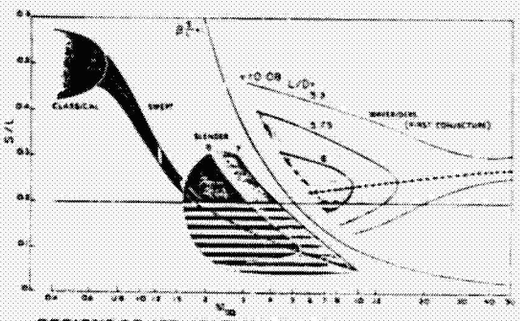

REGIONS OF APPLICATION OF VARIOUS AIRCRAFT TYPES (KÜCHEMANN 1965)

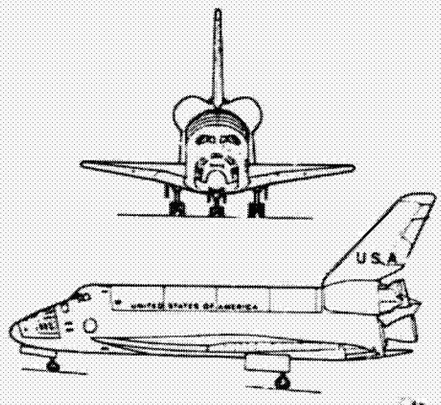

(d) EXISTING AND CONJECTURED AIRCRAFT TYPES FOR LONG RANGE FLIGHT COMPARED WITH SHUTTLE

Fig. 3 Concluded.

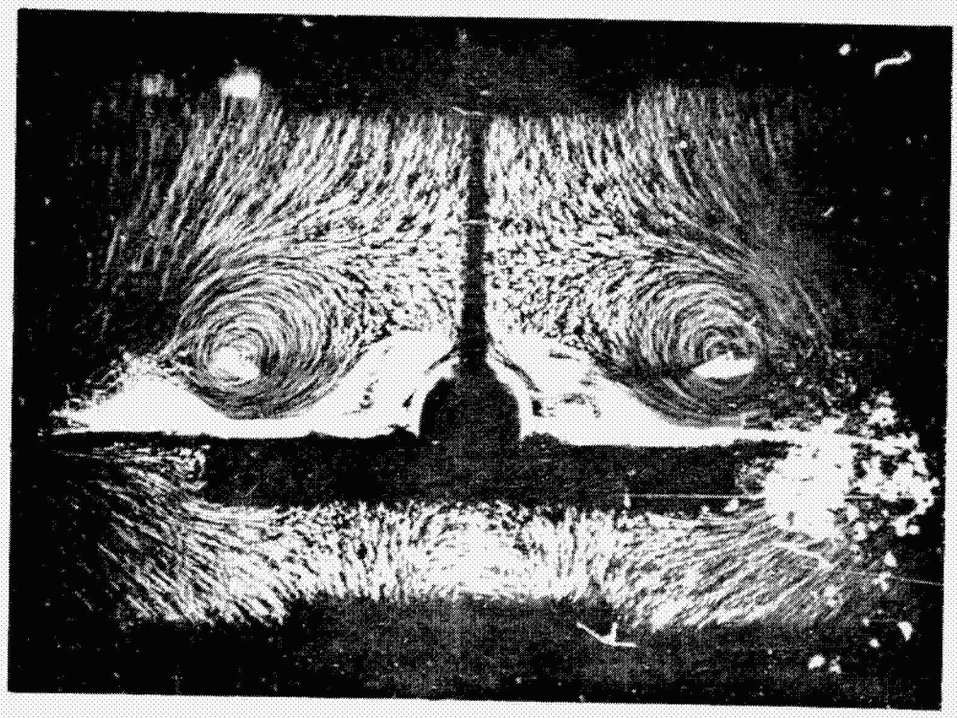

Fig. 4 Vortices from sharp swept leading edges of slender wing (courtesy of Aeronautical Journal).

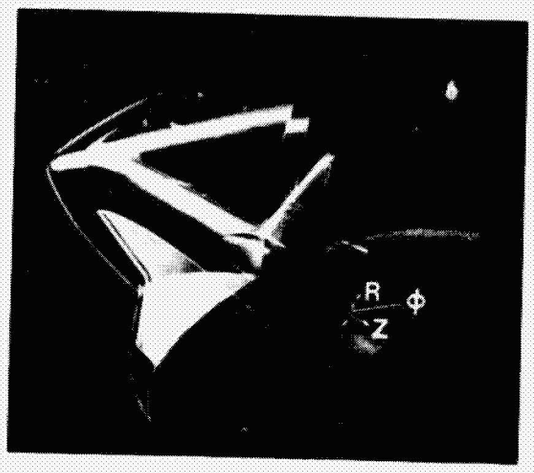

Fig. 5 Shock structure about Shuttle Orbiter at large angle of attack during atmospheric reentry (Reinhardt 1977).

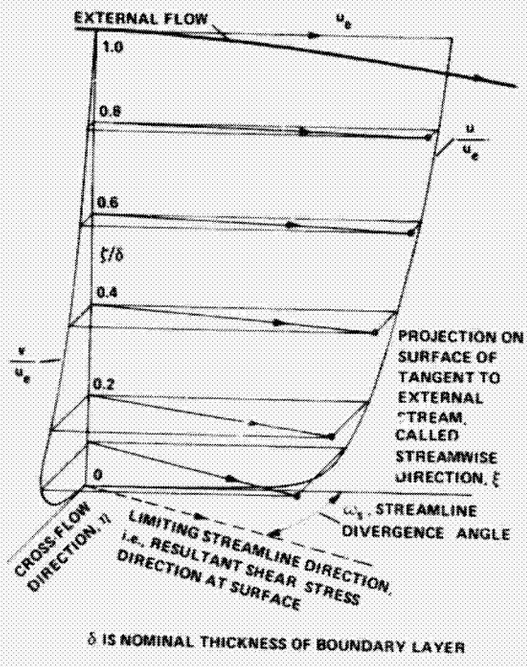

Fig. 7 Response of initially 2D boundary layer to a transverse pressure gradient.

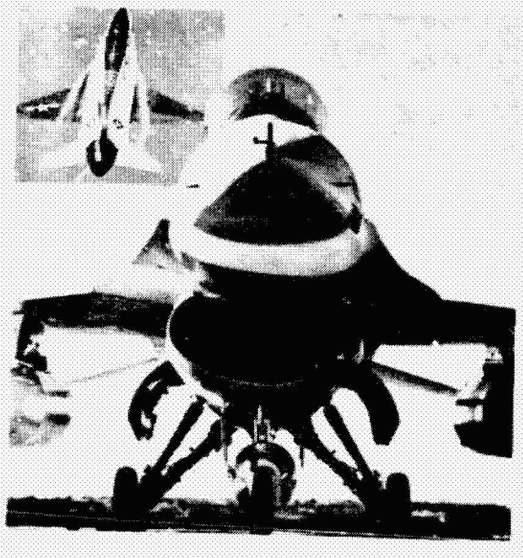

Fig. 6 Controlled flow separation from leading-edge extensions (strakes).

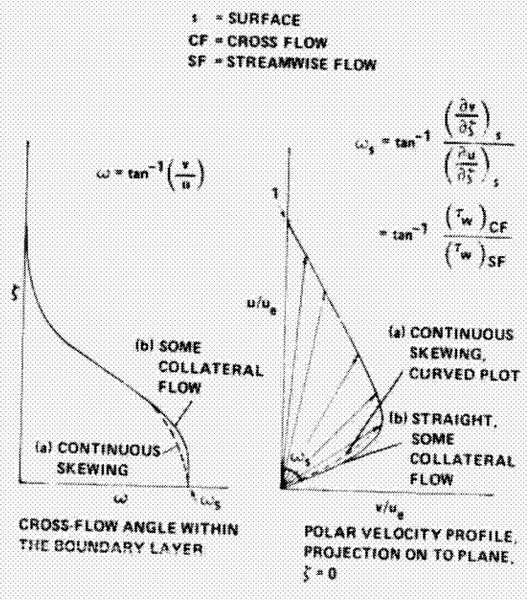

Fig. 8 Velocity vectors in 3D boundary layer near surface (streamline coordinates).

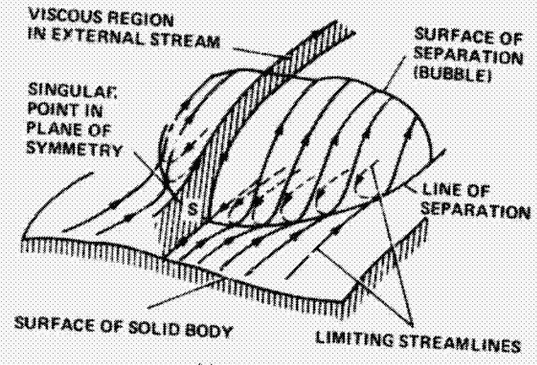

(a) BUBBLE

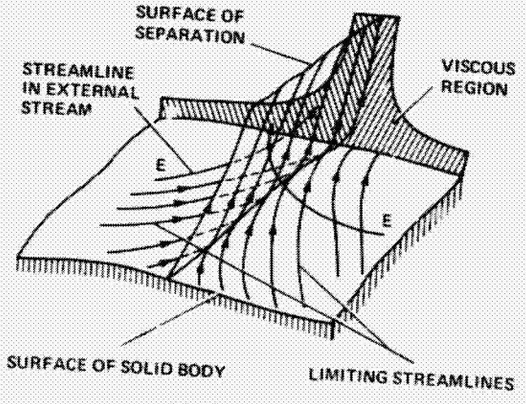

(b) FREE SHEAR LAYER

Fig. 9 3D separations (after Maskell 1955).

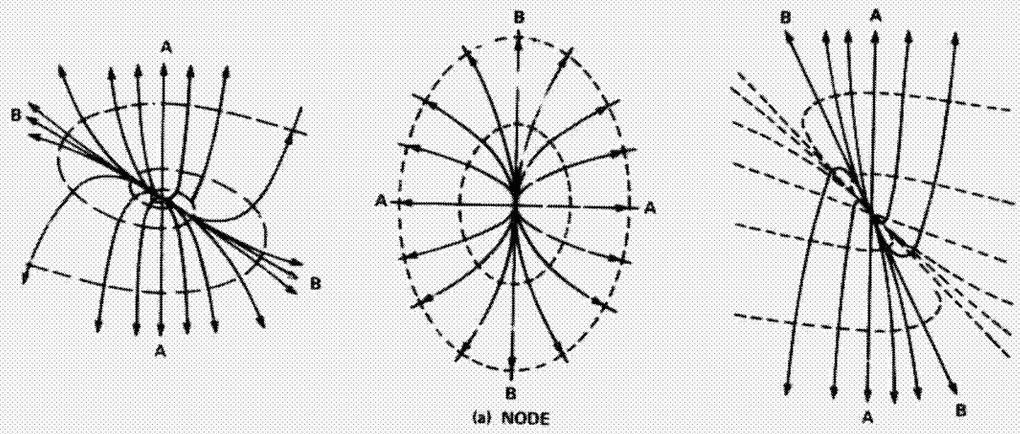

(a) NODE

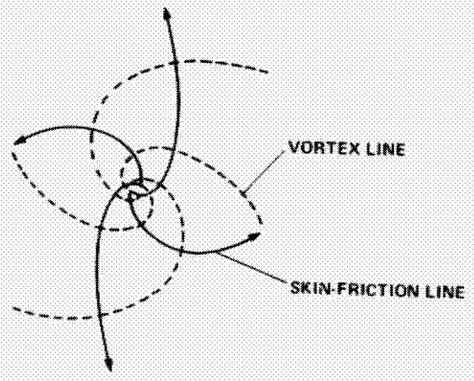

(b) FOCUS (NODE)

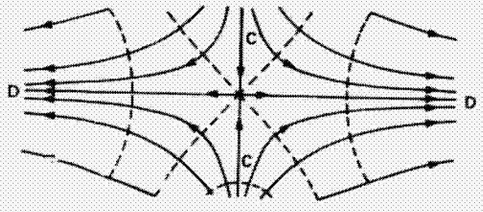

(c) SADDLE

Fig. 10 Singular points.

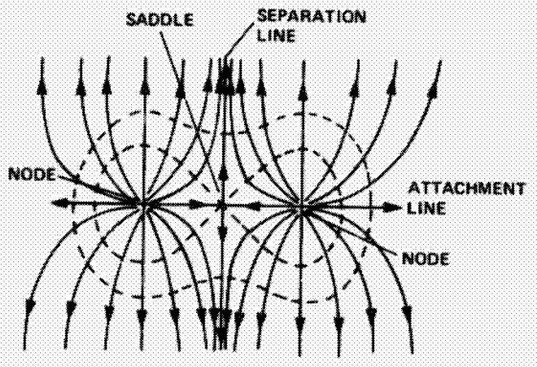

(a) LIGHTHILL 1963

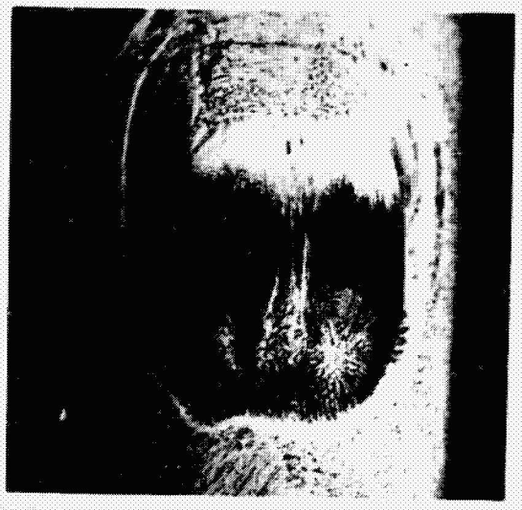

(b) PLAN VIEW OF SHUTTLE MODEL WINDSHIELD, $M_\infty = 7.4$, $R_{L_\infty} = 3.4 \times 10^6$, VEHICLE LENGTH, L = 1.3 ft; $\alpha = 15°$
(COURTESY L. SEEGMILLER, NASA-AMES)

FLOW DIRECTION

Fig. 11 Example of adjacent nodes and saddle point.

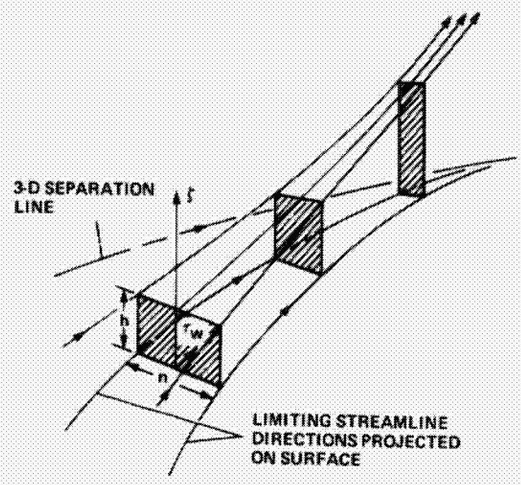

Fig. 12 Limiting streamlines near 3D separation line.

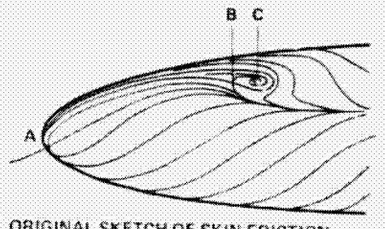

(a) ORIGINAL SKETCH OF SKIN-FRICTION LINES BY LEGENDRE 1965

A – NODAL ATTACHMENT POINT
B – SADDLE POINT
C – FOCUS OF SEPARATION

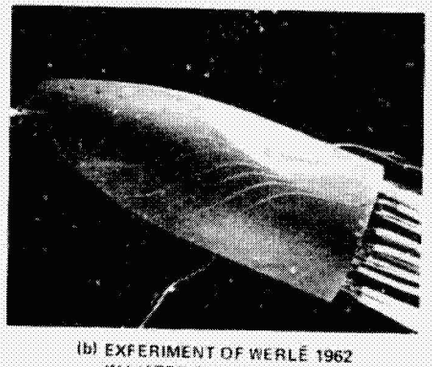

(b) EXFERIMENT OF WERLÉ 1962 IN WATER TUNNEL

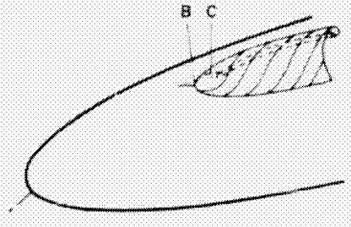

(c) EXTENSION OF FOCUS, LEGENDRE 1965

Fig. 13 Focus of separation.

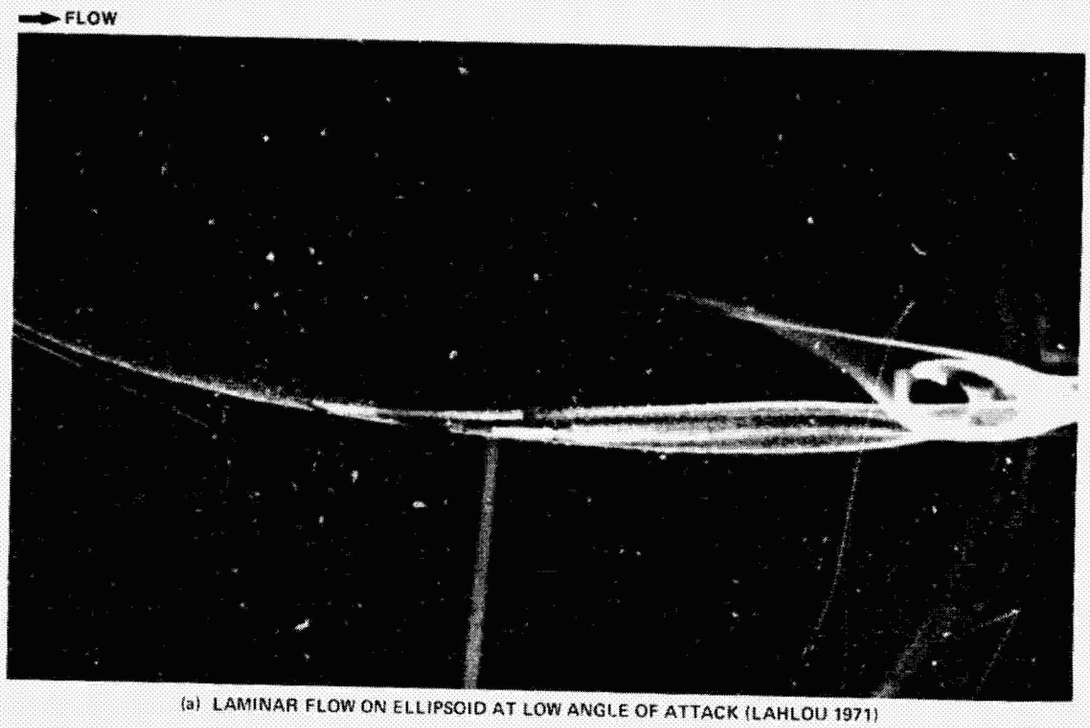

(a) LAMINAR FLOW ON ELLIPSOID AT LOW ANGLE OF ATTACK (LAHLOU 1971)

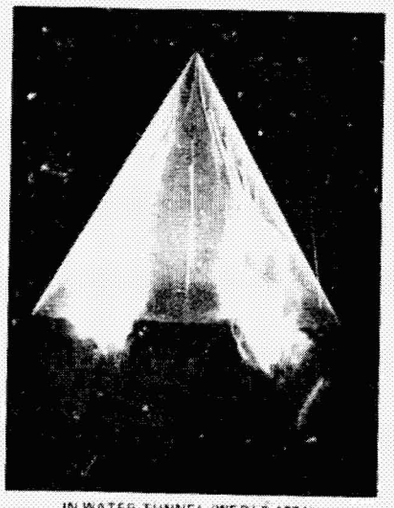

IN WATER TUNNEL (WERLÉ 1974)

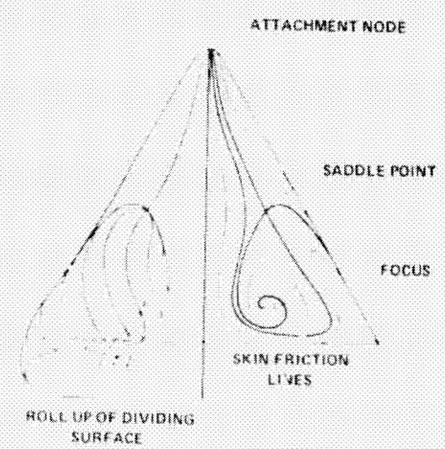

POSTULATED PATTERNS OF LEGENDRE 1965

(b) LAMINAR FLOW ON SLENDER DELTA WING AT HIGH ANGLE OF ATTACK

Fig. 14 Focus of separation on aerodynamic configurations.

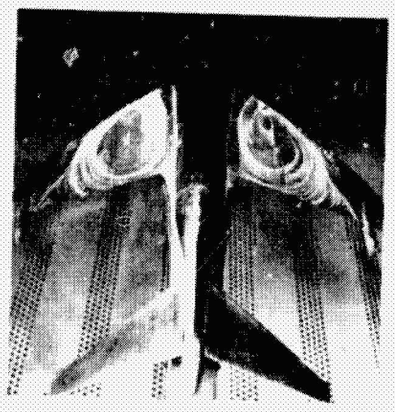

OIL FLOW PATTERN (COURTESY OF ARA, BEDFORD)

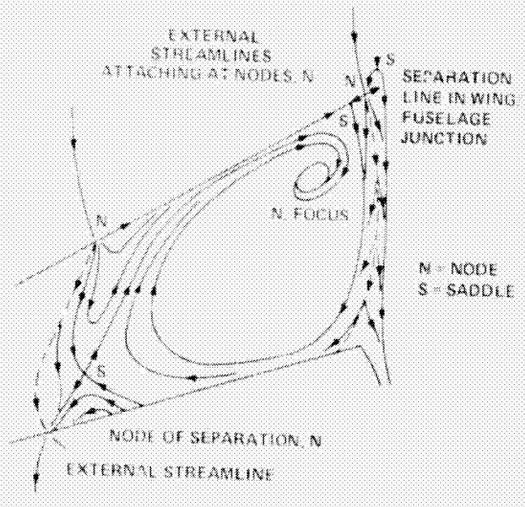

INTERPRETATION OF SKIN-FRICTION LINES ON TOP SURFACE OF PORT WING

(c) TURBULENT FLOW ON SWEPT WING OF FIGHTER AT HIGH LIFT

(d) TURBULENT FLOW ON INBOARD TRAILING-EDGE REGION OF LIFTING HIGH ASPECT RATIO SWEPT WING OF TRANSPORT AIRCRAFT AT HIGH SUBSONIC SPEED (COURTESY OF B. ELSENAAR, NLR)

Fig. 14 Continued.

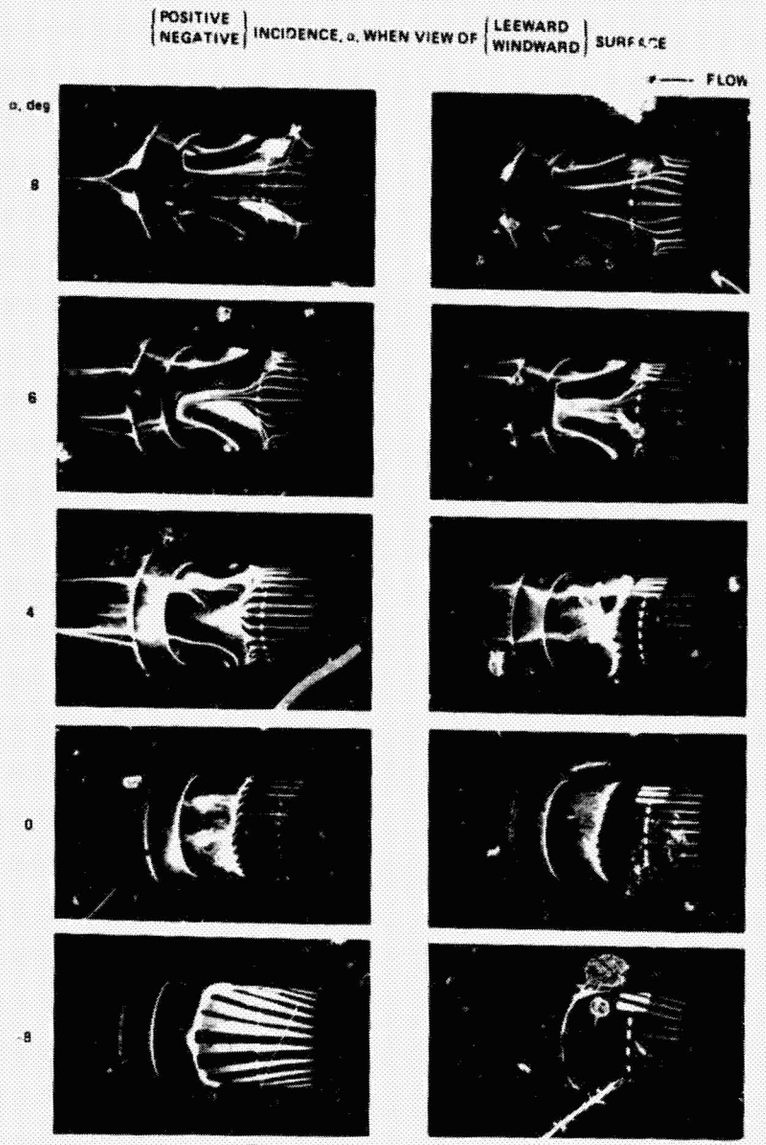

AXIAL LENGTH FROM NOSE TO FRUSTRUM = 70 in. (1.78 m)

(e) CYLINDER - FRUSTRUM AT $M_\infty = 2$ (COURTESY OF C.F. COE)

Fig. 14 Continued.

$\alpha_{W_B} = 8°$; PLUME

$\alpha_{W_B} = 8°$; NO PLUME

$\alpha_{W_B} = 0°$; PLUME

$\alpha_{W_B} = 0°$; NO PLUME

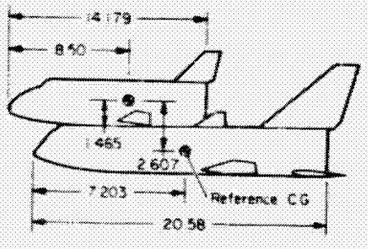

ALL DIMENSIONS IN INCHES
$R_{ft} = 2.51 \times 10^6$

(f) EFFECT OF PLUME ON STRAIGHT WING ORBITER MOUNTED TO STRAIGHT WING BOOSTER AT $M_\infty = 2$ (DODS AND CANGIE 1971)

Fig. 14 Concluded.

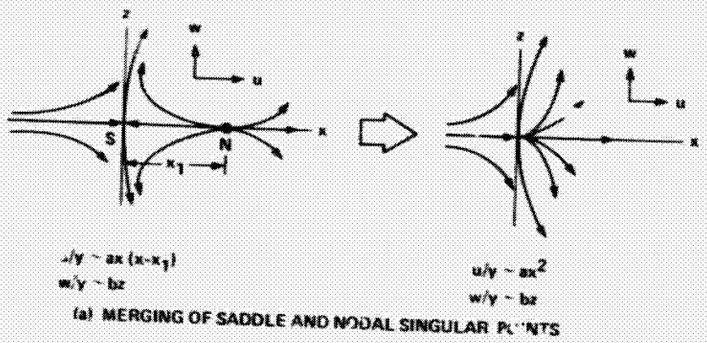

(a) MERGING OF SADDLE AND NODAL SINGULAR POINTS

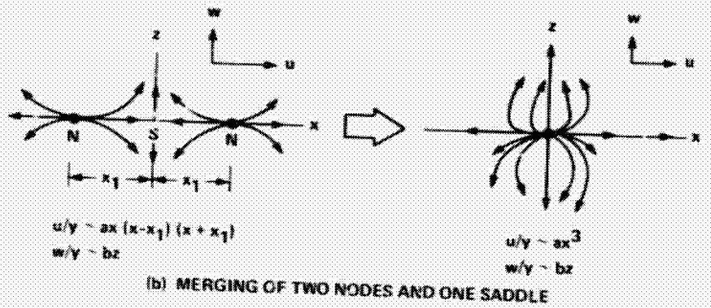

(b) MERGING OF TWO NODES AND ONE SADDLE

Fig. 15 Merging of singular points in skin-friction line pattern.

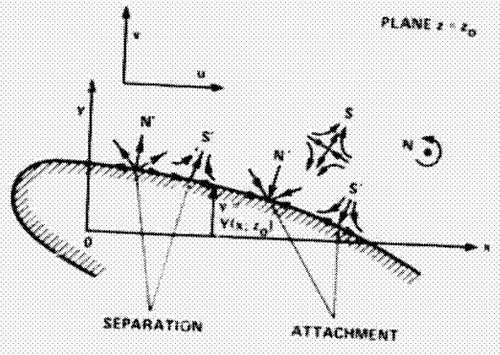

Fig. 16 Singular points in cross section of flow (J. C. R. Hunt et al. 1978).

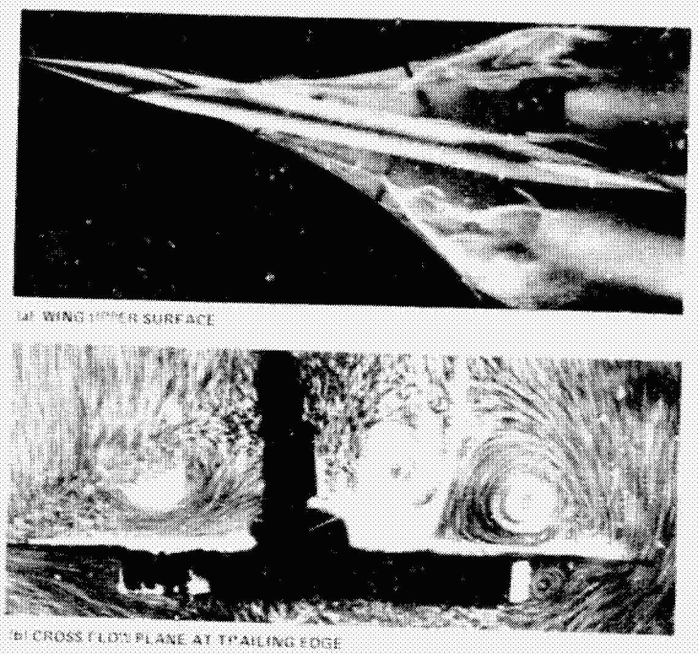

(a) WING UPPER SURFACE

(b) CROSS FLOW PLANE AT TRAILING EDGE

"CONCORDE" AT 12° ANGLE OF ATTACK AND 10° YAW IN WATER TUNNEL

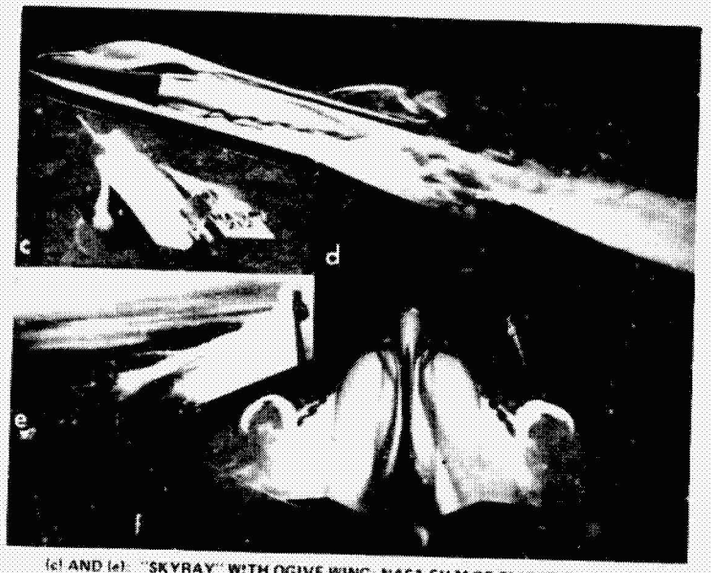

(c) AND (e): "SKYRAY" WITH OGIVE WING, NASA FILM OF FLIGHT TESTS, AND
(d) AND (f): AT 15° ANGLE OF ATTACK IN WATER TUNNEL

Fig. 17 Visualization of flow about slender wings (Werlé 1973).

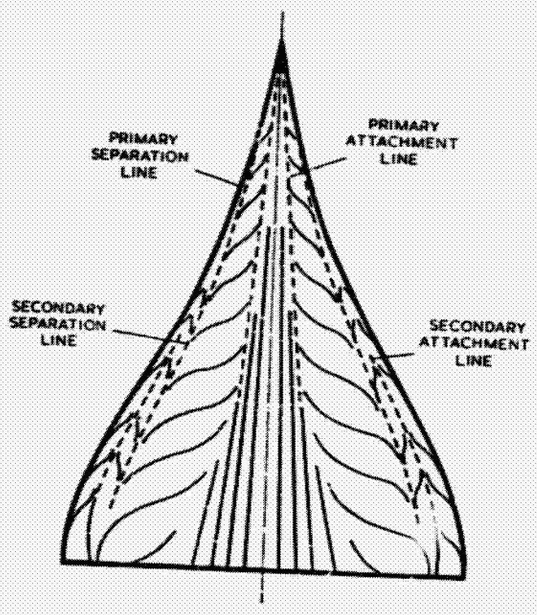

(a) SKIN-FRICTION LINE PATTERN ON UPPER SURFACE OF SLENDER WING AT LOW SPEEDS, $\alpha = 15°$

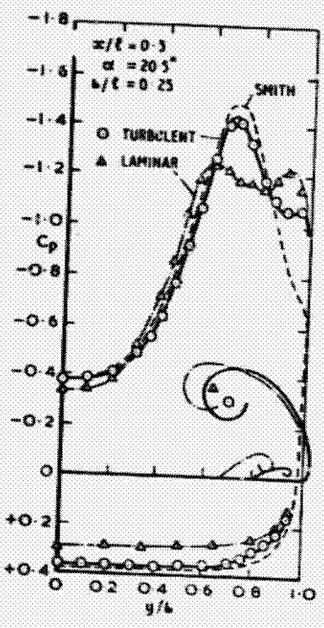

(b) PRESSURE DISTRIBUTIONS OVER A THIN DELTA WING AT LOW SPEEDS WITH LAMINAR AND WITH TURBULENT FLOW

Fig. 18 Surface pressures and skin-friction lines on slender wings with subsonic leading edges (after Küchemann 1975).

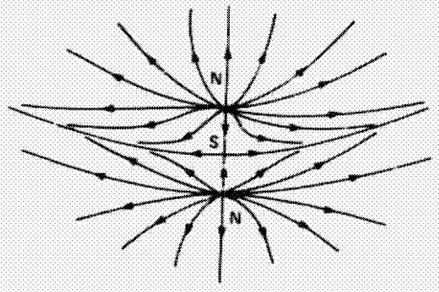

LIGHTHILL 1963

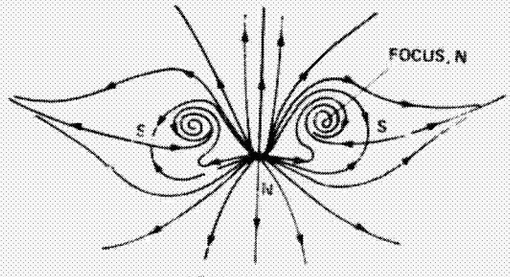

LEGENDRE 1972

Fig. 19 Skin-friction lines at rounded apex of delta wing.

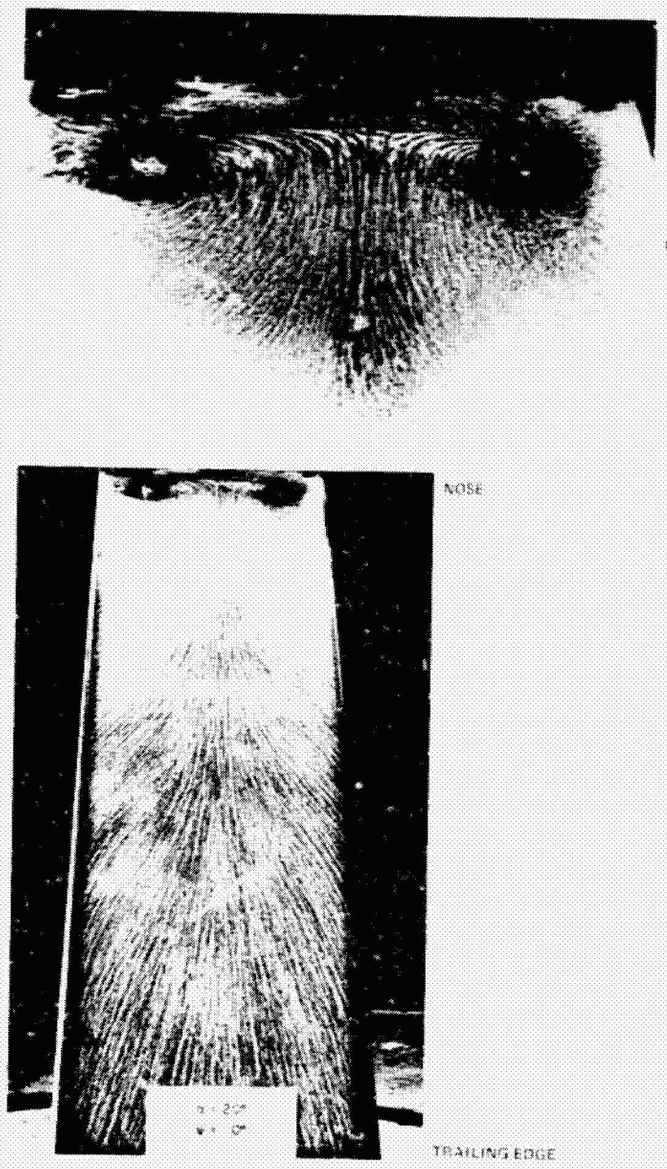

Fig. 20 Oil-flow pattern on slender, rectangular wing at α = 20° (Wickens 1966).

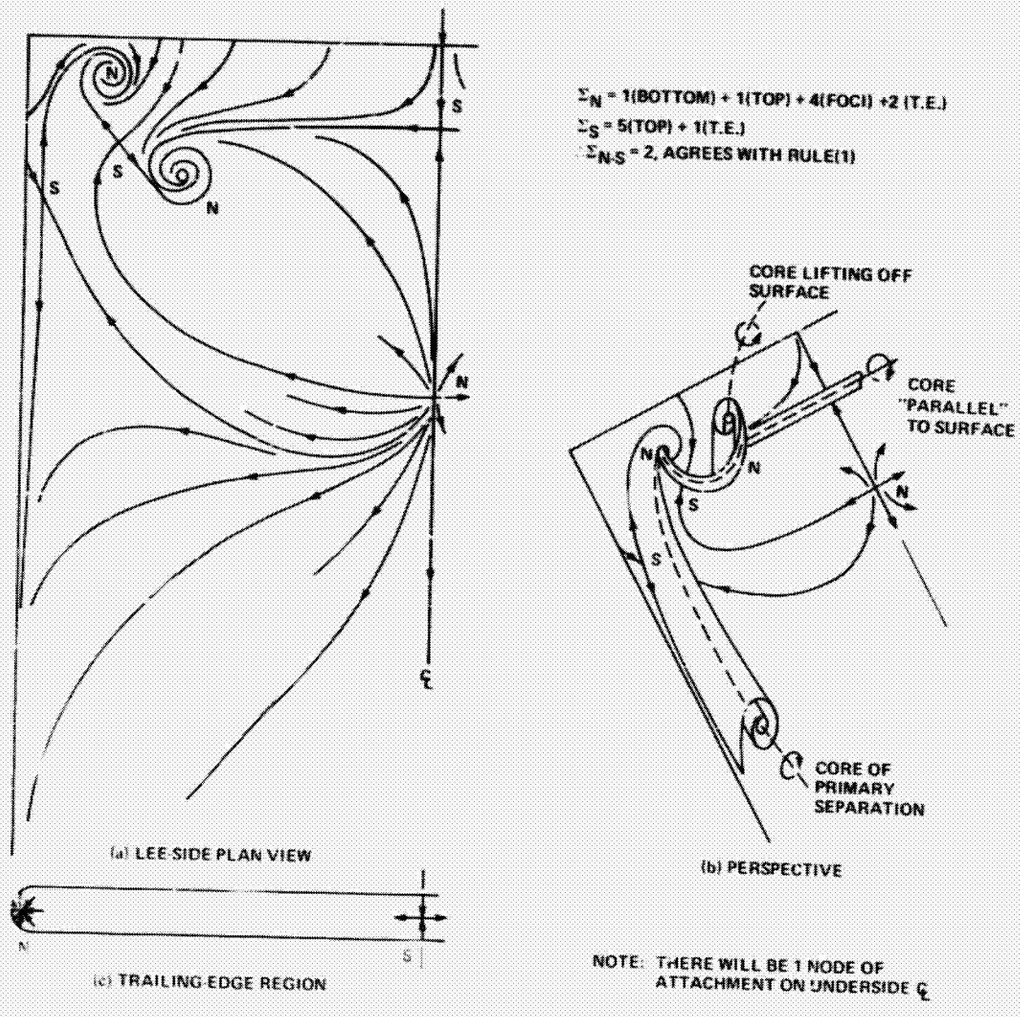

Fig. 21 Interpretation of skin-friction lines on slender, rectangular wing.

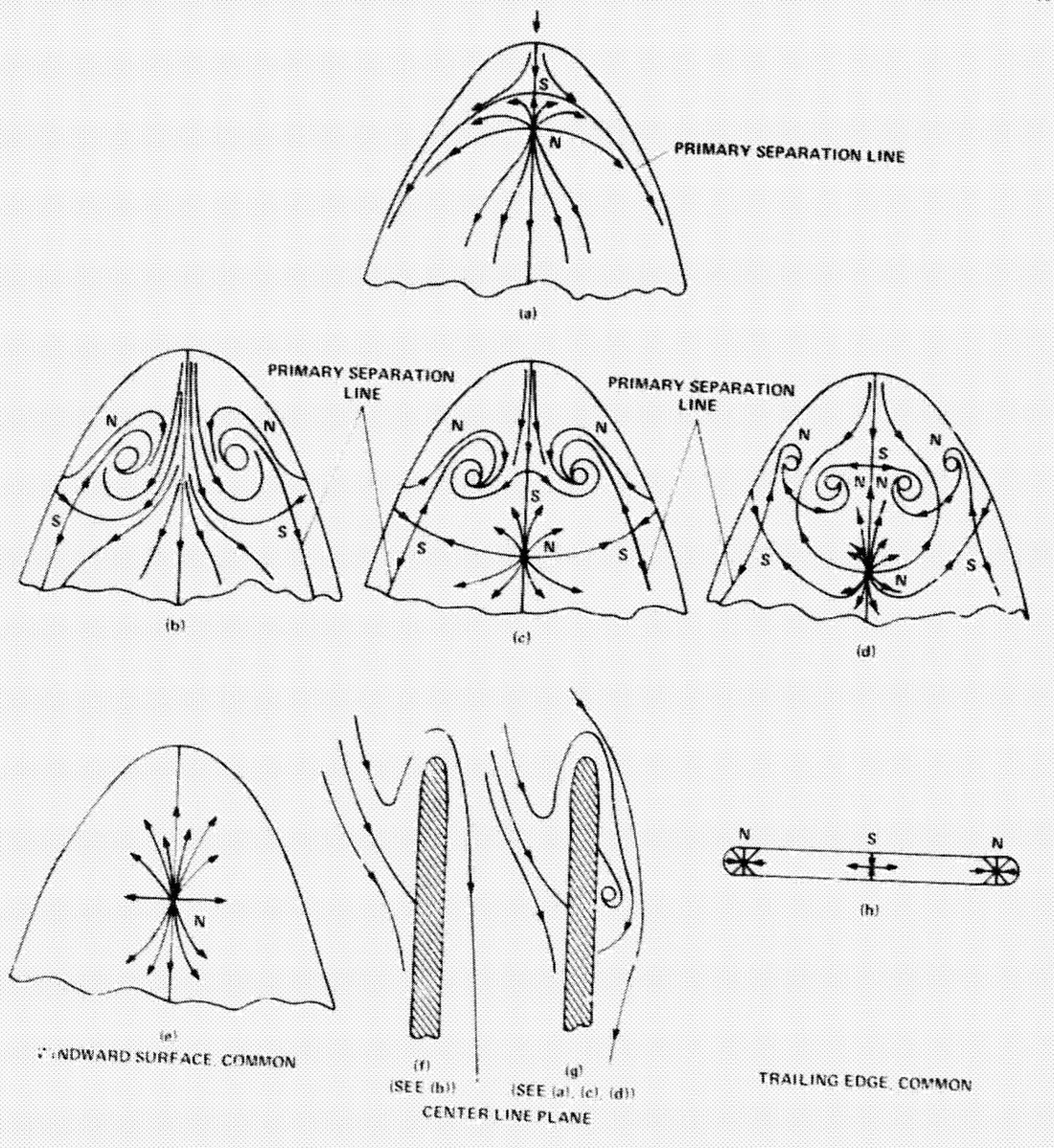

Fig. 22 Sequence of possible skin-friction line patterns in nose region of slender configuration.

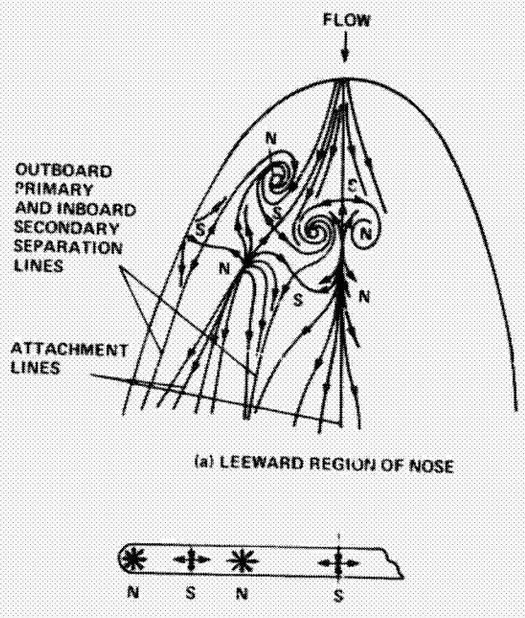

Fig. 23 Postulated skin-friction line pattern on nose region with primary and secondary separations.

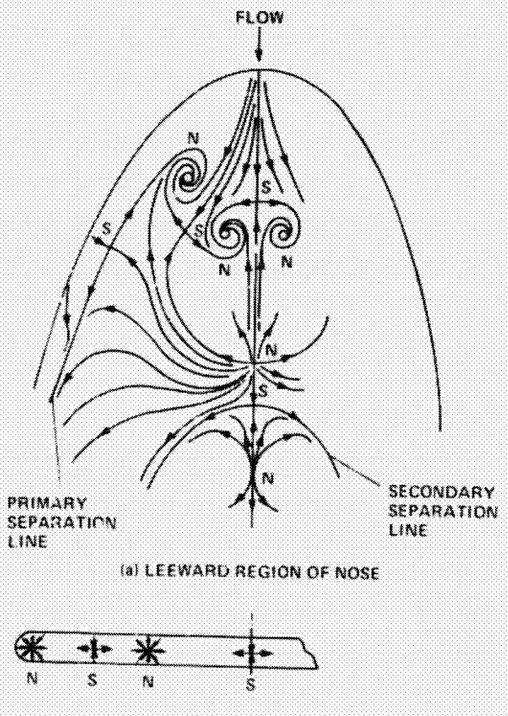

Fig. 24 Alternative postulate of skin-friction line pattern on nose region with primary and secondary separations.

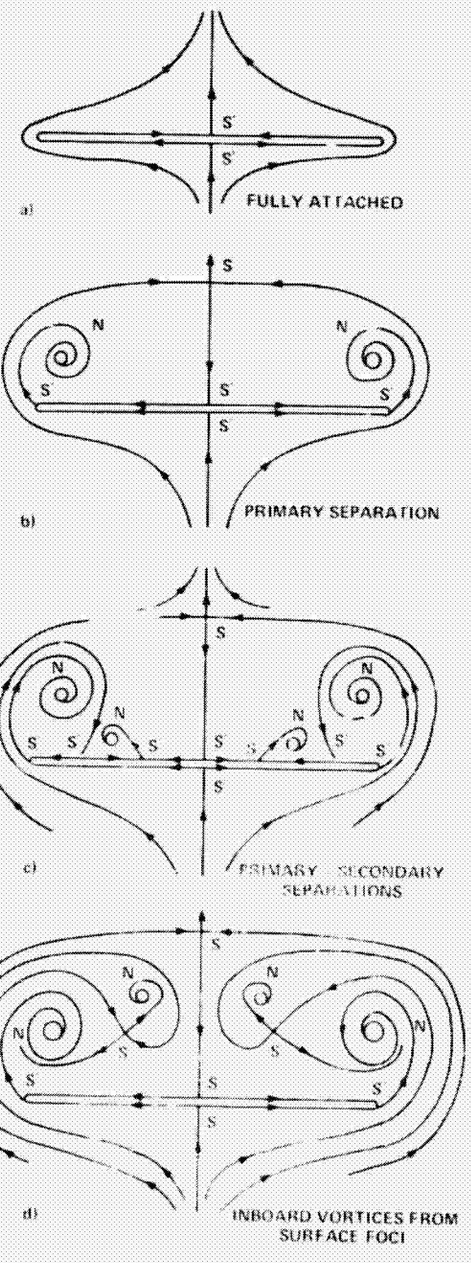

Fig. 25 Cross-flow streamlines about slender configuration at angle of attack.

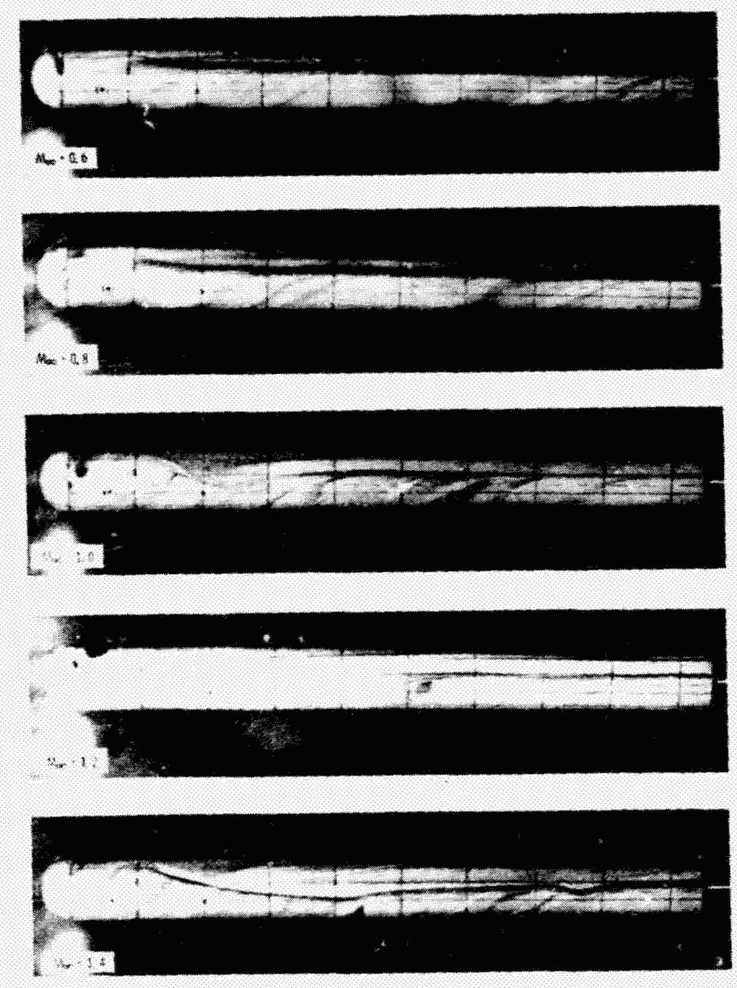

CYLINDER DIA., D = 1 m LENGTH = 10 m, R_D = 0.4 × 10^6

(a) EXPERIMENT, M_∞ = 0.6 TO 1.4, α = 19°, LAMINAR (HSIEH, 1977)

Fig. 26 Primary and secondary separations on hemisphere-cylinder at angle of attack.

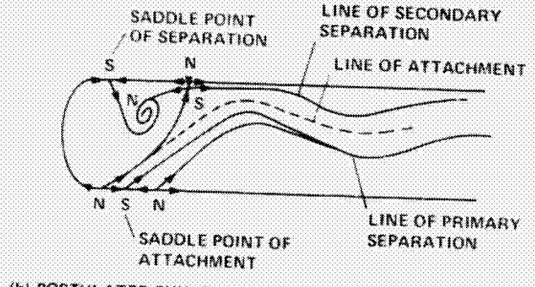

(b) POSTULATED SKIN-FRICTION LINE PATTERN, SIDE VIEW, OF $M_\infty = 1.4, \alpha = 19°$ FLOW

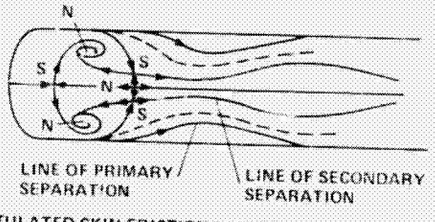

(c) POSTULATED SKIN-FRICTION PATTERN, TOP VIEW, OF $M_\infty = 1.4, \alpha = 19°$ FLOW

Fig. 26 Concluded.

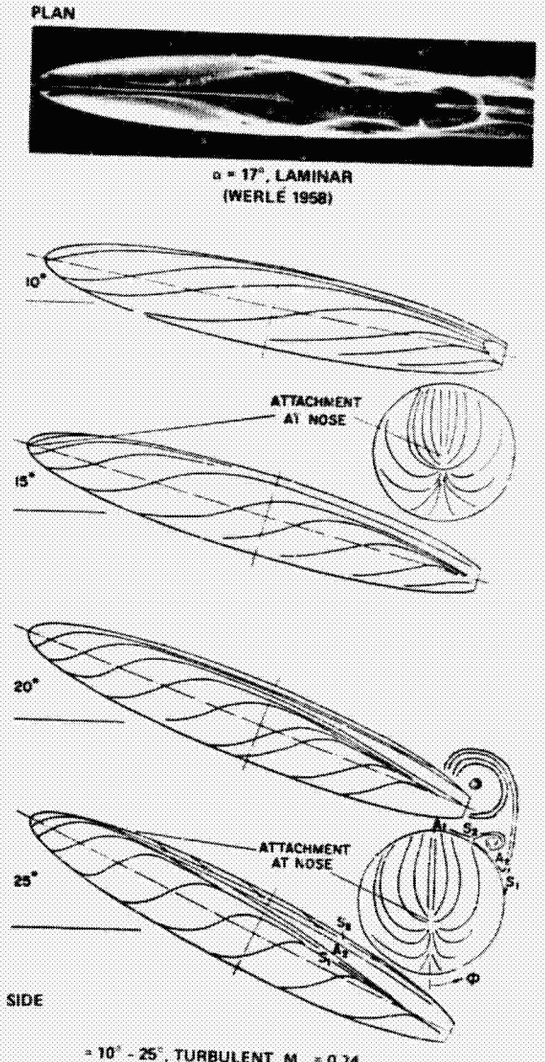

Fig. 27 Skin-friction lines and external flow about 6:1 ellipsoid at angle of attack.

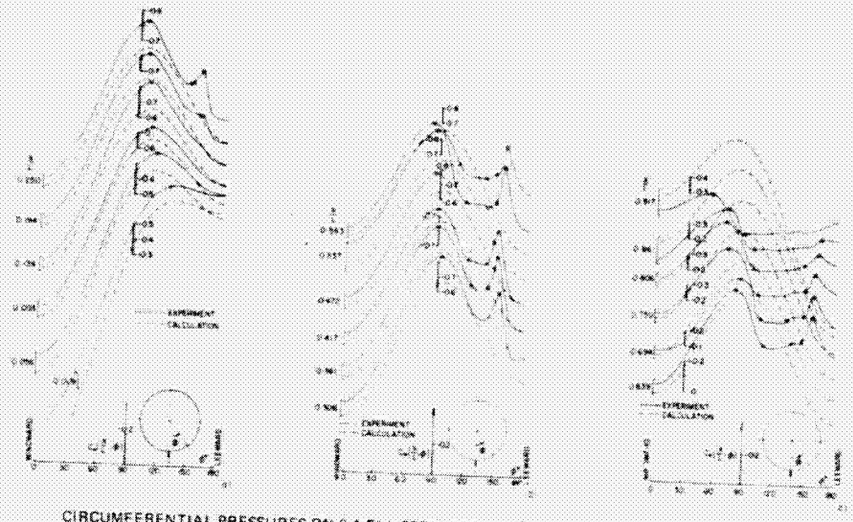

CIRCUMFERENTIAL PRESSURES ON 6:1 ELLIPSOID AT $\alpha = 25^{\circ}$, $M_{\infty} = 0.74$, AND $R_{L_{\infty}} = 44 \times 10^{6}$
▽ – MINIMUM PRESSURE, Δ – PRIMARY SEPARATION, ○ – SECONDARY ATTACHMENT,
□ – SECONDARY SEPARATION, ▽ – SUCTION PEAK FROM PRIMARY VORTEX

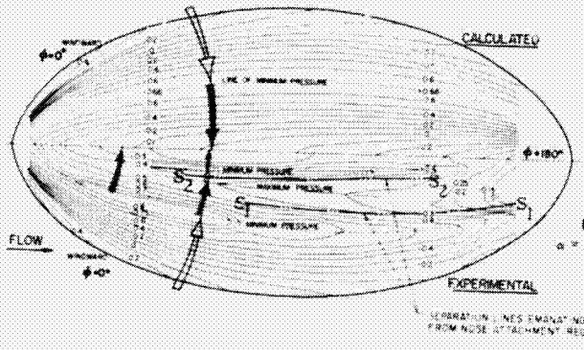

ISOBARS ON 6:1 ELLIPSOID AT
$\alpha = 25^{\circ}$, $M_{\infty} = 0.74$, AND $R_{L_{\infty}} = 44 \times 10^{6}$

Fig. 28 Surface pressures on 6:1 ellipsoid at 25° angle of attack with turbulent viscous flow (Peake, Rainbird, and Atraghji 1972).

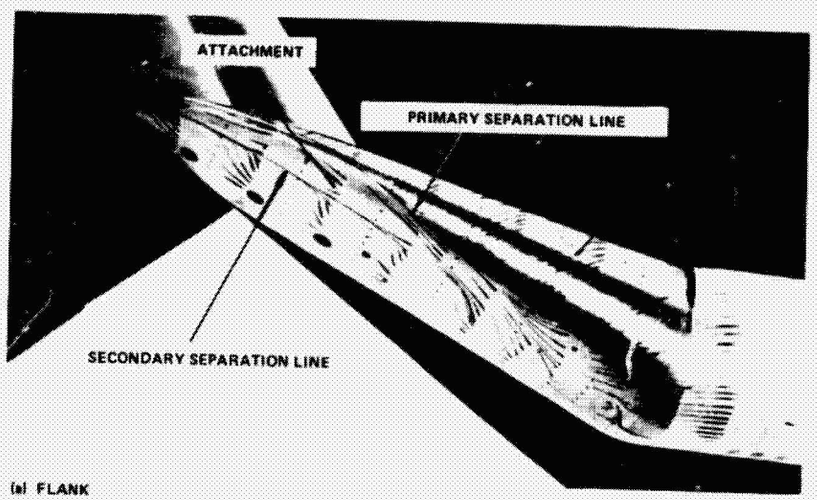

(a) FLANK

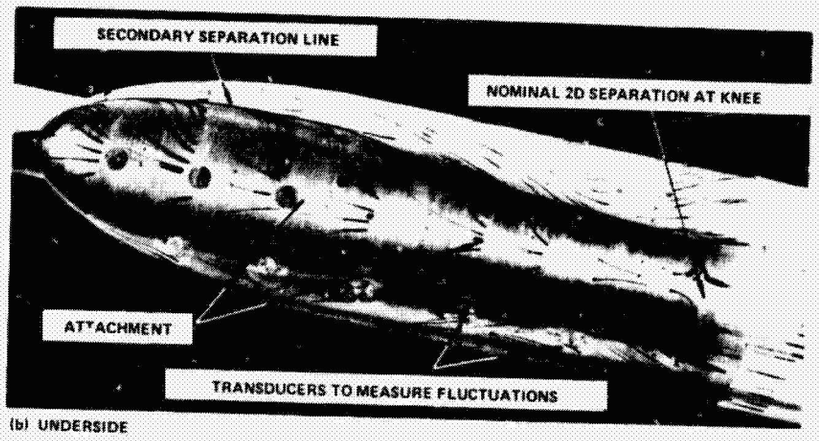

(b) UNDERSIDE

$M_\infty = 0.73$; $R_{ft} = 10 \times 10^6$ ft; AFTERBODY LENGTH = 17.2 in.; TURBULENT BOUNDARY LAYERS

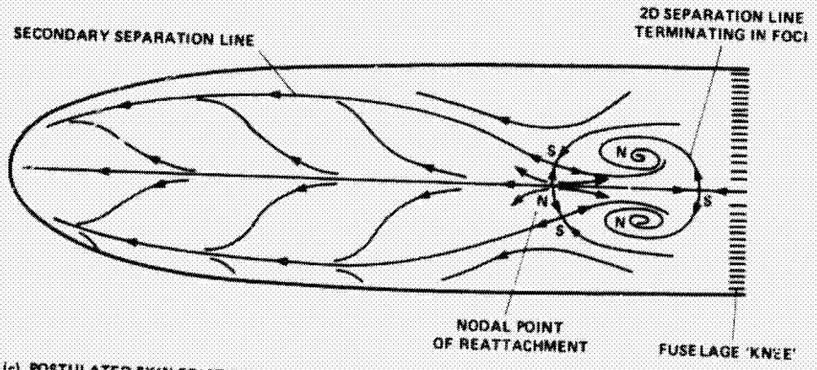

(c) POSTULATED SKIN-FRICTION LINE PATTERN ON UNDERSIDE

Fig. 29 Oil-flow pattern on "beaver-tail" afterbody at 20° upsweep (Peake 1968).

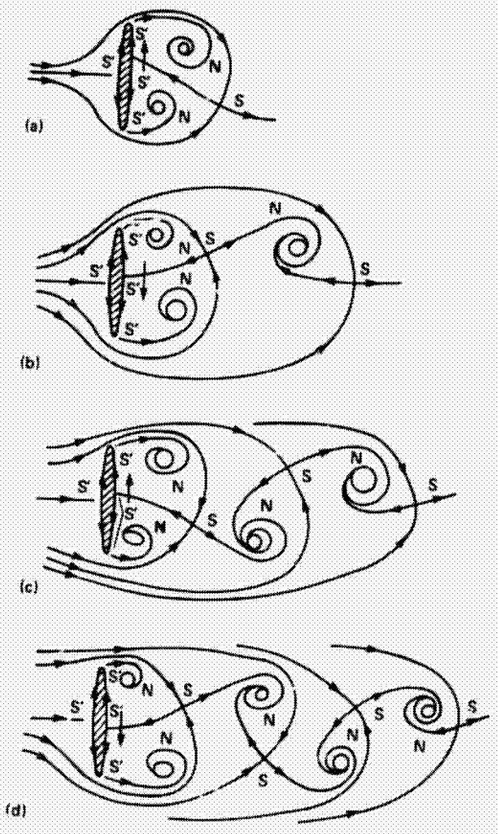

Fig. 30 Asymmetric flow behind cylinder: formation of wake.

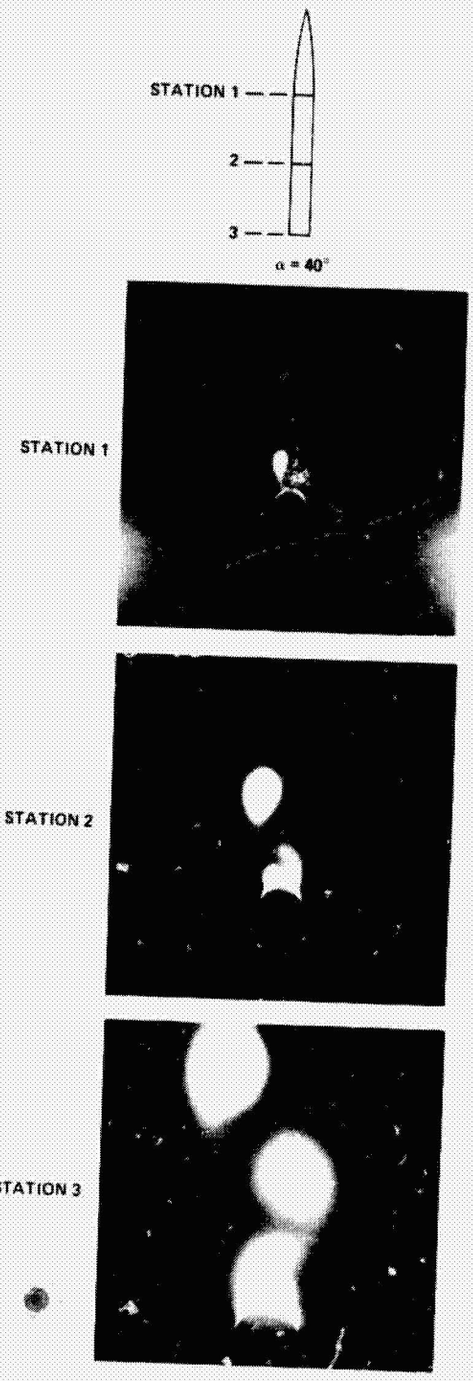

Fig. 31 Vapor-screen photographs of asymmetric flow along ogive-cylinder at $M_\infty = 0.6$ (Jorgensen 1977).

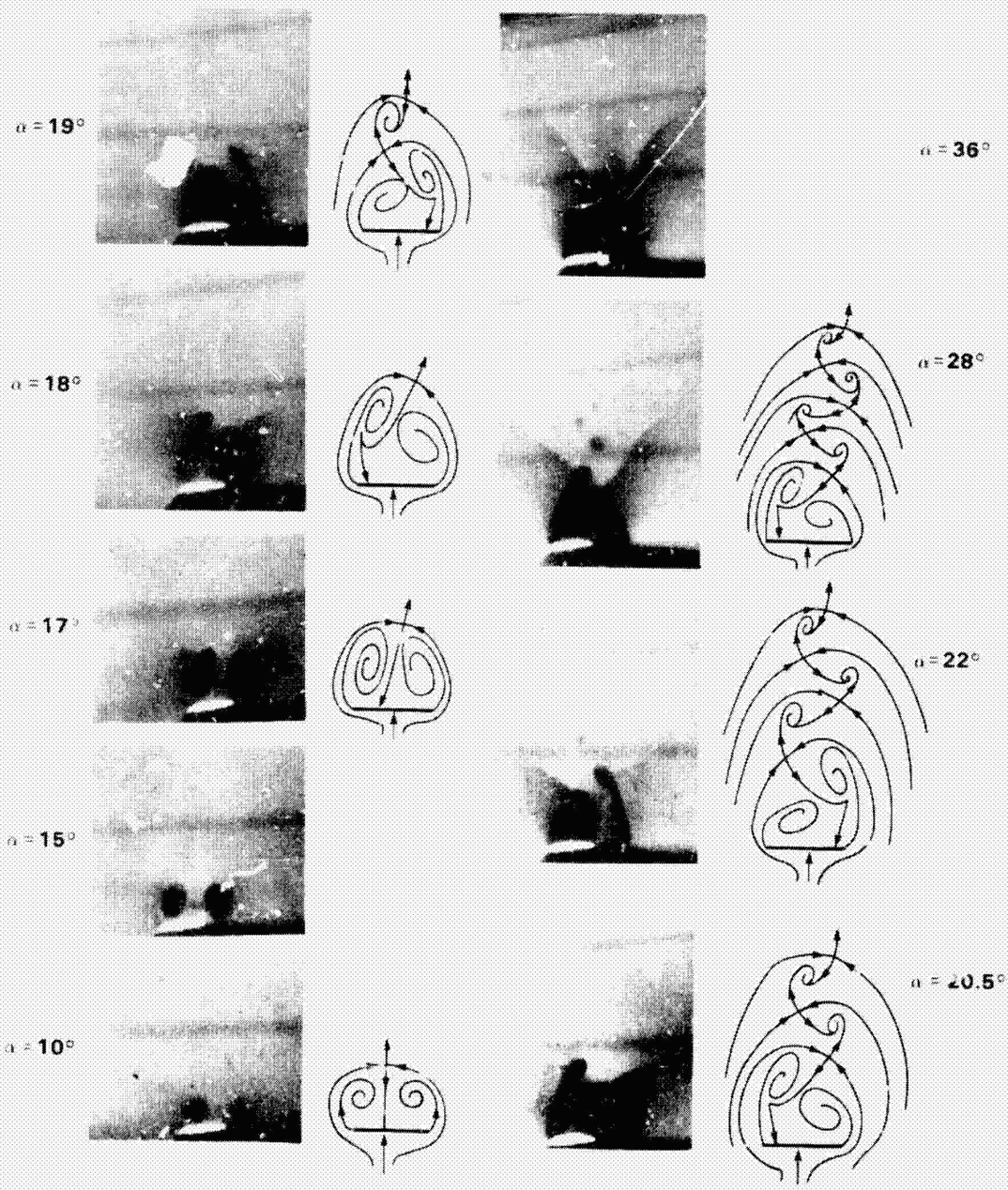

Fig. 32 Asymmetric flow over slender delta wing at angle of attack at $M_\infty = 2.8$ (Fellows and Carter 1969).

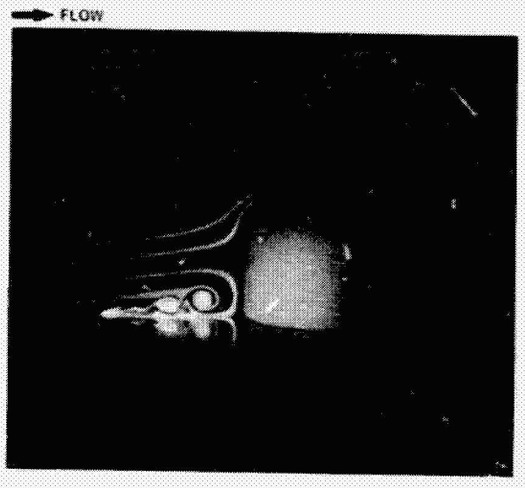

Fig. 33 Low-speed smoke flow about obstacle (Thwaites 1960).

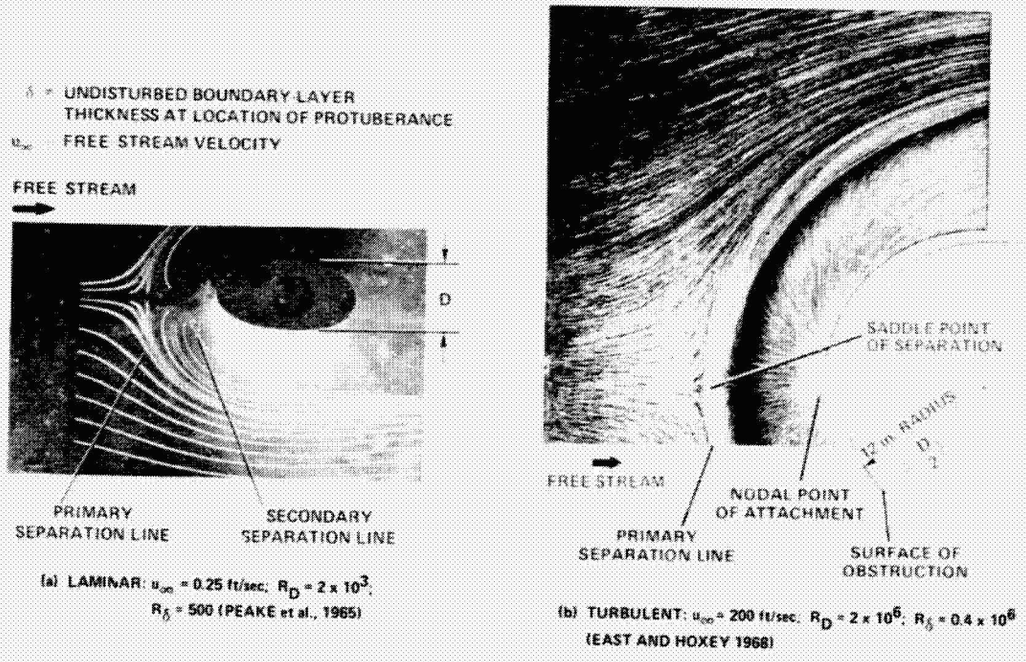

Fig. 34 Skin-friction lines on surfaces about protuberance.

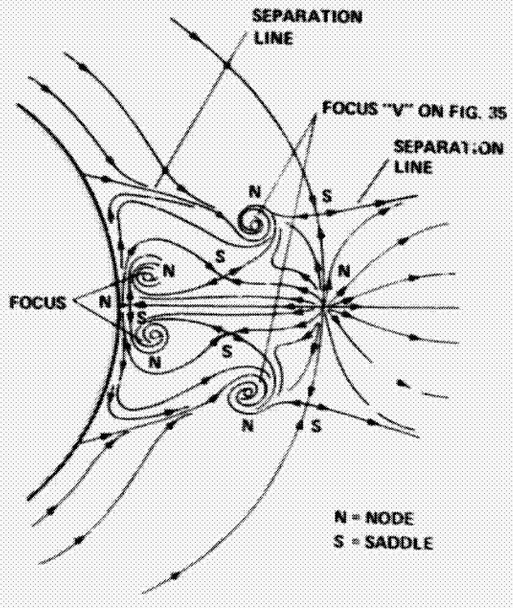

Fig. 36 Postulate of region of skin-friction lines aft of cylinder protuberance in supersonic flow.

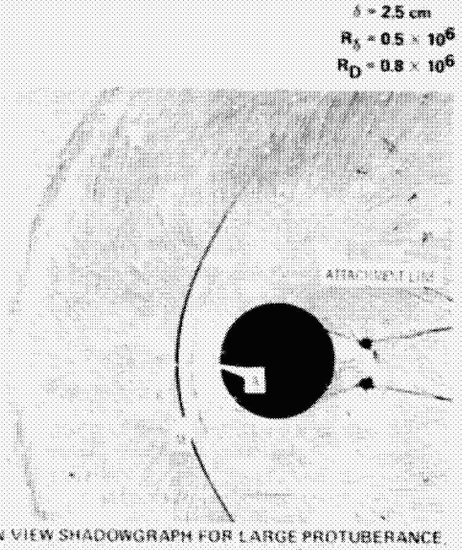

PLAN VIEW SHADOWGRAPH FOR LARGE PROTUBERANCE
$M_\infty = 2.50$, $R_\infty = 19.3 \times 10^6/m$
S – PRIMARY SEPARATION
B – BOW SHOCK
M – MACH STEM
A – ATTACHMENT LINE
V – VORTEX CORE
ATTACHMENT LINE INDICATED ORIGINATES AT POINT A

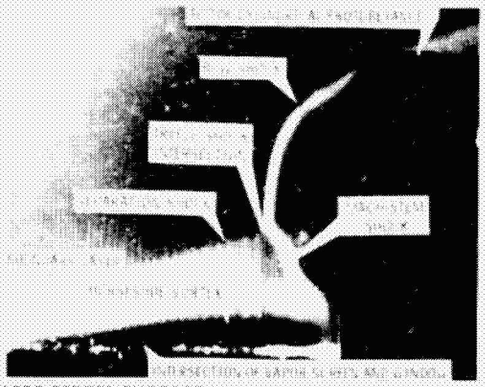

VAPOR SCREEN PHOTOGRAPH FOR LARGE PROTUBERANCE WITH LIGHT SHEET IN SYMMETRY PLANE AND CAMERA AT 30° TO SHEET. $M_\infty = 2.50$, $R_\infty = 9.3 \times 10^6/m$

Fig. 35 Cylinder protuberance in supersonic turbulent flow (Sedney and Kitchens 1975).

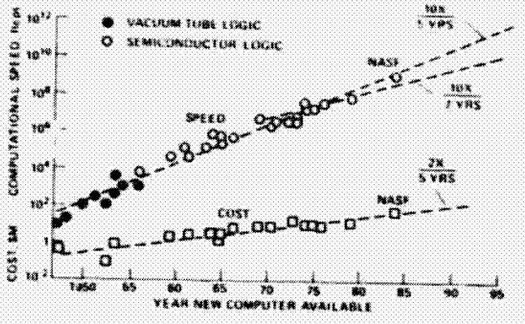

(a) TRENDS IN SPEED OF COMPUTATION AND IN COST OF LARGE COMPUTERS

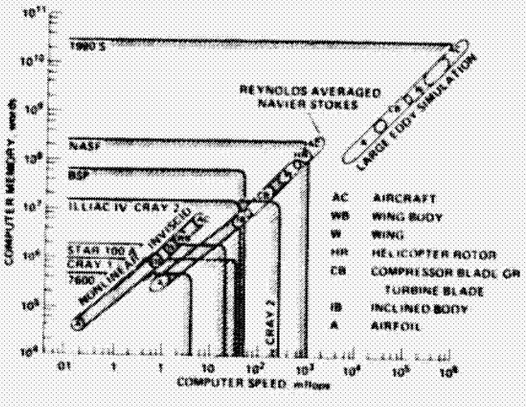

(b) COMPUTER SPEED AND MEMORY REQUIREMENTS COMPARED WITH LARGE COMPUTER CAPABILITIES

Fig. 37 Trends of computer speed (D. R. Chapman 1979).

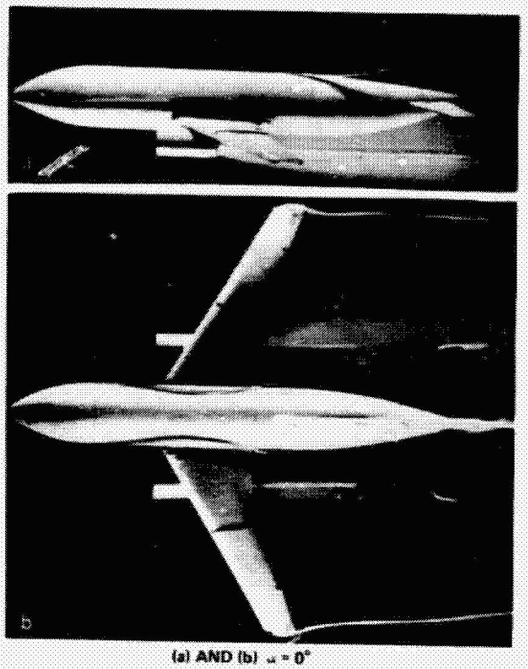

(a) AND (b) $\alpha = 0°$

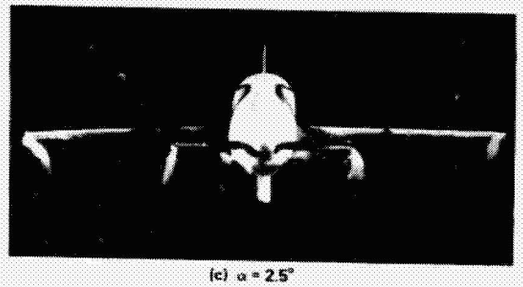

(c) $\alpha = 2.5°$

Fig. 38 Classical aircraft of "Airbus" type with attached flow over wing (L.E. and T.E. drooped) (Werlé 1974).

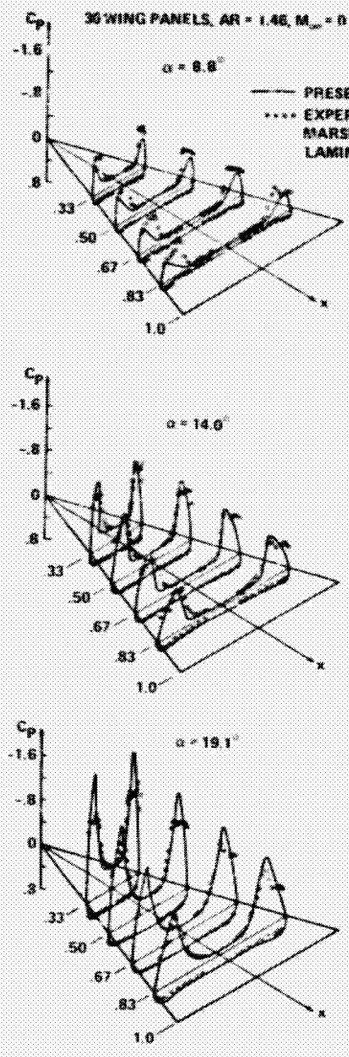

Fig. 39 Calculated pressures on slender wing with controlled separation at all three sharp edges (J. A. Weber et al. 1975).

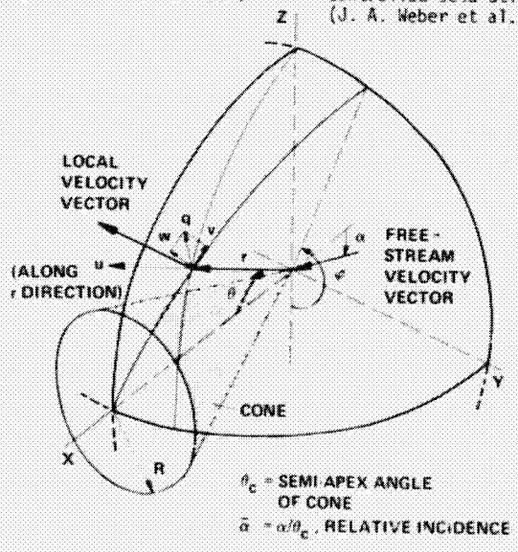

Fig. 40 Spherical polar coordinates in conical flow, with velocity components at sphere centered on vertex (Nebbeling and Bannink 1976).

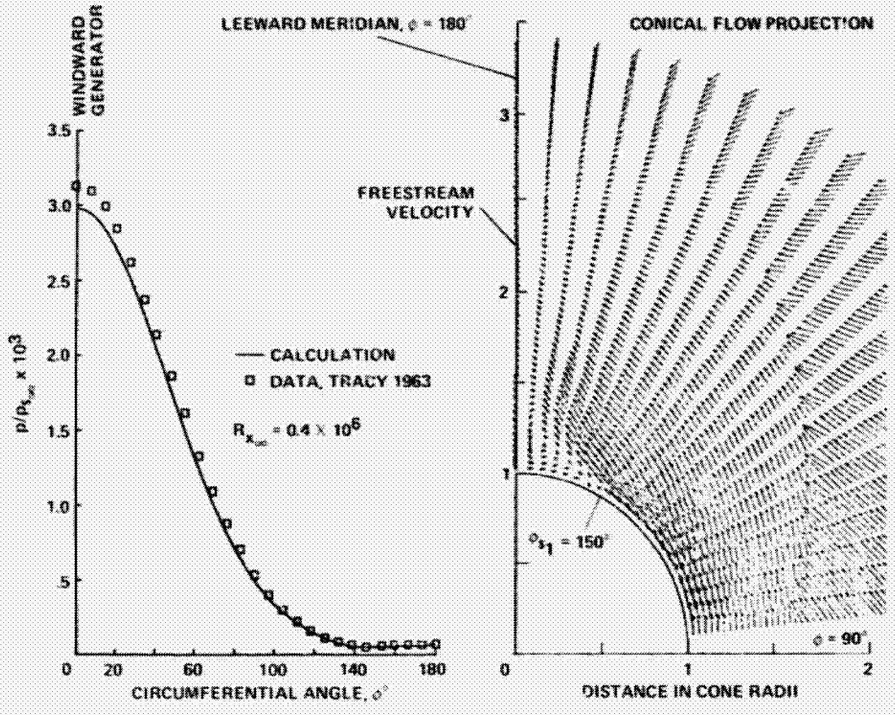

Fig. 41 Flow field about $\theta_c = 10°$ sharp cone in laminar flow at $M_\infty = 8$, $\alpha = 24°$; simplified Navier-Stokes solution of McRae (1976) compared with experimental result of Tracy (1963).

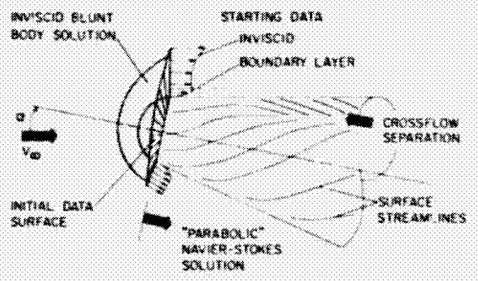

LAMINAR VISCOUS VORTEX FLOW OVER A BLUNT CONE

CALCULATION METHOD:
I VISCOUS IMPLICIT CODE
II INVISCID CHARACTERISTICS CODE

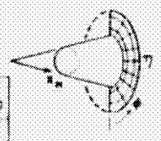

		I VISCOUS	II INVISCID
NUMBER OF MESH POINTS	η	50	21
	ϕ	19	19
	TOTAL	950	399
CDC-7600 COMPUTE TIME (min) $x/R_N = 14.7$	PER STEP	0.26	0.012
	TOTAL	22.9	6.0

COMPUTATIONAL MESH AND COMPUTER RUN TIME

Fig. 42 Calculation of viscous flow over sphere-cone at angle of attack (Rakich and Lubard 1975).

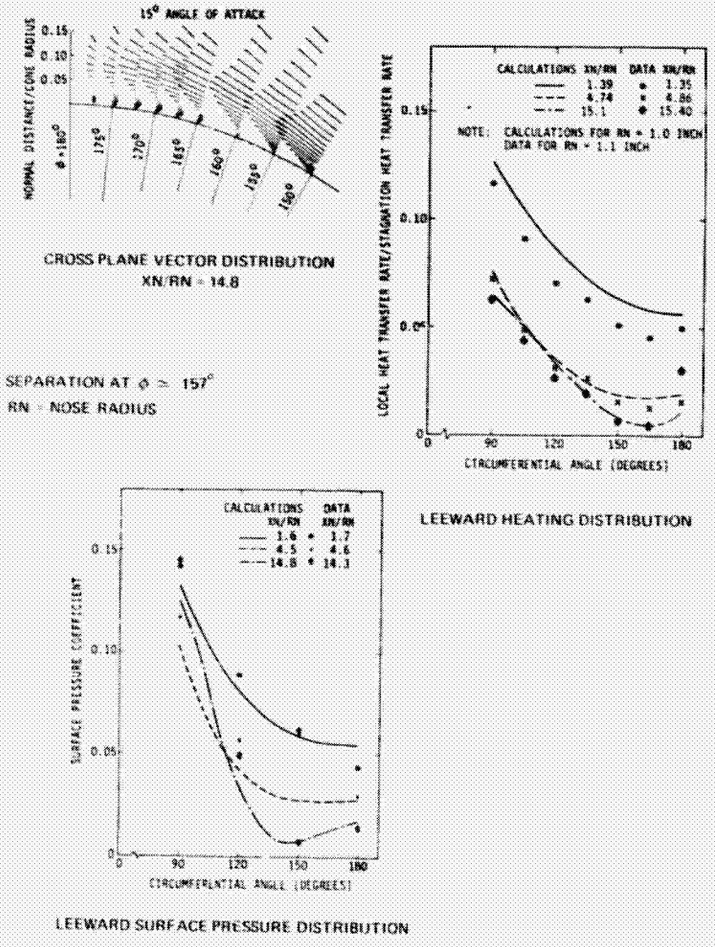

Fig. 43 Sphere-cone solution using "parabolic" Navier-Stokes equations: $\theta_C = 15°$, $M_\infty = 10.6$, laminar, $\alpha = 15°$, $T_{wall}/T_{total} = 0.26$ (Lubard and Rakich 1975).

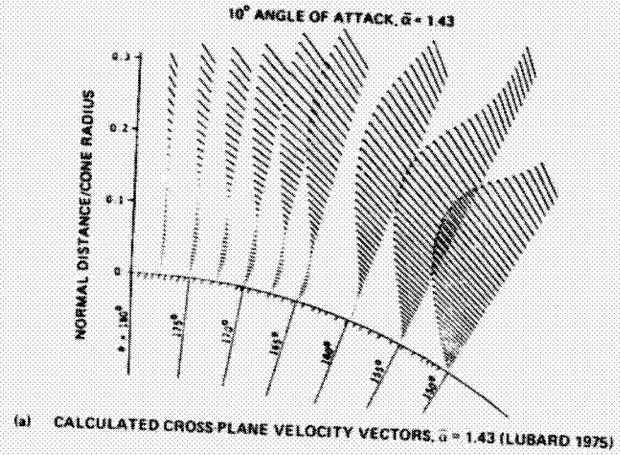

(a) CALCULATED CROSS-PLANE VELOCITY VECTORS, ᾱ = 1.43 (LUBARD 1975)

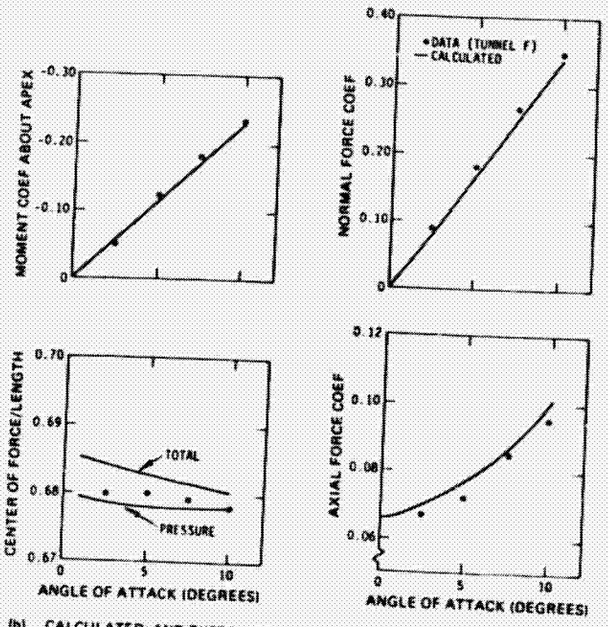

(b) CALCULATED, AND EXPERIMENTAL FORCES AND MOMENTS (PATE 1974)

Fig. 44 "Parabolized" Navier-Stokes laminar flow-field calculations about $\theta_c = 7°$ sharp cone: $M_\infty = 16.1$, $R_{L_\infty} = 10^6$.

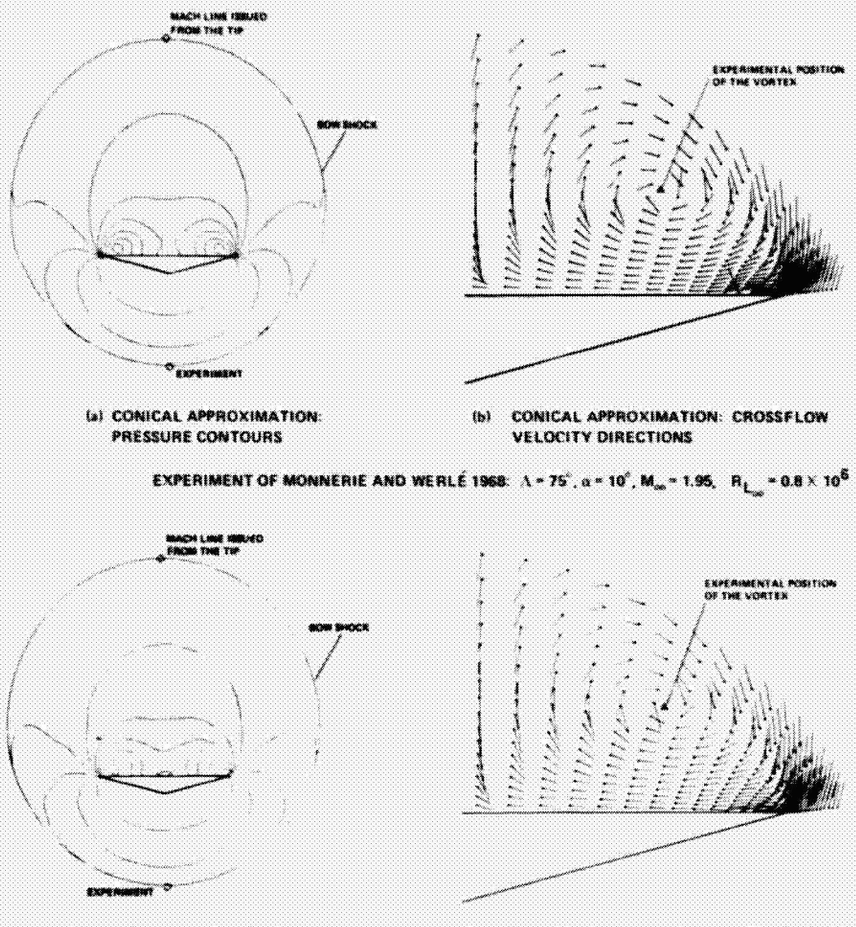

Fig. 45 Navier-Stokes computations of laminar flow about slender wing at $M_\infty = 1.95$ (Vigneron, Rakich, and Tannehill 1978).

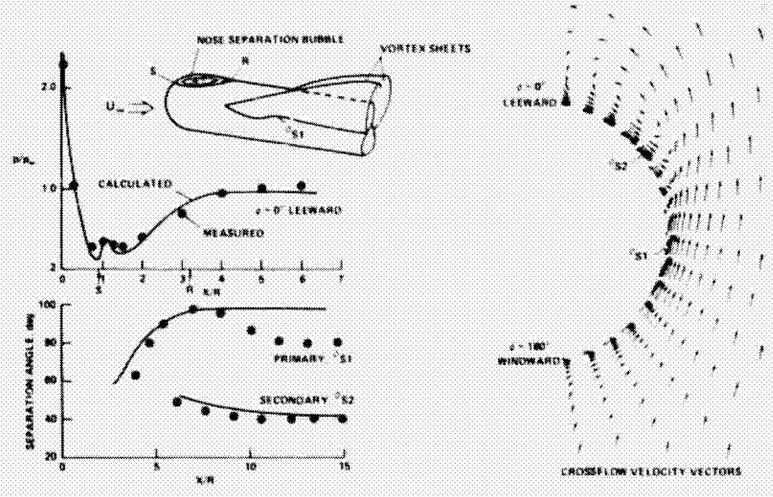

Fig. 46 Computed and measured laminar flow characteristics for an inclined hemisphere-cylinder body; Reynolds averaged Navier-Stokes computation: $M_\infty = 1.2$, $\alpha = 19°$, $R_D = 0.4 \times 10^6$ (Pulliam and Steger 1978).

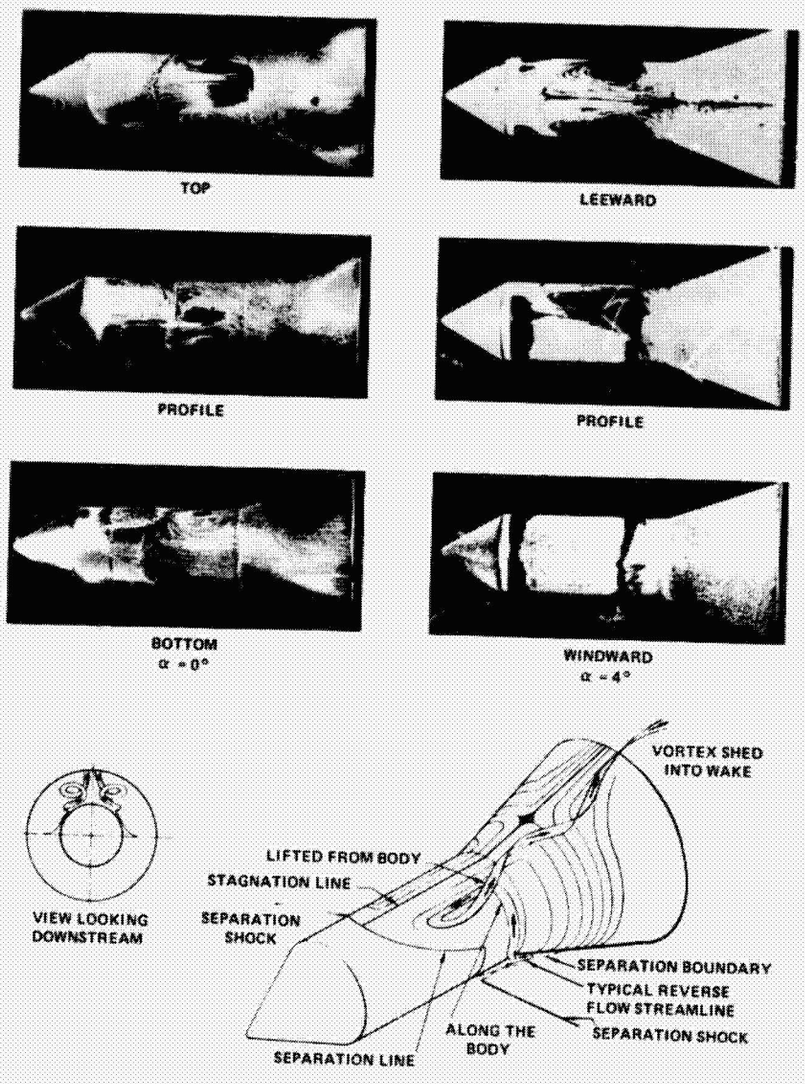

Fig. 47 China-clay patterns and model of laminar flow over cylinder-flare at $M_\infty = 1.2$ (Ericsson, Reding, and Guenther 1969).

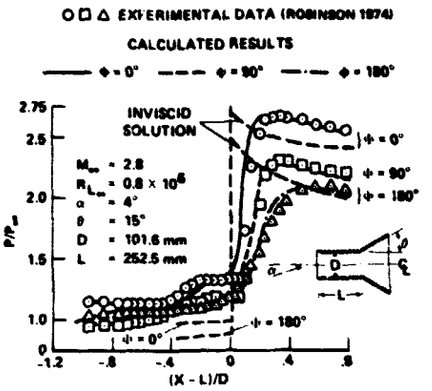

(a) COMPARISON BETWEEN EXPERIMENT OF ROBINSON 1974 AND CALCULATION BY HUNG 1979 OF SURFACE PRESSURES ALONG GENERATORS OF BODY

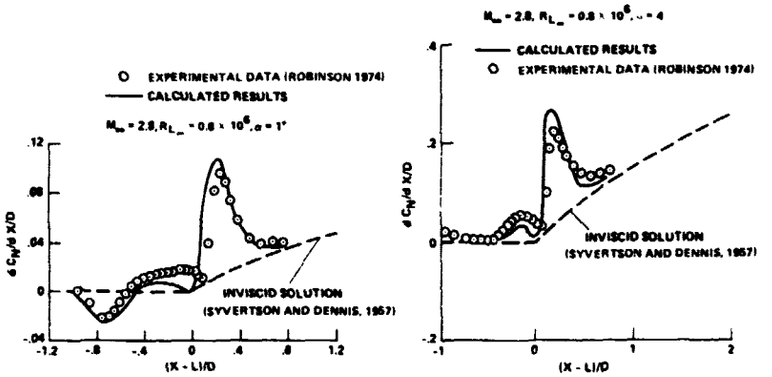

(b) NORMAL FORCE DISTRIBUTION: EXPERIMENT OF ROBINSON 1974 AND CALCULATION OF HUNG 1979

$$\frac{d\,C_N}{d\,x/D} = \frac{4}{\pi}\frac{2r_b}{D}\int_0^{\pi}\frac{2p}{\rho_\infty u_\infty{}^2}\cos\phi\,d\phi$$

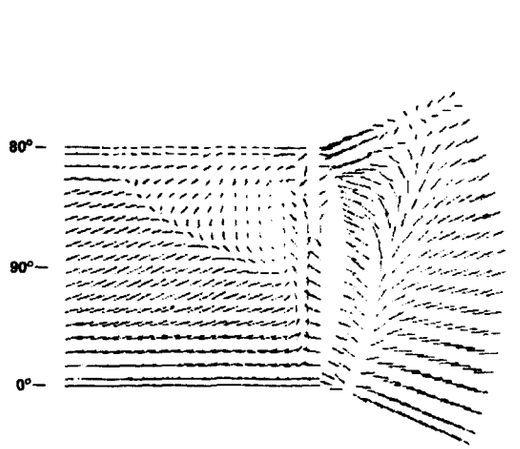

(c) UNWRAPPING OF SURFACE TO SHOW CALCULATED LIMITING STREAMLINE DIRECTIONS (HUNG 1979)

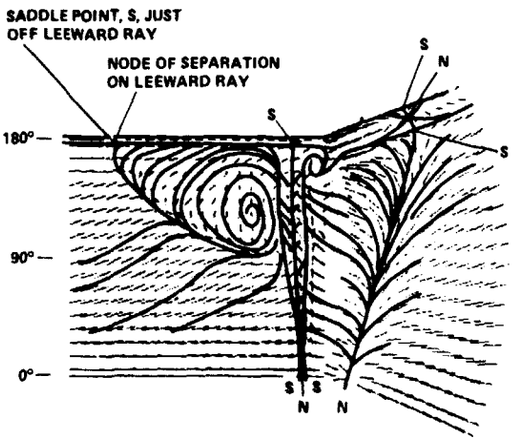

(d) CONJECTURED SKIN-FRICTION LINE DEVELOPMENT SUPERIMPOSED OVER CALCULATION

Fig. 48 Pressures and skin-friction lines on cylinder-flares at 4° angle of attack at $M_\infty = 2.8$.

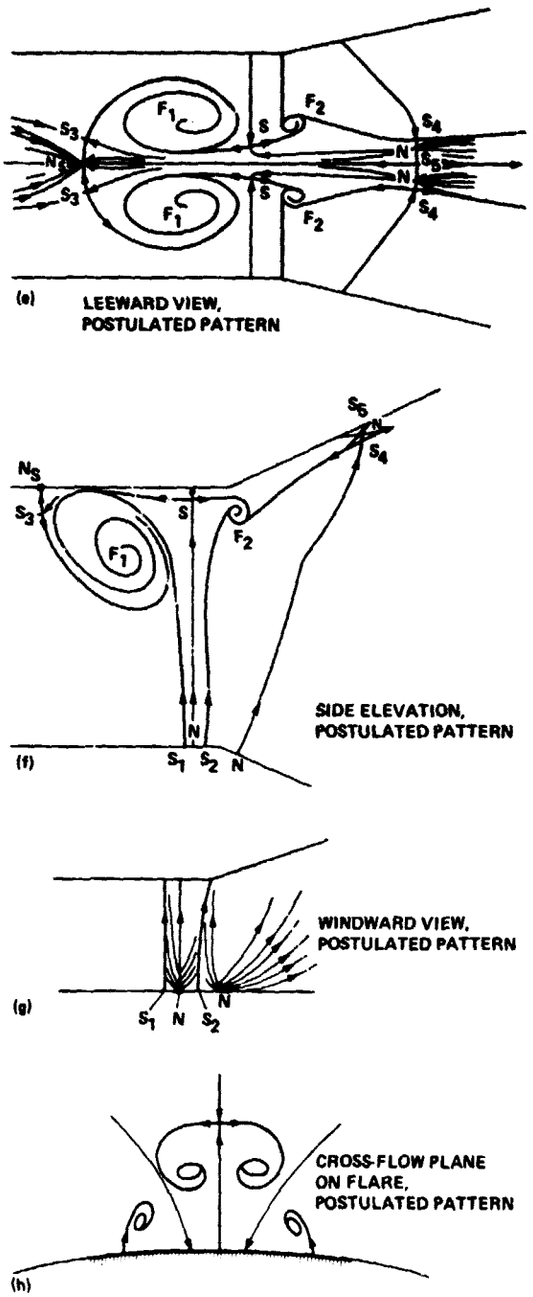

Fig. 48 Concluded.

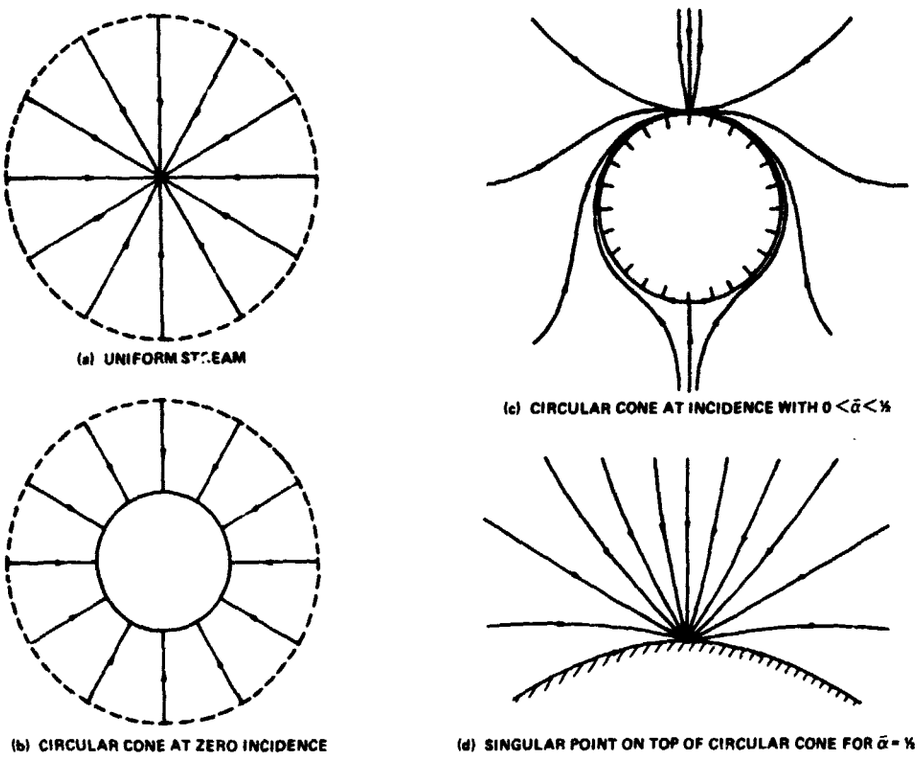

Fig. 49 Patterns of conical streamlines in inviscid flow inboard of bow shock wave (J. H. B. Smith 1969).

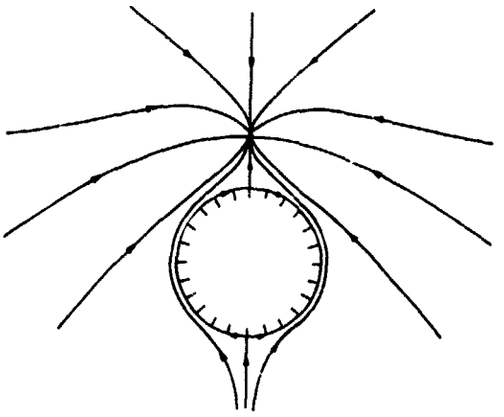

(e) CIRCULAR CONE AT ANGLE OF ATTACK $\bar{\alpha} > 1$

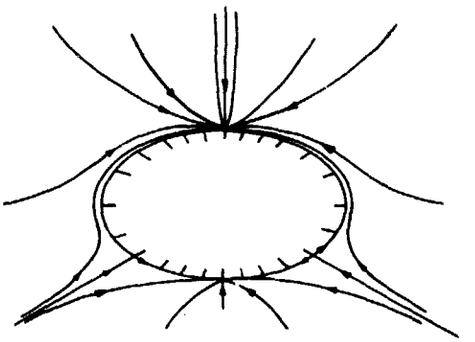

(g) ELLIPTIC CONE AT MODERATE ANGLE OF ATTACK

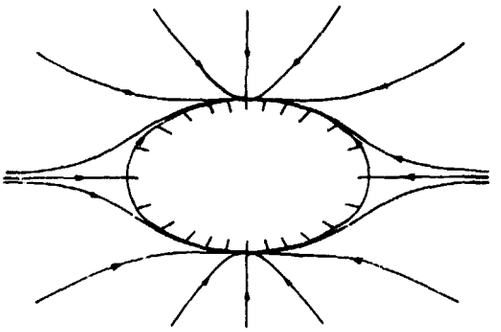

(f) ELLIPTIC CONE AT ZERO ANGLE OF ATTACK

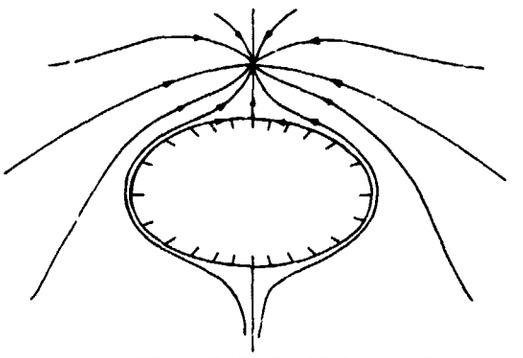

(h) ELLIPTIC CONE AT HIGH ANGLE OF ATTACK

$\bar{\alpha} = \alpha / \theta_c$; θ_c = SEMI-APEX ANGLE OF CONE

Fig. 49 Concluded.

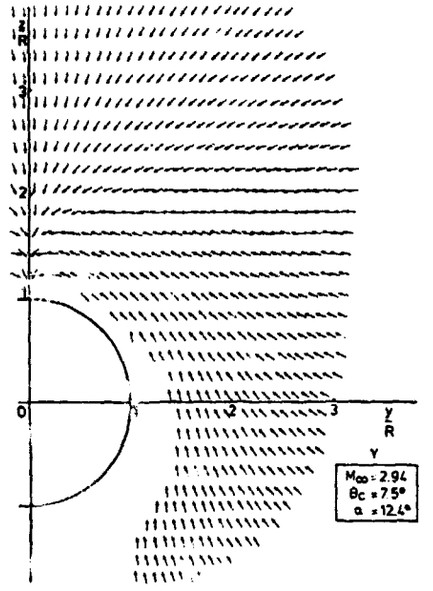

(a) DIRECTION OF CONICAL STREAMLINES

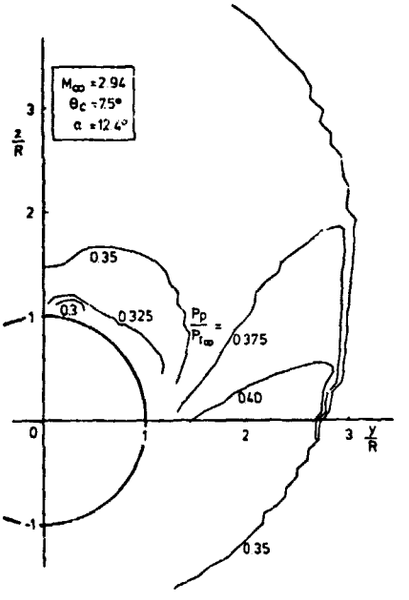

(b) LINES OF CONSTANT PITOT PRESSURE

Fig. 50 Measurement of conical streamlines about $\theta_c = 7.5°$ cone at moderate relative incidence: $\bar{\alpha} = 1.65$, $M_\infty = 2.94$, $R_{L_\infty} = 7 \times 10^6$, turbulent (Nebbeling and Bannink 1976).

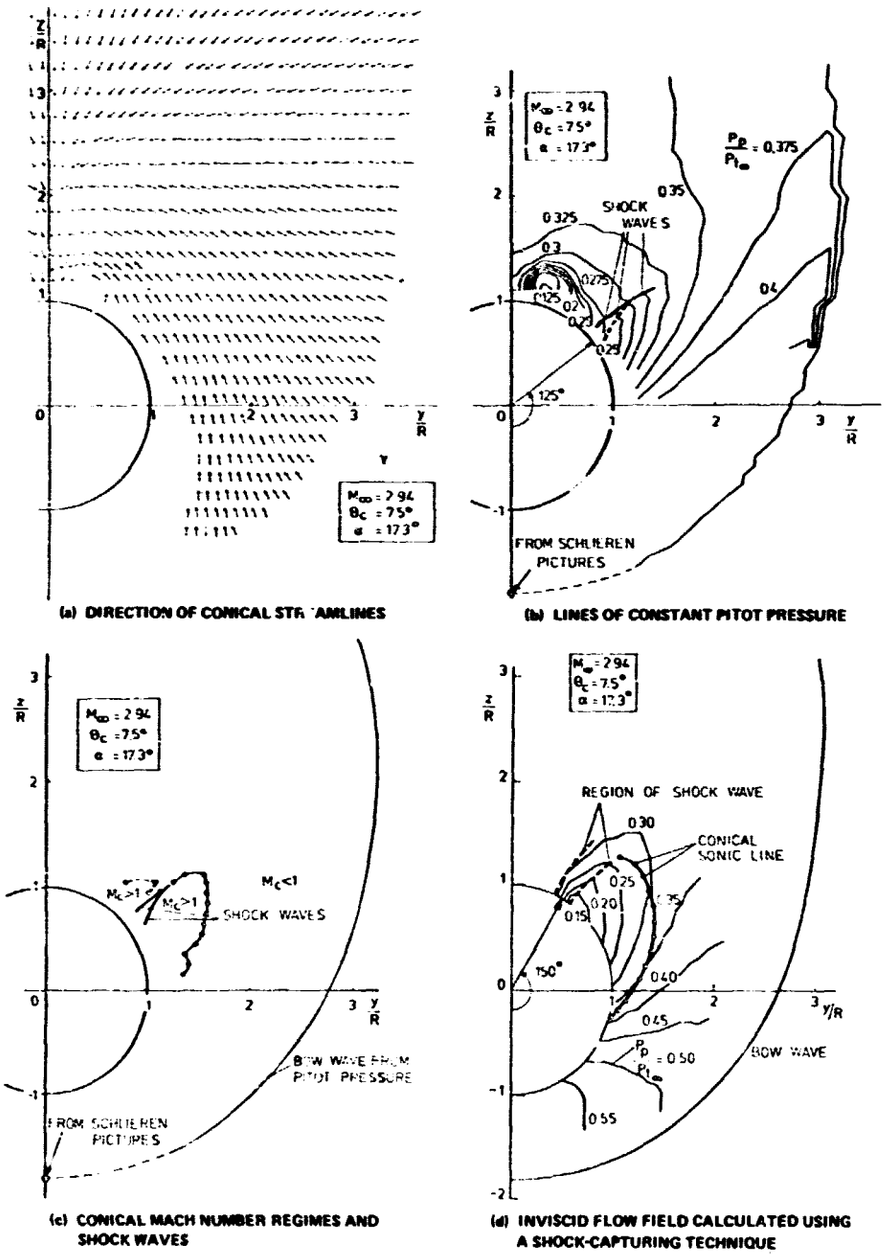

Fig. 51 Measurement of conical streamlines about $\theta_c = 7.5°$ cone at high relative incidence: $\bar{\alpha} = 1.65$, $M_\infty = 2.94$, $R_{L_\infty} = 7 \times 10^6$, turbulent (Nebbeling and Bannink 1976).

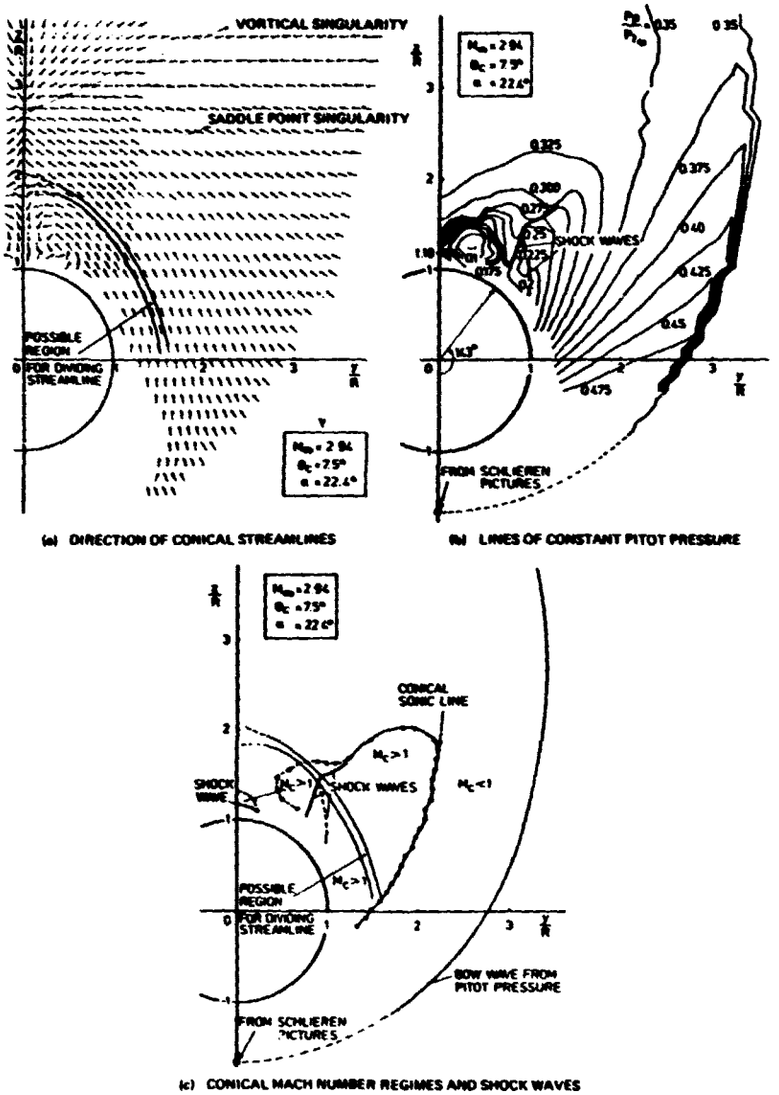

(a) DIRECTION OF CONICAL STREAMLINES

(b) LINES OF CONSTANT PITOT PRESSURE

(c) CONICAL MACH NUMBER REGIMES AND SHOCK WAVES

Fig. 52 Measurement of conical streamlines about $\theta_c = 7.5°$ cone at very high relative incidence: $\tilde{\alpha} = 3$, $M_\infty = 2.94$, $R_{L_\infty} = 7 \times 10^6$, turbulent (Nebbeling and Bannink 1976).

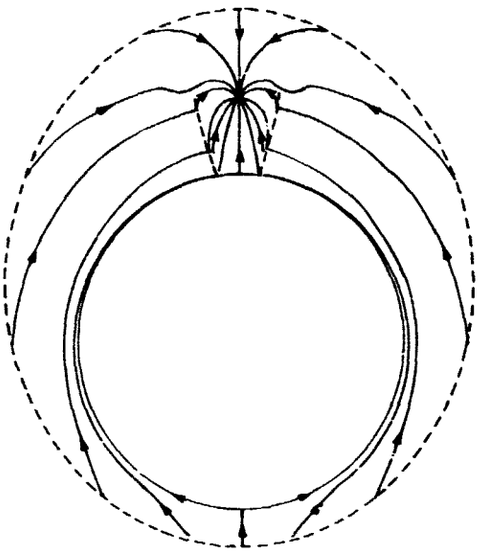

Fig. 53 Inviscid conical streamline pattern with transonic crossflow about $\theta_c = 20°$ cone at moderate relative incidence: $\bar{\alpha} = 1.5$ and $M_\infty = 7$ (Fletcher 1974).

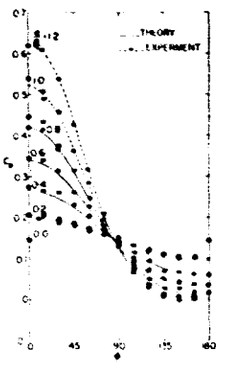

(a) PRESSURE DISTRIBUTIONS ON A 15° CIRCULAR CONE AT $M_\infty = 10.4$, $R_{x_\infty} = 10^6$

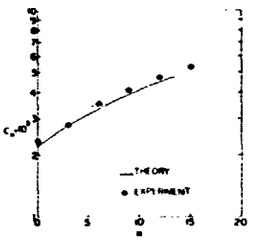

(b) HEAT-TRANSFER COEFFICIENT (STANTON NUMBER) AT THE MOST WINDWARD GENERATOR ON A 15° CIRCULAR CONE AT $M_\infty = 10.4$, $R_{x_\infty} = 10^6$

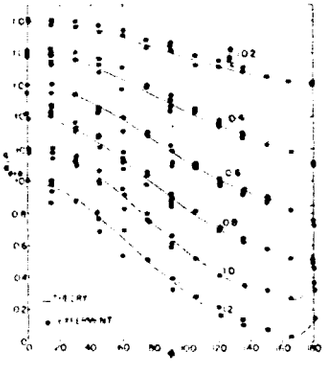

(c) HEAT-TRANSFER DISTRIBUTIONS ON A 15° CIRCULAR CONE AT $M_\infty = 10.4$, $R_{x_\infty} = 10^6$

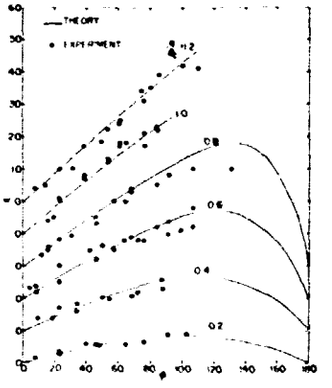

(d) SURFACE FLOW DIRECTIONS ON A 15° CIRCULAR CONE AT $M_\infty = 10.4$, $R_{x_\infty} = 10^6$

CONE LENGTH, L = 4 IN
MEASURING STATION, $x/L = 0.875$
$T_{WALL}/T_{STAG} = 0.23$

Fig. 54 Circumferential pressures, heat transfer and skin-friction line directions on surface of $\theta_c = 15°$ circular cone at angle of attack in hypersonic flow: $M_\infty = 10.4$, $R_{x_\infty} = 10^6$, laminar (Cnan 1969).

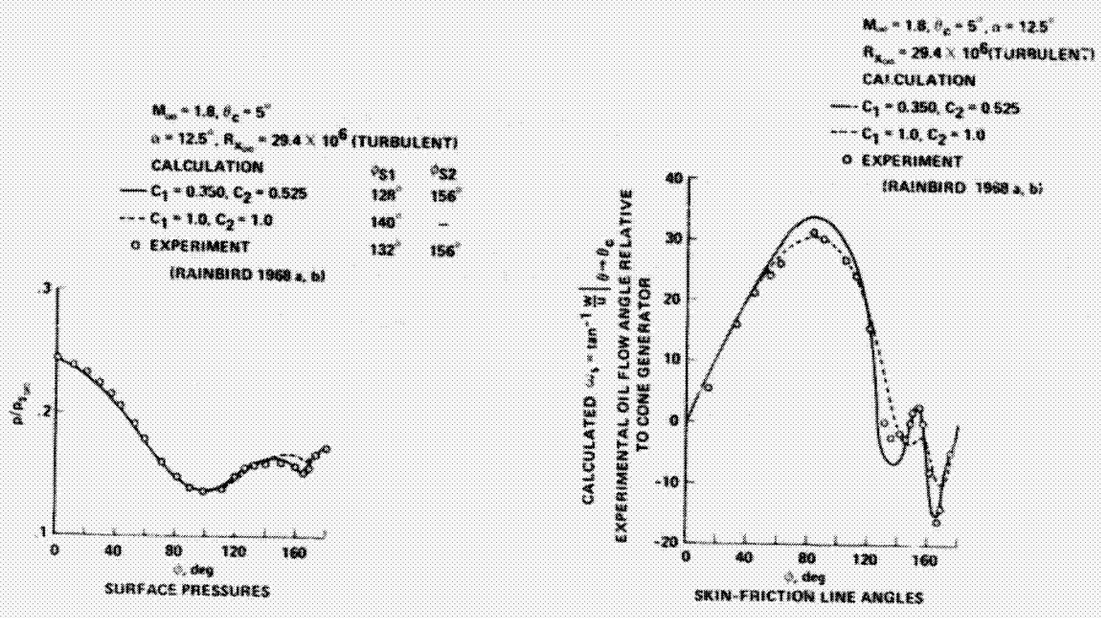

Fig. 55 Comparison of surface pressures and skin-friction line angles; calculation of McRae and Hussaini (1978) and experiment of Rainbird (1968a,b).

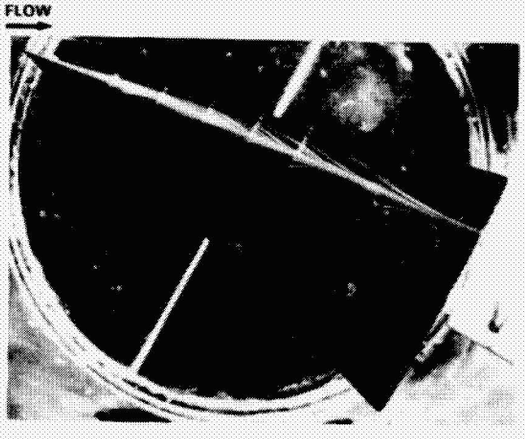

Fig. 56 Limiting streamlines on a 1.5:1 elliptic cone at 30° angle of attack in a water tunnel: laminar, $R_{L_\infty} = 2.7 \times 10^5$ (Crabbe 1965).

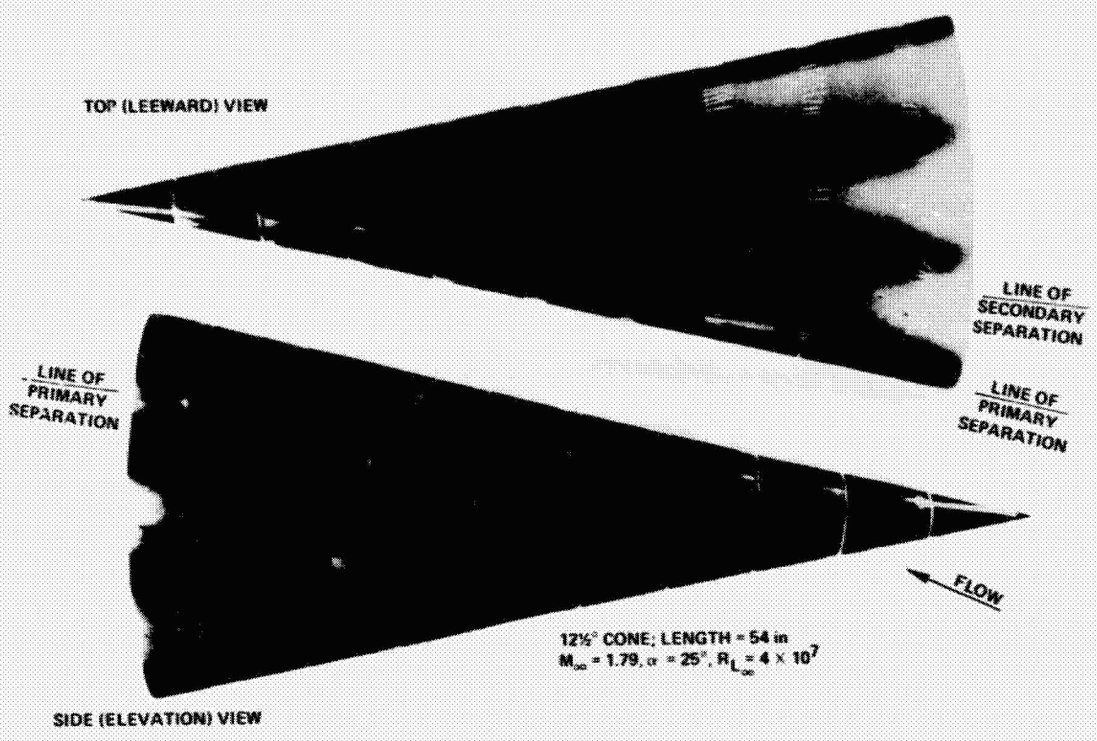

Fig. 57 Oil-dot surface flow visualization on circular cone at high relative incidence, $\bar{\alpha}$ = 2, with turbulent boundary layers (Rainbird et al. 1966).

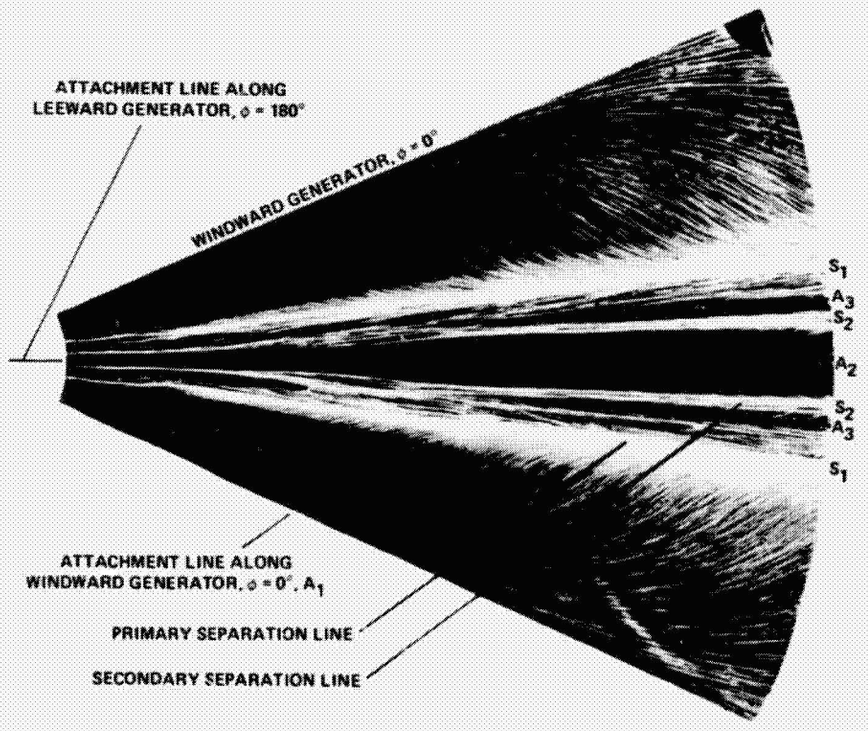

Fig. 58 Symmetrical oil-flow visualization on "unpeeled" surface of θ_c = 7.5° circular cone at M_∞ = 2.0: turbulent, $\bar{\alpha}$ = 2.1 (Bannink and Nebbeling 1978).

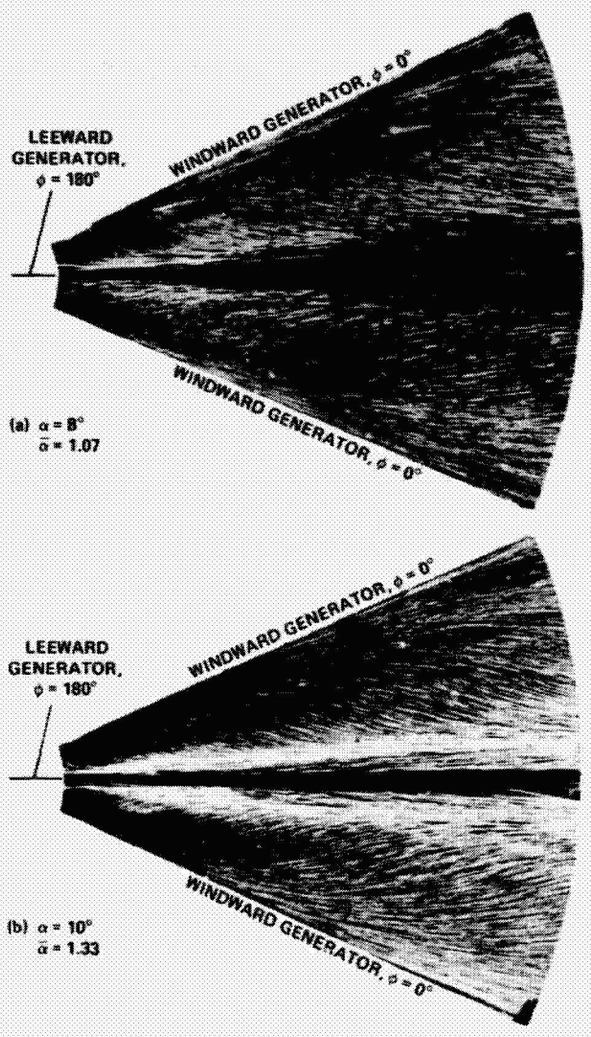

Fig. 59 Symmetrical oil-flow visualization on "unpeeled" surface of $\theta_c = 7.5°$ circular cone at $M_\infty = 2.94$: turbulent, $R_{L_\infty} = 7 \times 10^6$ (Bannink and Nebbeling 1978).

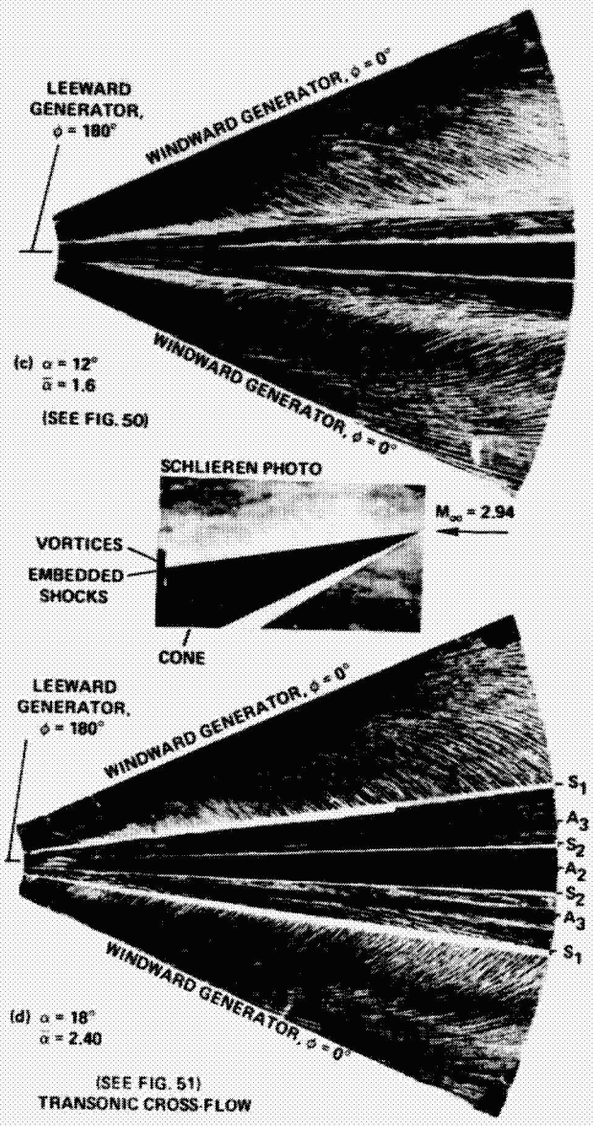

Fig. 59 Continued.

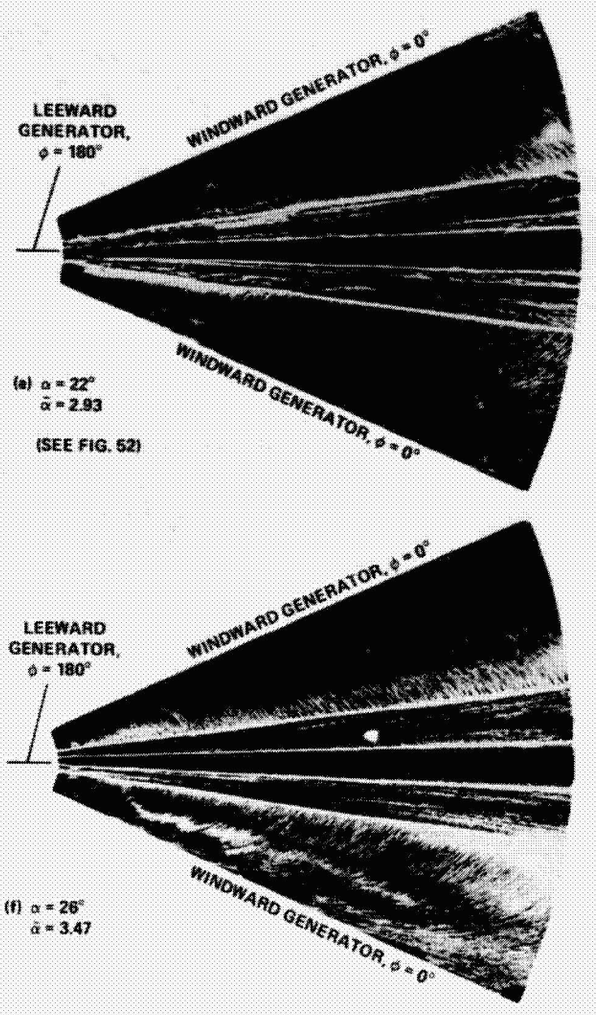

Fig. 59 Concluded.

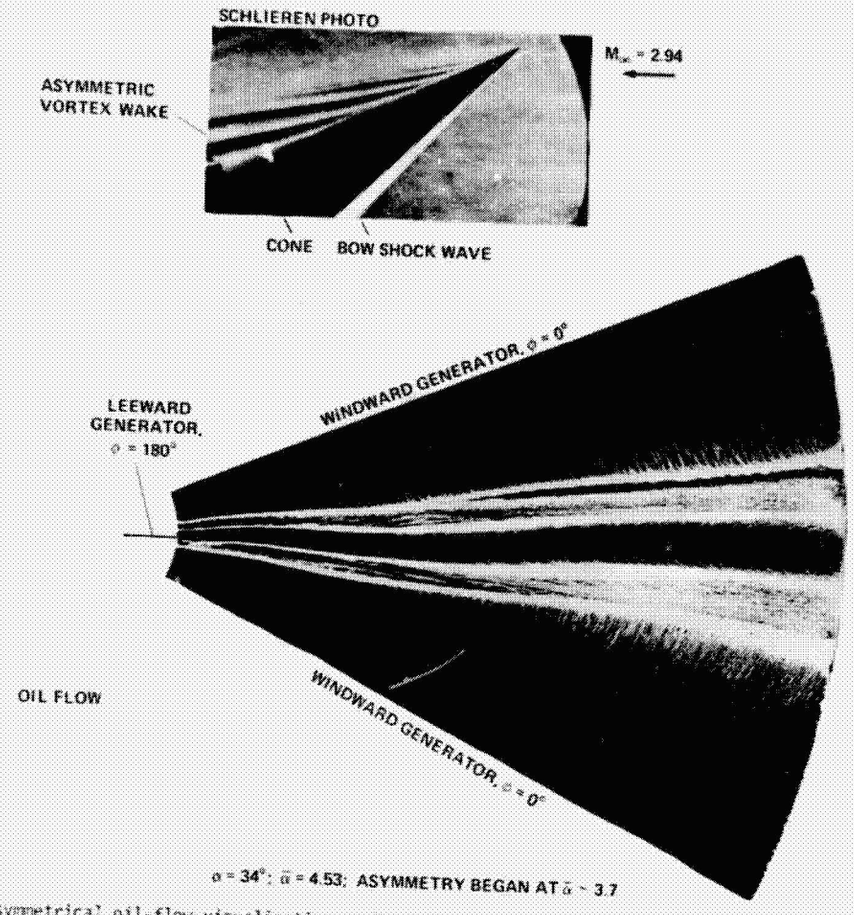

Fig. 60 Asymmetrical oil-flow visualization on "unpeeled" surface and Schlieren photograph of $\theta_c = 7.5°$ circular cone at $M_\infty = 2.94$; turbulent, $R_{L_\infty} = 7 \times 10^6$ (Bannink and Nebbeling 1978).

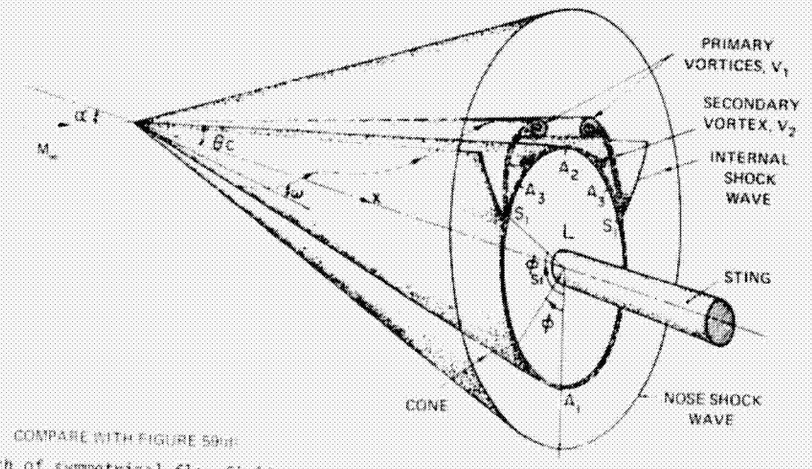

COMPARE WITH FIGURE 50(d)

Fig. 61 Sketch of symmetrical flow field past cone at large relative incidence ($\bar{\alpha} \sim 2.5$) with turbulent viscous flow at high Reynolds number, $R_{L_\infty} \sim 4 \times 10^7$ (Rainbird 1968a,b).

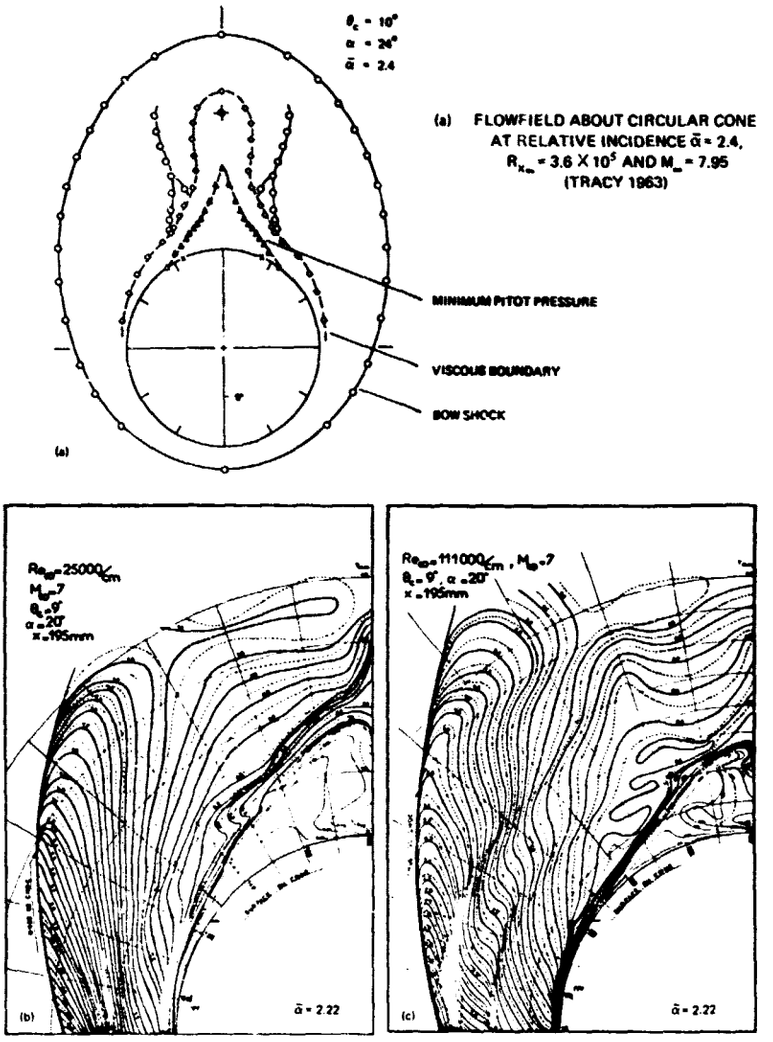

(b),(c) PITOT PRESSURE CONTOURS IN FLOWFIELD ABOUT CIRCULAR CONE AT RELATIVE INCIDENCE $\bar{\alpha}$ = 2.22, AT M_∞ = 7 (b) R_{x_∞} = 4.9 X 10^5 AND (c) R_{x_∞} = 21.6 X 10^5 (GUFFROY ET AL.1968)

Fig. 62 Laminar viscous flow field about circular cone at high relative incidence.

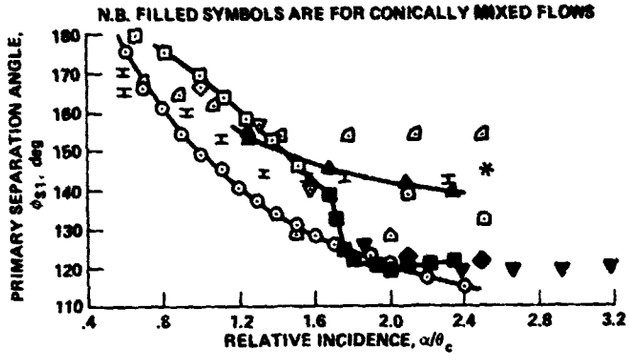

AUTHOR	SYMBOL	M_∞	θ_c deg	R_{L_∞}	TYPE
RAINBIRD et al., 1963	○	~ 0	12.5	2.7×10^4	LAMINAR
GUFFROY et al., 1968	⌶	7.0	9.0	$\sim 5.0 \times 10^5$	
STETSON 1971	◿	14.2	5.6	8.0×10^5	
RAINBIRD 1968a, b	□	1.80	12.5	2.5×10^7	TURBULENT
	△	4.25	12.5	5.1×10^7	
	⬡	1.80	5.0	3.4×10^7	
	◇	4.25	5.0	6.8×10^7	
PEAKE et al., 1978	✳	0.60	5.0	1.4×10^7	
NEBBELING AND BANNINK 1976	▽	2.94	7.5	7.0×10^6	
McELDERRY 1974	⌂	6.05	6.0	16.0×10^6	

Fig. 63 Primary separation angles on cones at angle of attack.

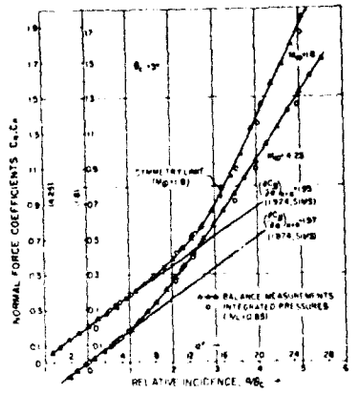

Fig. 64 Normal force characteristics of $\theta_C = 5°$ cone at $M_\infty = 1.8$ and 4.25: turbulent, $R_{L_\infty} = 3.4 \rightarrow 6.8 \times 10^7$ (Rainbird 1968a,b).

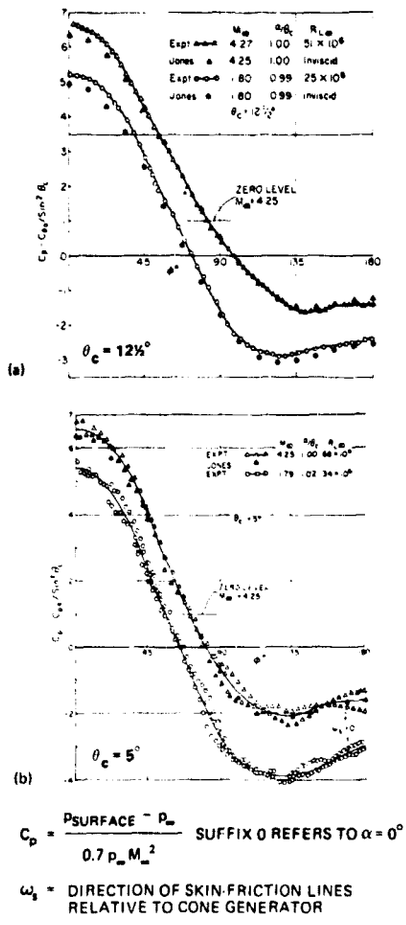

Fig. 65 Comparison of experimental circumferential surface static pressure distributions at x/L = 0.85 on θ_c = 5° and 12.5° circular cones at relative incidences $\bar{\alpha} \sim 1$ with numerical solutions of D. J. Jones (1969) (from Rainbird 1968a,b).

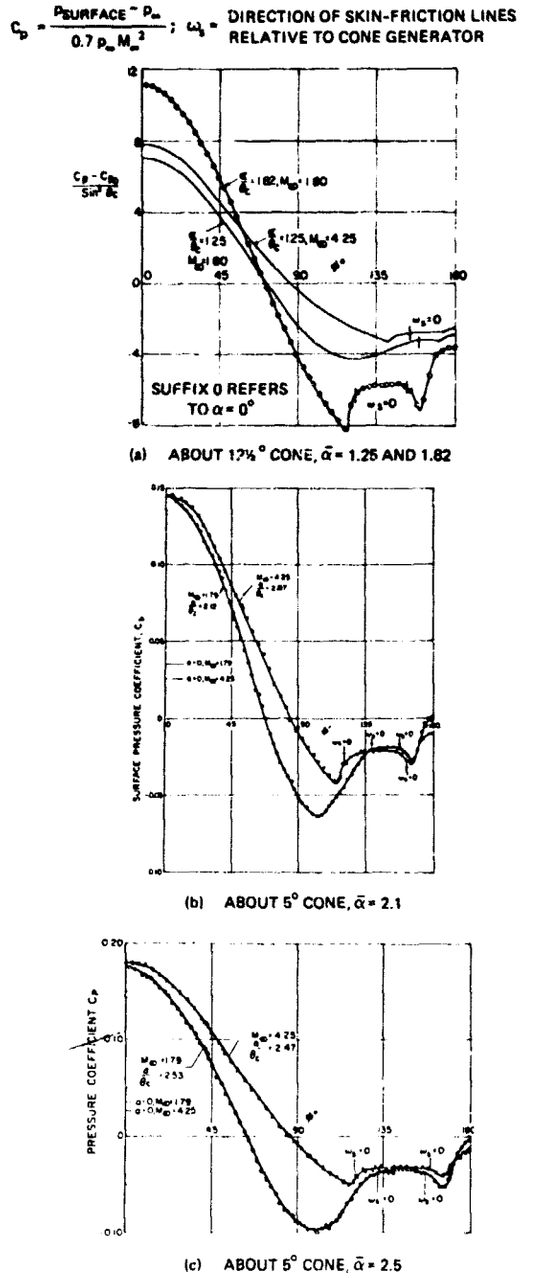

Fig. 66 Experimental circumferential static pressure distributions at x/L = 0.85 about θ_c = 5° and 12.5° circular cones at moderate to high relative incidence (Rainbird (1968a,b).

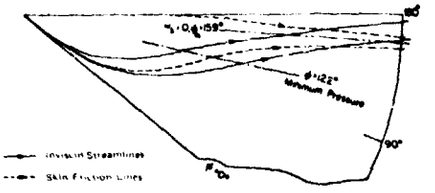

(a) INVISCID AND SKIN-FRICTION LINE DIRECTIONS ON DEVELOPED SURFACE OF CONE: $\bar{\alpha} = 1.25$

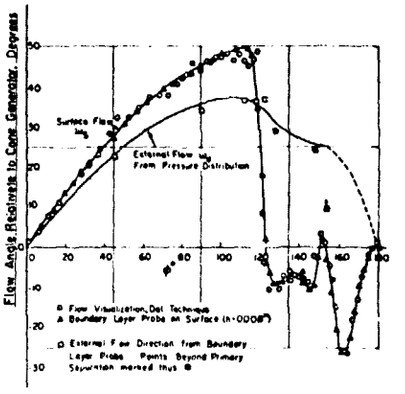

(b) SURFACE AND EXTERNAL FLOW DIRECTIONS, $\bar{\alpha} = 1.82$

Fig. 67 Surface and external flow directions about $\theta_c = 12.5°$ cone at $M_\infty = 1.8$, $\bar{\alpha} = 1.25$ and 1.82 (Rainbird 1968a,b).

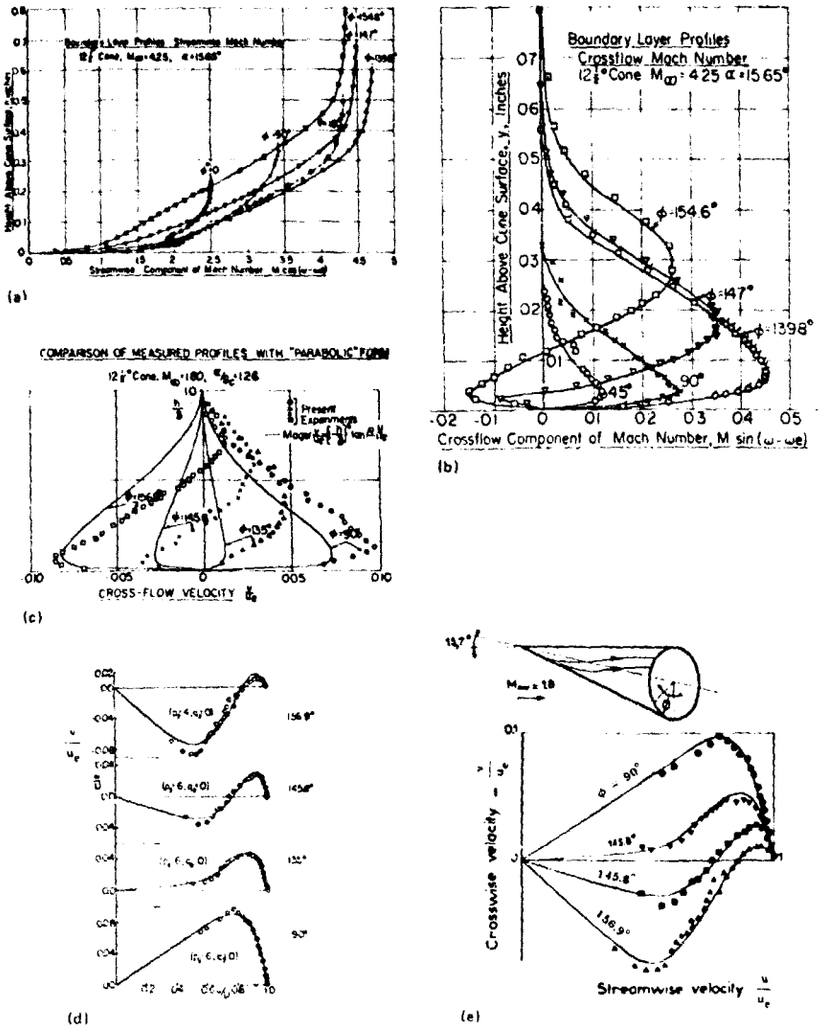

Fig. 68 Experimental and calculated 3D boundary-layer profiles about θ_c = 12.5° cone at M_∞ = 1.8 and 4.25.

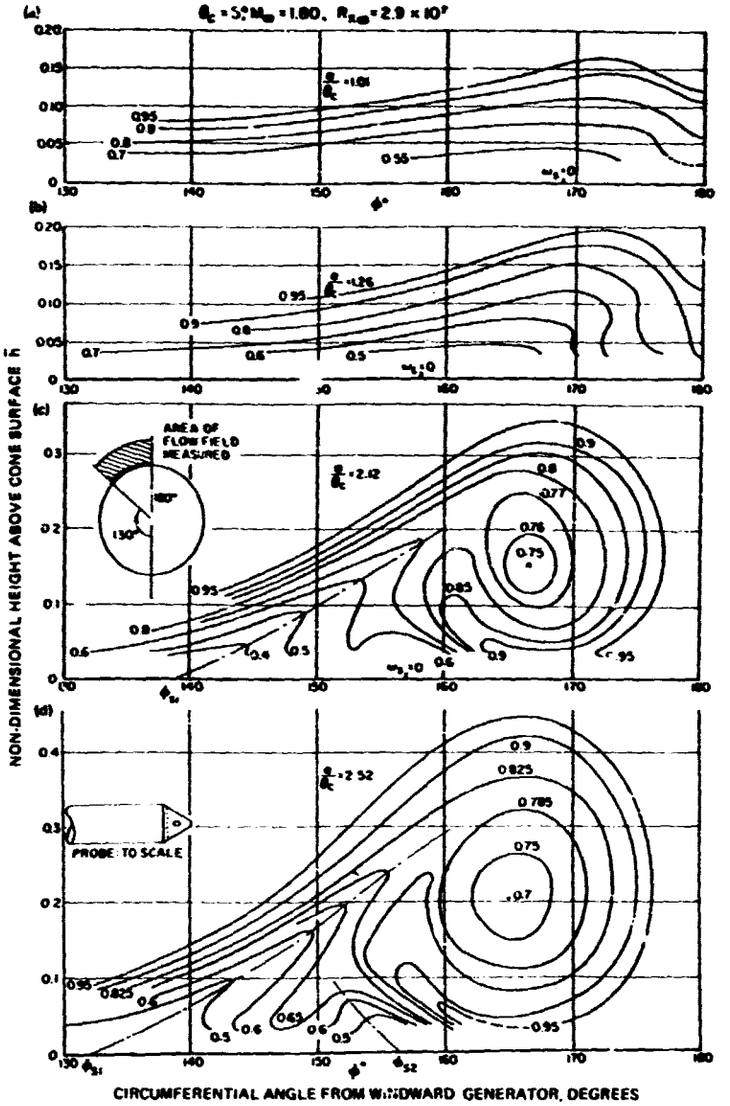

Fig. 69 Pitot pressure contours in flow field above 5° cone at M_∞ = 1.8 and at relative incidences $\bar{\alpha}$ = 1.01, 1.26, 2.12, and 2.52 (Rainbird 1968a,b).

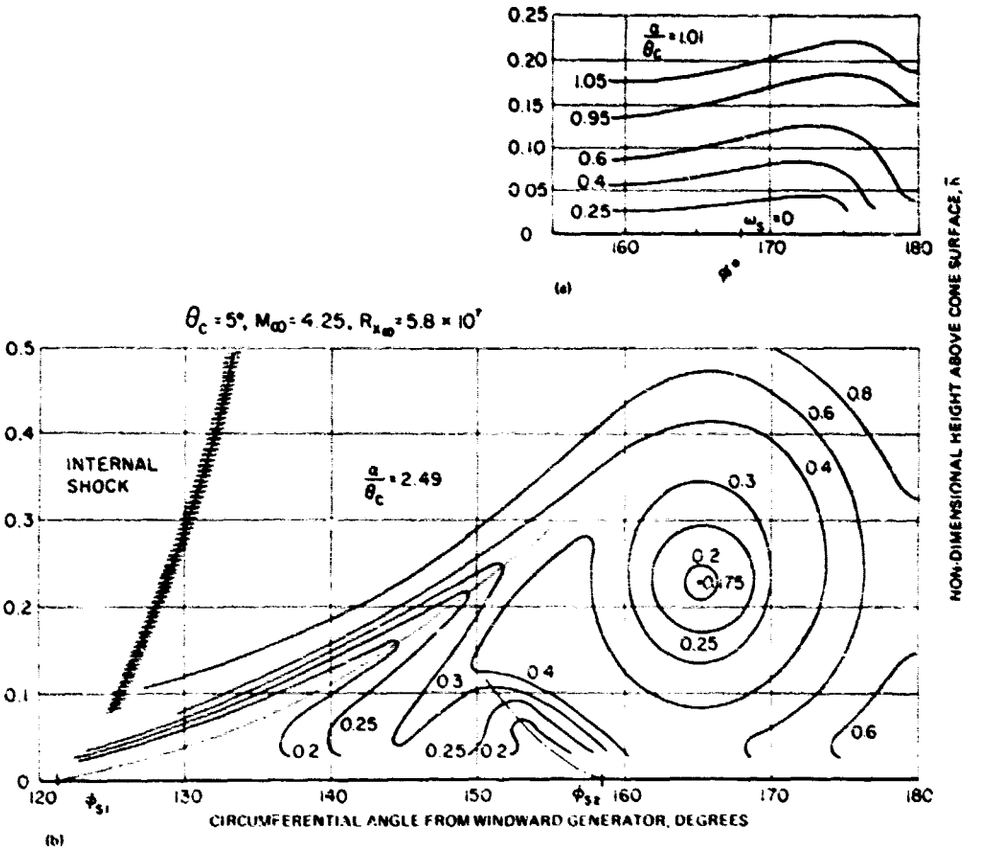

Fig. 70 Pitot pressure contours in flow field above 5° cone at M_∞ = 4.25 and at relative incidences α/θ_c = 1.01 and 2.49 (Rainbird 1968a,b).

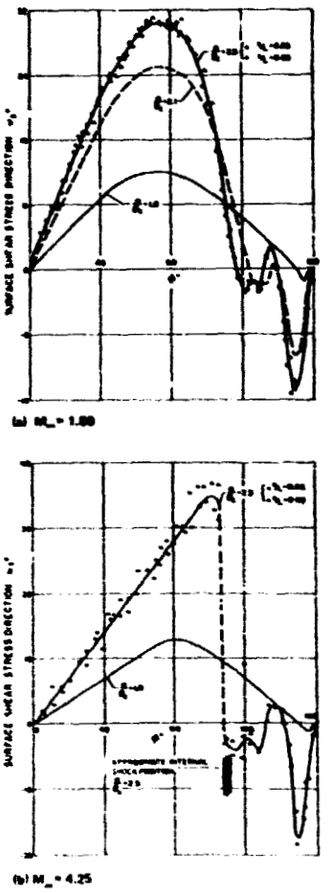

Fig. 71 Surface shear stress directions on 5° cone at M_∞ = 1.8 and 4.25 at moderate to high relative incidence (Rainbird 1968a,b).

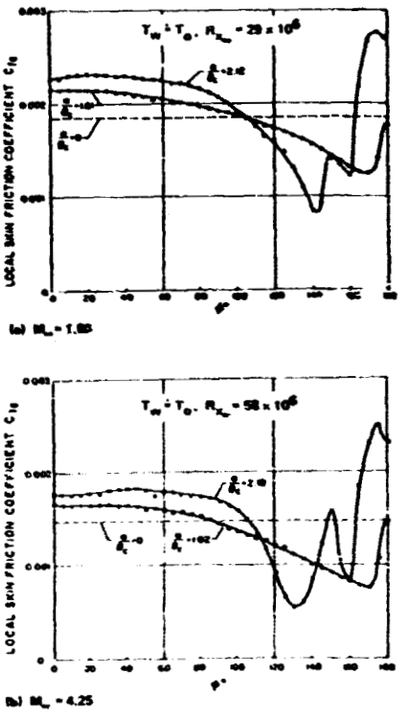

Fig. 72 Distributions of skin-friction coefficient on 5° cone at M_∞ = 1.80 at moderate to high relative incidence (Rainbird 1968a,b).

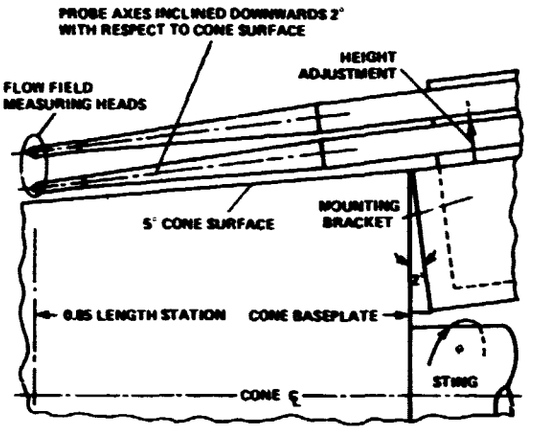

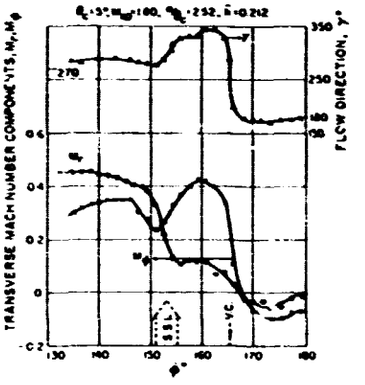

γ = CIRCUMFERENTIAL ANGLE OF RESULTANT VELOCITY VECTOR RELATIVE TO FLOWFIELD PROBE

M_ϕ = CIRCUMFERENTIAL COMPONENT OF MACH NUMBER

M_r = RADIAL COMPONENT OF MACH NUMBER

$\bar{h}$ = DISTANCE ABOVE CONE SURFACE NORMALIZED BY LOCAL RADIUS

Fig. 73 Circumferential distribution of Mach number components, M_∞ = 1.8, $\bar{a}$ = 2.52 for the 5° cone (Rainbird 1968a,b).

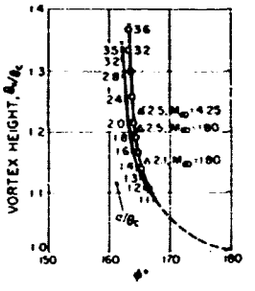

SYMBOL	M_∞	θ_c°	$R_{L\infty}$	
⊸	≈0	12½	2.7×10^6	LAMINAR, RAINBIRD 1963
⊸	≈0	7½	2.7×10^6	
▲	1.80	5	3.4×10^7	TURBULENT, RAINBIRD 1968a, b
◢	4.25	5	6.8×10^7	

Fig. 74 Vortex core positions at various relative incidences in laminar and turbulent flow.

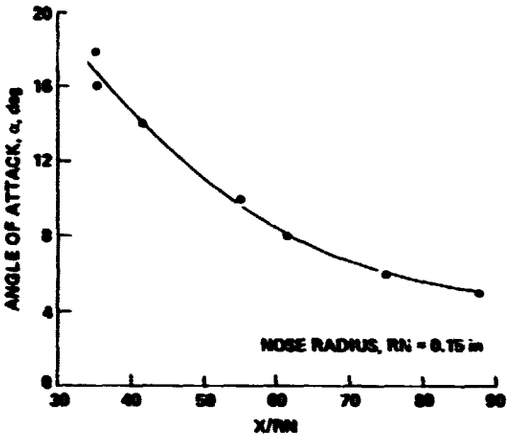

Fig. 75 Distance to return to conical (laminar) flow conditions on leeward side of θ_c = 5.6° blunt cone (10% bluntness) at M_∞ = 14.2, $R_{L_\infty} \sim 0.4 \times 10^6$ (Stetson 1971).

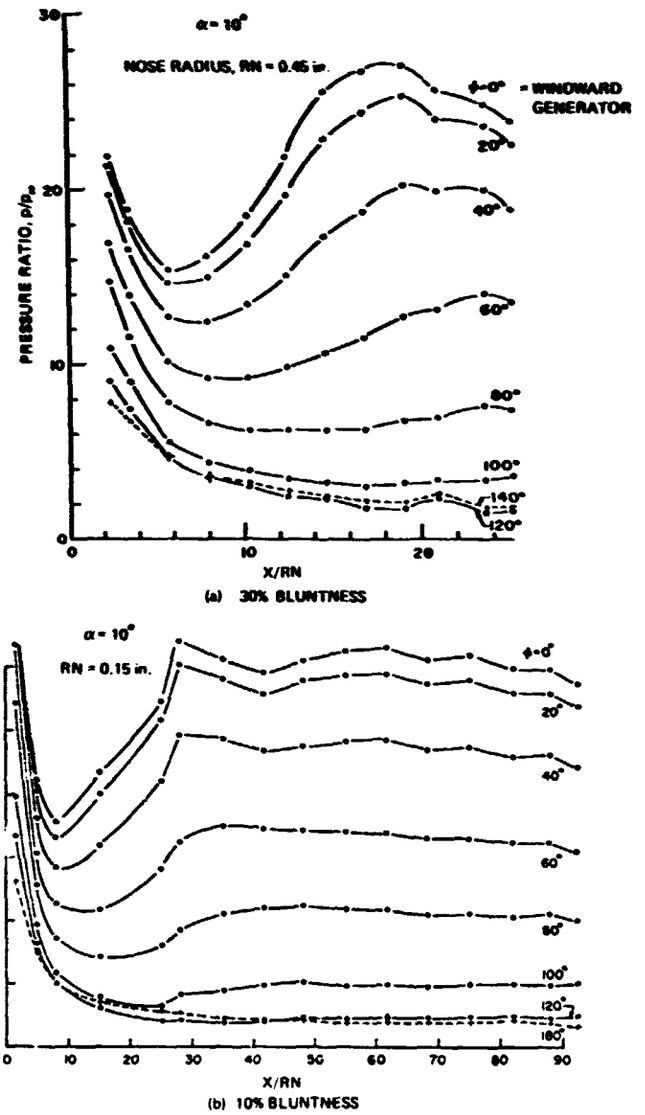

Fig. 76 Longitudinal pressure distributions on θ_c = 5.6° blunt cones at M_∞ = 14.2 and $R_{L_\infty} \sim 0.4 \times 10^6$: laminar, $\bar{\alpha}$ = 1.79 (Stetson 1971).

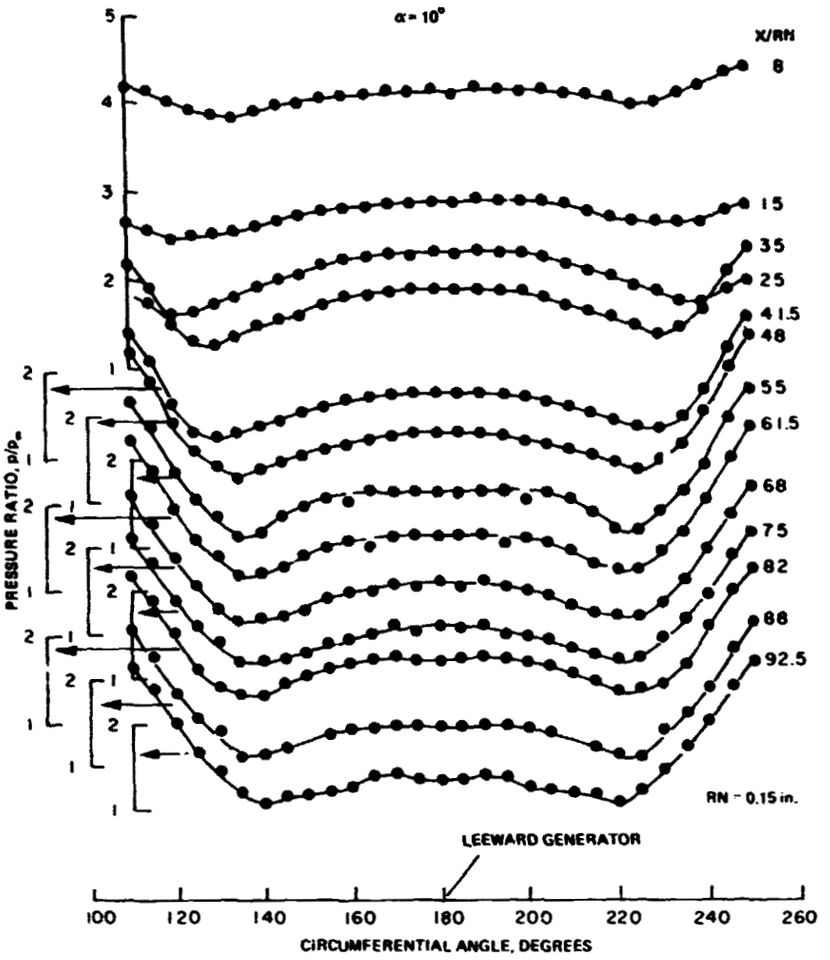

Fig. 77 Circumferential pressure distributions on leeward side of θ_c = 5.6° blunt cone (10% bluntness) at M_∞ = 14.2 and $R_{L_\infty} \sim 0.4 \times 10^6$: laminar, and $\bar{\alpha}$ = 1.79 (Stetson 1971).

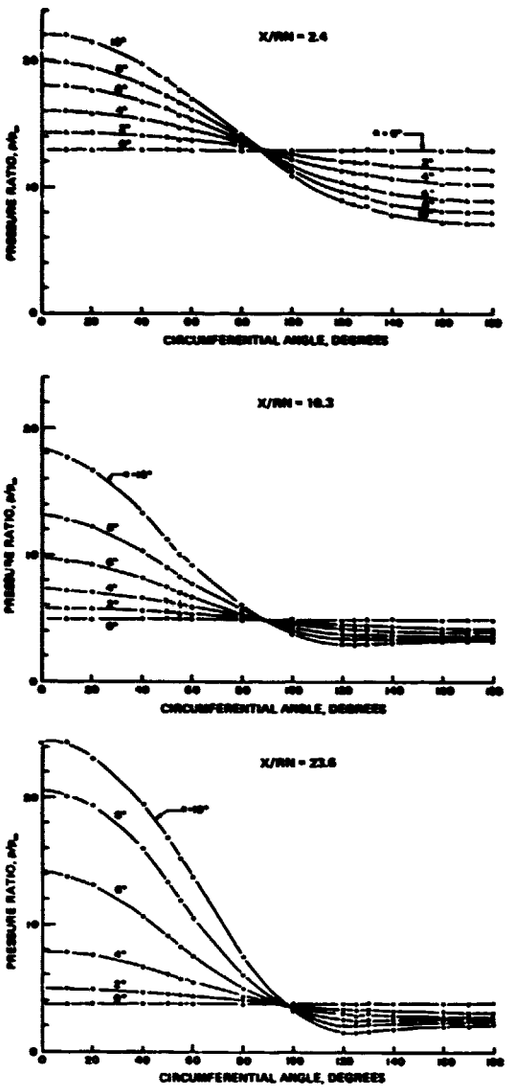

Fig. 78 Circumferential pressure distributions about $\theta_c = 5.6°$ blunt cone (30% bluntness) at $M_\infty = 14.2$, $R_{L_\infty} \sim 0.4 \times 10^6$; laminar, up to $\bar{\alpha} = 1.79$ (Stetson 1971).

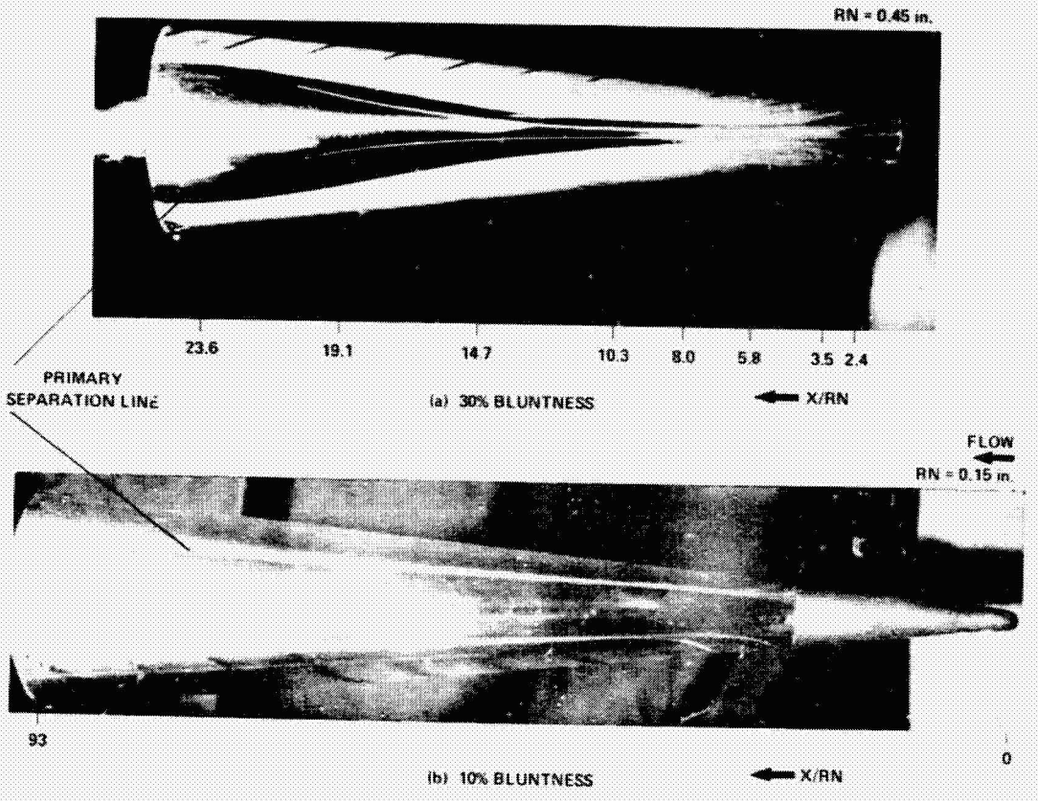

Fig. 79 Leeward-side oil flow on $\theta_c = 5.6°$ blunt cones at $\bar{\gamma} = 1.79$, $M_\infty = 14.2$, $R_{L_\infty} \sim 0.4 \times 10^6$; laminar (Stetson 1971).

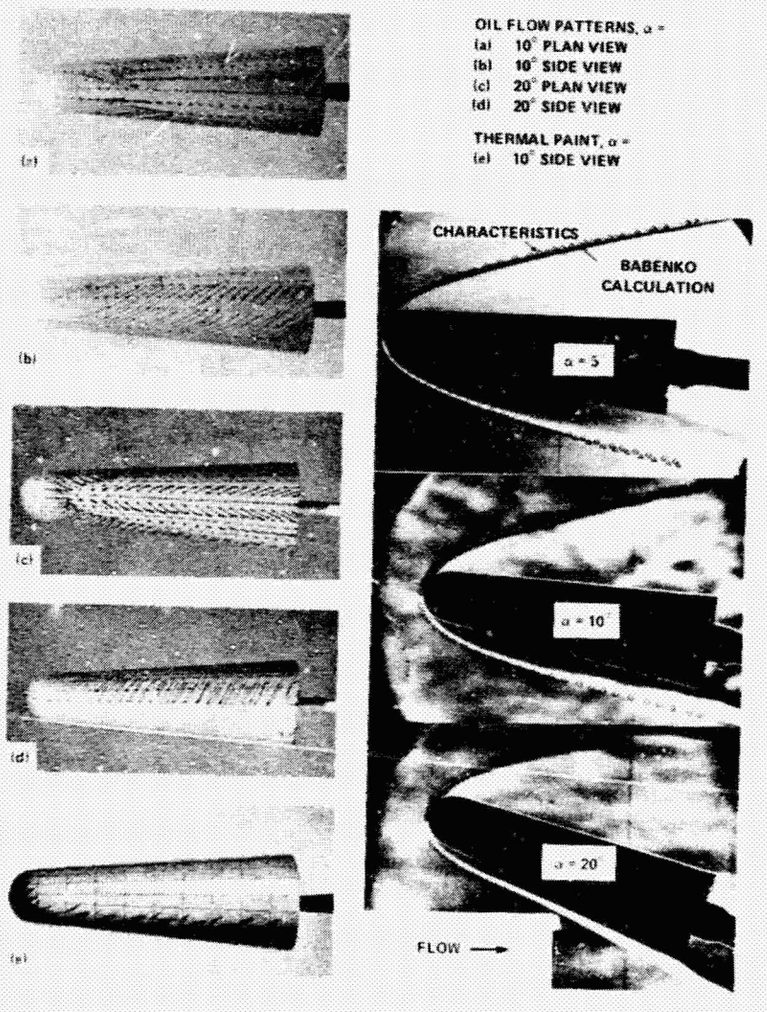

Fig. 80 Surface oil flow patterns and external shock shape about $\theta_c = 4.7°$, 56% blunt cone at $M_\infty = 10$, $R_{L_\infty} = 2.3 \times 10^6$ at high relative incidences (Cérésuela, Kretzschmer, and Rehbach 1968).

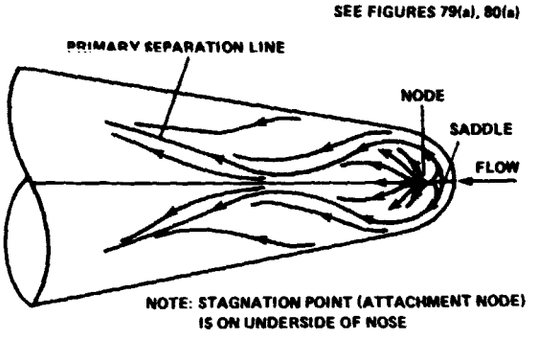

(a) PRIMARY SEPARATION ONLY

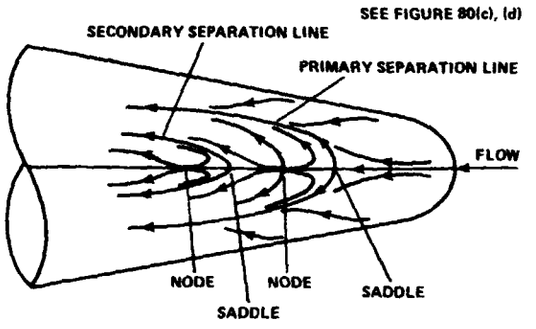

(b) PRIMARY AND SECONDARY SEPARATIONS

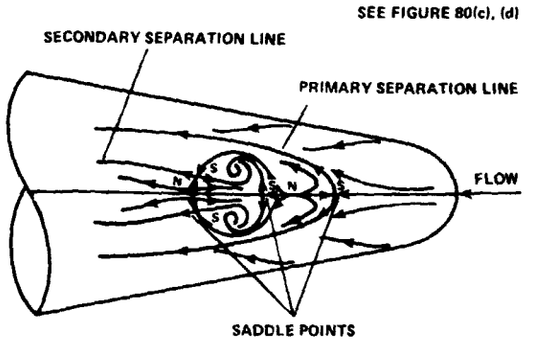

(c) ALTERNATIVE FOR PRIMARY AND SECONDARY SEPARATIONS

Fig. 81 Conjectured skin-friction line patterns on leeward side of blunt cone.

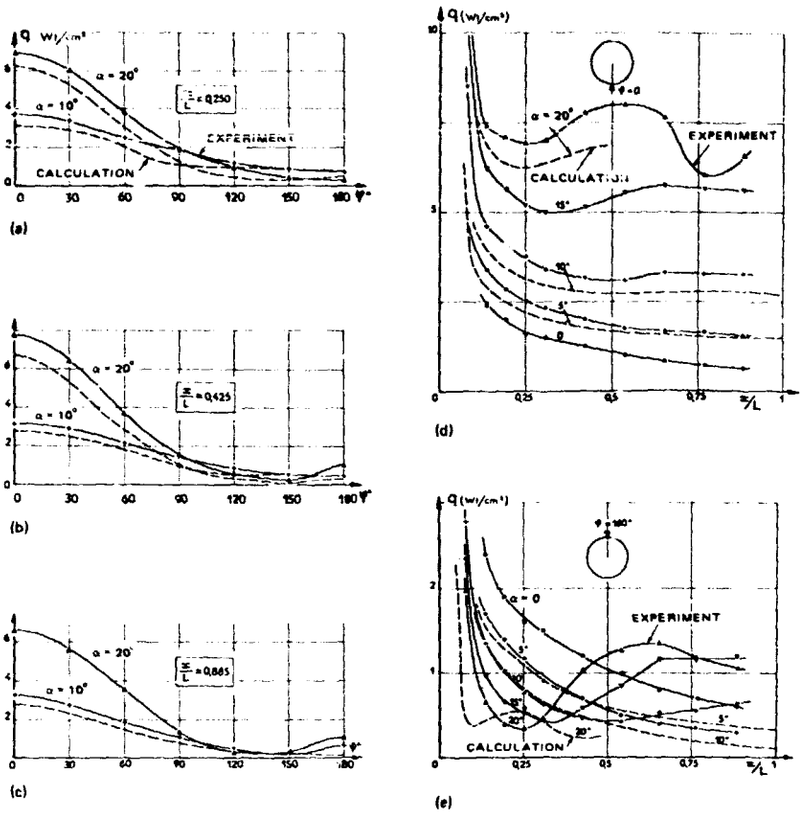

Fig. 82 Heat flux distributions on 56% blunt, θ_c = 4.7° cone at M_∞ = 10, R_{L_∞} = 2.3 × 10^6, laminar, up to very high relative incidence (Cérésuela, Kretzschmer, and Rehbach 1968).

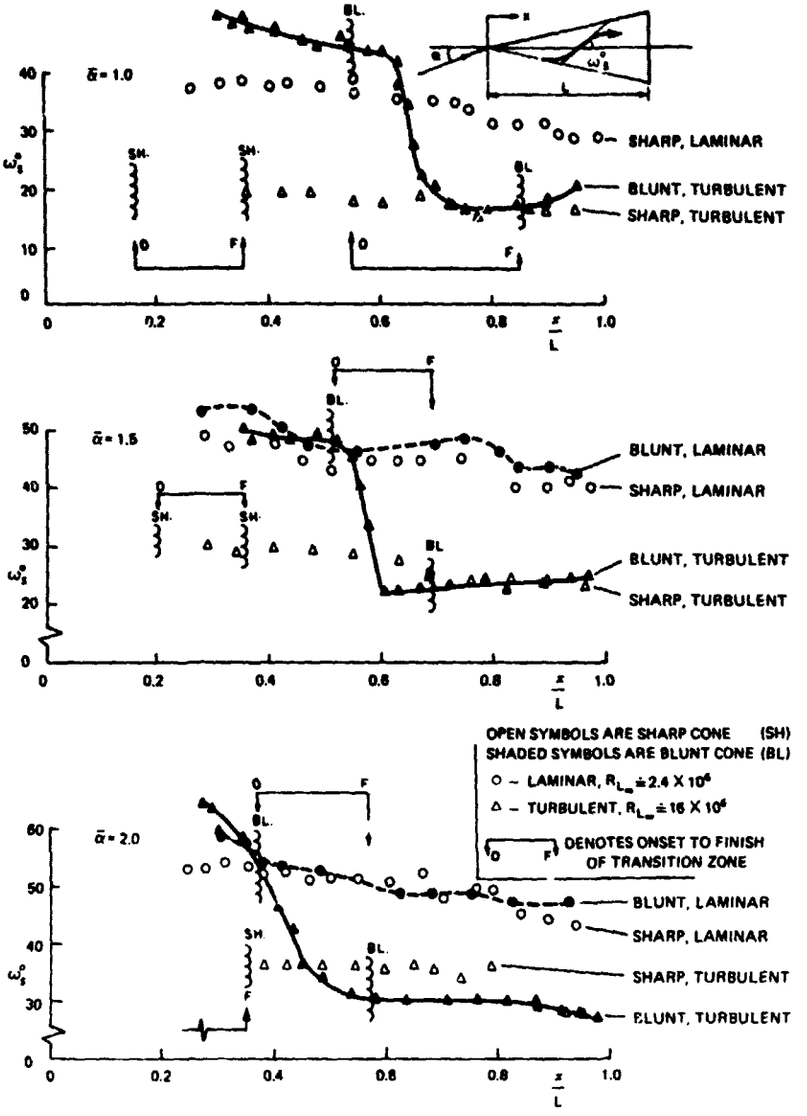

Fig. 83 Comparison of skin-friction line directions along $\phi = 90°$ for $\theta_c = 6°$ sharp and 10% blunt cones, demonstrating different boundary-layer states at $M_\infty = 6.05$ (McElderry 1974).

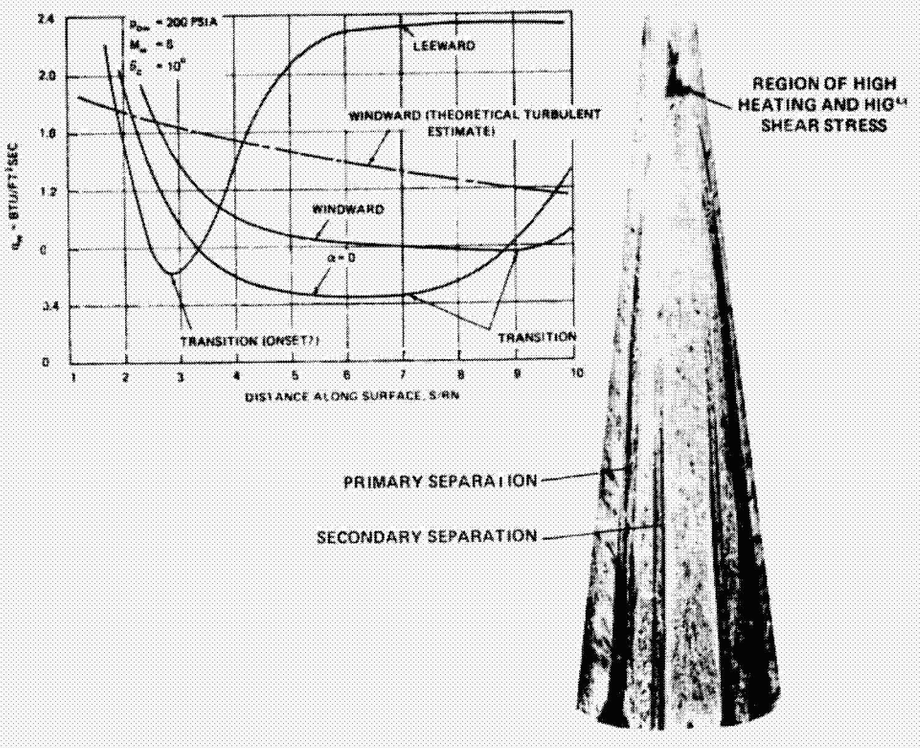

Fig. 84 Measured heat transfer rates and oil flow on surface of θ_c = 10° blunt cone, M_∞ = 6 at $\bar{\alpha} \sim 2$; laminar, transition and turbulent boundary layers (Zakkay et al. 1972).

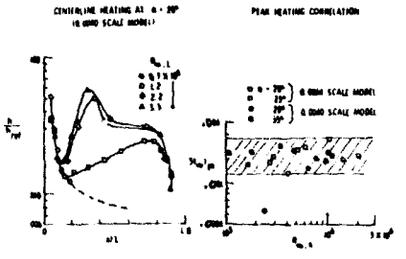

Fig. 85 Effect of Reynolds number on heating to leeward generator of conceptual shuttle model at $M_\infty = 6$ (Whitehead, Hefner, and Rao 1972).

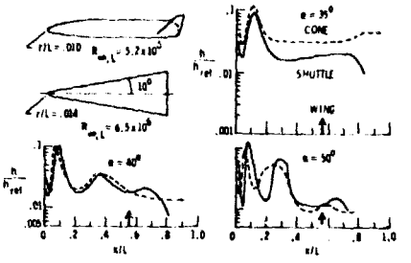

Fig. 86 Leeward meridian heating on Shuttle and 10° blunted cone at $M_\infty = 6$ (Whitehead, Hefner, and Rao 1972).

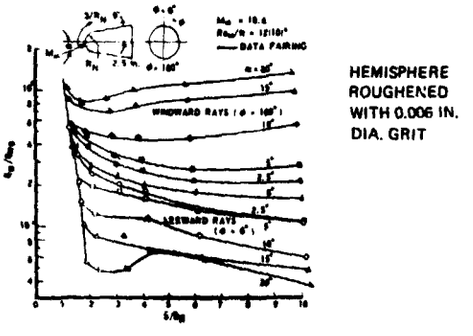

Fig. 87 Measured turbulent heat transfer distributions along the windward and leeward rays of $\theta_c = 9°$ blunt cone for various angles of attack at $M_\infty = 10.6$, $R_{L_\infty} = 25 \times 10^6$ (Widhopf 1971a).

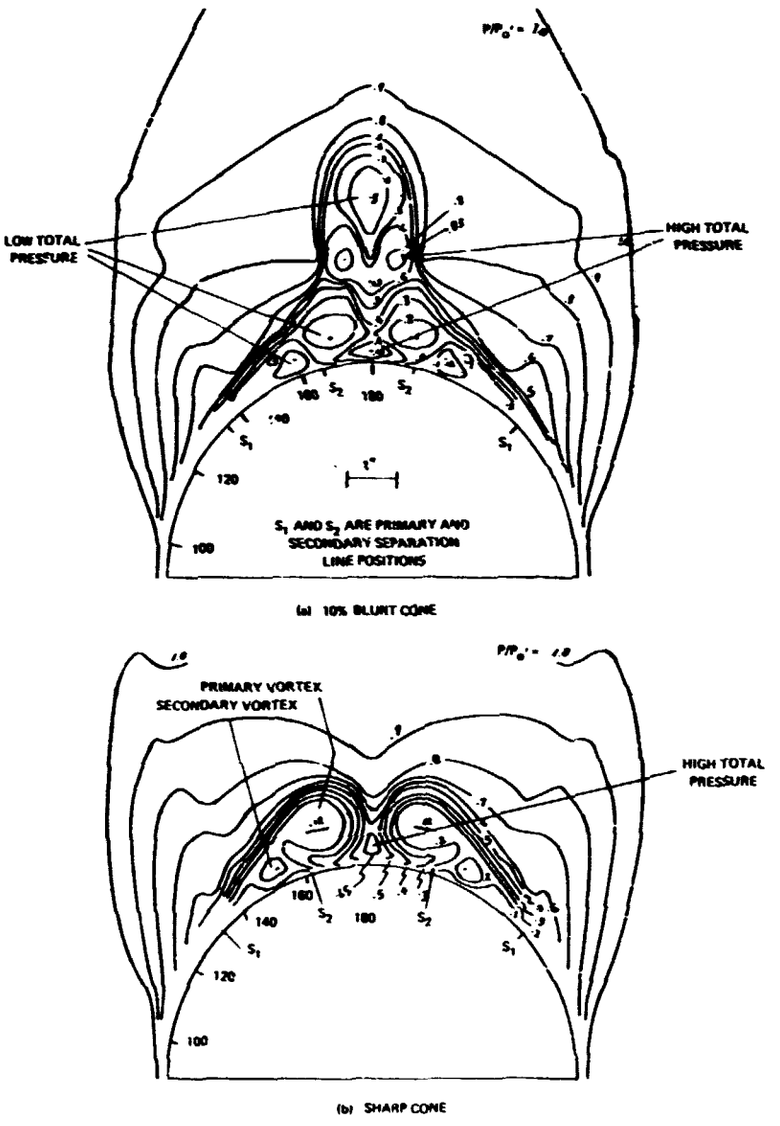

Fig. 88 Pitot pressure contours at x/L = 0.967 about 10% blunt cone and sharp cone, θ_c = 6° at M_∞ = 6.05, R_{L_∞} = 15.8 × 10^6, turbulent and $\bar{\alpha}$ = 2 (McElderry 1974).

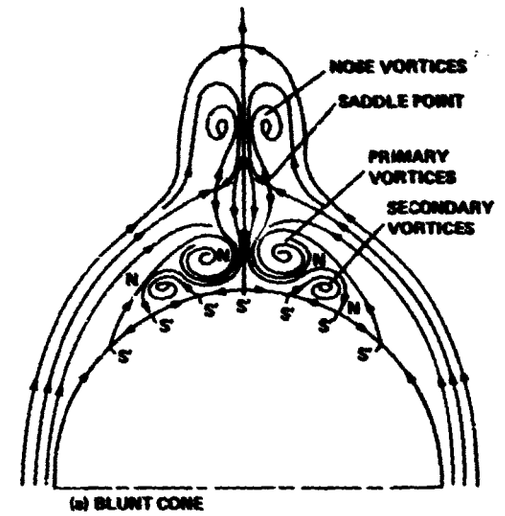

(a) BLUNT CONE

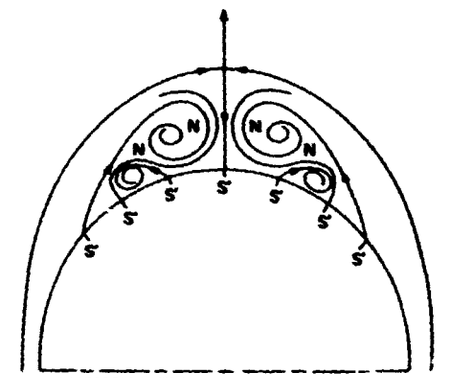

(b) SHARP CONE

NOTE: FOR BOTH CONES, A HALF-SADDLE POINT S' ALSO EXISTS ON WINDWARD RAY. SUM OF SINGULAR POINTS SATISFIES TOPOLOGY RULE NO. 3

Fig. 89 Postulate of flow structures in crossflow plane about blunt and sharp cones corresponding with pitot measurements of McElderry (1974).

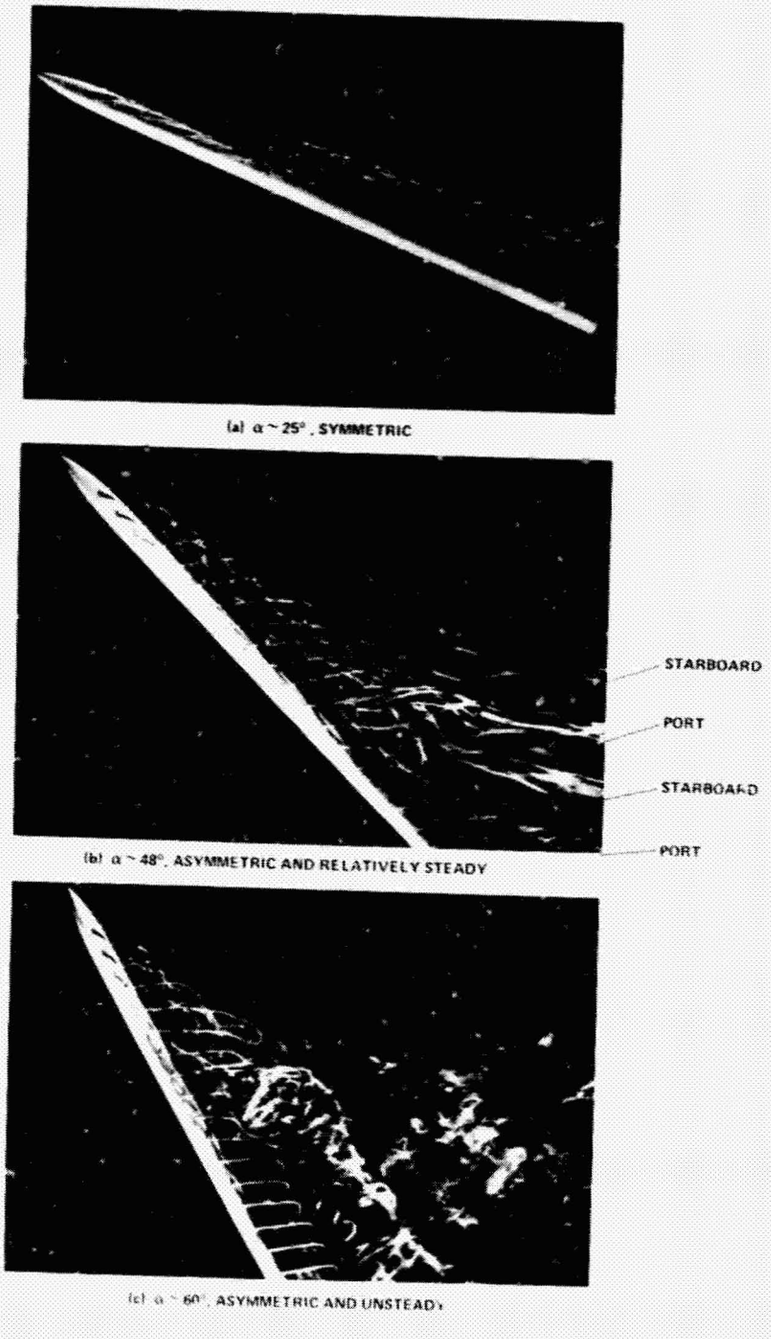

Fig. 90 Leeward-side vortex wake about θ_c = 18° tangent-ogive-cylinder at angle of attack in water tunnel (Fiechter 1966).

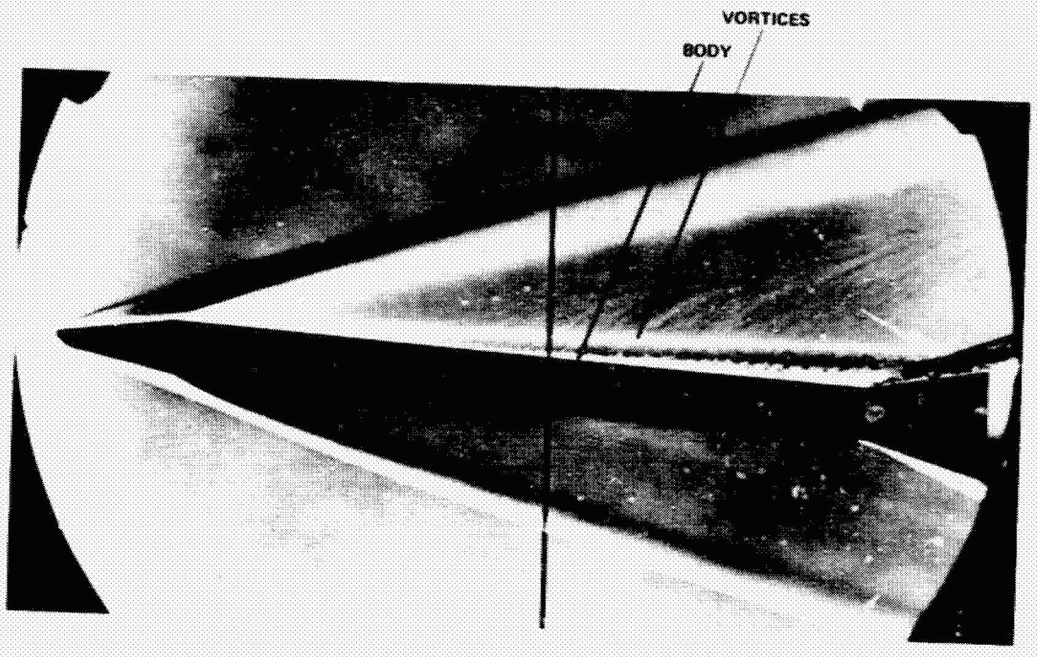

Fig. 91 Body separations on $\theta_c = 10°$ blunted cone-cylinder-flare at $M_\infty = 4$ and $\bar{\gamma} \sim 0.5$ (courtesy of Computing Devices of Canada).

(a) SYMMETRIC CROSS FLOW, WATER TUNNEL, $M_\infty \sim 0$, $\alpha = 20°$ (WERLÉ 1974)

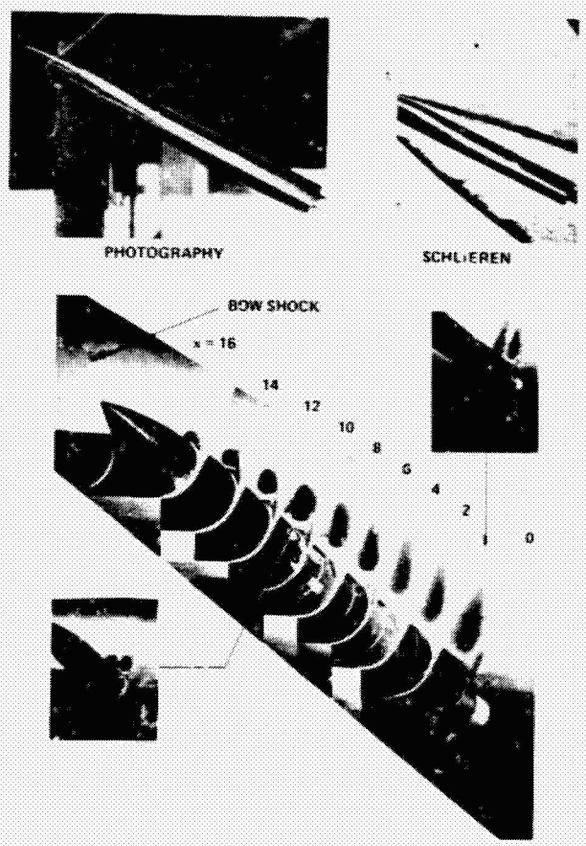

(b) LASER VAPOR SCREEN, OIL FLOW AND SCHLIEREN FLOW VISUALIZATION, $M_\infty = 2$, $\alpha = 26°$ (O'HARE AND JONES 1973)

Fig. 92 Views of the symmetric vortex wake in the cross-flow plane about tangent-ogive cylinders at angle of attack.

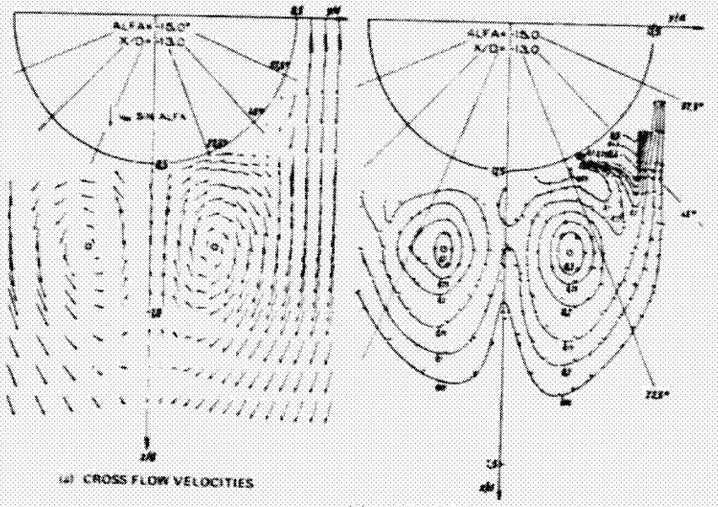

FLOW FIELD AT THE PLANE X/D = -13, ANGLE OF ATTACK α = -15°, WINGLESS BODY

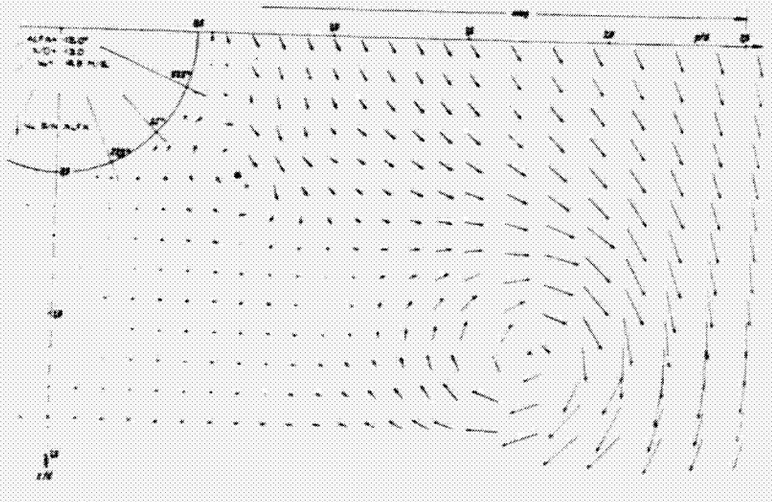

(c) CROSS FLOW VELOCITIES AT THE PLANE X/D = -13, ANGLE OF ATTACK α = -15°, WITH DELTA WING

Fig. 93 Body vortices about θ_c = 18° tangent-ogive cylinder in low-speed turbulent flow at $\bar{x}$ = 0.8 (Grosche 1970).

(a) SIDE ELEVATION, $R_{L_\infty} \sim 10 \times 10^6$, $R_D = 1.3 \times 10^6$

LENGTH, L = 38.2 cm (15 in.); D = 5.0 cm (1.97 in.)

S_1 = PRIMARY SEPARATION OF BOUNDARY LAYER DEVELOPING FROM WINDWARD GENERATOR

S_2 = SECONDARY SEPARATION

A_1 = PRIMARY ATTACHMENT LINE

A_2 = SECONDARY ATTACHMENT

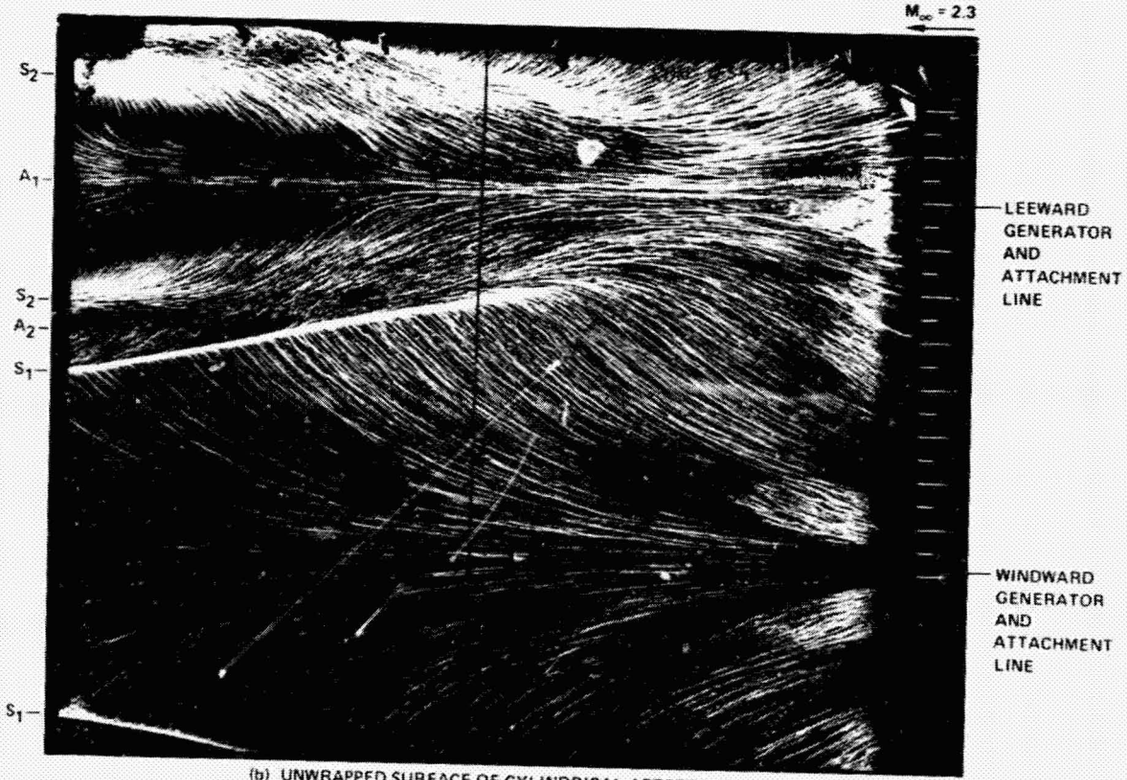

(b) UNWRAPPED SURFACE OF CYLINDRICAL AFTERBODY, $R_{L_\infty} \sim 10 \times 10^6$, $R_D = 1.3 \times 10^6$

Fig. 94 Surface oil flow patterns on $\theta_c = 20°$ blunted cone-cylinder at $\bar{x} = 0.6$, $M_\infty = 2.4$, with turbulent boundary layers (Boersen 1975).

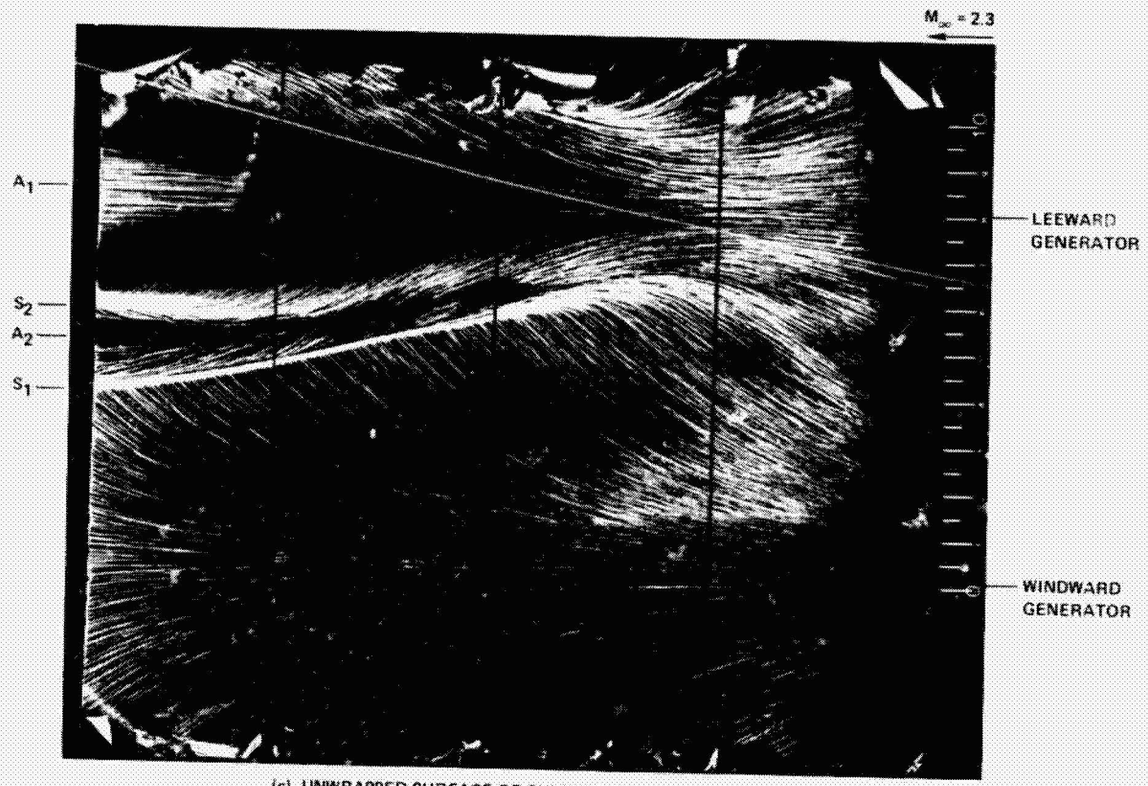

(c) UNWRAPPED SURFACE OF CYLINDRICAL AFTERBODY, $R_{L_\infty} \sim 30 \times 10^6$, $R_D = 4 \times 10^6$

Fig. 94 Concluded.

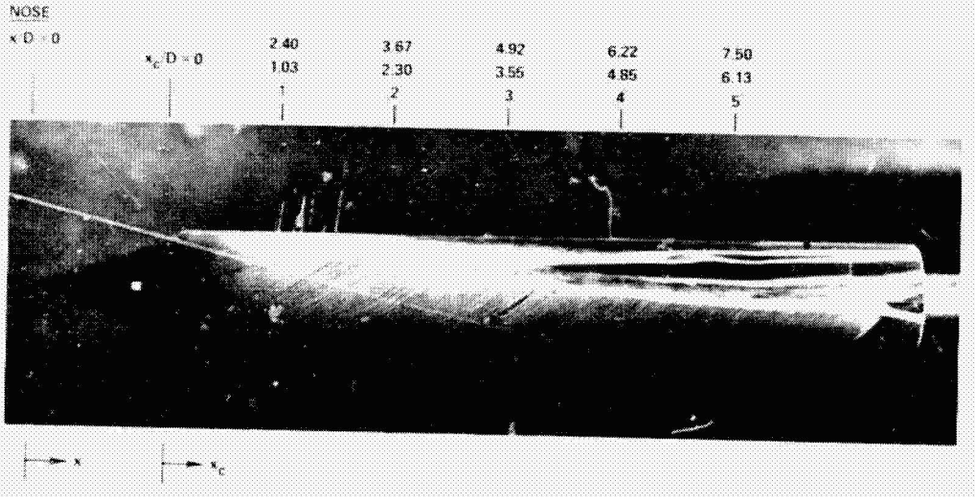

(a) SIDE ELEVATION, $R_{L_\infty} = 32 \times 10^6$ ($R_D = 4 \times 10^6$)

LENGTH, L = 40 cm (15.75 in.), D = 5.0 cm (1.97 in.)

Fig. 95 Surface oil-flow patterns and circumferential pressures on $\theta_c = 20°$ pointed cone-cylinder at $T_\infty = 0.6$, $M_\infty = 2.3$ with turbulent boundary layers (Boersen 1975).

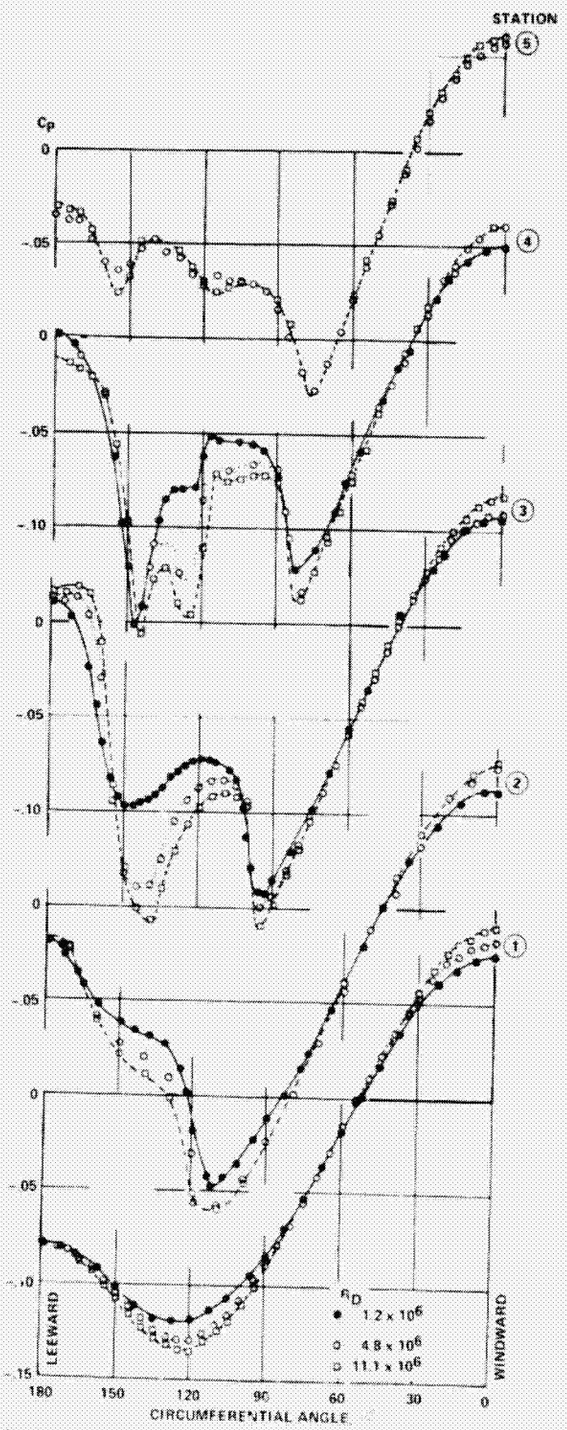

(b) CIRCUMFERENTIAL PRESSURE DISTRIBUTIONS ON AFTERBODY OF CONE CYLINDER

Fig. 95 Continued.

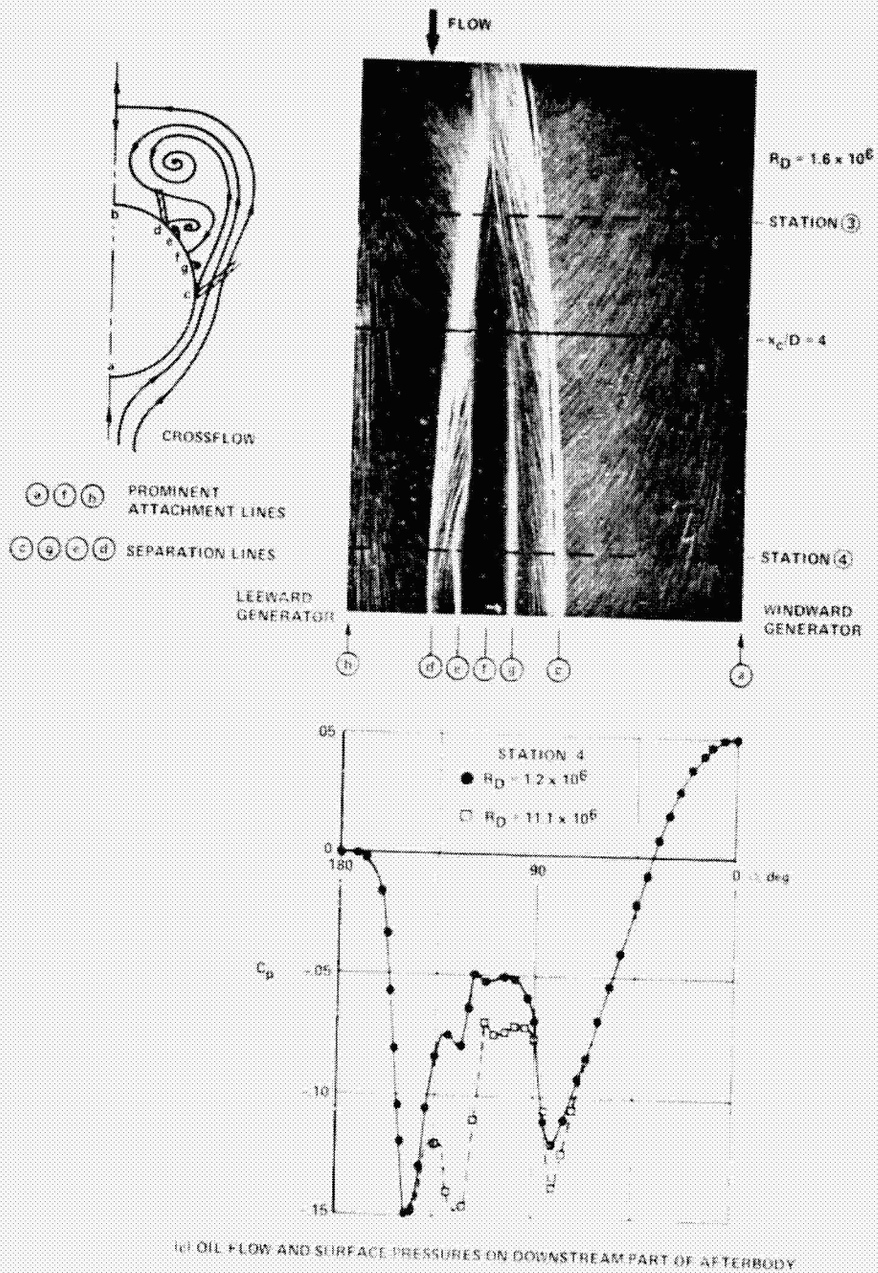

(c) OIL FLOW AND SURFACE PRESSURES ON DOWNSTREAM PART OF AFTERBODY

Fig. 95 Concluded.

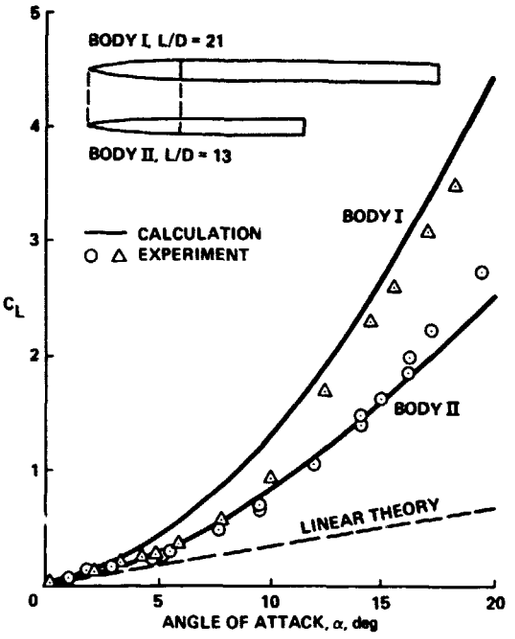

Fig. 96 Overall lift of two bodies of revolution (see Küchemann 1973).

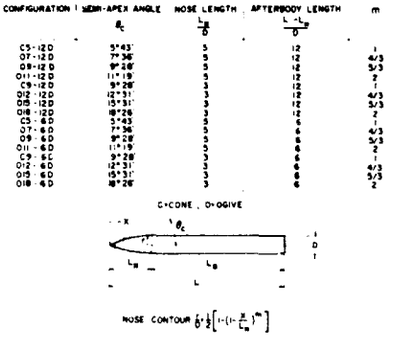

Fig. 97 Details of long, pointed slender bodies (Peake, Rainbird, and Atraghji 1972).

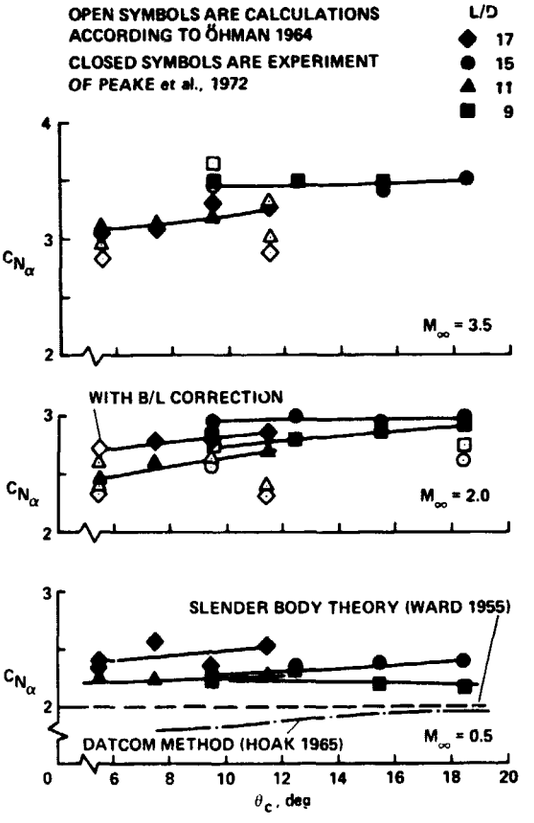

Fig. 98 Low angle-of-attack performance of long, pointed slender bodies in terms of normal force slope vs semi-nose angle at M_∞ = 0.5, 2.0, and 3.5 at R_D = 1 × 10^6 to 4 × 10^6 (Peake, Rainbird, and Atraghji 1972).

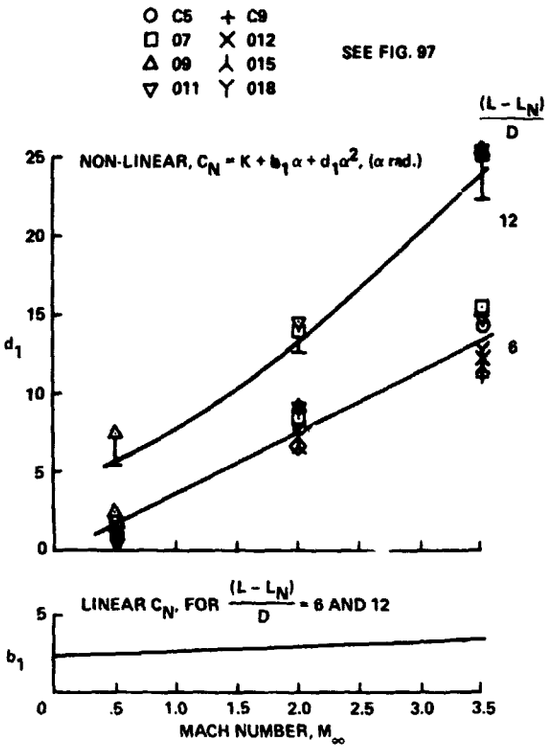

Fig. 99 Linear and nonlinear lift on long, pointed slender bodies at $R_D = 1 \times 10^6$ to 4×10^6 (Peake, Rainbird, and Atraghji 1972).

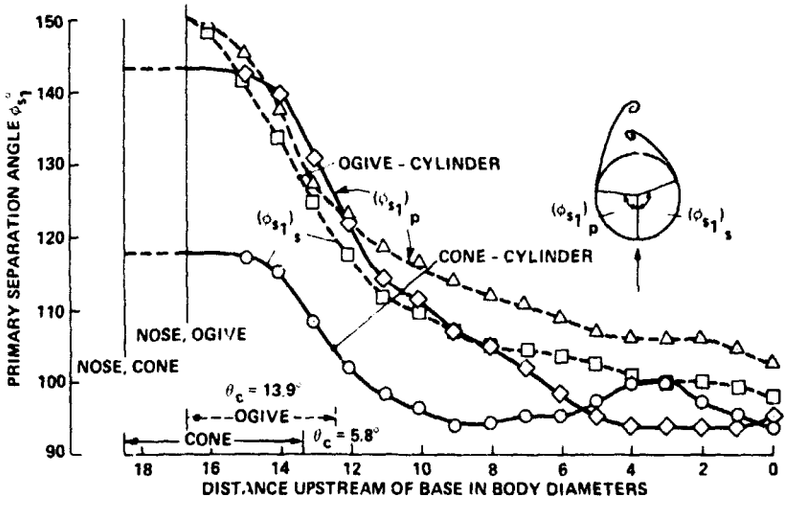

Fig. 100 Asymmetric primary separation on cone and ogive-cylinders, $\alpha = 18°$, $M_\infty = 0.6$, $R_{L_\infty} = 3.5 \times 10^7$ (Rainbird et al. 1966).

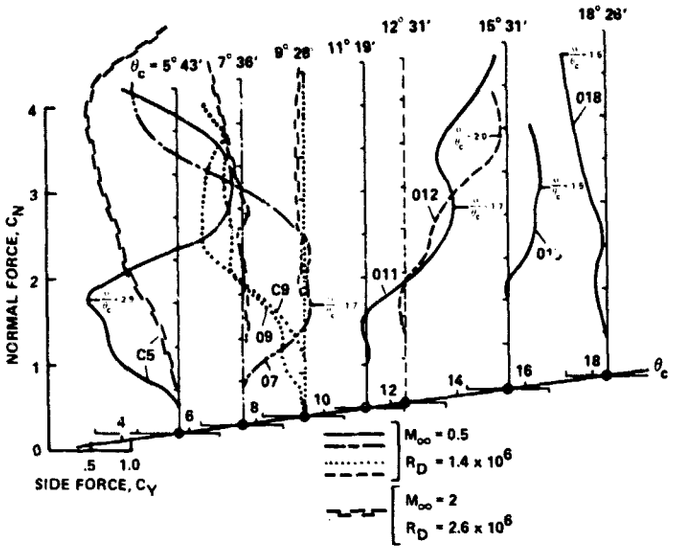

Fig. 101 Influence of semi-nose angle θ_c on side-force-normal-force polar for afterbody length of 12D at $R_D = 1 \times 10^6$ to 4×10^6 (Peake, Rainbird, and Atraghji 1972).

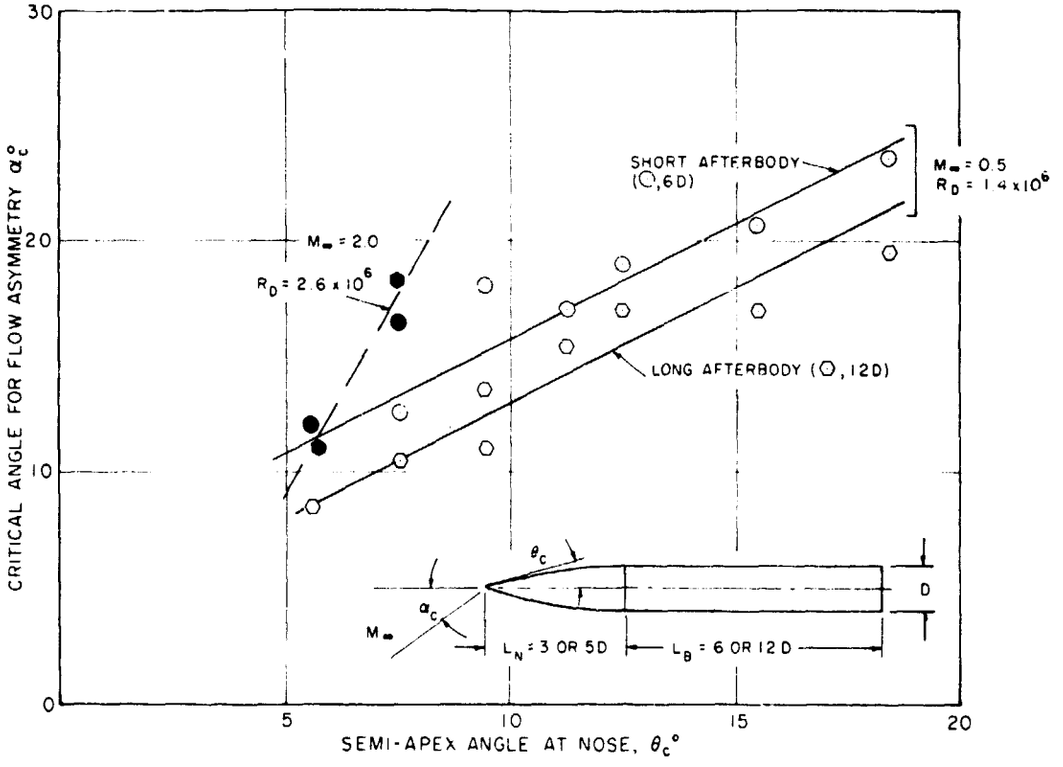

Fig. 102 Critical angle of attack for onset of flow asymmetry (Peake, Rainbird and Atraghji 1972).

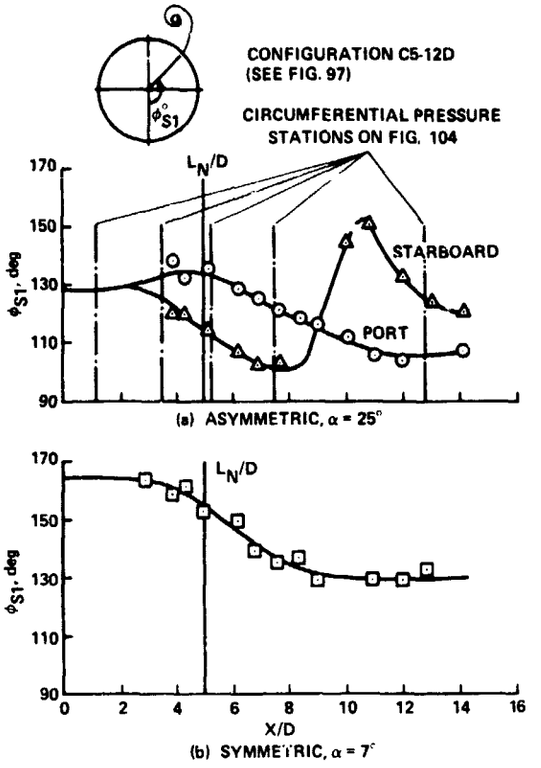

Fig. 103 Asymmetric and symmetric primary separation angles on a 5.7° cone-cylinder at M_∞ = 0.5 and R_D = 1.4 × 10^6 (Peake, Rainbird, and Atrayhji 1972).

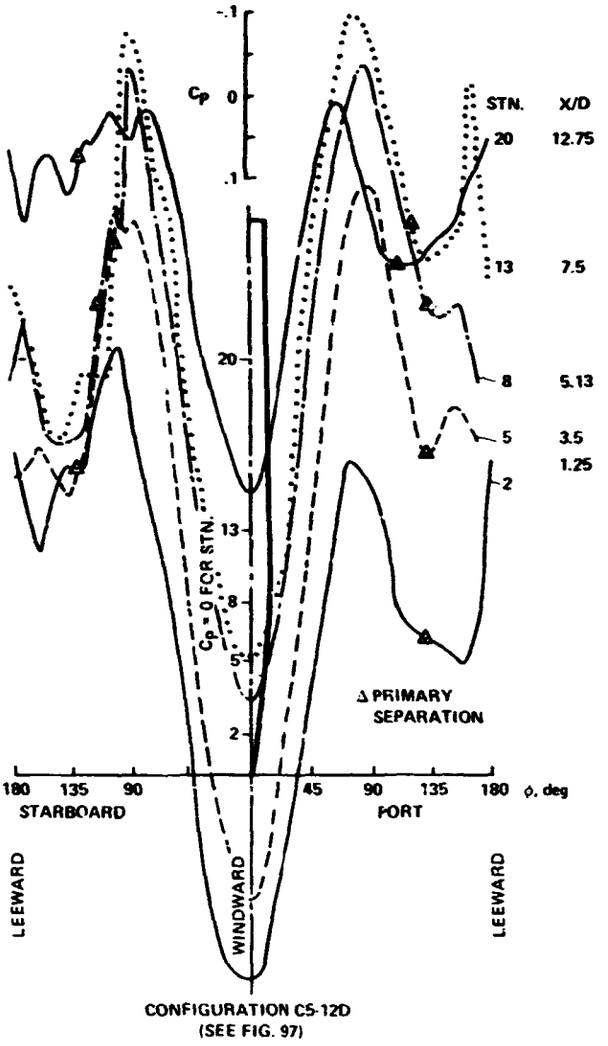

Fig. 104 Circumferential pressures on a 5.7° cone-cylinder at α = 25°, M_∞ = 0.5, and R_D = 1.4 × 10^6 with asymmetric separation line positions.

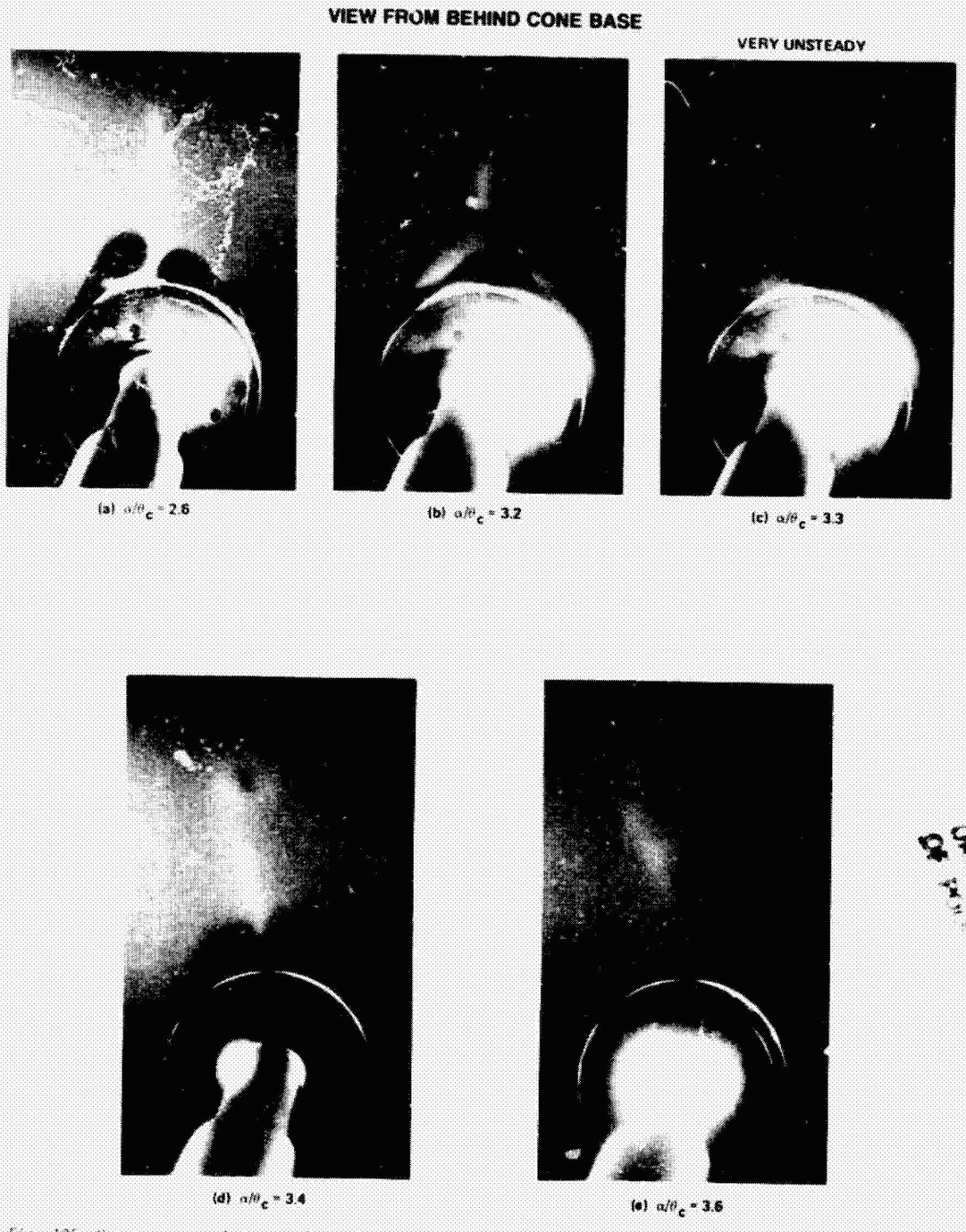

Fig. 105 Vapor-screen pictures of development of asymmetric vortex wake in cross-flow plane about sharp $\theta_c = 5°$ cone, $M_\infty = 0.6$, $R_{L_\infty} = 11 \times 10^6$ (Peake, Owen and Johnson 1980).

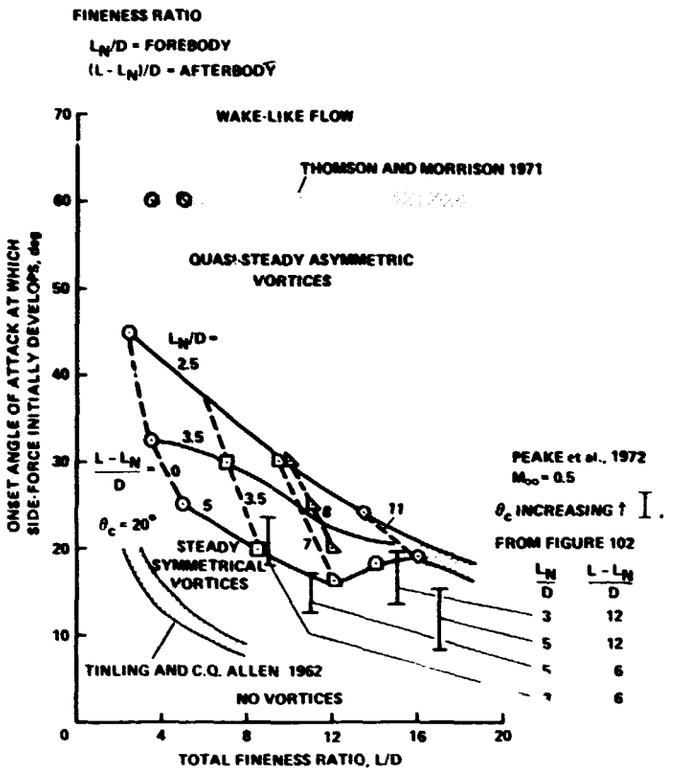

Fig. 106 Boundaries for various types of leeward flow separation about tangent-ogive cylinders, at M_∞ = 0.6 (Keener, G. T. Chapman, and Kruse 1976).

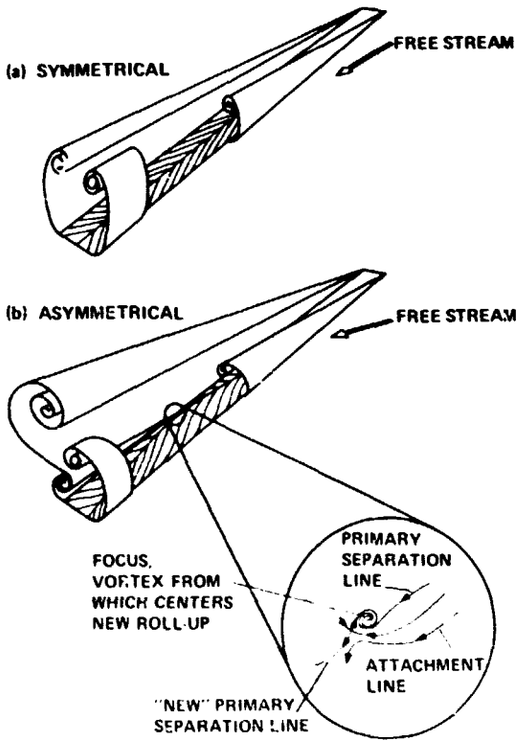

Fig. 107 Development of dividing surface from long, flat plates: after Maltby (see Küchemann 1972).

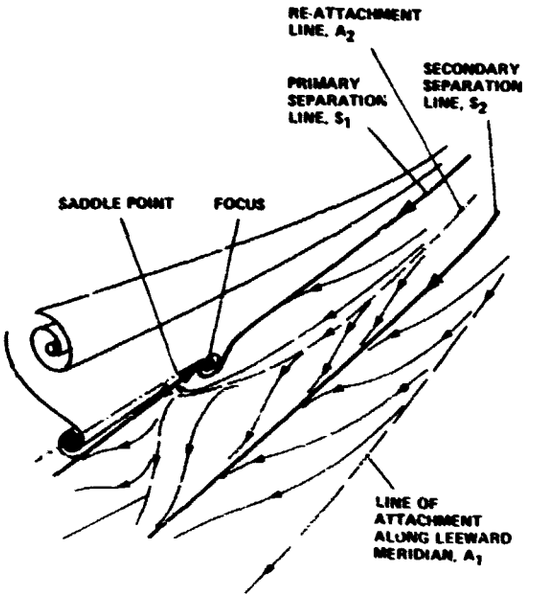

Fig. 108 Postulated development of "double-branching" of primary vortex.

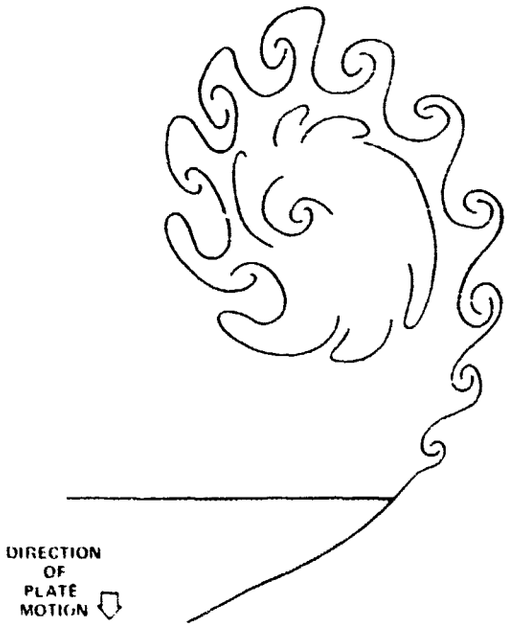

Fig. 109 Dividing surface behind body moving uniformly downwards in still air (Pierce 1961).

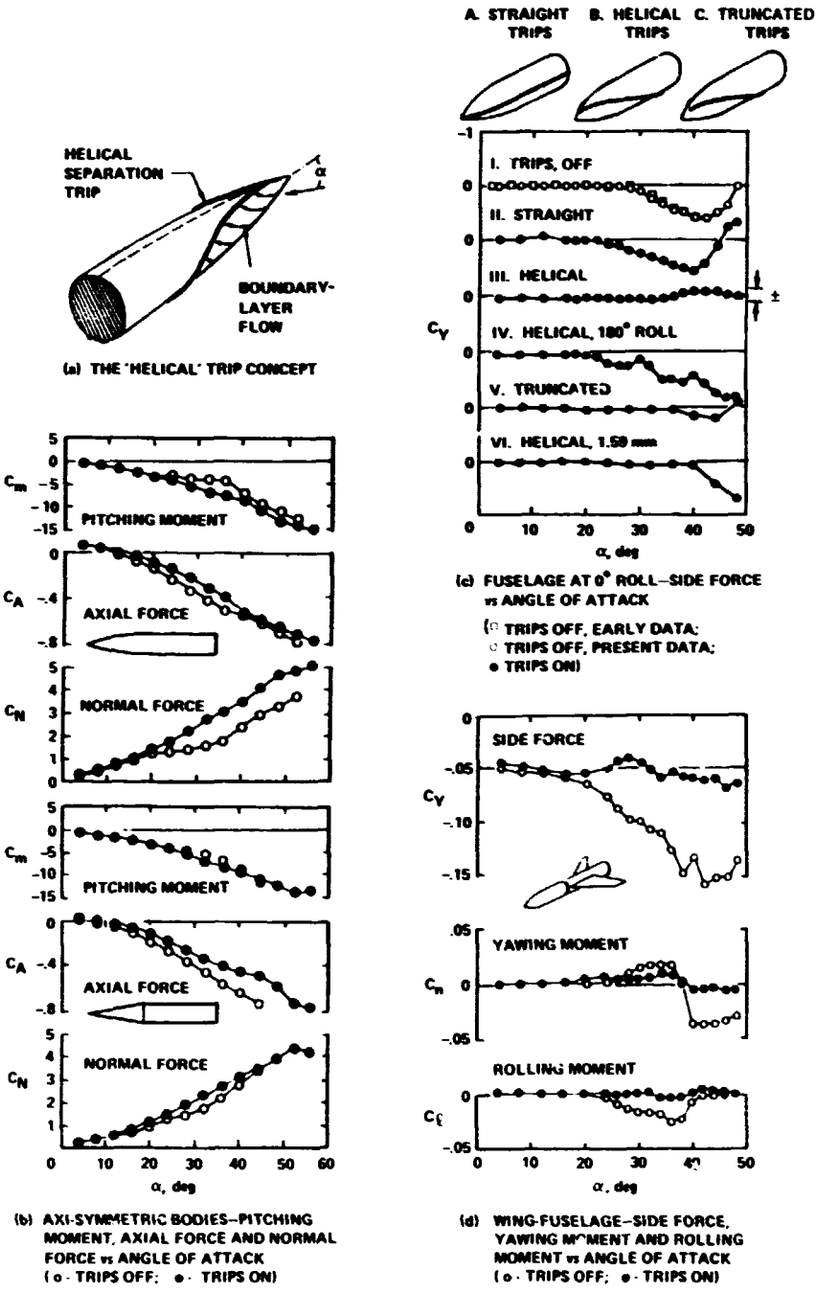

(a) THE 'HELICAL' TRIP CONCEPT

(b) AXI-SYMMETRIC BODIES—PITCHING MOMENT, AXIAL FORCE AND NORMAL FORCE vs ANGLE OF ATTACK (o - TRIPS OFF; ● - TRIPS ON)

(c) FUSELAGE AT 0° ROLL—SIDE FORCE vs ANGLE OF ATTACK

(○ TRIPS OFF, EARLY DATA; ○ TRIPS OFF, PRESENT DATA; ● TRIPS ON)

(d) WING-FUSELAGE—SIDE FORCE, YAWING MOMENT AND ROLLING MOMENT vs ANGLE OF ATTACK (o - TRIPS OFF; ● - TRIPS ON)

Fig. 110 Effectiveness of helical trip in alleviating asymmetrical forces and moments (D. S. Rao 1978).

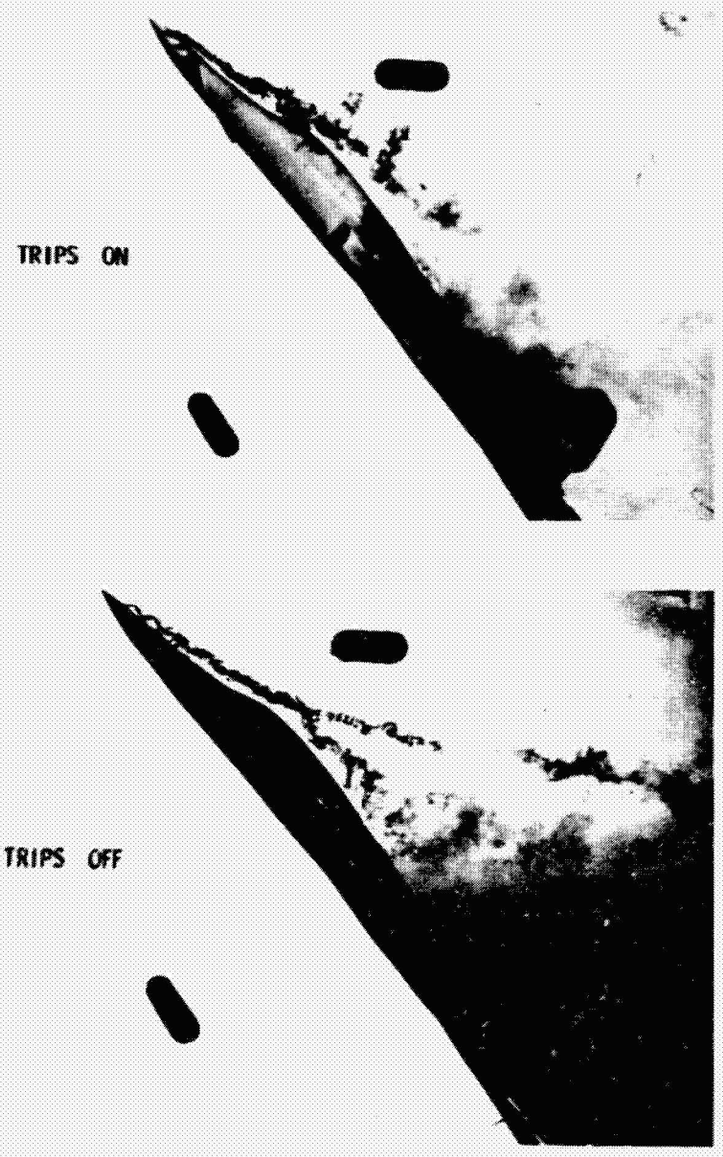

Fig. III Water tunnel flow visualization of effectiveness of helical trip about nose of slender aircraft (Erickson 1979).

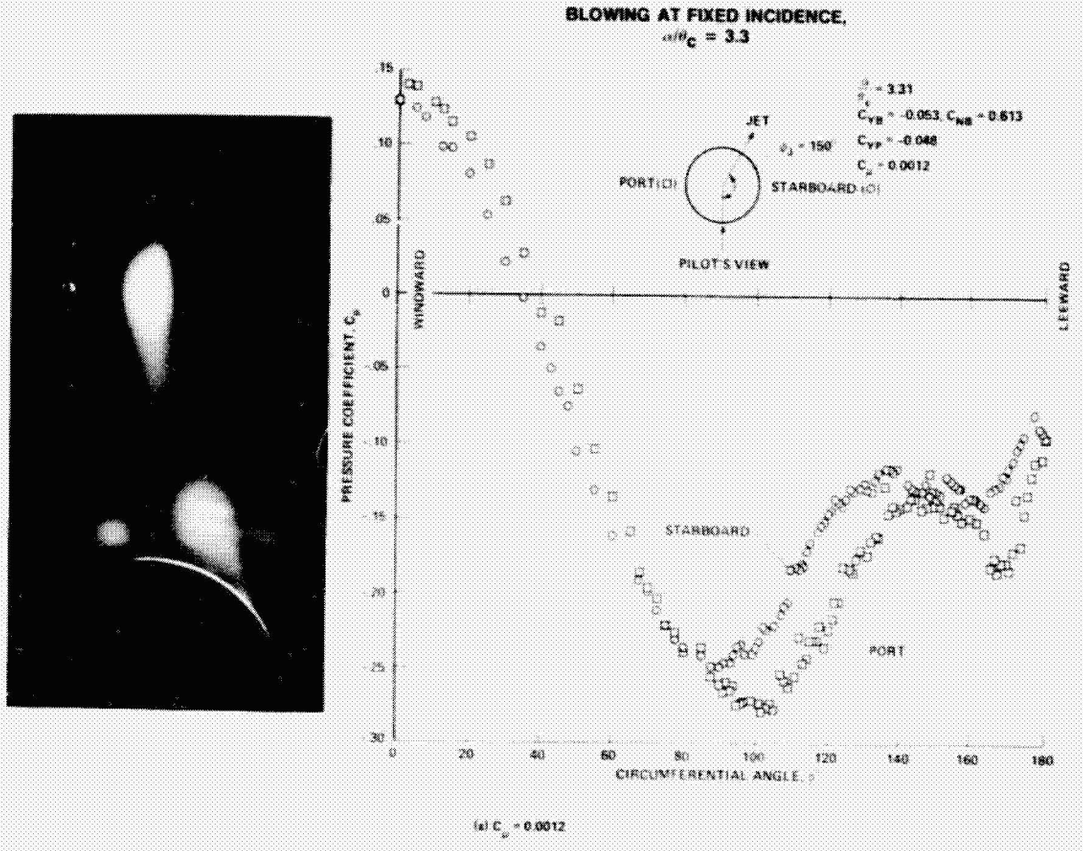

Fig. 112 Control of forebody vortex orientation by novel blowing scheme at $\bar{\alpha}$ = 3.3 on slightly blunted θ_c = 5° cone: M_∞ = 0.6, turbulent boundary layers (Peake and Owen 1979).

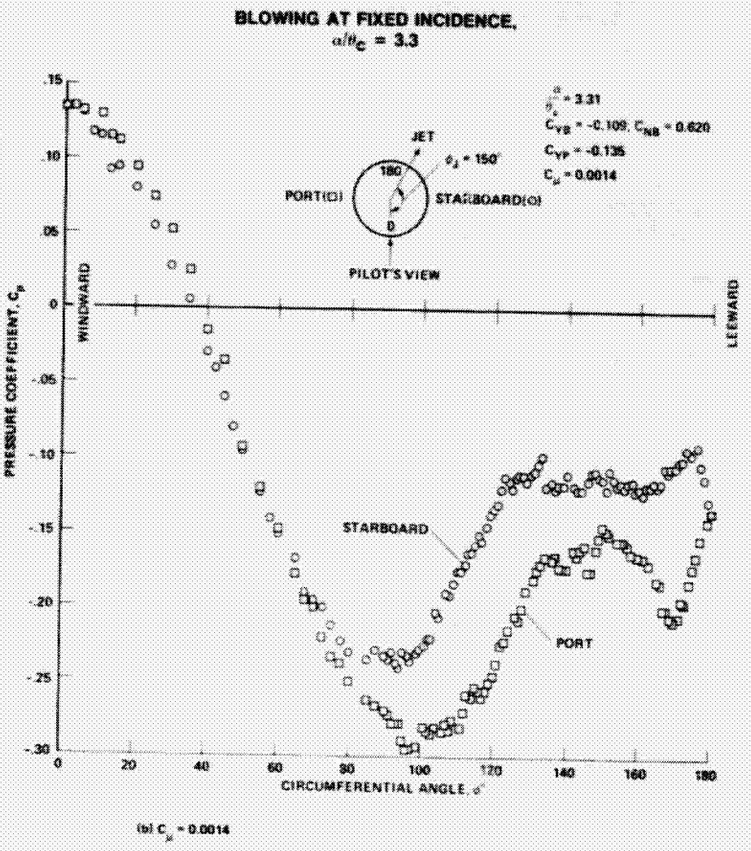

(b) C_μ = 0.0014

Fig. 112 Continued.

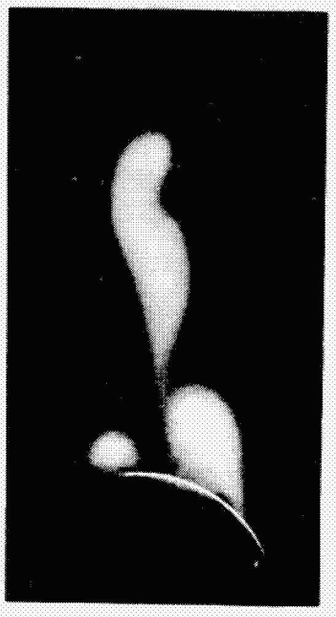

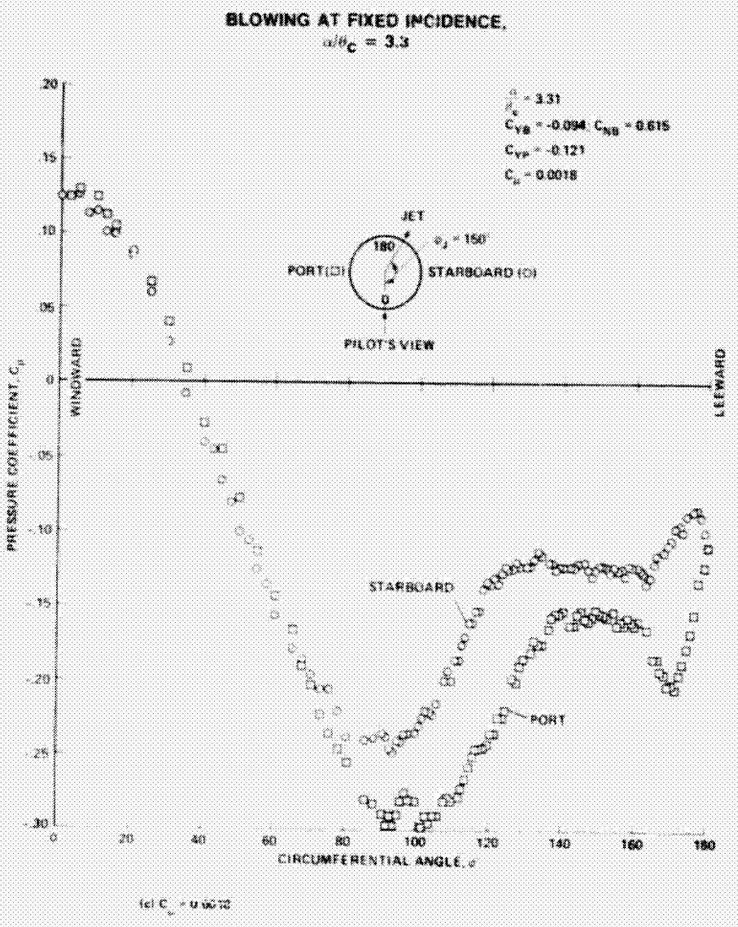

Fig. 112 Continued.

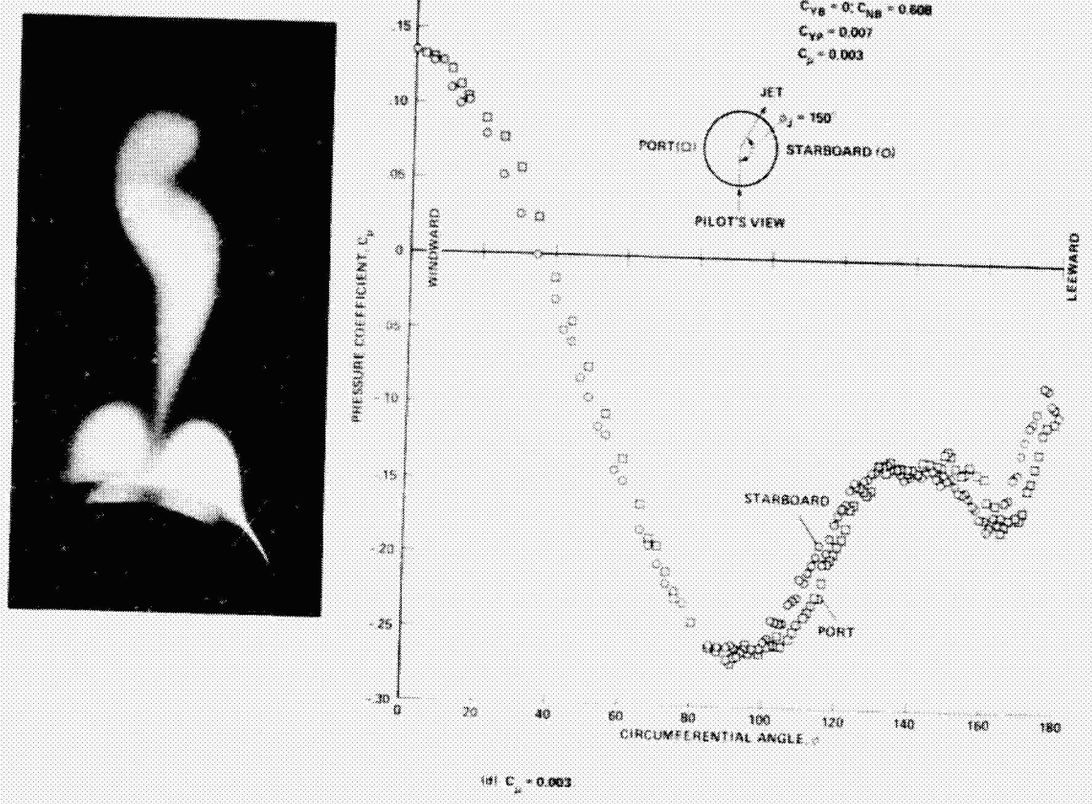

Fig. 112 Continued.

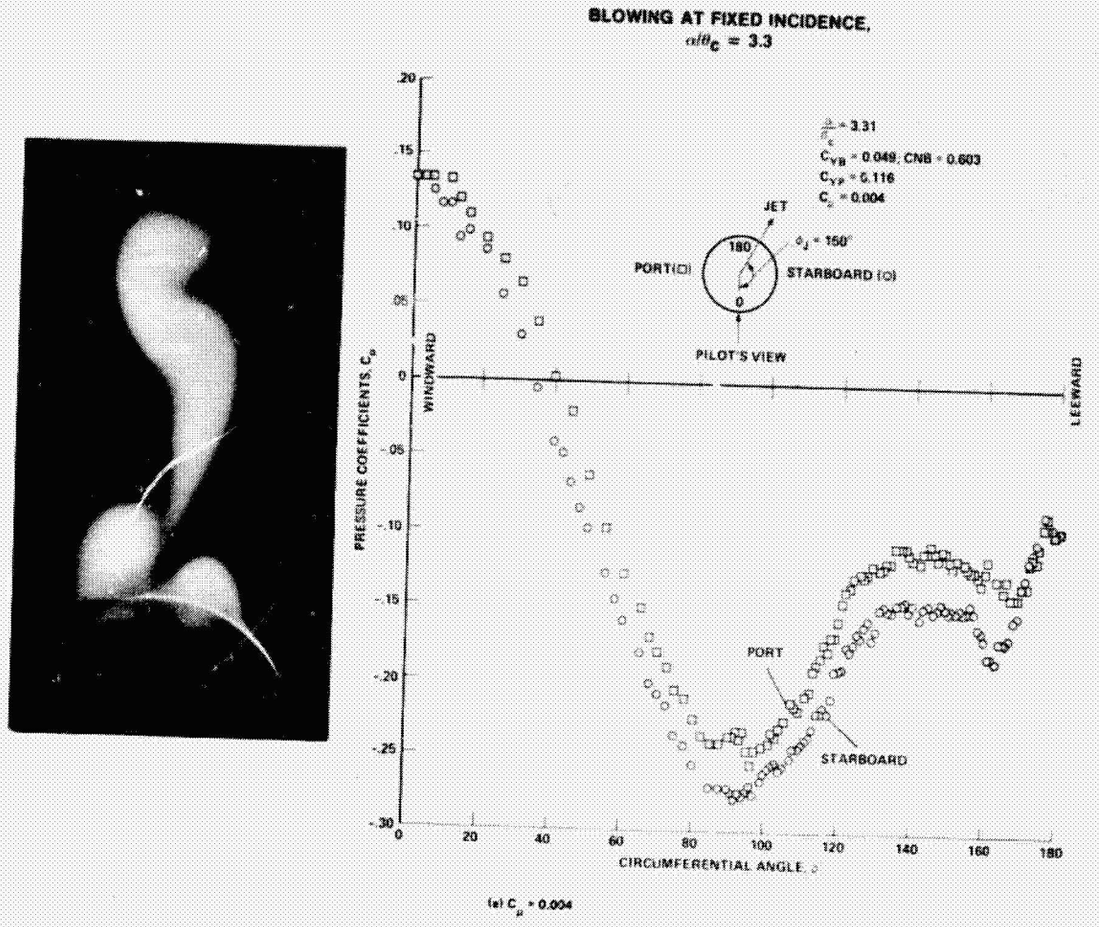

Fig. 112 Continued.

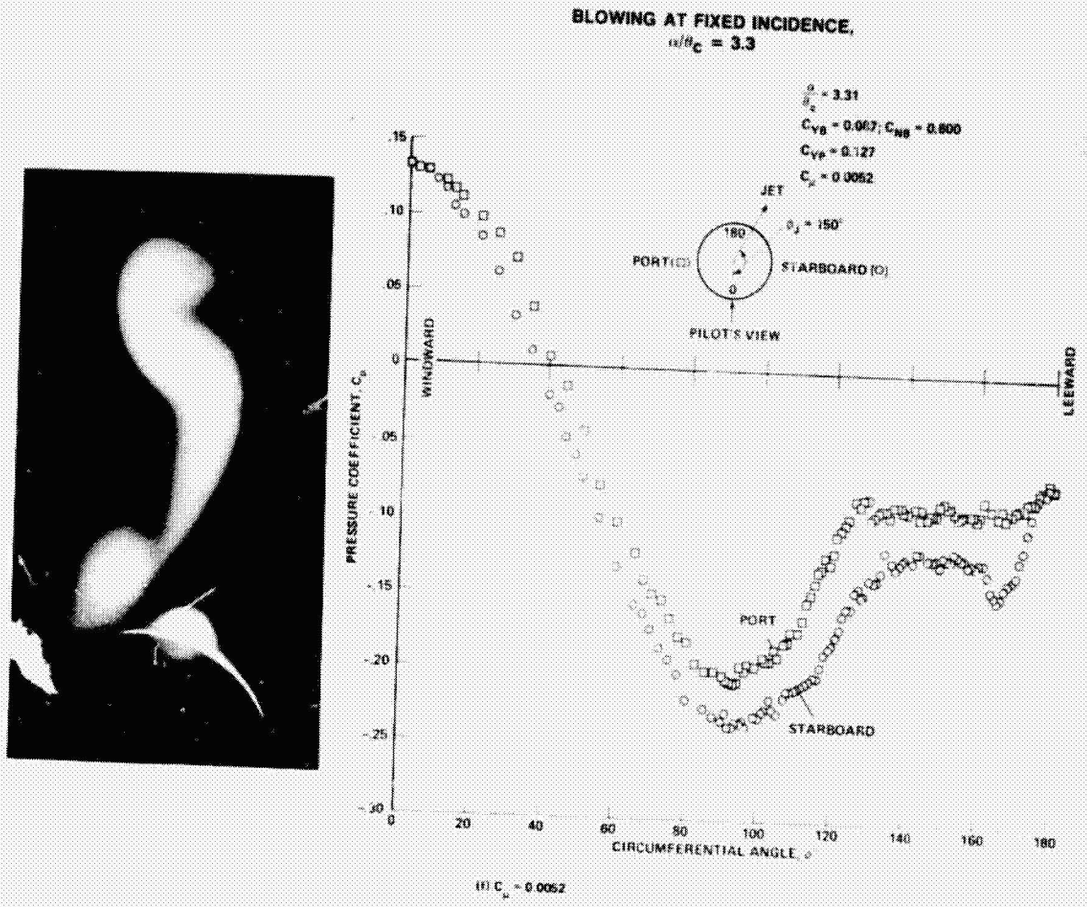

Fig. 112 Continued.

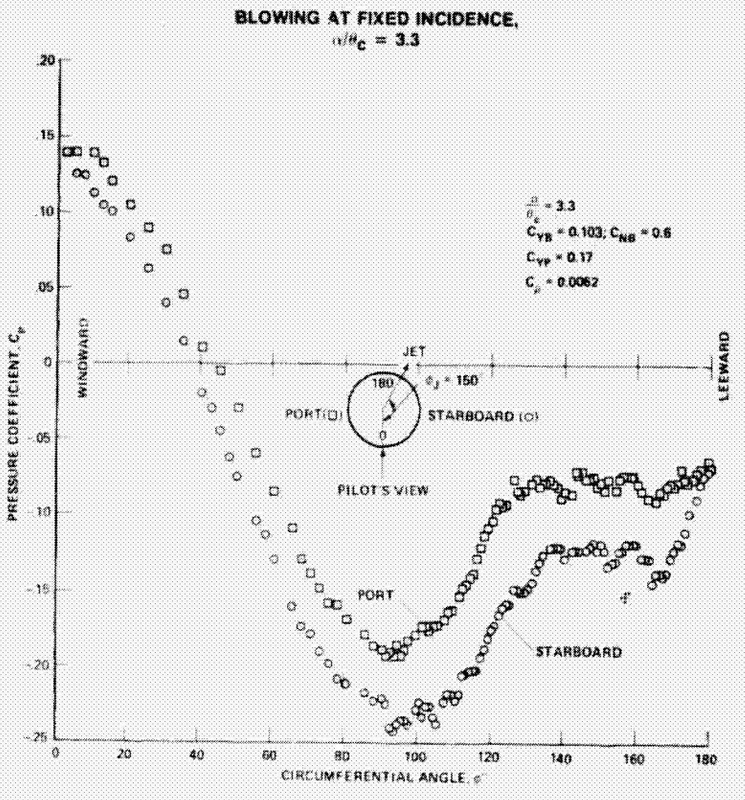

(g) C_{μ} = 0.0062

Fig. 112 Concluded.

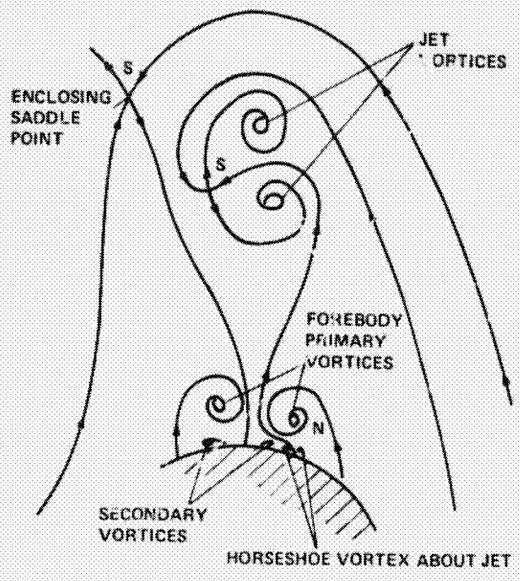

Fig. 113 Postulate of jet and forebody vortices (Peake, Owen, and Johnson 1980).

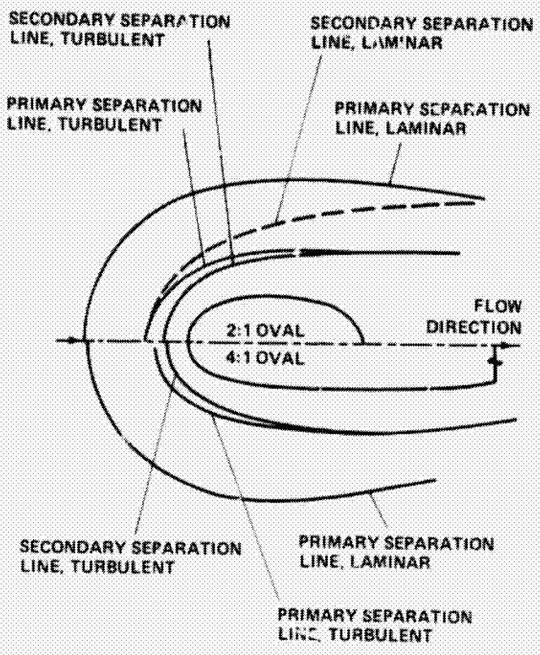

Fig. 115 Comparison between experimental separation line positions in laminar and turbulent flows about 2:1 and 4:1 oval cylinders (Peake, Galway, and Rainbird 1965).

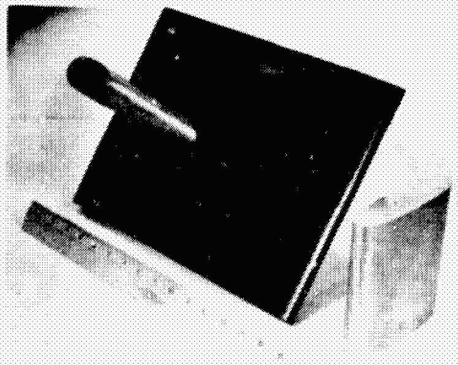

Fig. 114 Oval protuberance/flat plate model used in water-tunnel and wind-tunnel tests (Peake, Galway, and Rainbird 1965).

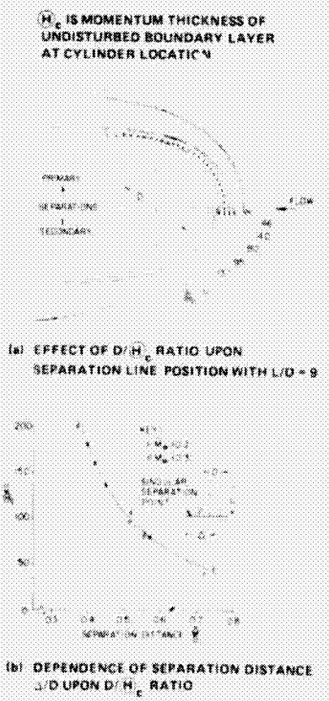

Fig. 116 Separation line positions about circular cylinder protuberances in subsonic flow (Peake, Rainbird, and Atraghji 1972).

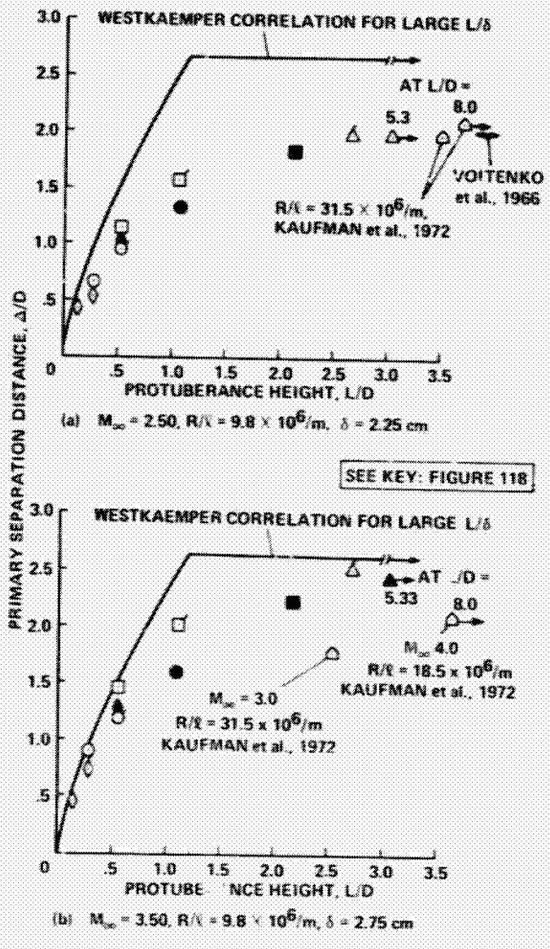

Fig. 117 Separation line positions about circular cylinder protuberances in supersonic flow (Sedney and Kitchens 1975).

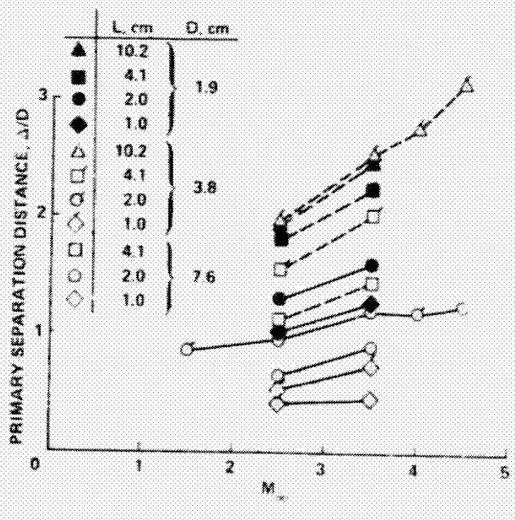

Fig. 118 Influence of Mach number on distance of primary separation from cylinder protuberance (Sedney and Kitchens 1975).

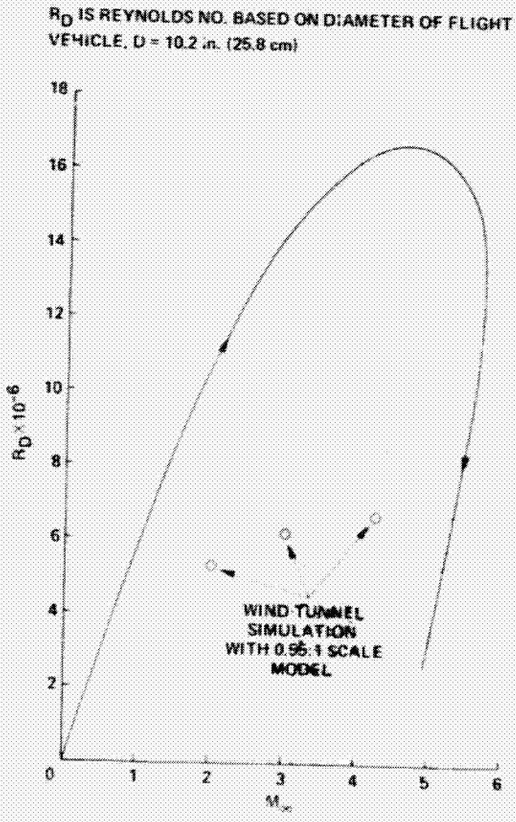

Fig. 119 Reynolds number-Mach number trajectory for flight of rocket with protuberance (Meyer 1968).

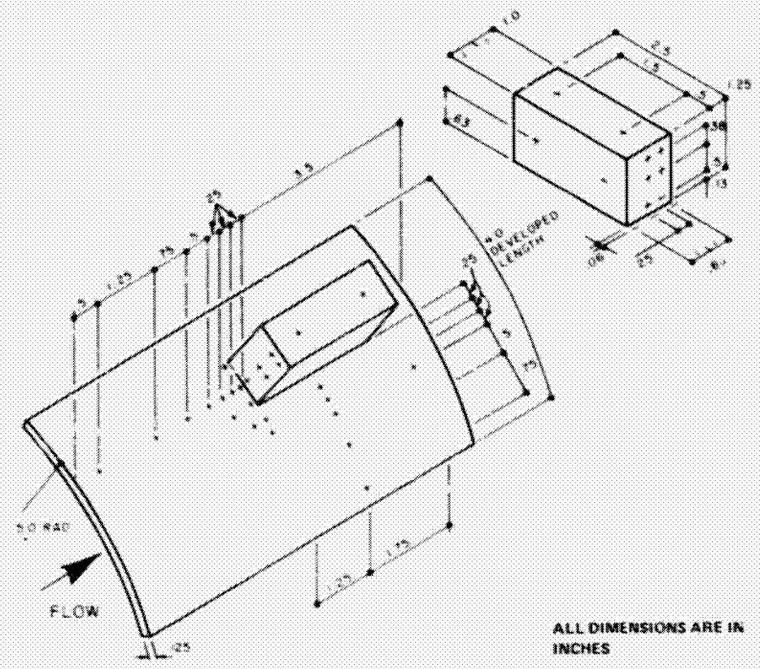

(a) THERMOCOUPLES ON PROTUBERANCE PANEL OF ROCKET FLIGHT VEHICLE

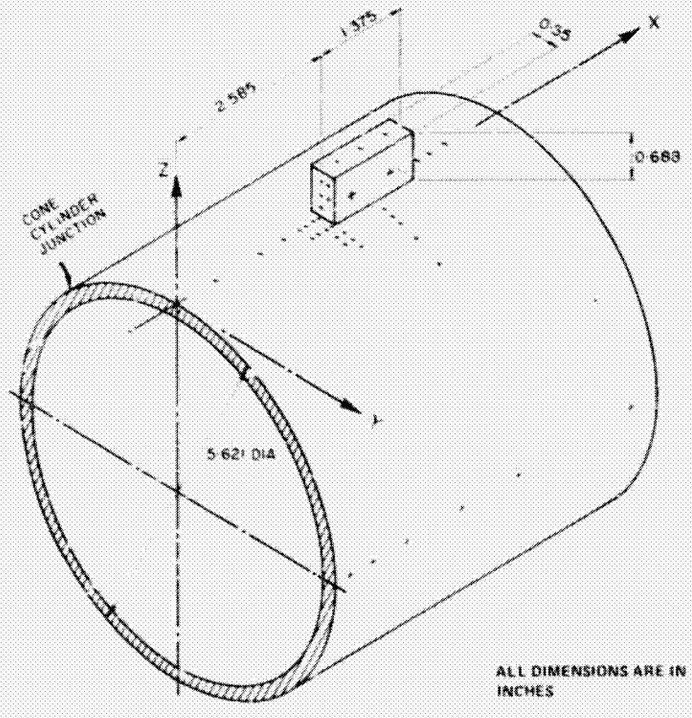

(b) PRESSURE ORIFICES ON WIND-TUNNEL MODEL OF ROCKET AND PROTUBERANCE

Fig. 120 Instrumentation on rocket flight vehicle and 0.55:1 scale wind-tunnel model (Meyer 1968).

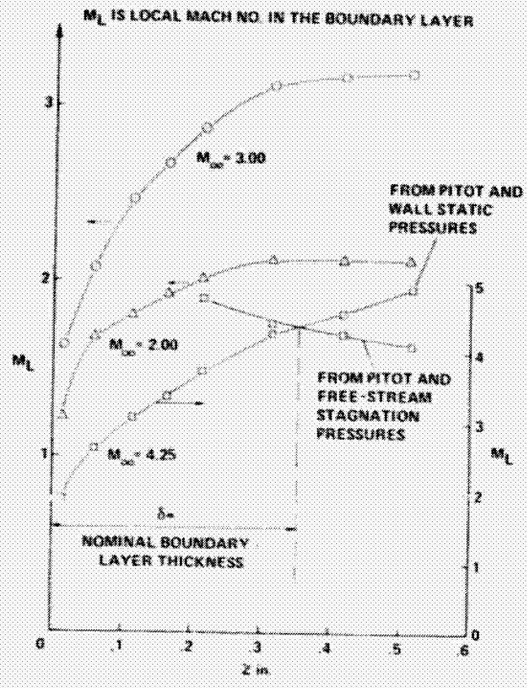

Fig. 121 Boundary-layer Mach number distributions on wind-tunnel model for M_∞ = 2.0, 3.0, and 4.25 (Meyer 1968).

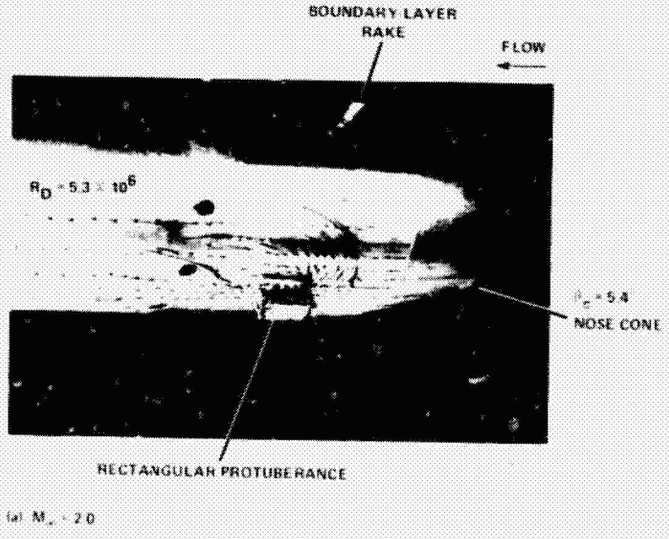

(a) M_∞ = 2.0

Fig. 122 Oil-flow patterns on rocket and protuberance in wind tunnel (Meyer 1968).

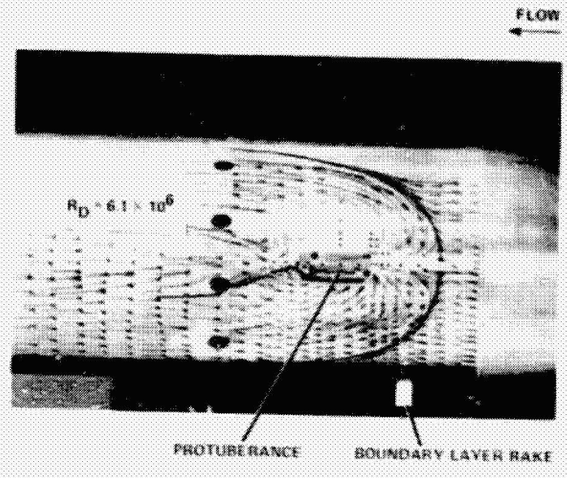

(b) $M_\infty = 3.0$

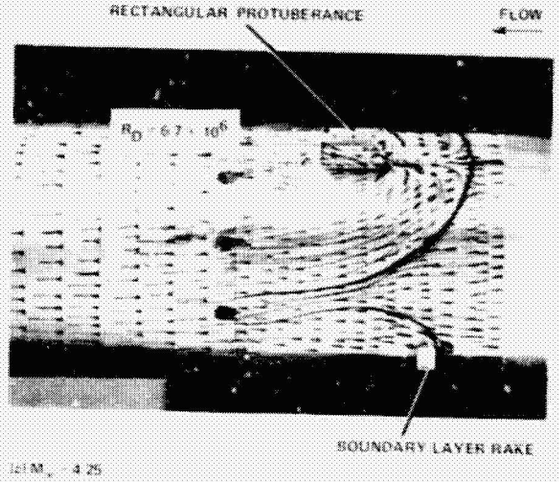

(c) $M_\infty = 4.25$

Fig. 122 Concluded.

$$\Sigma_N - (\Sigma_S + \frac{1}{2}\Sigma_{S'}) = 5 - (0 + \frac{10}{2}) = 0$$ (RULE 4, SECTION 2.7)

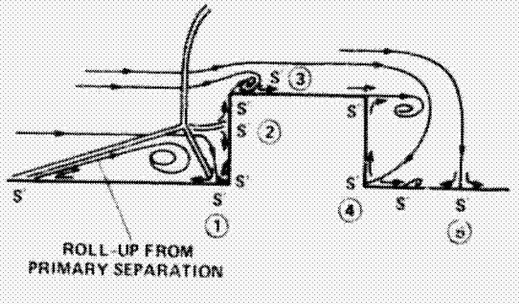

① – ⑤ ARE REATTACHMENT POINTS

Fig. 123 Conjectured flow pattern in plane of symmetry of rectangular protuberance.

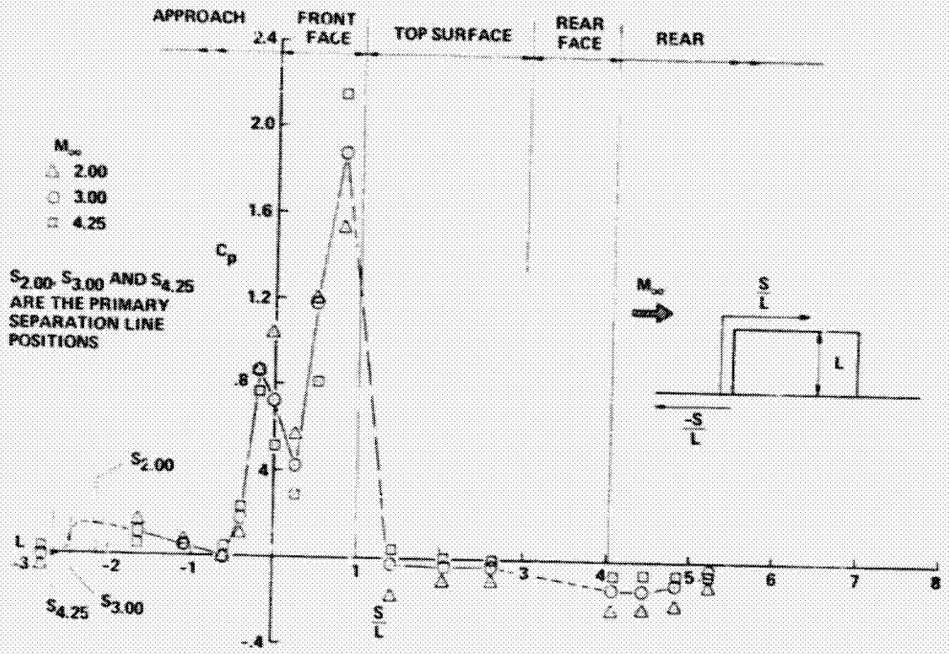

Fig. 124 Distribution of pressure coefficient along centerline of protuberance on wind-tunnel model (Meyer 1968).

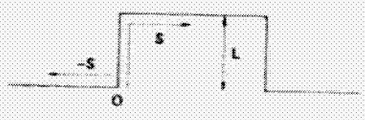

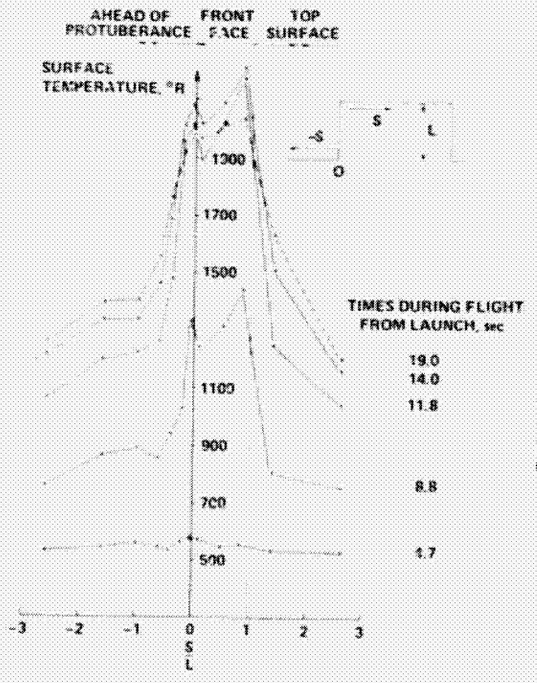

Fig. 125 Temperature distribution along protuberance centerline at several times during flight trajectory (Meyer 1968).

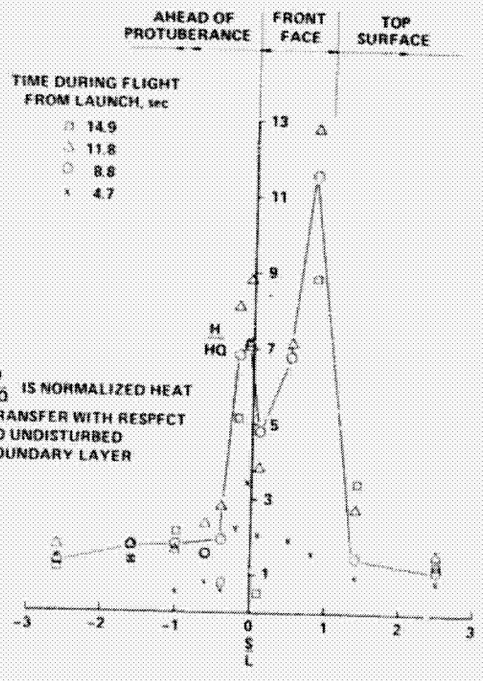

Fig. 126 Normalized heat transfer along protuberance centerline at several instants during flight trajectory (Meyer 1968).

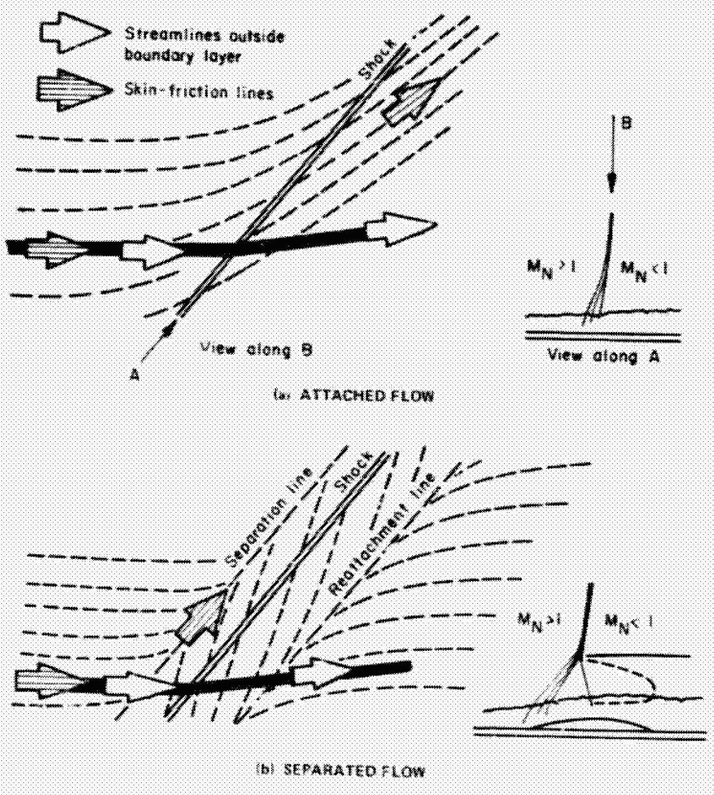

Fig. 127 Schematic diagram of skin-friction line patterns beneath swept shocks (Green 1970).

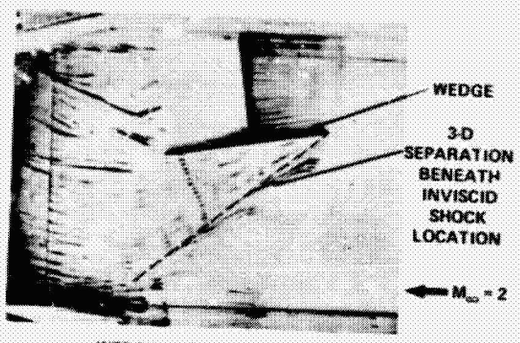

WEDGE INCLINATION TO FLOW $\theta = 10°$,
$\left[\frac{P_{WALL}}{P_\infty}\right]_{INVISCID} = 1.71$, $Re_{\theta_{BL}} = 14{,}000$

(a) $M_\infty = 2$

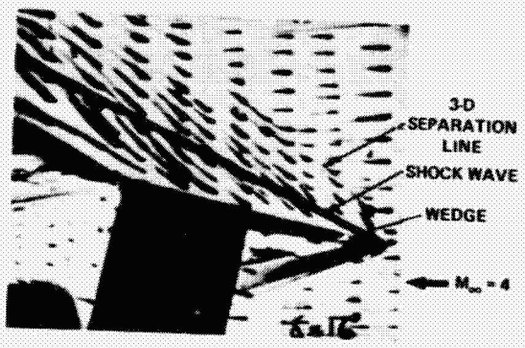

WEDGE INCLINATION TO FLOW $\theta = 16°$
$\left[\frac{P_{WALL}}{P_\infty}\right]_{INVISCID} = 3.97$, $Re_{\theta_{BL}} = 25{,}000$

(b) COMBINED SCHLIEREN/OIL DOT PHOTOGRAPH SHOWING LARGE "UPSTREAM INFLUENCE" AT $M_\infty = 4$

Fig. 128 Experimental skin-friction line patterns in turbulent boundary-layer-swept-shock interactions (Peake, Jones, and Rainbird 1970).

h_p = HEAT-TRANSFER COEFFICIENT AT HIGHER PEAK
h_o = HEAT-TRANSFER COEFFICIENT IN UNDISTURBED BOUNDARY LAYER
ℓ_o = DISTANCE FROM L. E. OF PLATE TO L. E. OF WEDGE
x_p = DISTANCE FROM WEDGE L. E. TO HIGHER PEAK
δ_o = UNDISTURBED BOUNDARY-LAYER THICKNESS
θ = WEDGE DEFLECTION ANGLE

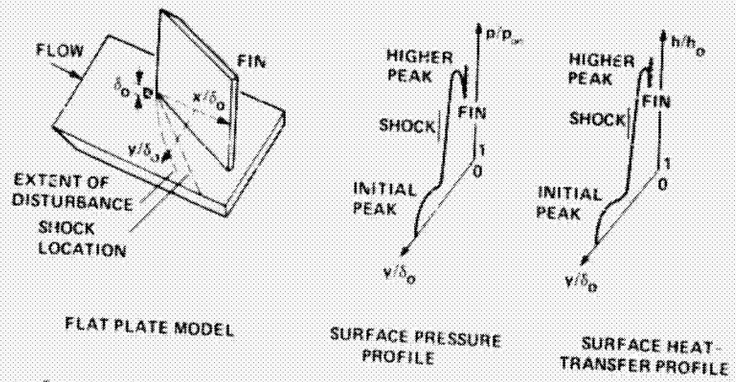

FLAT PLATE MODEL | SURFACE PRESSURE PROFILE | SURFACE HEAT-TRANSFER PROFILE

Fig. 129 Typical surface heating and surface pressure profiles normalized with respect to undisturbed values in corner with one surface deflected (Scuderi 1978).

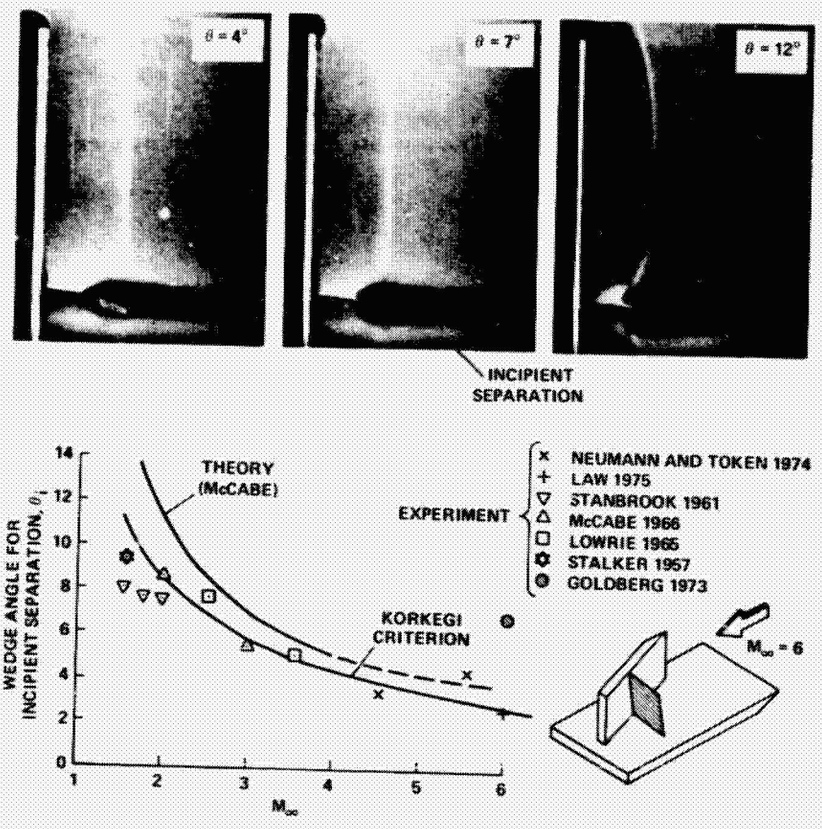

Fig. 130 Incipient separation in glancing shock interaction (D. S. Rao 1978: personal communication).

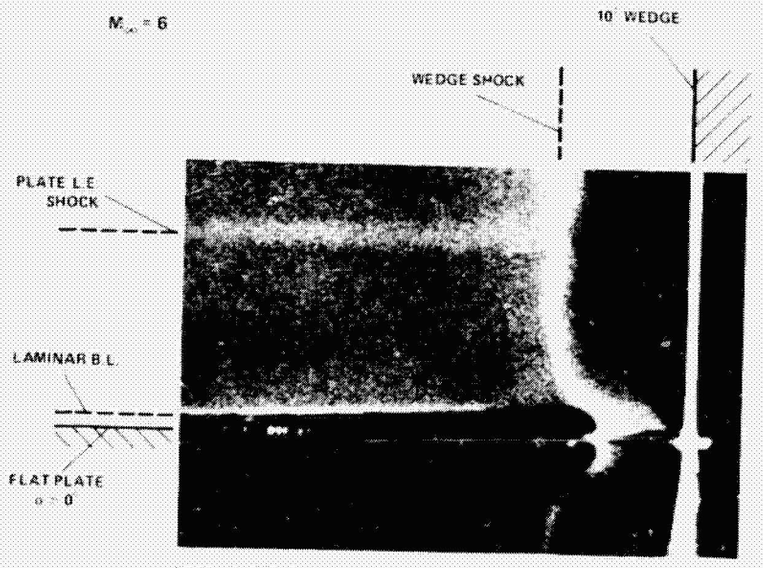

Fig. 131 Coiled free shear layer development from 3D separation line in swept-shock-boundary-layer interaction: vapor screen in plane perpendicular to free stream (D. S. Rao 1978: personal communication).

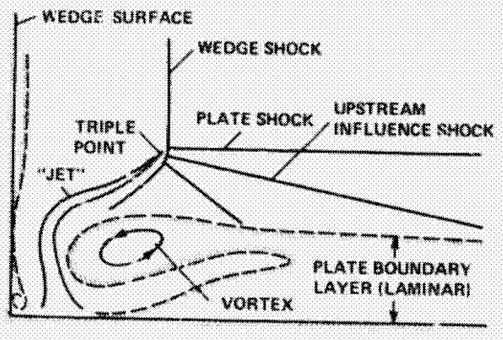

Fig. 132 Schematic representation of model of cross-flow in swept-shock laminar boundary-layer interaction in Figs. 130 and 131 (D. S. Rao 1978: personal communication).

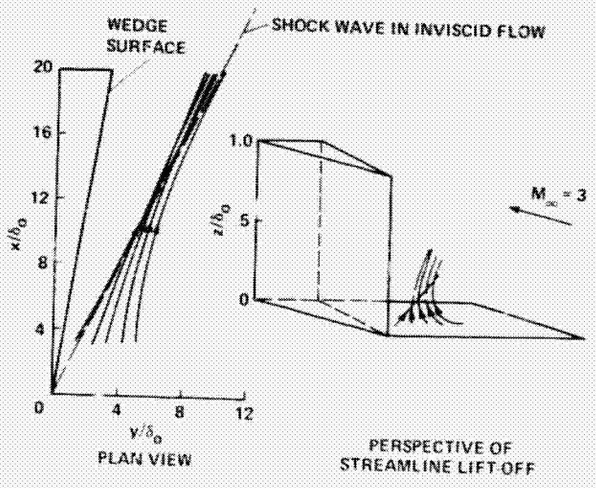

Fig. 133 Streamline merging and lift-off at 3D separation in $\theta = 10°$ wedge-angle flow of Oskam (1976) (Horstman and Hung 1979).

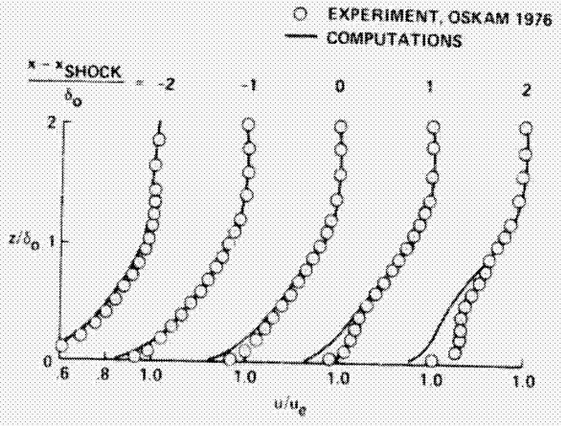

Fig. 134 Comparison of computed and Oskam's measured streamwise velocity profiles, $M_\infty = 3$, $\theta = 10°$, $y/\delta_o = 8$ (Horstman and Hung 1979).

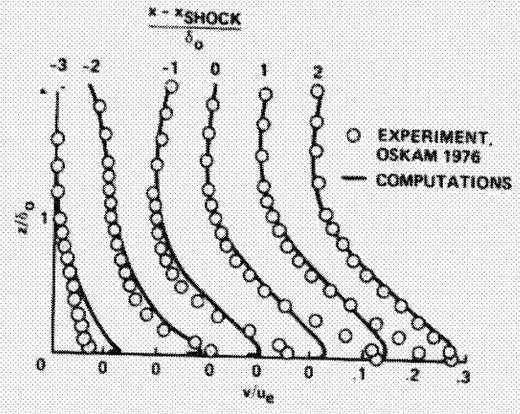

Fig. 135 Comparison of computed and Oskam's measured crossflow velocity profiles, $M_\infty = 3$, $\theta = 10°$, $y/\delta_0 = 8$ (Horstman and Hung 1979).

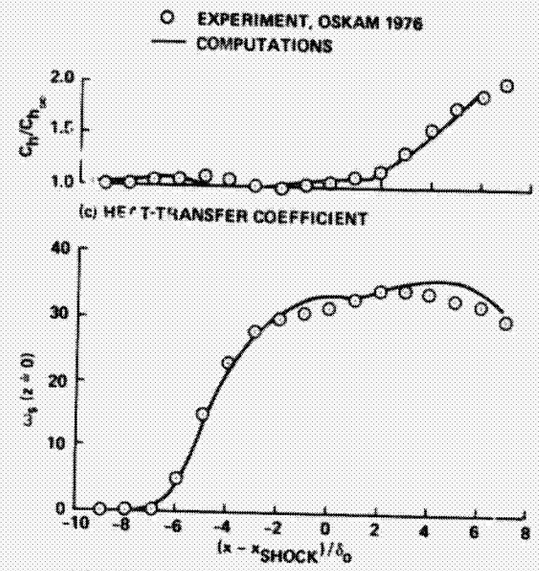

Fig. 136 Concluded.

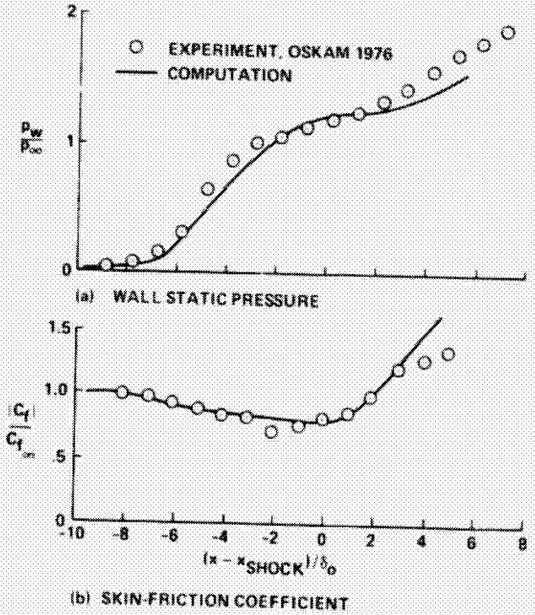

Fig. 136 Comparison of computations with Oskam's data in streamwise direction: $M_\infty = 3$, $\theta = 10°$, $y/\delta_0 = 8$ (Horstman and Hung 1979).

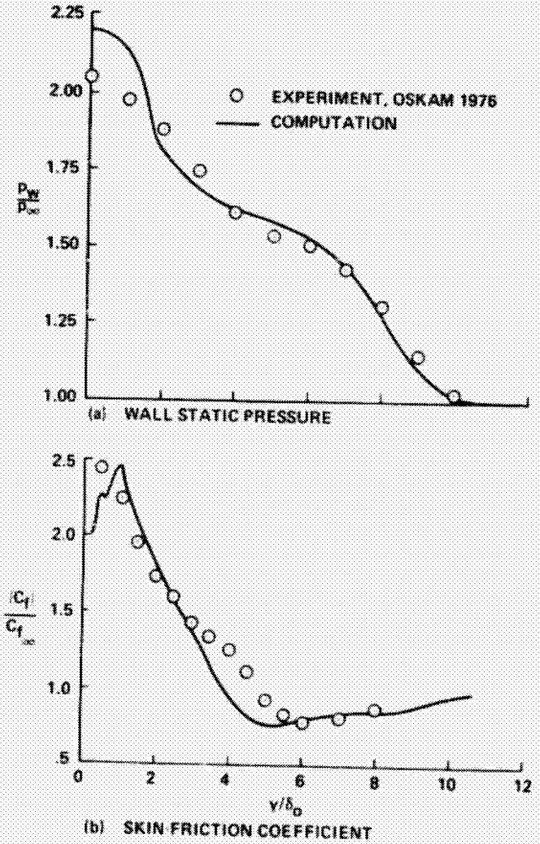

Fig. 137 Comparison of computations with Oskam's data in crossflow sense: $M_\infty = 3$, $\theta = 10°$, $x/\delta_0 = 15$ (Horstman and Hung 1979).

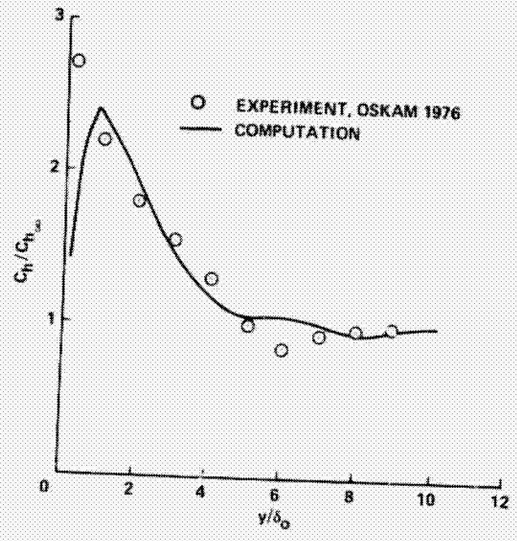

(c) HEAT-TRANSFER COEFFICIENT

Fig. 137 Concluded.

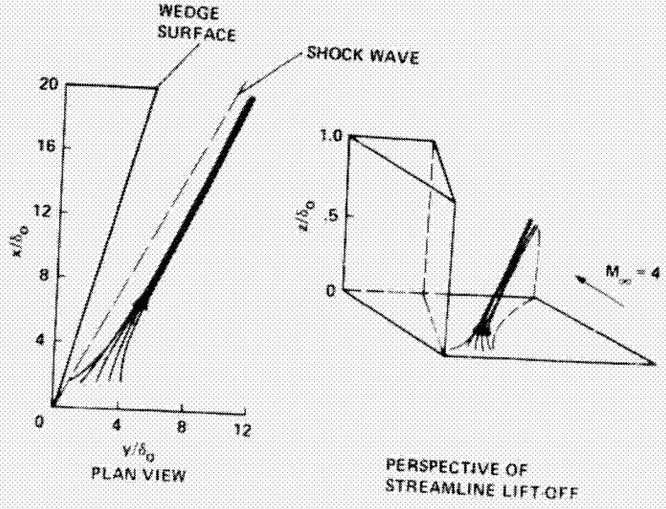

Fig. 138 Streamline convergence and lift-off at 3D separation in ϕ = 16° wedge-angle flow of Peake (1975) (Horstman and Hung 1979).

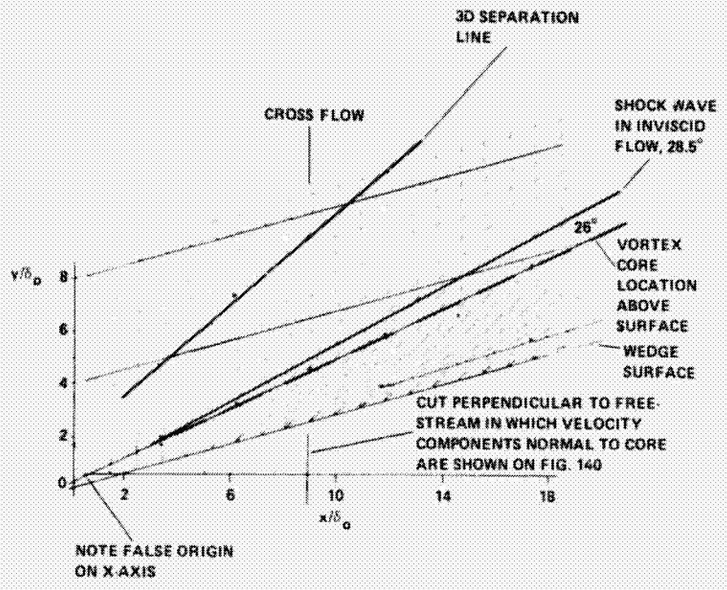

Fig. 139 Computed velocity vectors very close to surface at $z/\delta_0 = 0.0003$, $M_\infty = 4$, $\theta = 16°$ wedge-angle flow of Peake (1975) (Horstman and Hung 1979).

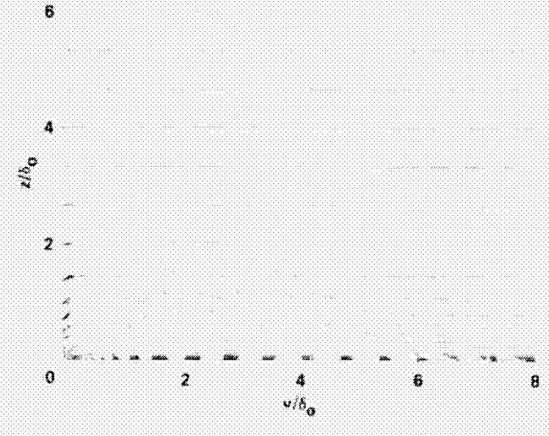

NOTE: (i) SEPARATION LINE POSITION IS AT $y/\delta_0 = 9.7$
(ii) PLANE AT $x/\delta_0 = 9$ IS PERPENDICULAR TO FREE STREAM

Fig. 140 Computed velocity vectors normal to direction of vortex core at $x/\delta_0 = 9$, $\theta = 16°$ wedge-angle flow of Peake (1975), $M_\infty = 4$.

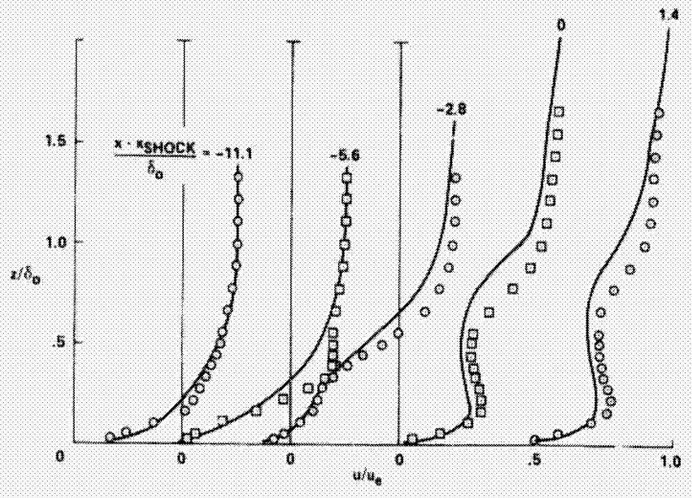

Fig. 141 Comparison between computed and Peake's measured streamwise velocity profiles in strong interaction: $M_\infty = 4$, $\theta = 16°$, $y/\delta_0 = 5$ (Horstman and Hung 1979).

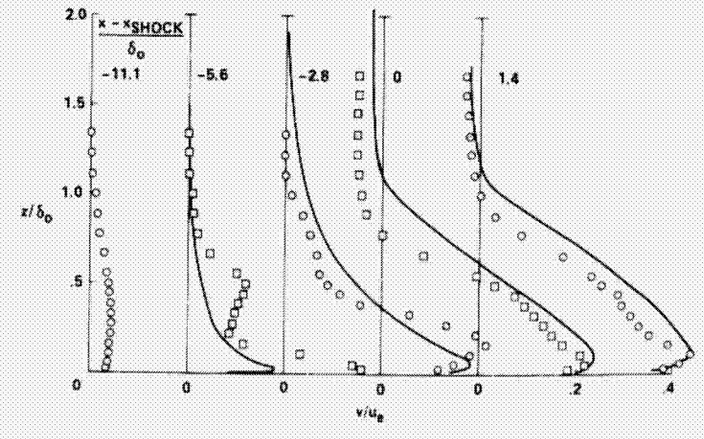

Fig. 142 Comparison between computed and Peake's measured streamwise velocity profiles in strong interaction: $M_\infty = 4$, $\theta = 16°$, $y/\delta_0 = 5$ (Horstman and Hung 1979).

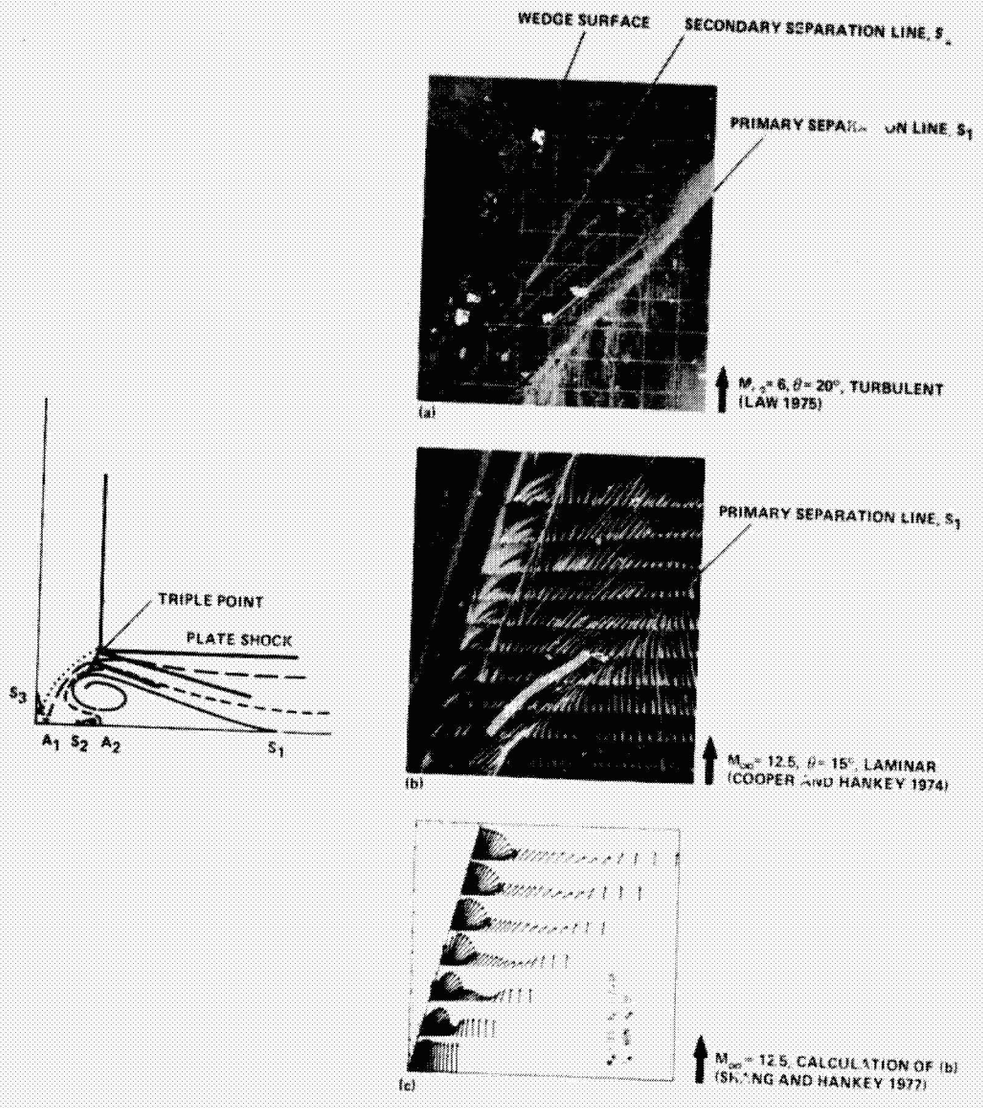

Fig. 143 Skin-friction line patterns in quasi-conical skewed shock interactions with secondary separations.

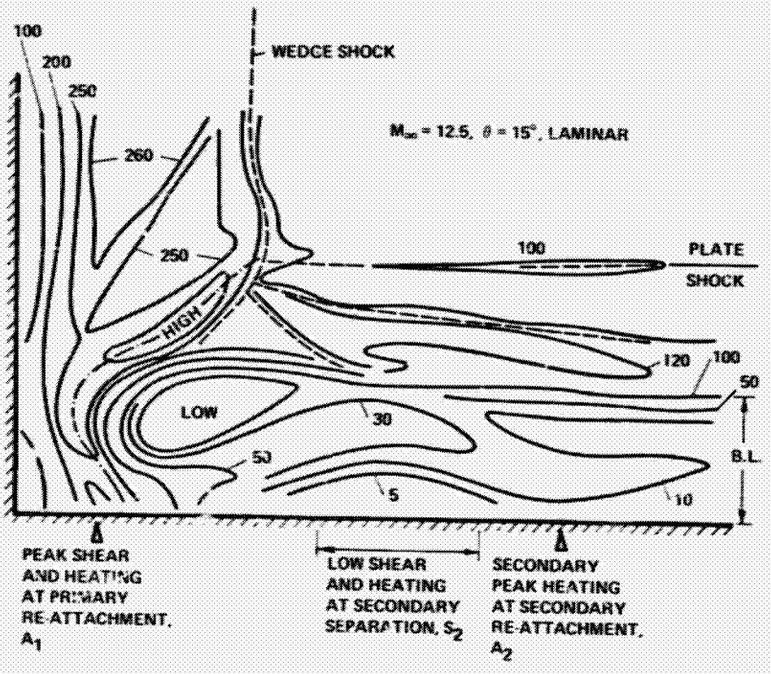

Fig. 142 Smoothed impact pressure contours in crossflow plane of corner flow with secondary separation (based on data of Cooper and Hankey 1973; D. W. Rao 1978: personal communication).

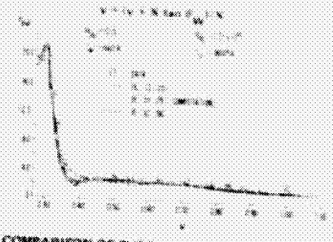

(a) COMPARISON OF SURFACE PRESSURE DISTRIBUTION FOR DIFFERENT MESH SIZES

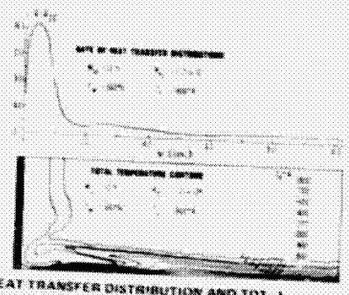

(b) HEAT TRANSFER DISTRIBUTION AND TOTAL TEMPERATURE CONTOURS

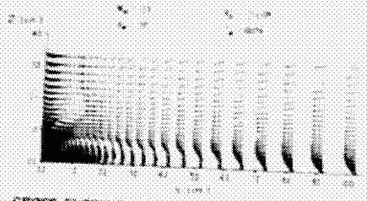

(c) CROSS-FLOW VECTOR VELOCITY PLOT IN CONICAL COORDINATES (x = 12 in.)

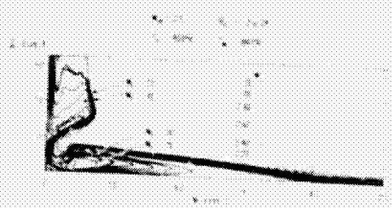

(d) CROSS-FLOW MACH NUMBER CONTOURS

Fig. 145 Calculations of $M_\infty = 12.5$ corner interaction in laminar flow (Shang and Hankey 1977).

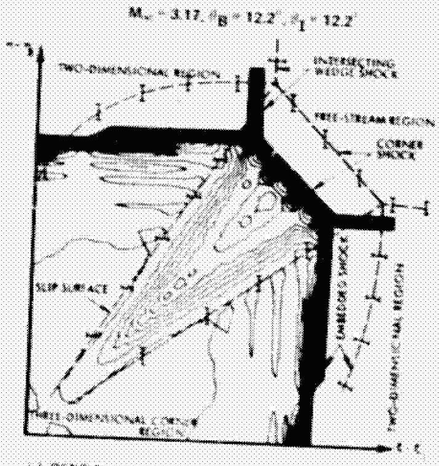

(a) DENSITY CONTOUR PLOT IN TRANSVERSE PLANE. I – EXPERIMENTAL RESULTS

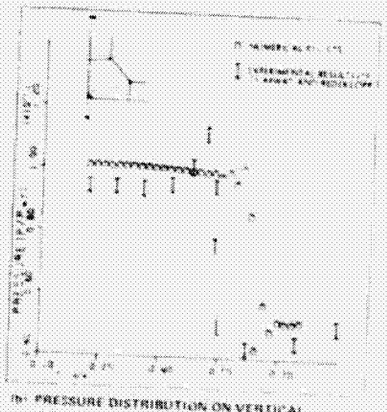

(b) PRESSURE DISTRIBUTION ON VERTICAL INTERSECTING WEDGE SURFACE

Fig. 147 Inviscid corner flow calculations of Shankar, Anderson, and Kutler (1975) compared with laminar flow experimental result of Charwat and Redekeopp (1967).

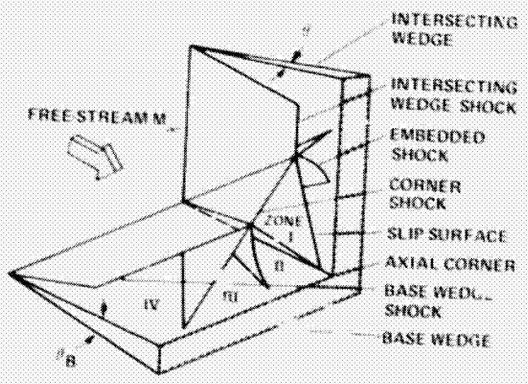

Fig. 146 Shock-wave structure in axial corner comprised of two intersecting wedges (Charwat and Redekeopp 1967).

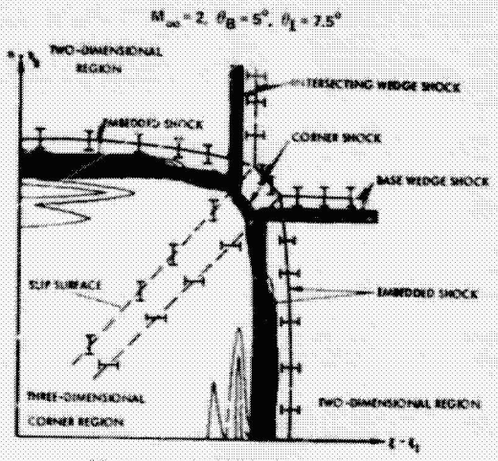

(a) DENSITY CONTOUR PLOT IN TRANSVERSE PLANE I - EXPERIMENTAL RESULTS

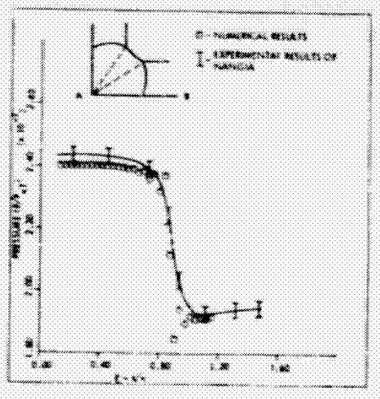

(b) PRESSURE DISTRIBUTION ON BASE WEDGE SURFACE

Fig. 148 Inviscid corner flow calculations of Shankar, Anderson, and Kutler (1975) compared with turbulent flow experimental result of Nangia (1974).

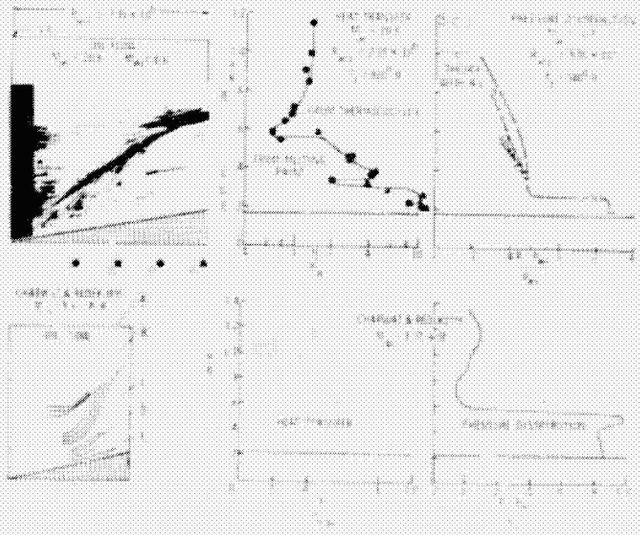

Fig. 149 Oil flow, heat transfer, and pressure distributions from experiments in helium with $\theta_I = \theta_B = 10°$ and from the work of Charwat and Redekeopp (1966) in air with $\theta_I = \theta_B = 12.2°$ (Bertram and Henderson 1969).

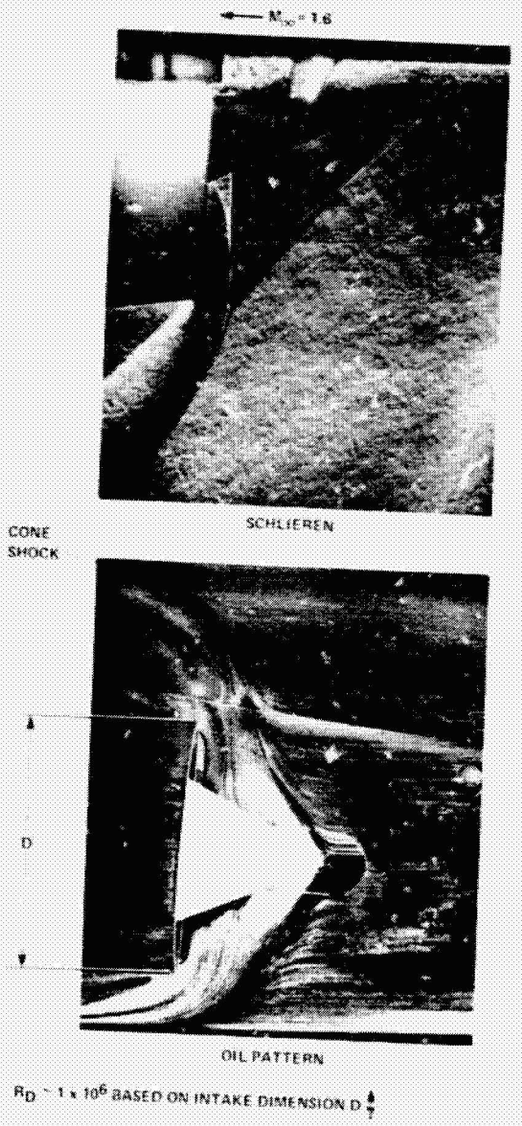

Fig. 150 Oil-flow pattern due to swept-shock-induced 3D separation about half-cone intake at $M_\infty = 1.6$ (Culley 1972a,b).

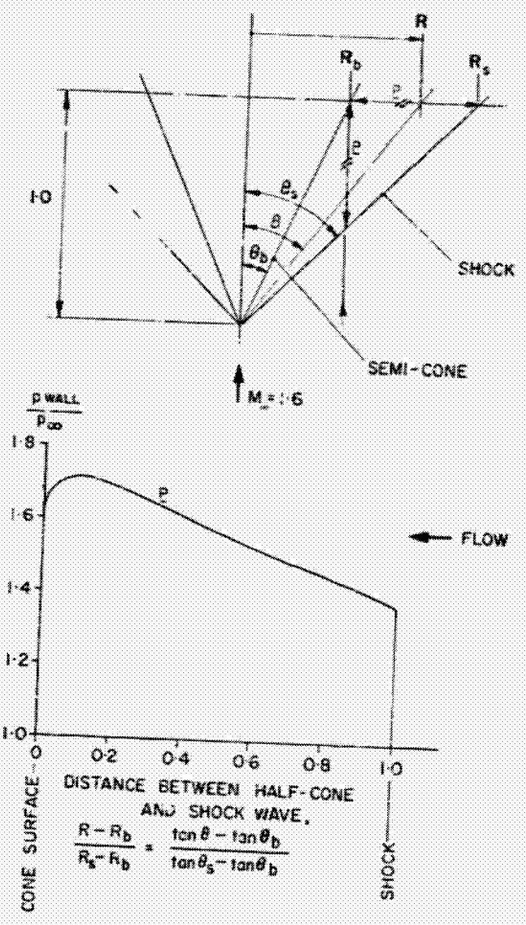

Fig. 151 Calculated pressure field between shock wave and Fourier half-cone at $M_\infty = 1.6$ (Peake, Jones, and Rainbird 1971).

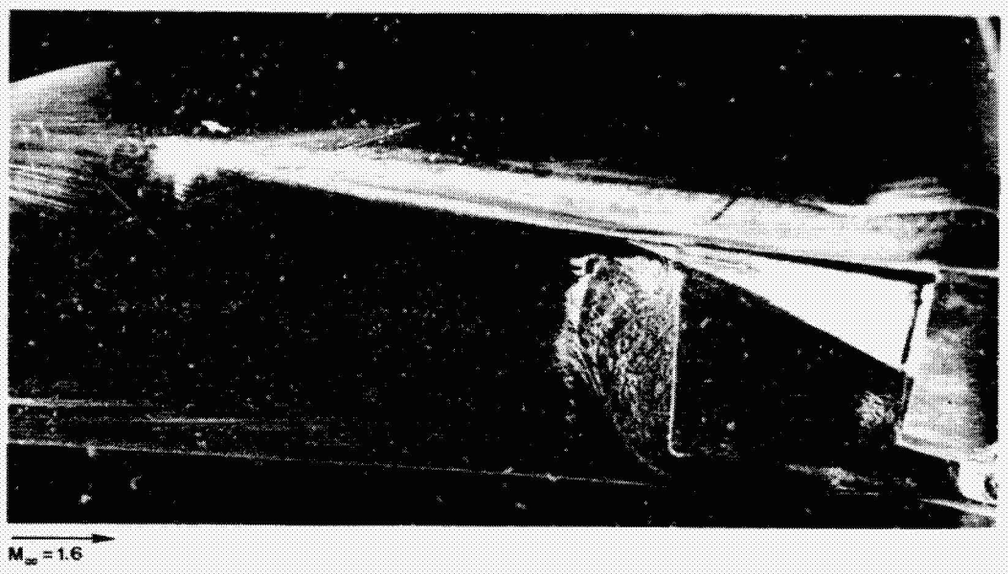

Fig. 152 Side view of 3D separation of fuselage boundary layer induced by boundary-layer splitter-plate-quarter-cone inlet; model angle of attack = 4.5°, M_∞ = 1.6 (Culley 1972b, 1975).

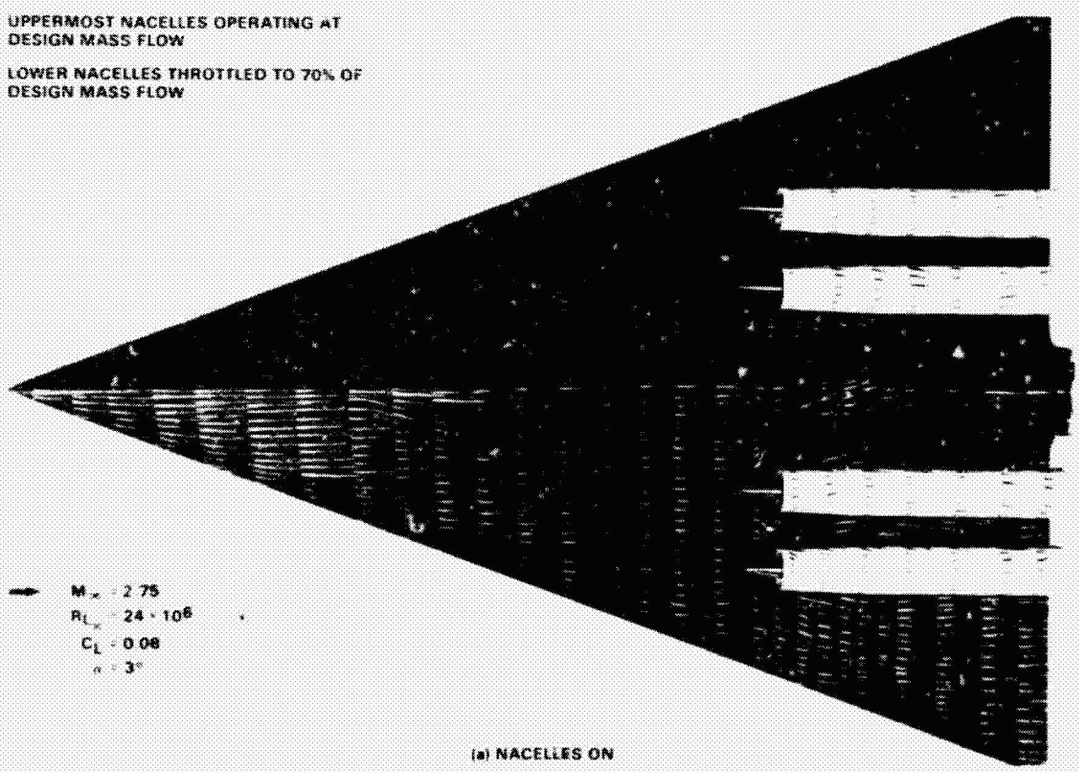

Fig. 153 Oil-dot flow visualization on lower surface of 70° delta wing showing swept-shock turbulent boundary-layer interactions associated with propulsion nacelles (Peake and Rainbird 1973).

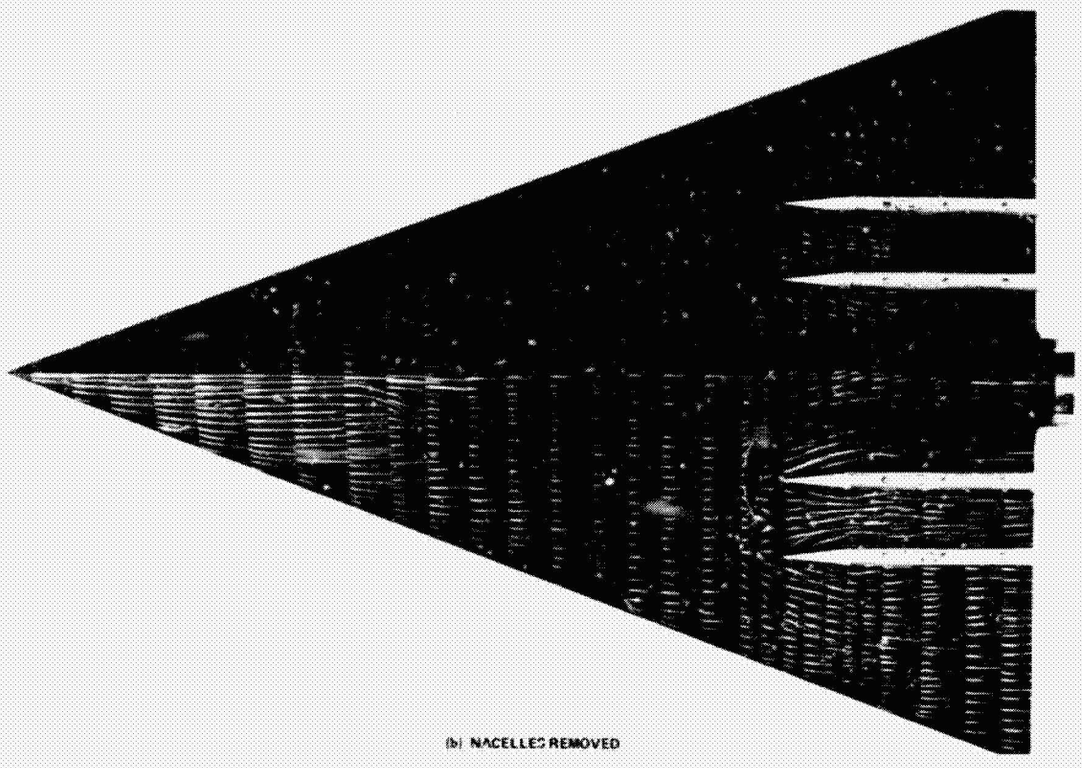

(b) NACELLES REMOVED

Fig. 153 Continued.

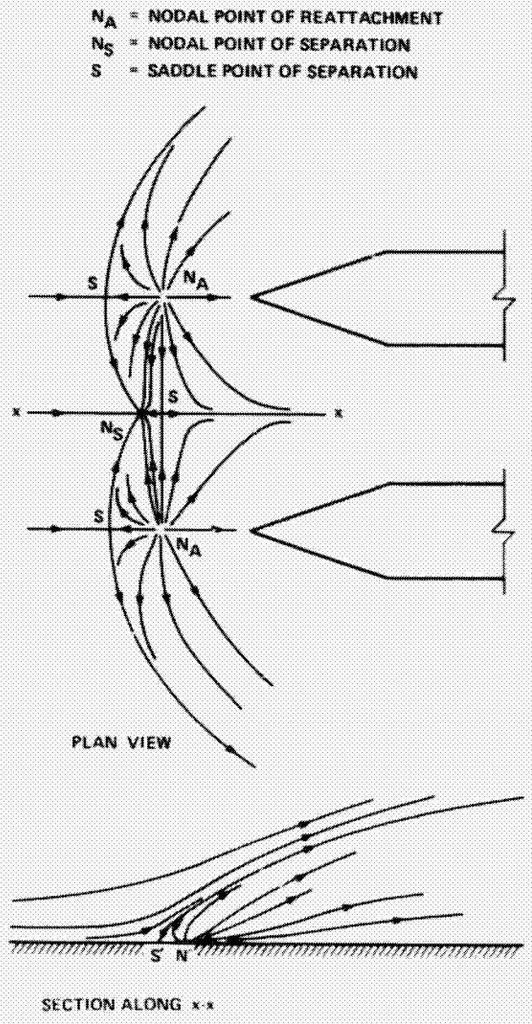

(c) POSTULATED PATTERNS OF SKIN-FRICTION LINES AND EXTERNAL FLOW STREAMLINES

Fig. 153. Concluded.

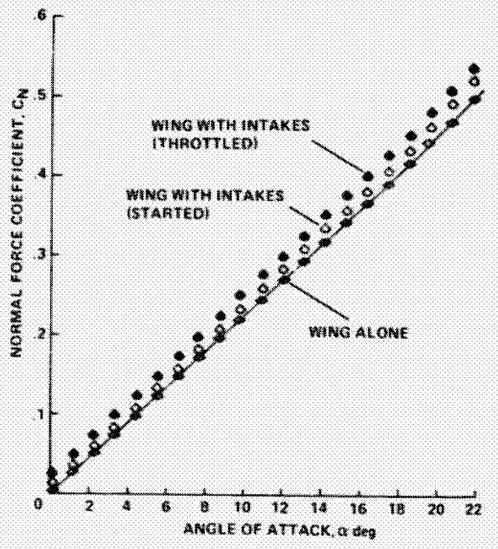

Fig. 154 "Favorable interference" effect on lift of 70° delta wing at $M_\infty = 2.75$, $R_{L_\infty} = 24 \times 10^6$ (Peake and Rainbird 1973).

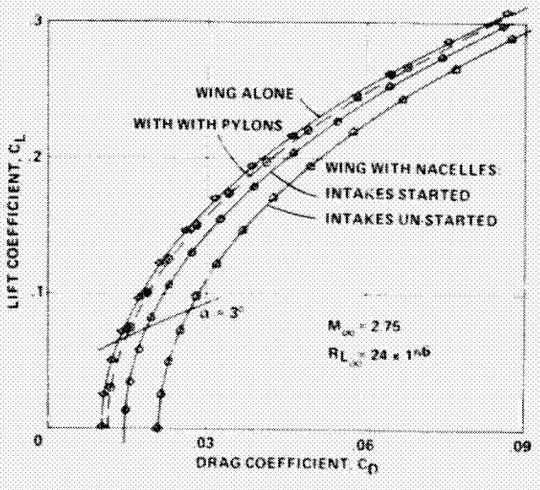

Fig. 155 Lift-drag polars: 70° delta wing with four nacelles supported on pylons at design Mach number, $M_\infty = 2.75$ (Peake and Rainbird 1973).

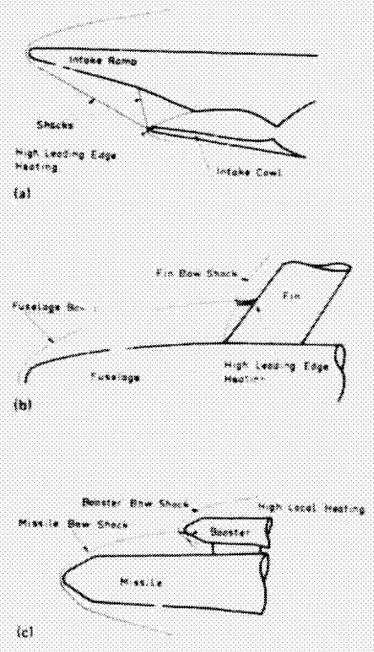

Fig. 156 Practical examples of shock-impingement heating (Edney 1968).

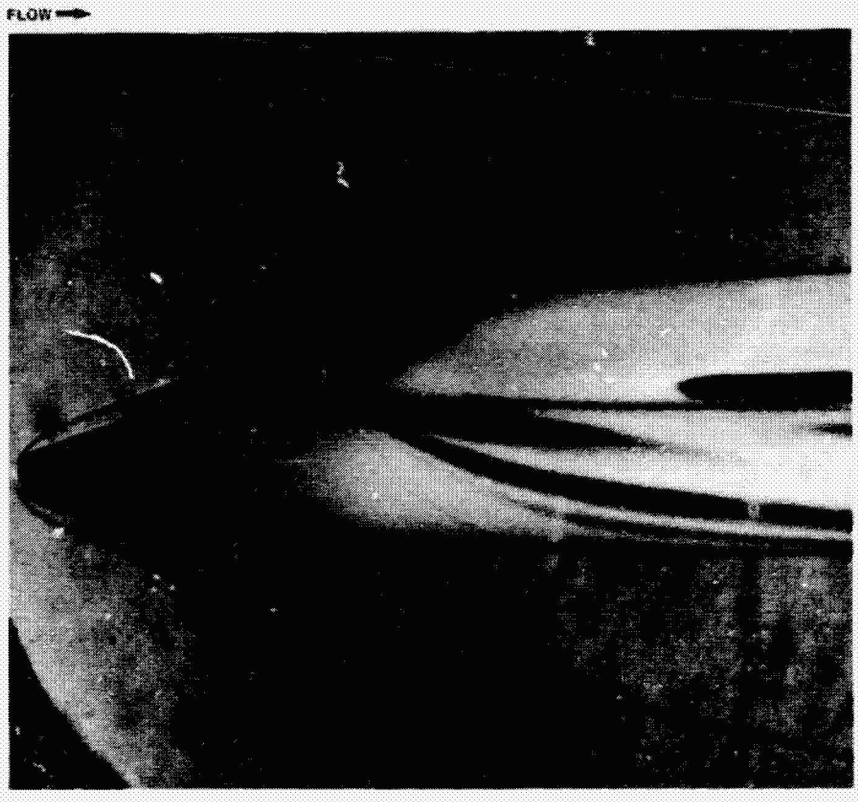

Fig. 157 Combined Schlieren and phase-change coating techniques revealing shock-on-shock interactions and aerodynamic interference heating (Creel and J. L. Hunt 1972).

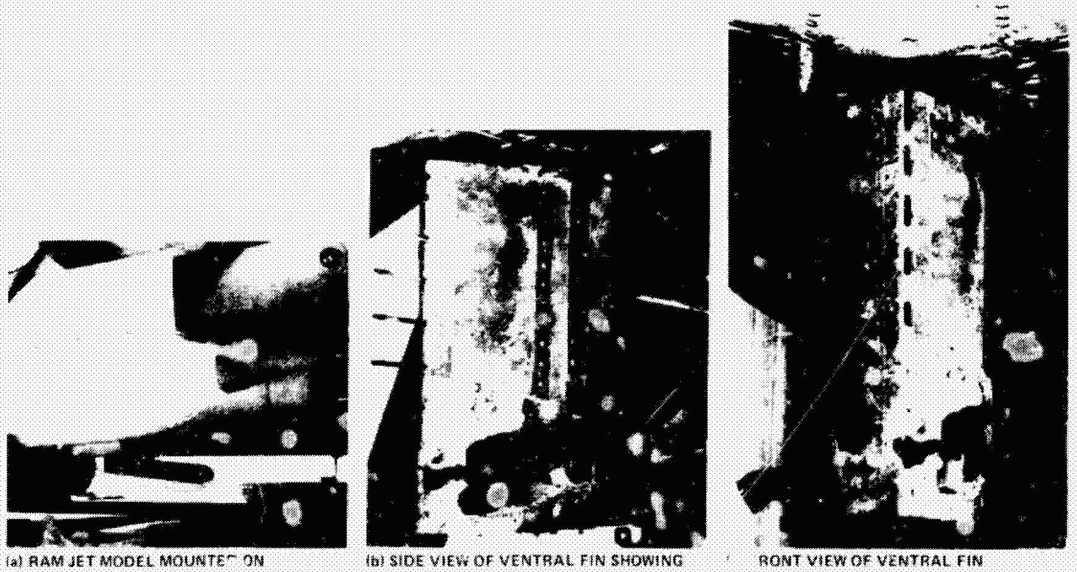

(a) RAM JET MODEL MOUNTED ON VENTRAL FIN OF X-15A-2 AIRCRAFT PRIOR TO TEST FLIGHT. (PHOTO COURTESY OF NASA)

(b) SIDE VIEW OF VENTRAL FIN SHOWING DAMAGE DUE TO SHOCK IMPINGEMENT. (PHOTO COURTESY OF NASA)

FRONT VIEW OF VENTRAL FIN SHOWING DAMAGE DUE TO SHOCK IMPINGEMENT. (PHOTO COURTESY OF NASA)

Fig. 158 Damage to ventral fin on NASA X-15A-2 aircraft from shock impingement (courtesy of NASA).

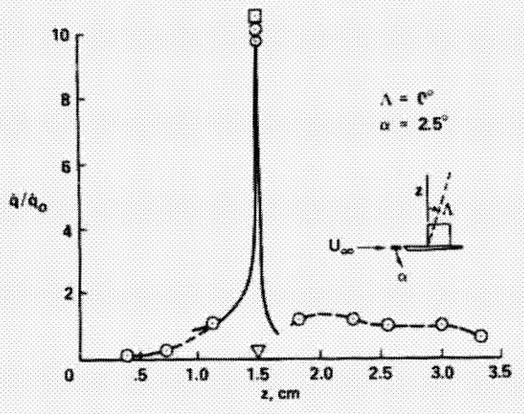

Fig. 159 Effect of shock impingement on fin leading-edge heat transfer at $M_\infty = 14$ (Hiers and Loubsky 1967).

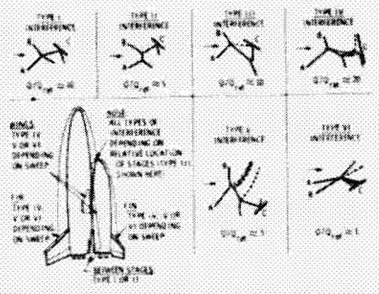

(a) THE SIX TYPES OF SHOCK INTERFERENCE

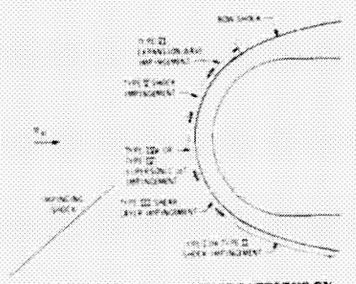

(b) LOCATION OF INTERFERENCE PATTERNS ON A HEMISPHERE

Fig. 160 Types of shock-on-shock interactions diagnosed by Edney (1968) (Hains and Keyes 1972).

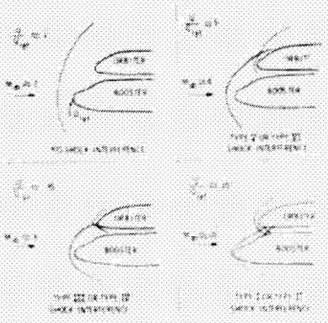

Fig. 161 Shock-interference patterns on Space Shuttle during ascent (Hains and Keyes 1972).

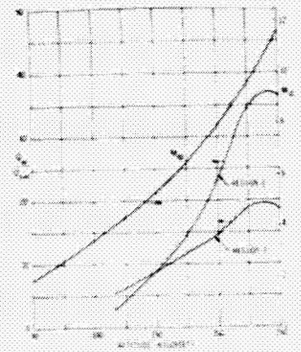

Fig. 162 Peak heat-transfer amplification for Type IV interference on typical Space Shuttle ascent trajectory ($\gamma = 1.40$)(Hains and Keyes 1972).

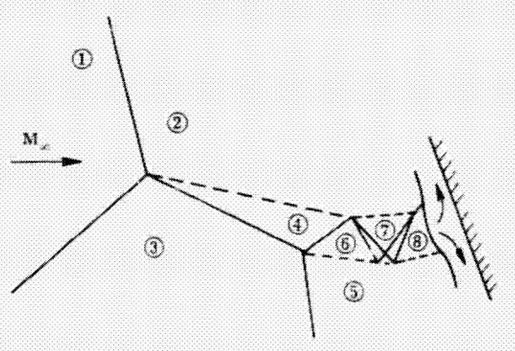

(a) DOWNWARD SLOPING SHEAR LAYER

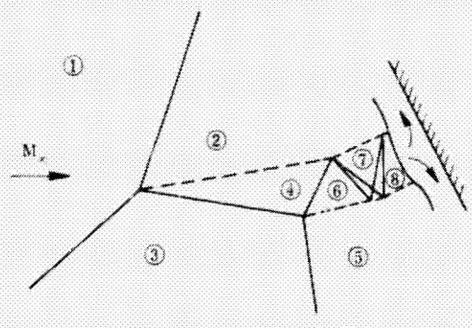

(b) UPWARD SLOPING SHEAR LAYER

Fig. 163 Jet configuration for downward and upward sloping shear layers with jet bow shock in Region 8 (Keyes and Hains 1973).

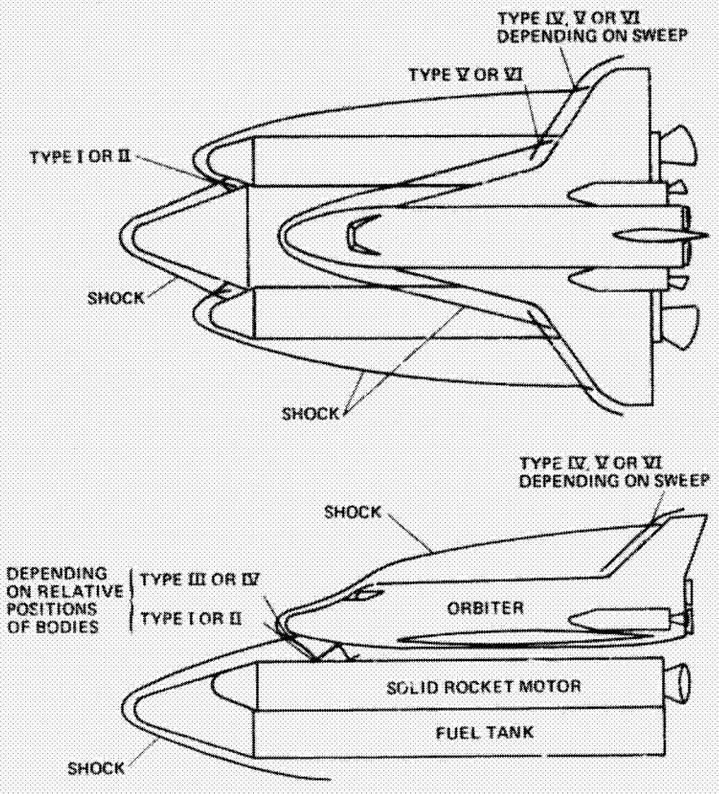

Fig. 164 Locations of types of interference heating on mated Shuttle-booster configuration at $M_\infty \sim 20$ (Keyes and Hains 1973).

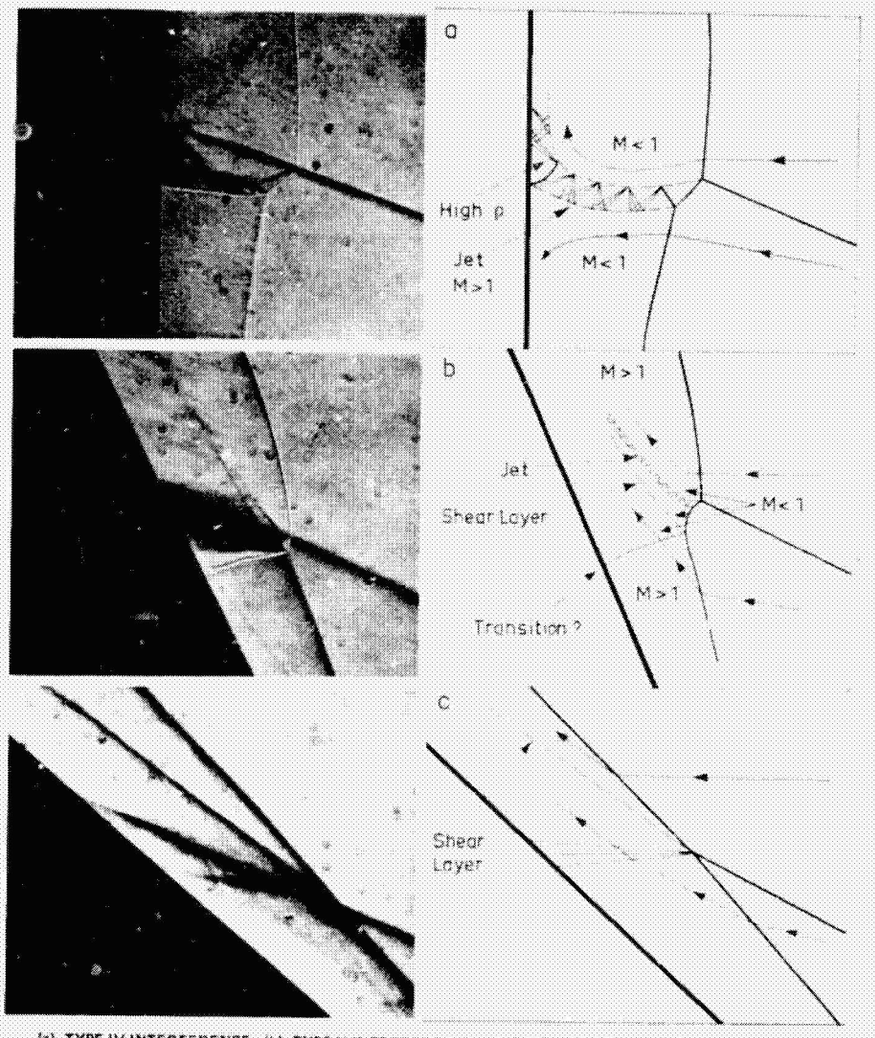

(a) TYPE IV INTERFERENCE. (b) TYPE V INTERFERENCE. (c) TYPE VI INTERFERENCE. $M_\infty = 4.6$, $\theta = 5°$ (SHOCK GENERATOR DEFLECTION)

Fig. 165 Effect of varying sweep angle of cylindrical fin on pattern of interference heating (Edney 1968).

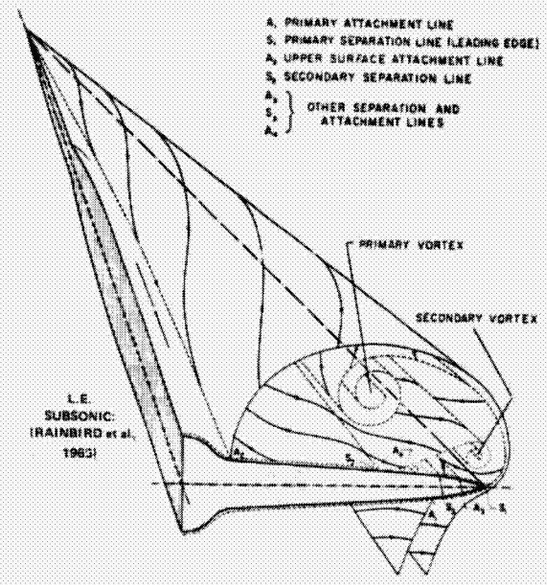

(a) INTERPRETATION OF FLOW ABOUT 70° DELTA WING AT 16.6° ANGLE OF ATTACK

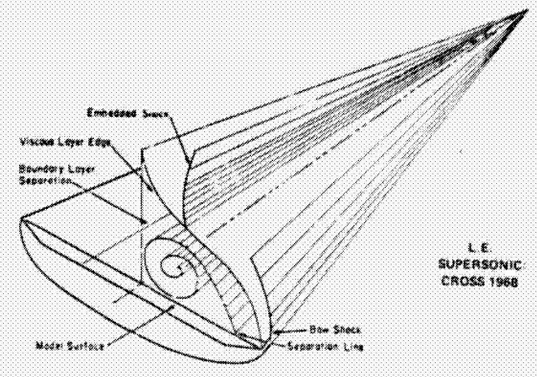

(b) DOMINANT FEATURES OF LEE SIDE FLOW FIELD ABOUT 75° DELTA WING

Fig. 166 Leeward flows over delta wings at angle of attack.

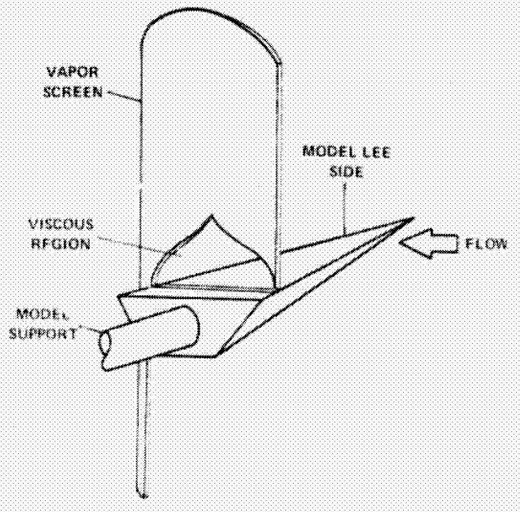

(a) ARRANGEMENT OF MODEL AND VAPOR SCREEN

(b) VAPOR SCREEN FLOW VISUALIZATION OF EXPANSION FLOW FIELD

Fig. 168 75° delta wing vapor-screen experiment at $M_\infty = 12$ (Cross 1968).

NOTE: b IS LOCAL SEMI-SPAN

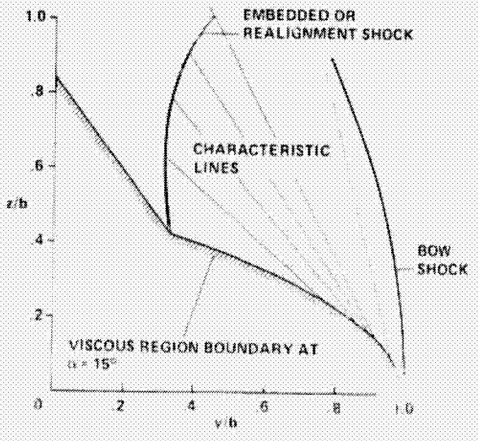

Fig. 167 Crossflow plane for delta wing with supersonic leading edges (Cross 1968).

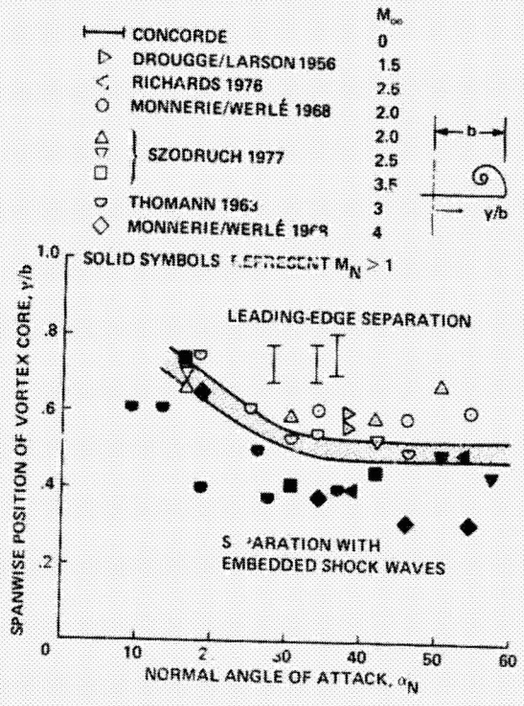

Fig. 169 Vortex position exhibiting certain types of delta-wing flow (Szodruch and Peake 1980).

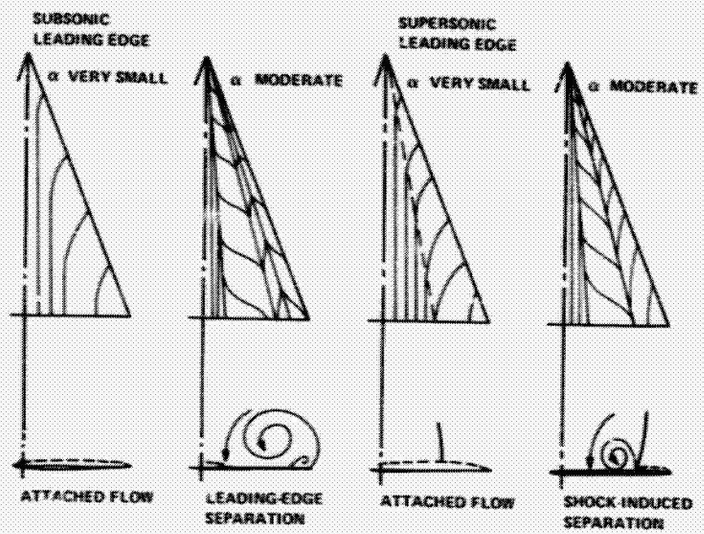

(a) STANBROOK-SQUIRE 1964, THIN WING

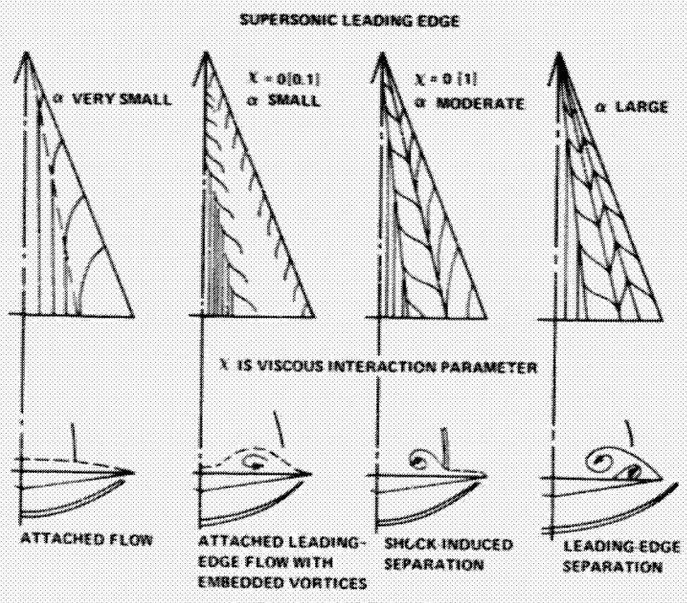

(b) NARAYAN 1978, THICK WING

Fig. 170 Skin-friction line and cross-flow regimes over flat-topped delta wings (Szodruch and Peake 1980).

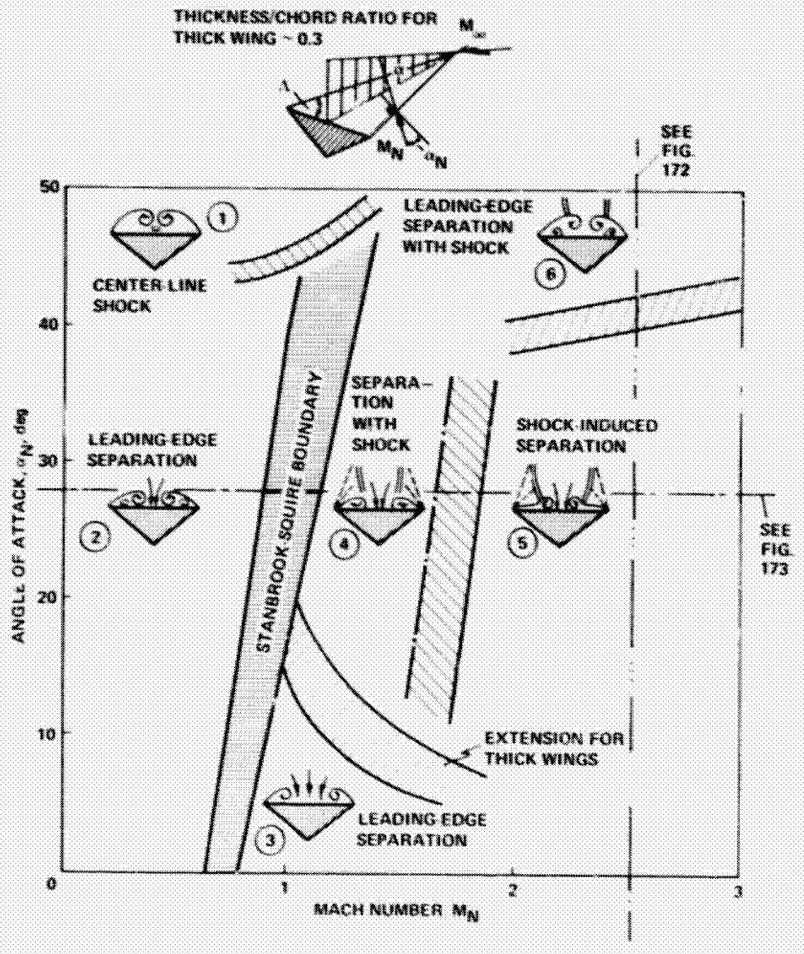

Fig. 171 Leeward flow regimes over thick delta wings on α_N-M_N diagram (after Szodruch 1977).

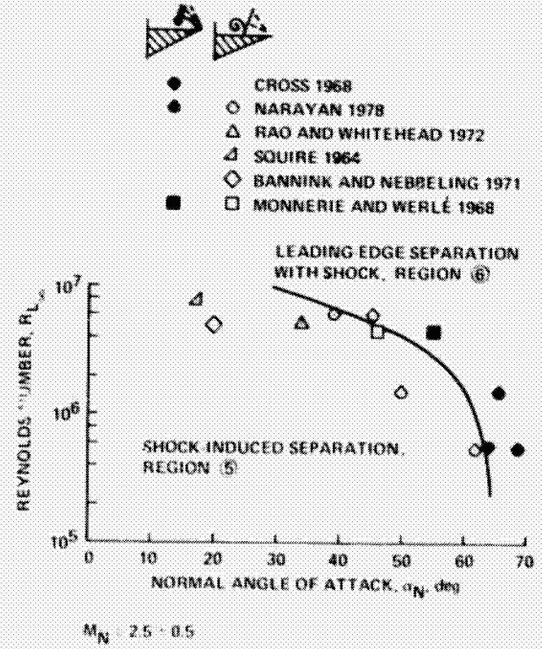

Fig. 172 Influence of Reynolds number on flow types and boundaries at M_N = constant (Szodruch and Peake 1980).

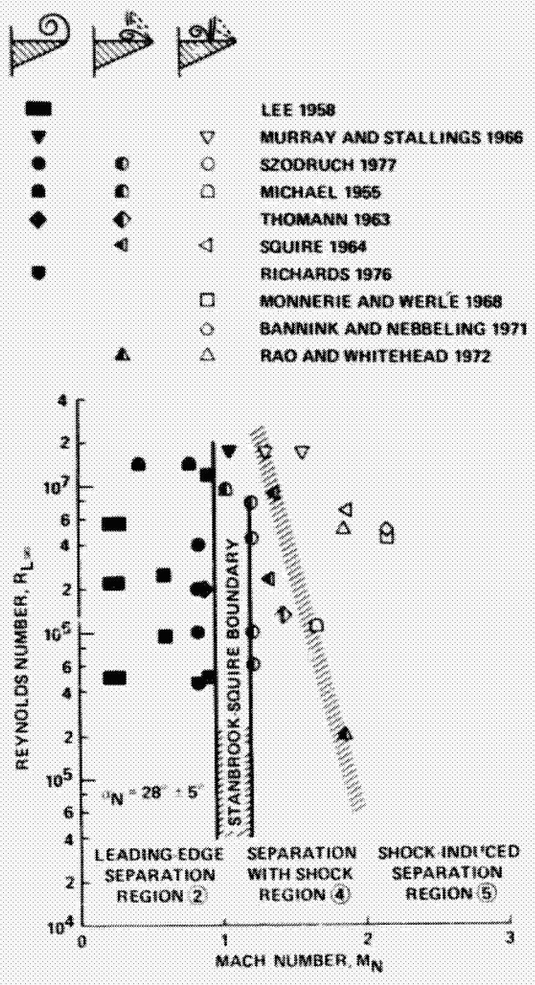

Fig. 173 Influence of Reynolds number on flow types and boundaries at $\alpha_N \sim$ constant (Szodruch and Peake 1980).

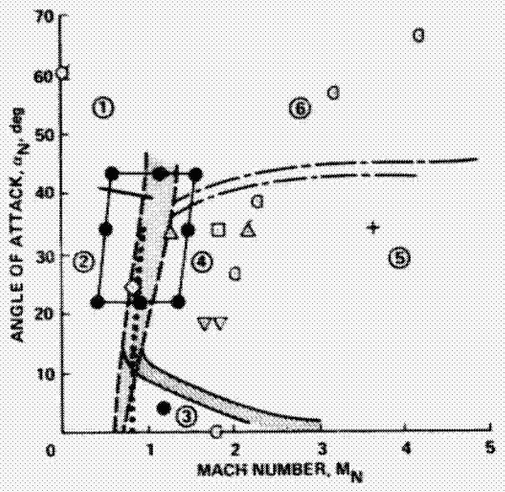

KEY	AUTHOR	Λ°	M_∞	α°	M_N	α_N°	$R_{L_\infty} \times 10^{-6}$
♂	MONNERIE AND WERLÉ 1968	75	0	25	0	61	0.01
○			1.95	25	0.94	61	1→4.5
△			4	10	1.2	34	
△			7	10	2.2	34	
◇	THOMANN 1963	76	3	6.5	0.8	25	2
▽	RAO AND WHITEHEAD 1972	75	6.8	5	1.85	19	0.6→8
□			6	10	1.85	34	
○	NARAYAN 1978	80	10	0→22	1.8 →4.2	0→67	1.5
+	CROSS 1968	75	10→14	0→50	2.6 →7.8	0→78	0.2→0.5
• • •	MALTBY 1962	65	1.75	4→18	0.75→0.9	9→38	2
			1.88	0→10	0.8 →0.85	0→23	
●	SZODRUCH 1977	73	2.5→3.5	0→30	0.4 →1.6	0→43	0.1→0.6

BOUNDARIES:

STANBROOK-SQUIRE BOUNDARY FOR THIN WINGS

EXTENSION FOR THICK WINGS AT LOW ANGLES OF ATTACK

EXTENSION FOR THICK WINGS AT HIGH ANGLES OF ATTACK

CENTER LINE SHOCK

Fig. 174 Some chosen experimental conditions represented on α_N - M_N diagram to be presented in Figs. 175 to 187.

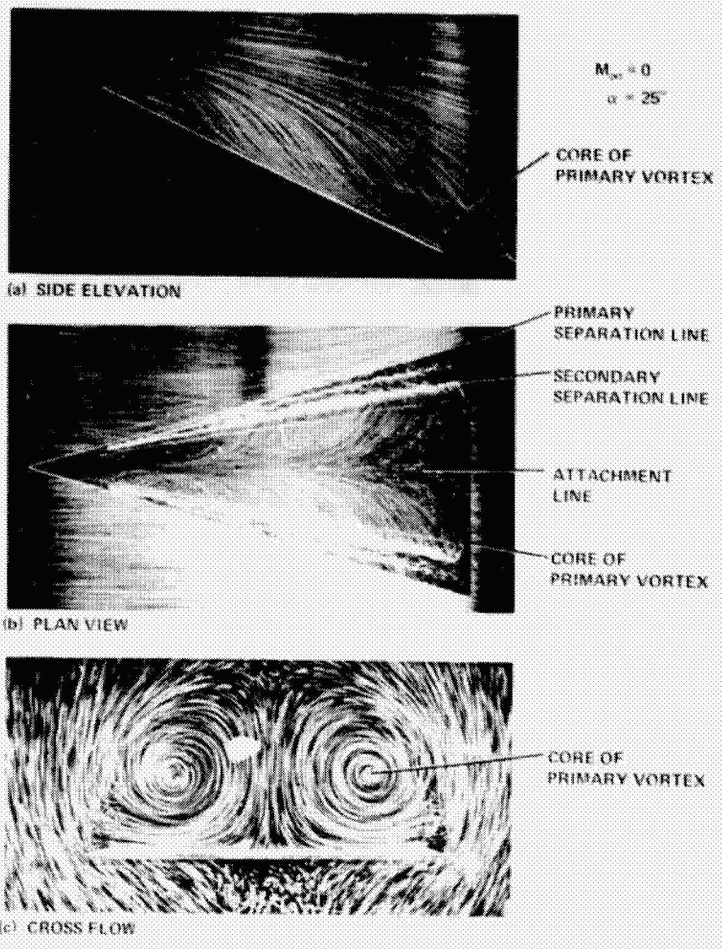

Fig. 175 Very low-speed 75° delta wing flow of Monnerie and Werlé (1968).

(a) SCHLIEREN

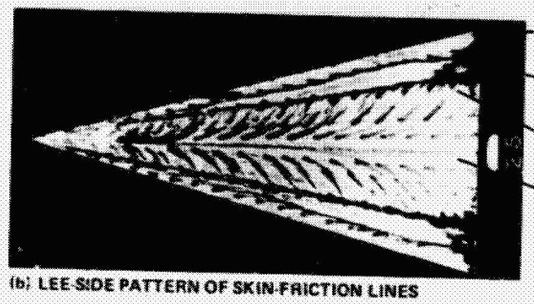

(b) LEE-SIDE PATTERN OF SKIN-FRICTION LINES

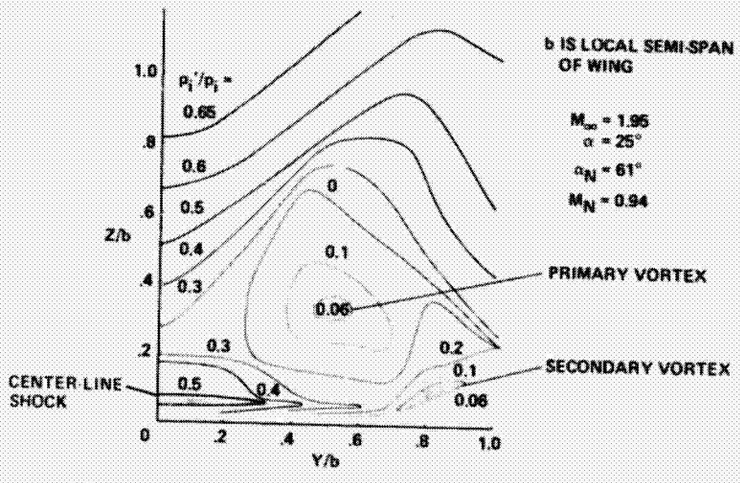

(c) CONTOURS OF CONSTANT PITOT PRESSURE

Fig. 176 75° delta wing flow of Monnerie and Werlé (1968) with subsonic leading edges.

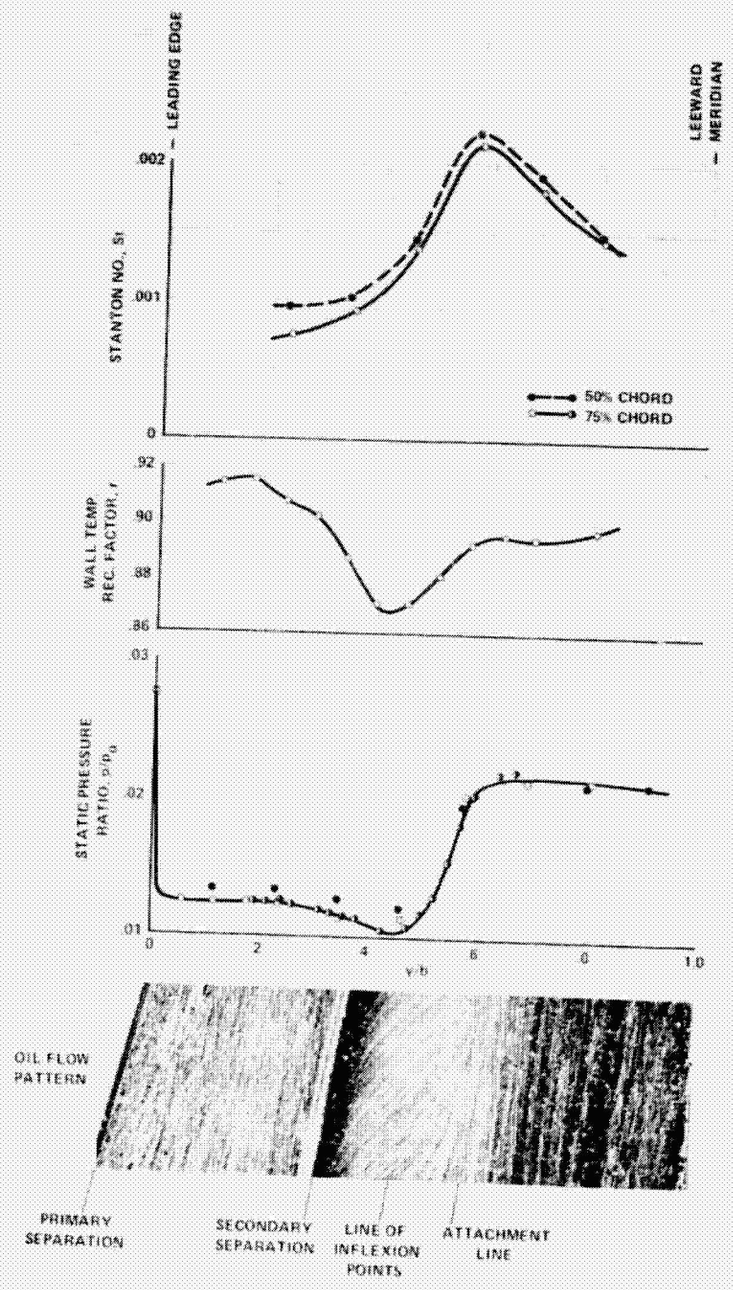

Fig. 177 Heat-transfer, recovery factor, and pressure distribution on 76° delta wing, α = 6.5°, $R_{L_\infty} = 2 \times 10^6$, $M_\infty = 3$ (Thomann 1963).

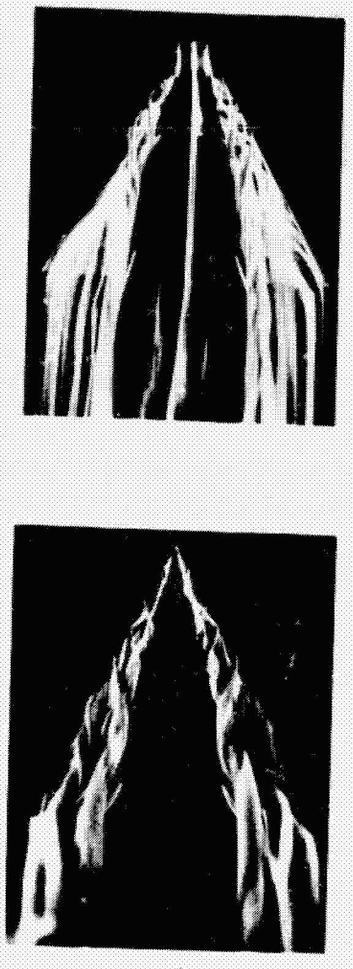

$\alpha = 12^{\circ}$

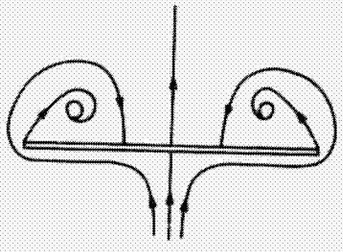

POSTULATE OF FLOW PATTERN

Fig. 178 Leeward behavior of flow about delta wing at low angle of attack in a water tunnel (Werlé 1958).

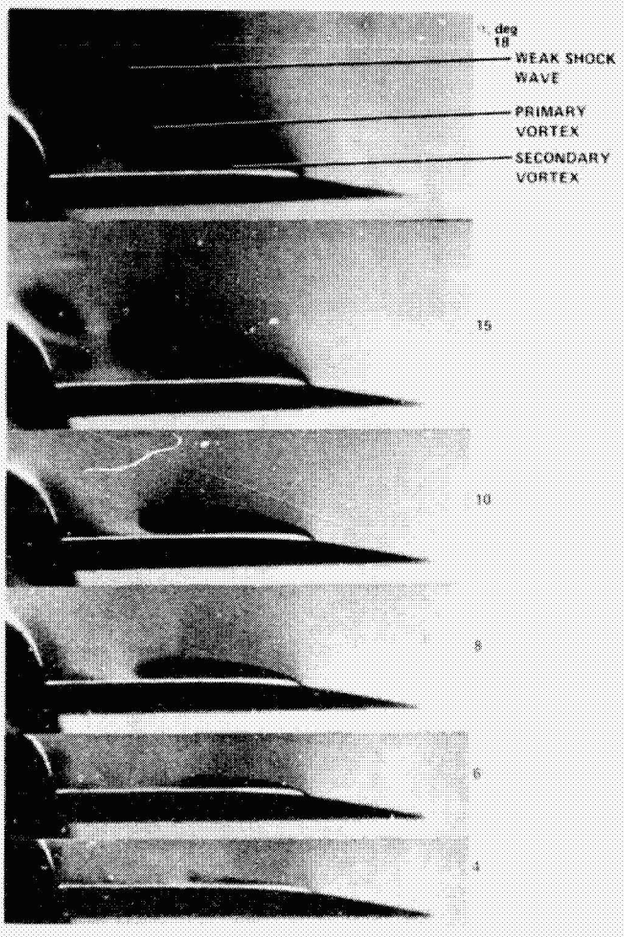

Fig. 179 Vapor-screen photographs of flow over upper surface of plane, slender wing at $M_\infty = 1.75$ (Maltby 1962).

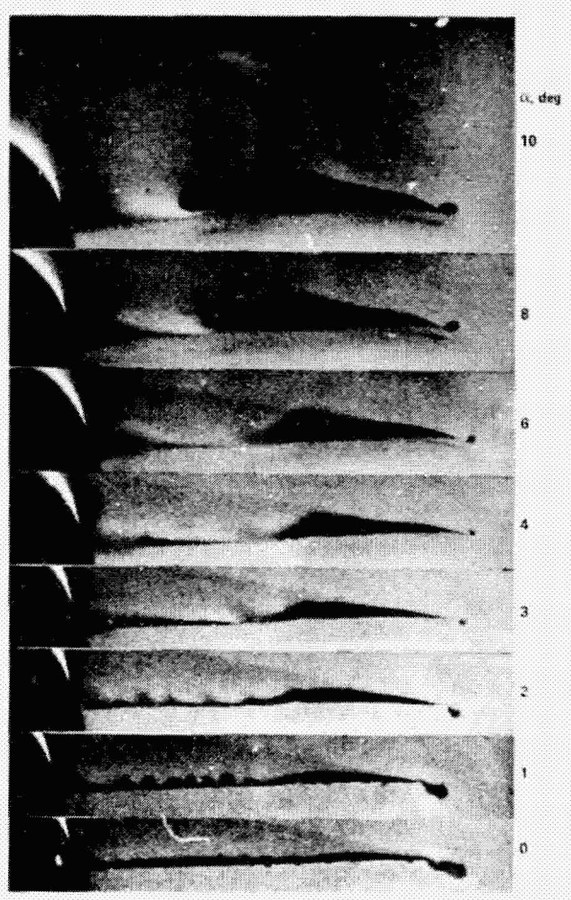

Fig. 180 Vapor-screen photographs of flow behind cambered delta wing at $M_\infty = 1.88$ (Maltby 1962).

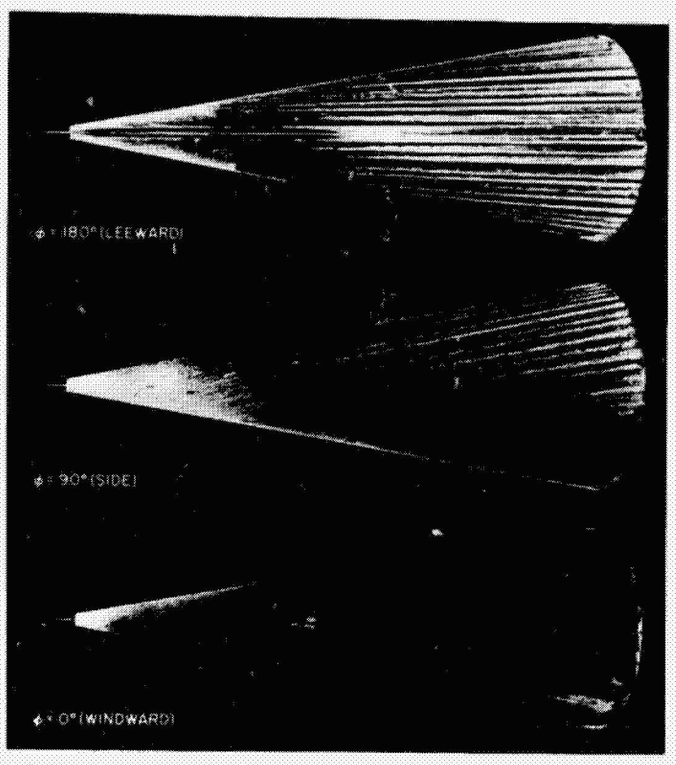

(a) THREE VIEWS OF CONE SURFACE

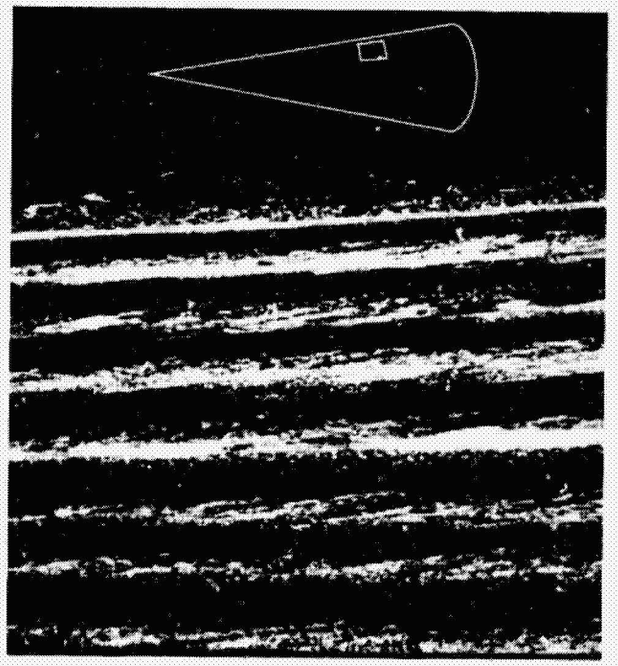

(b) ENLARGED VIEW OF PORTION, LEEWARD SURFACE ($\phi \sim 135°$, $x/L \sim 0.7$)

Fig. 181 Oil-film study on $\theta_c = 10°$ cone at $\alpha = 5°$ with transitional boundary layer; $M_\infty = 7.4$, $R_{L_\infty} = 3 \times 10^6$, $T_T = 1050°$ K (McDevitt and Mellenthin 1969).

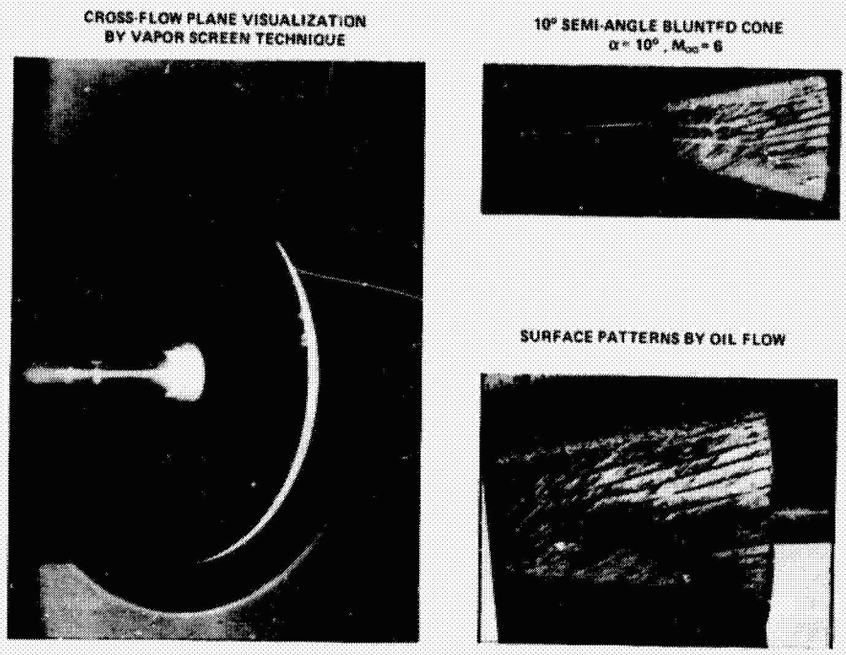

Fig. 182 Streamwise vortices in boundary layer of lifting cone (D. S. Rao 1978: personal communication).

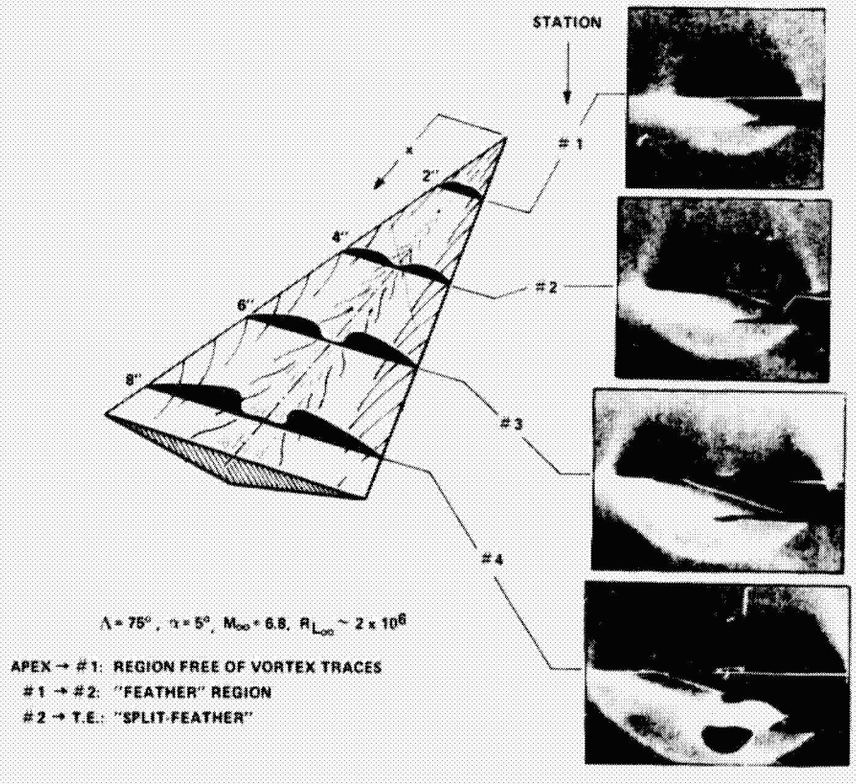

Fig. 183 Vapor-screen flow visualization about 75° delta wing at M_∞ = 6.8 (Rao and Whitehead 1972).

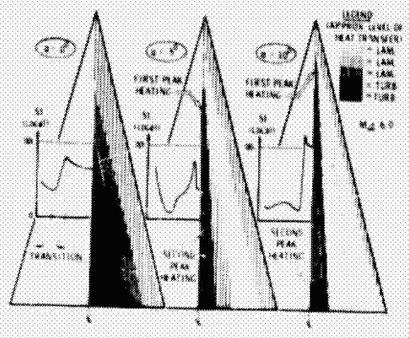

Fig. 184 Leeward-surface heating patterns at $M_\infty = 6$ (Rao and Whitehead 1972).

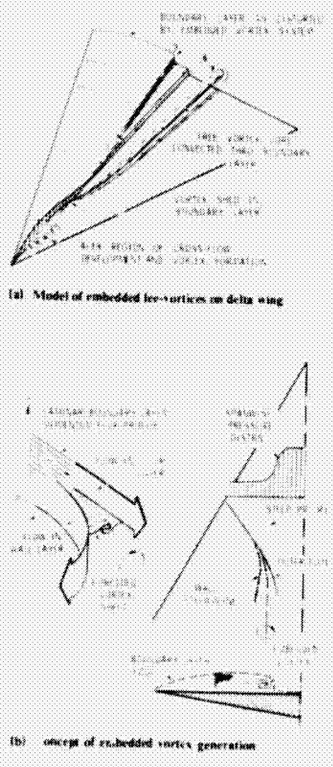

(a) Model of embedded lee-vortices on delta wing

(b) Concept of embedded vortex generation

Fig. 185 Concept of embeded vortices on leeward side of delta wing at low angle of attack and hypersonic Mach numbers (Rao and Whitehead 1972).

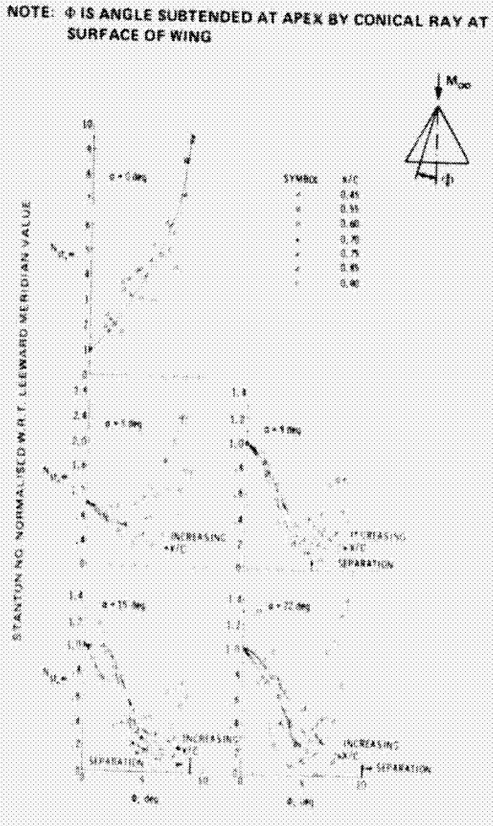

Fig. 186 Spanwise heat-transfer variation across 80° delta wing, $M_\infty = 10$, $R_{L_\infty} = 1.5 \times 10^6$, with inboard or leading-edge separations (Narayan 1978).

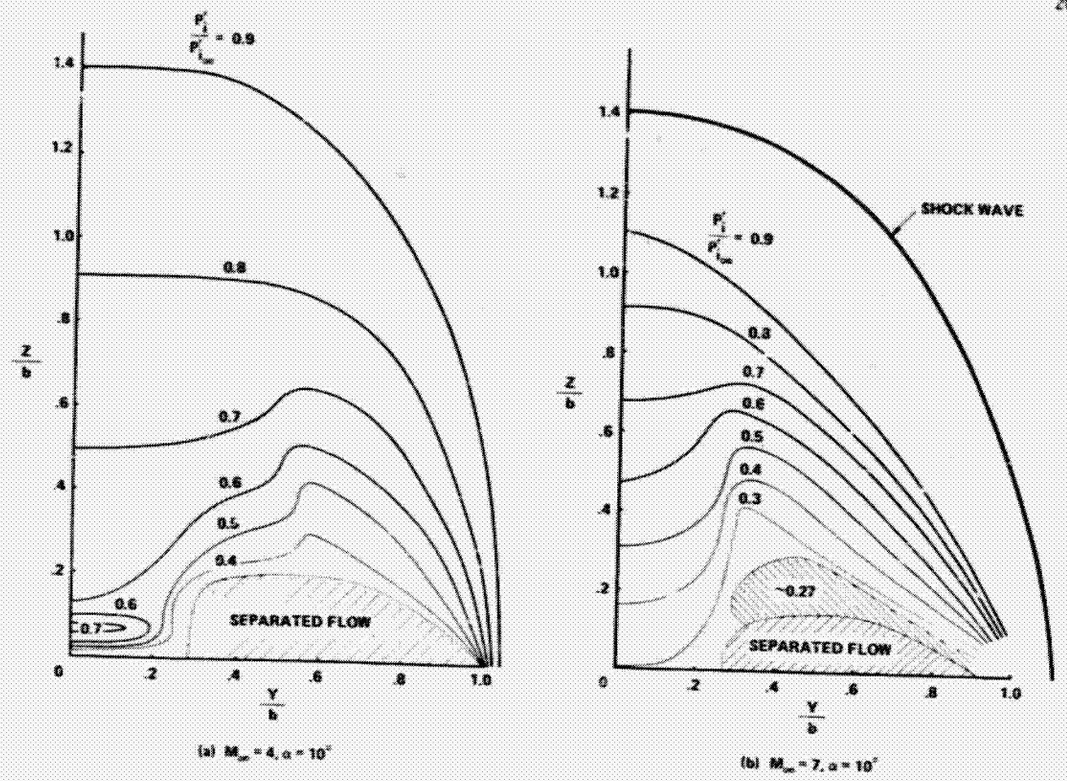

(a) $M_\infty = 4, \alpha = 10°$ (b) $M_\infty = 7, \alpha = 10°$

Fig. 187 Contours of constant pitot pressure about 75° delta wing at M_∞ = 4 and 7 (Monnerie and Werlé 1968).

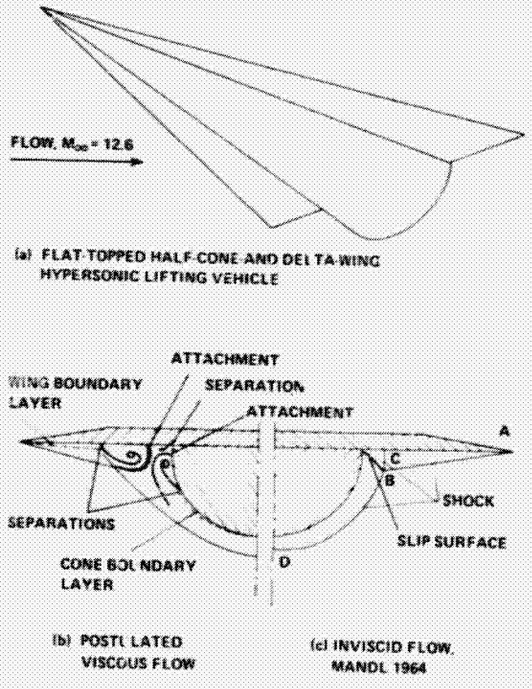

(a) FLAT-TOPPED HALF-CONE-AND DELTA-WING HYPERSONIC LIFTING VEHICLE

(b) POSTULATED VISCOUS FLOW (c) INVISCID FLOW, MANDL 1964

Fig. 188 Lifting hypersonic half-cone-delta wing at M_∞ =12.6, α = 15°.

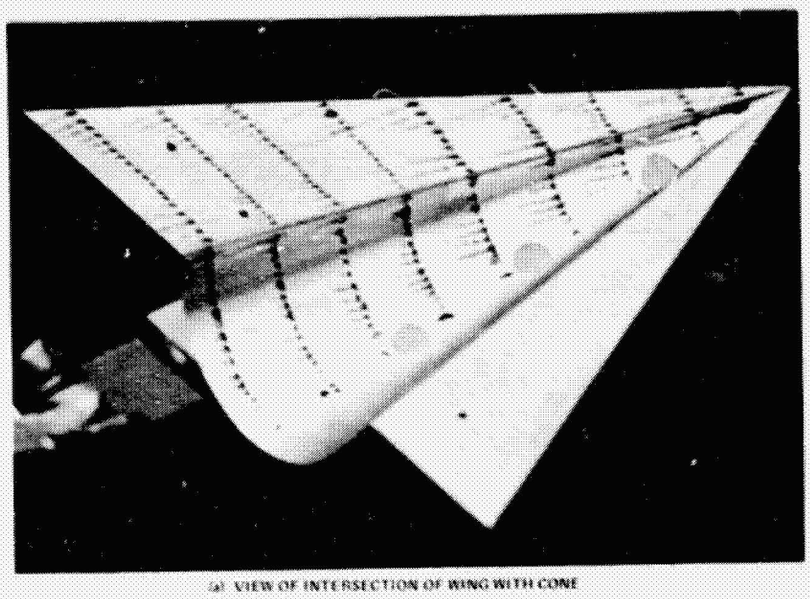

(a) VIEW OF INTERSECTION OF WING WITH CONE

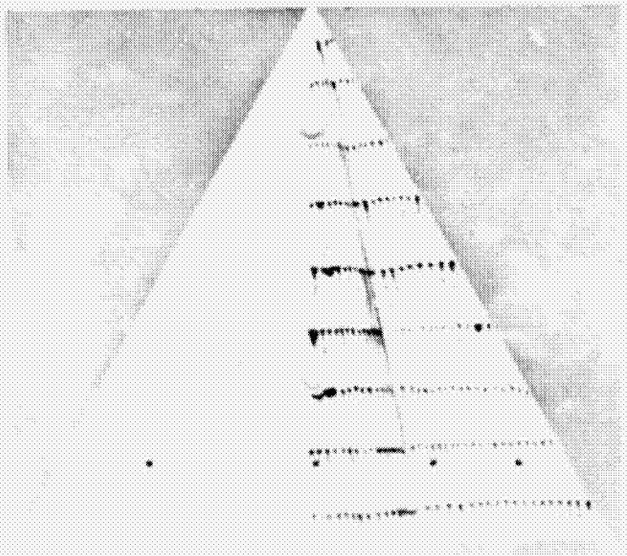

(b) WINDWARD VIEW

Fig. 189 Surface flow pattern on delta wing with half-cone: $\alpha = 15°$, $M_\infty = 12.6$, $R_{L,\infty} = 4.4 \times 10^5$ (Meyer and Vail 1967).

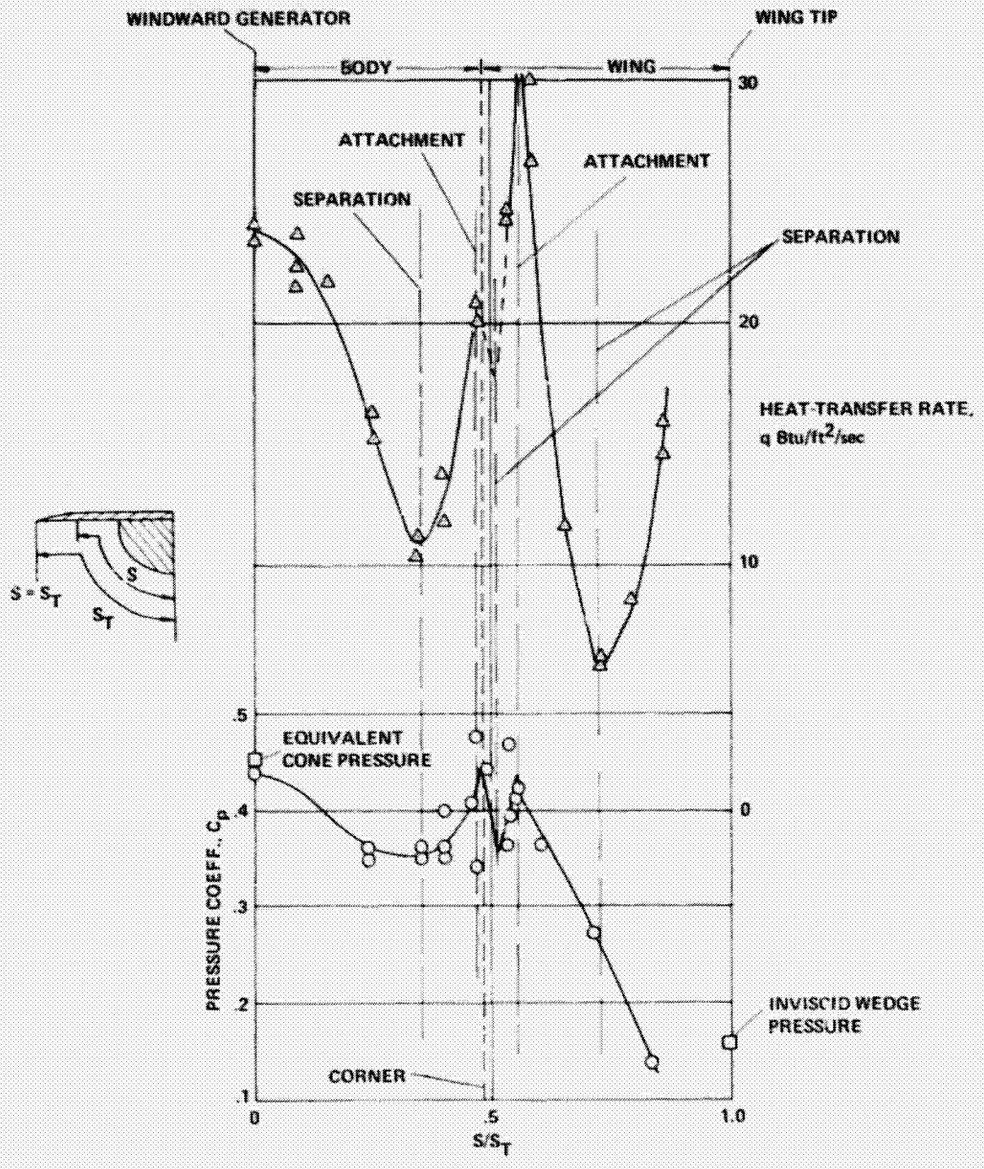

Fig. 190 Heat transfer and surface pressures on half-cone-delta wing: $\alpha = 15^{\circ}$, $M_{\infty} = 12.6$, $R_{L_{\infty}} = 4.4 \times 10^{5}$ (Meyer and Vail 1967).

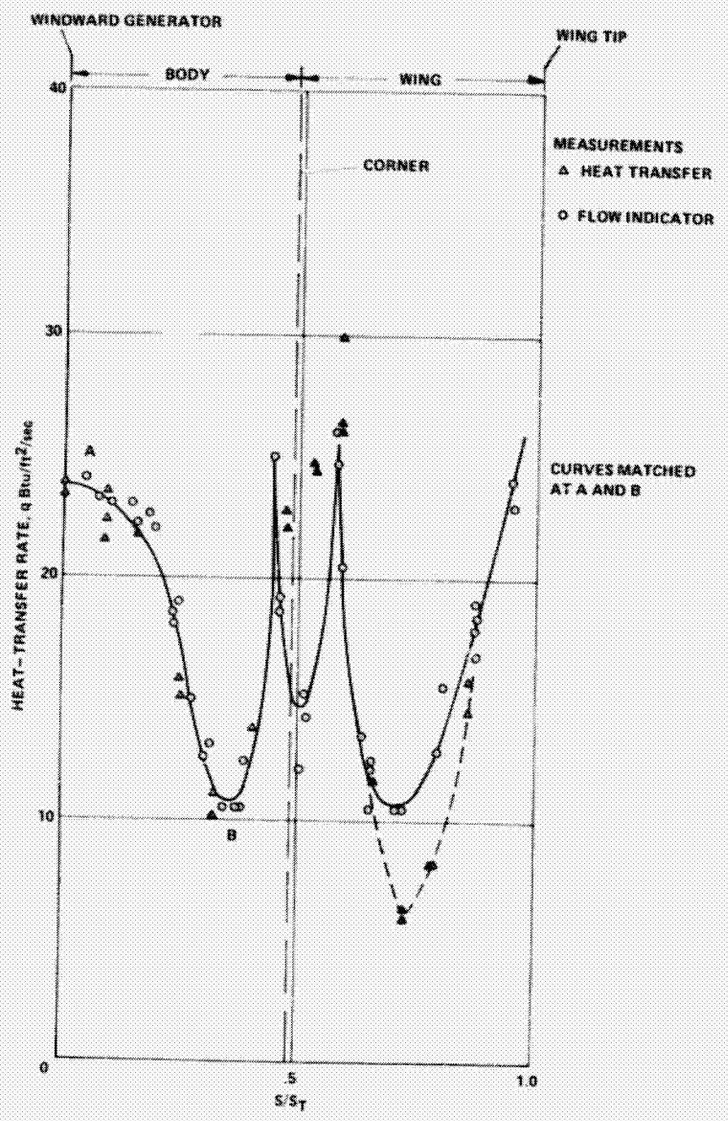

Fig. 191 Comparison of streak length and heat transfer distributions on half-cone-delta wing: $\alpha = 15°$, $M_\infty = 12.6$, $R_{L_\infty} = 4.4 \times 10^5$ (Meyer and Vail 1967).

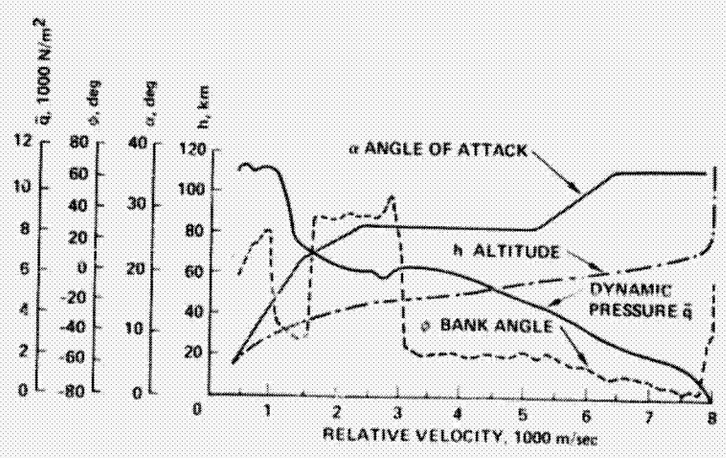

Fig. 192 Atmospheric reentry trajectory of Space Shuttle Orbiter (Bornemann and Surber 1978).

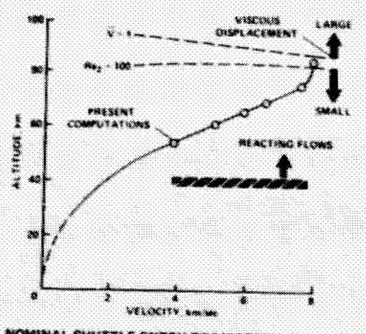

(a) NOMINAL SHUTTLE ENTRY TRAJECTORY AND VISCOUS FLOW REGIMES DEFINED BY FLAT PLATE AND BLUNT BODY INTERACTION PARAMETERS: $\bar{V} = M_\infty R_{L_\infty}^{-.5}$, $Re_2 = V_2 \rho_2 RN/\mu_2$, RN = BLUNT BODY NOSE RADIUS, SUBSCRIPT 2 REFERS TO CONDITIONS DOWNSTREAM OF BOW SHOCK WAVE

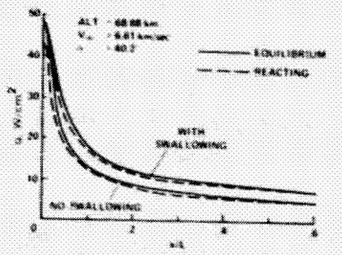

(c) CALCULATED WINDWARD CENTERLINE HEATING FOR FLIGHT CONDITIONS

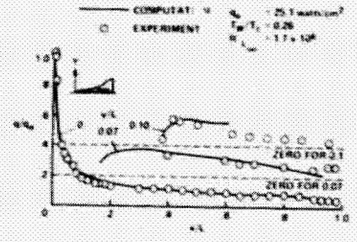

(b) SHUTTLE WINDWARD SURFACE HEATING FOR WIND TUNNEL CONDITIONS, $M_\infty = 7.3$, $\alpha = 30°$

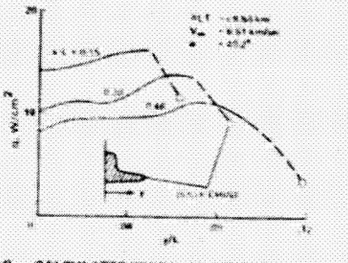

(d) CALCULATED WINDWARD SPANWISE HEATING FOR EQUILIBRIUM FLIGHT CONDITIONS INCLUDING SWALLOWING EFFECTS

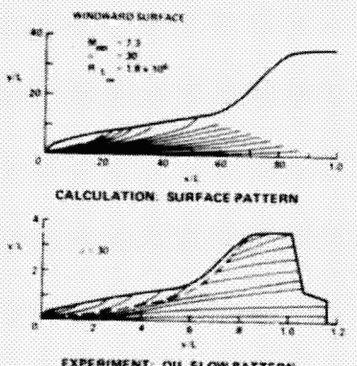

(e) SURFACE FLOW PATTERNS ON SHUTTLE WINDWARD SIDE

Fig. 193 Heating on windward side of Space Shuttle (Rakich and Lanfranco 1976).

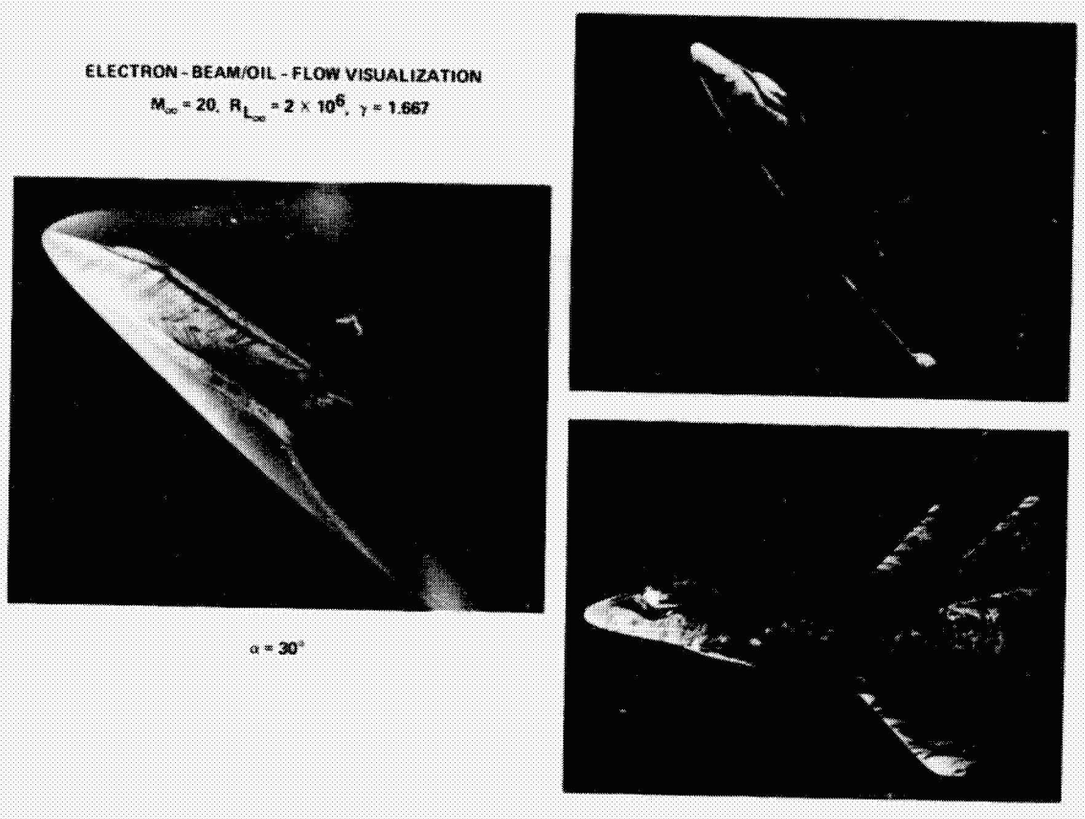

Fig. 194 Electron beam-oil-flow visualization about Shuttle Orbiter at $M_\infty = 20$ (Woods and Arrington 1972).

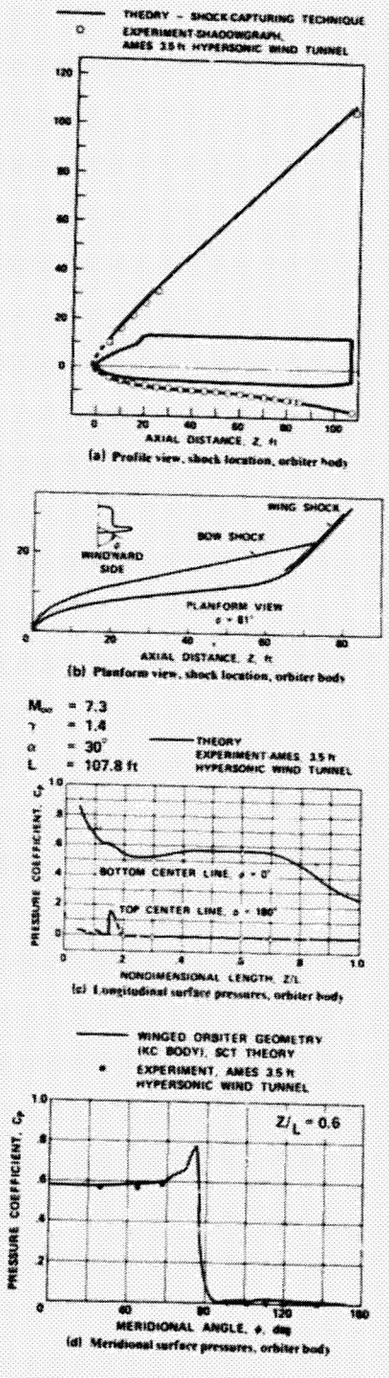

Fig. 195 Shuttle Orbiter experimental shock shapes and surface pressures compared with "shock-capture" computation (Chaussee, Holtz, and Kutler 1976).

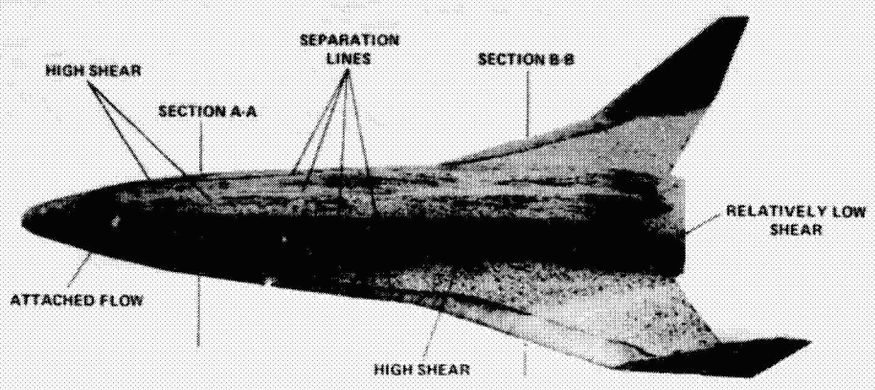

(a) EXPERIMENT, $M_\infty = 6$, $\alpha = 20°$, $R_{L_\infty} = 5.2 \times 10^6$ (HEFNER 1972)

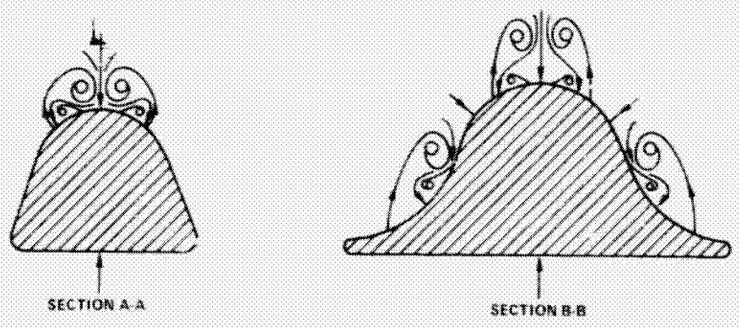

(b) POSTULATE OF CROSS FLOW

Fig. 196 Leeward-surface flow characteristics on conceptual delta-wing Orbiter at $M_\infty = 6$.

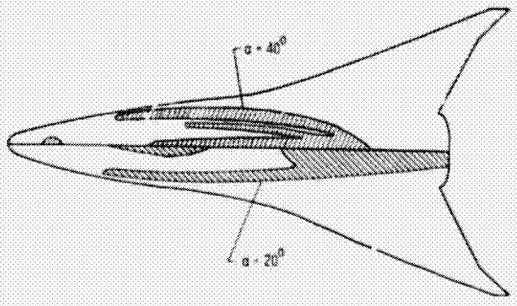

Fig. 197 Regions of increased heating on leeward surface of conceptual delta-wing Orbiter: $M_\infty = 6$, $R_{L_\infty} = 5.2 \times 10^6$ (Hefner 1972).

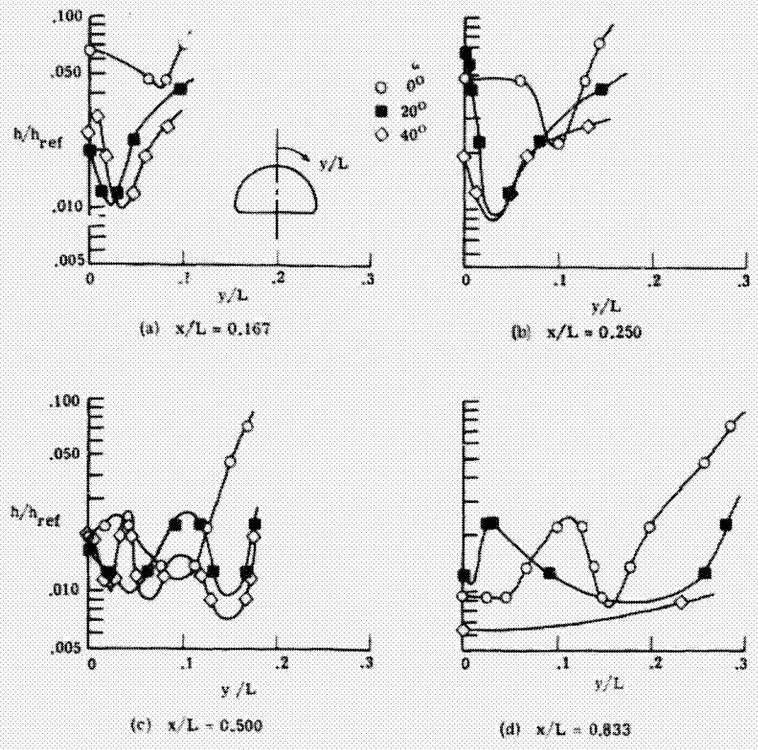

Fig. 198 Spanwise heating distribution on leeward surface of conceptual delta-wing Orbiter: $M_\infty = 6$, $R_{L_\infty} = 5.2 \times 10^6$ (Hefner 1972).

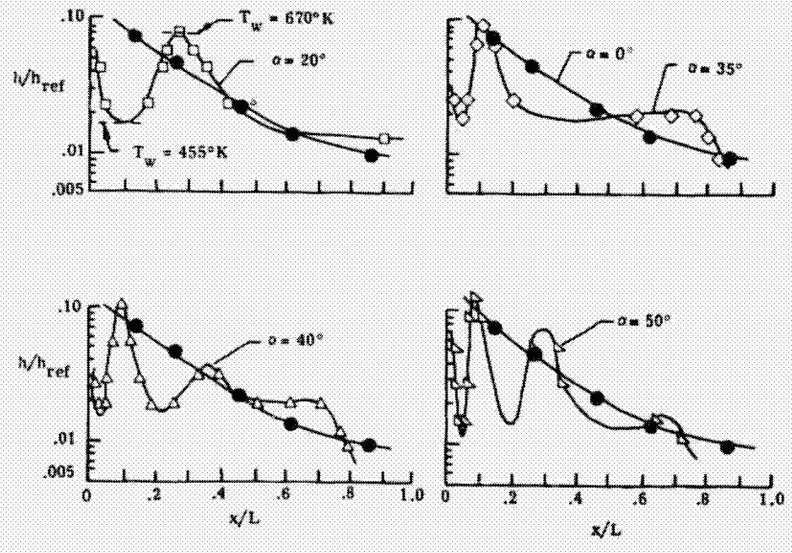

Fig. 199 Heating along leeward-surface meridian of delta-wing Orbiter at angle of attack: $M_\infty = 6$, $R_{L_\infty} = 5.2 \times 10^6$ (Hefner 1972).

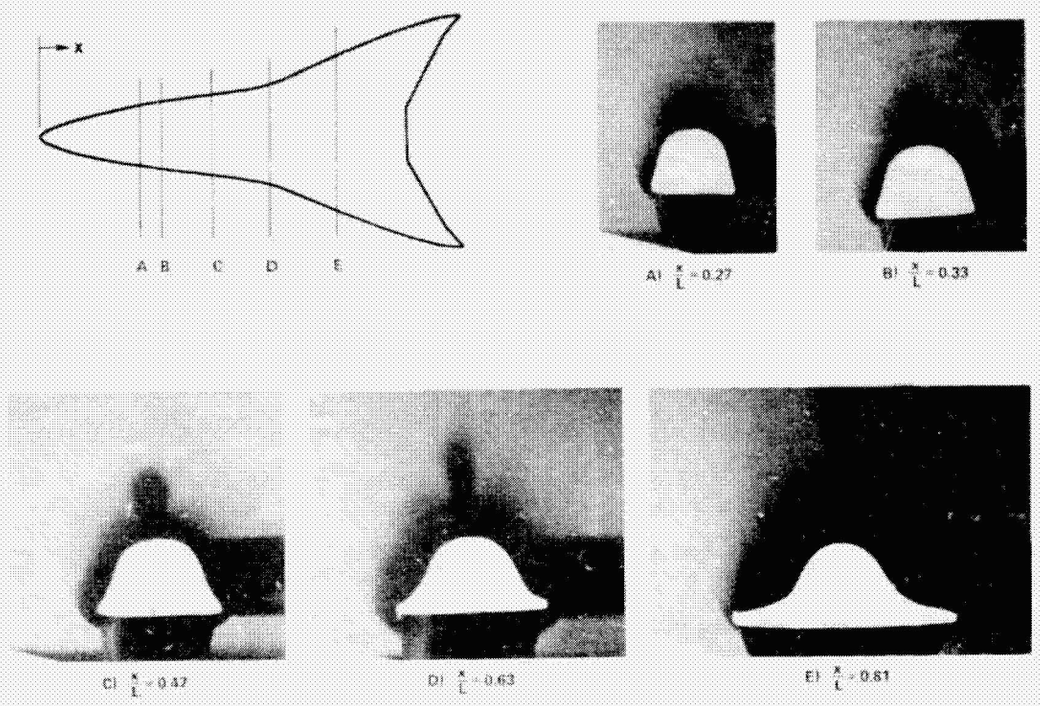

Fig. 200 Vapor-screen photographs of flow about conceptual delta-wing Orbiter: $M_\infty = 6$, $\alpha = 20°$, $R_{L_\infty} = 5.2 \times 10^6$ (Hefner 1972).

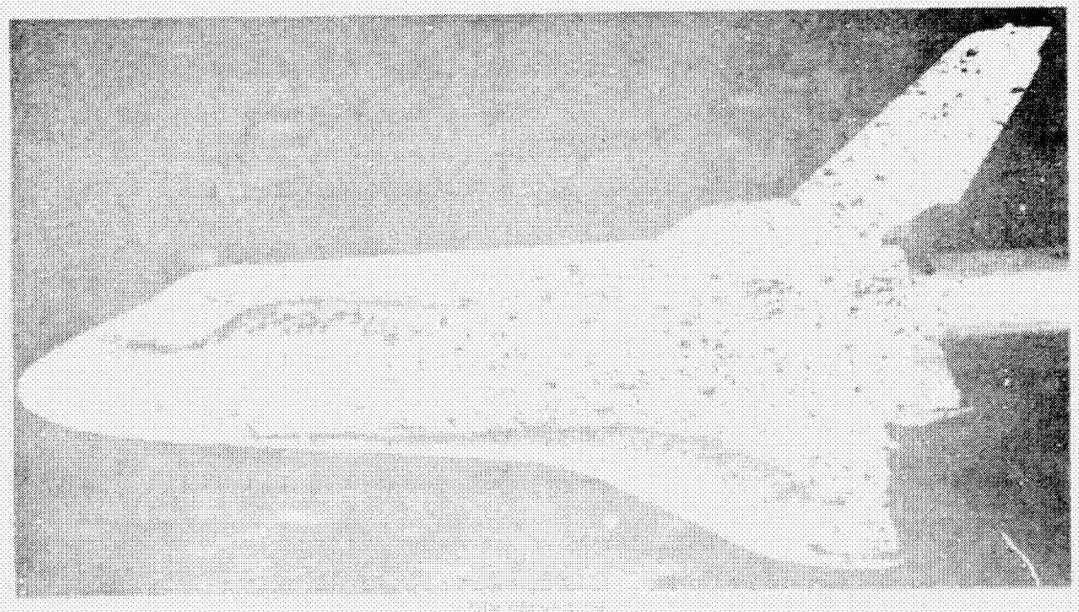

Fig. 201 Space Shuttle Orbiter at 30° angle of attack: $M_\infty = 20$ and $R_{L_\infty} \sim 1 \times 10^6$ (Stone and Mulfinger 1974).

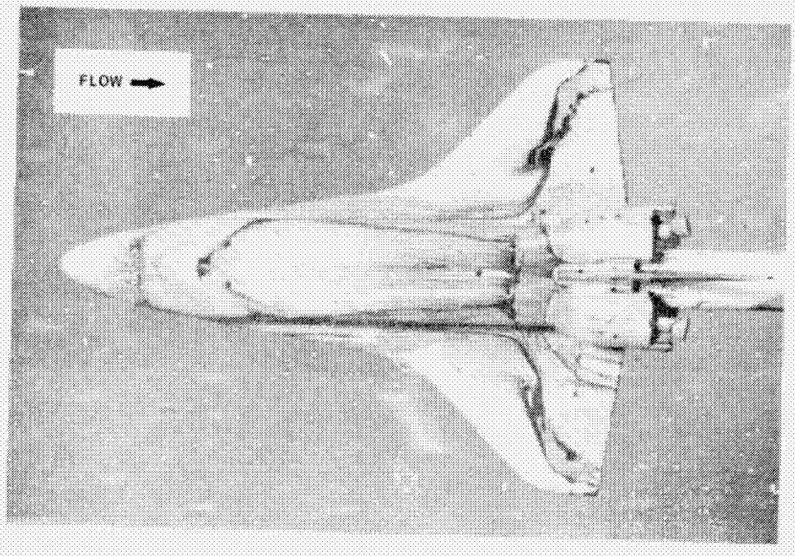

Fig. 202 Oil-flow pattern on Shuttle Orbiter at $M_\infty = 1.2$, $\alpha = 0°$ (Ericsson and Reding 1976).

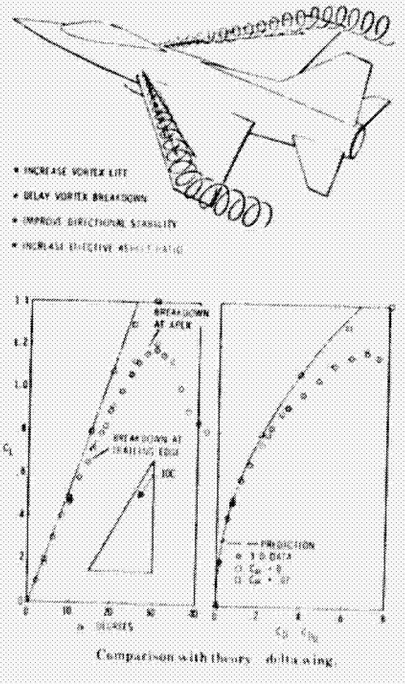

Fig. 203 Spanwise blowing along leading edge (Bradley and Wray 1974).

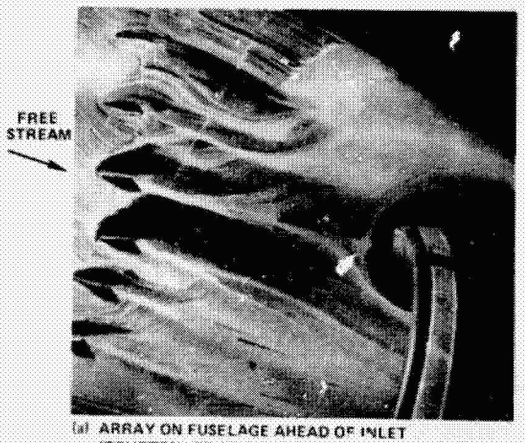

(a) ARRAY ON FUSELAGE AHEAD OF INLET
(COURTESY OF ARA, BEDFORD)

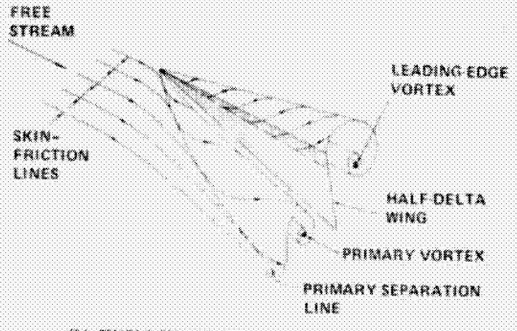

(b) SINGLE (SHEN 1967)

Fig. 204 Controlled separation from swept edges of vortex generators.

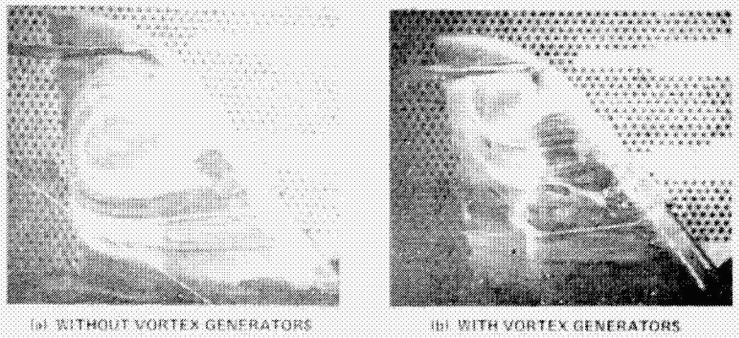

(a) WITHOUT VORTEX GENERATORS (b) WITH VORTEX GENERATORS

EFFECT OF VORTEX GENERATORS ON SPREAD OF SEPARATION

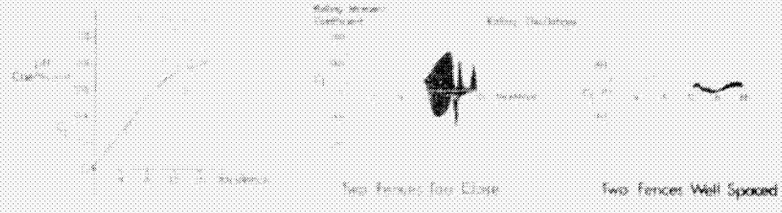

(a) EFFECTS OF FENCES (b) ROLL UNSTEADINESS WITH TWO FENCES

Fig. 205 Control of focus position on transonic swept wing in buffet (Bore 1972).

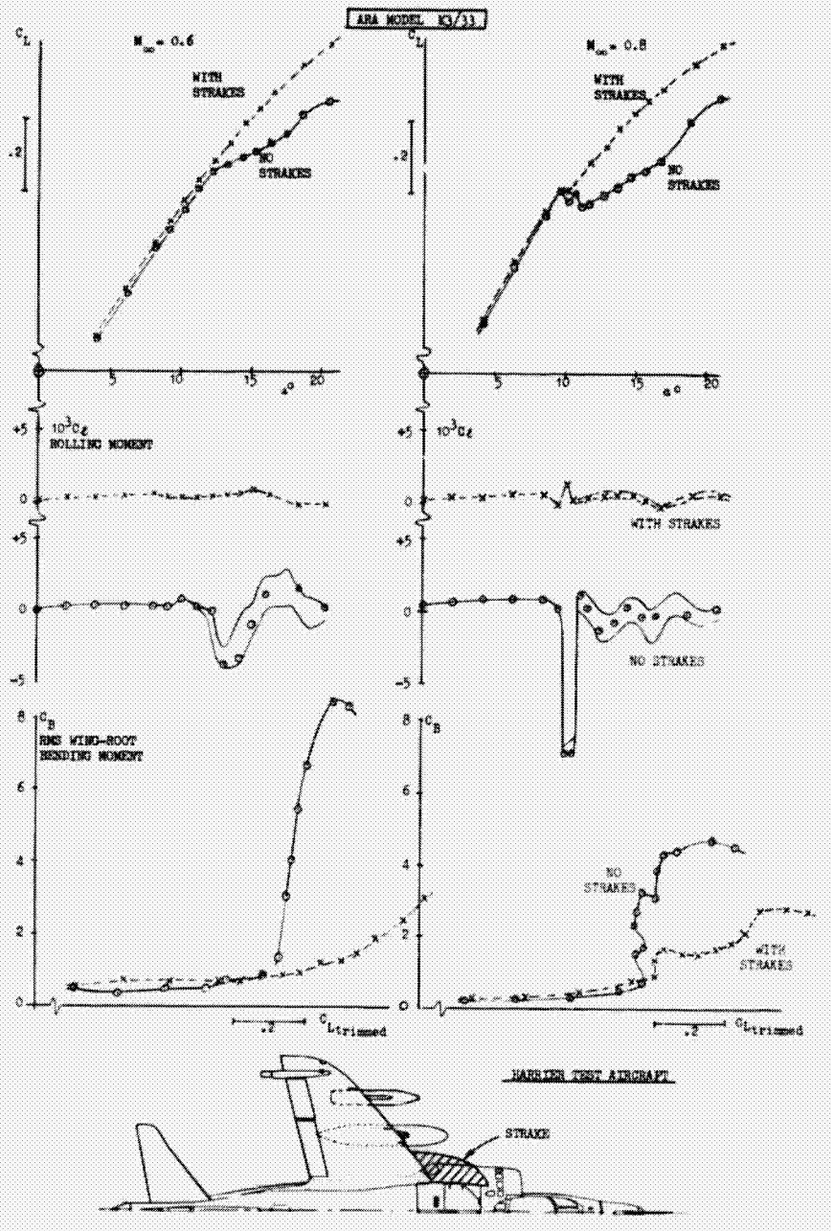

Fig. 206 Effect of strakes on wing buffet and unsteady rolling moment (Moss 1978).

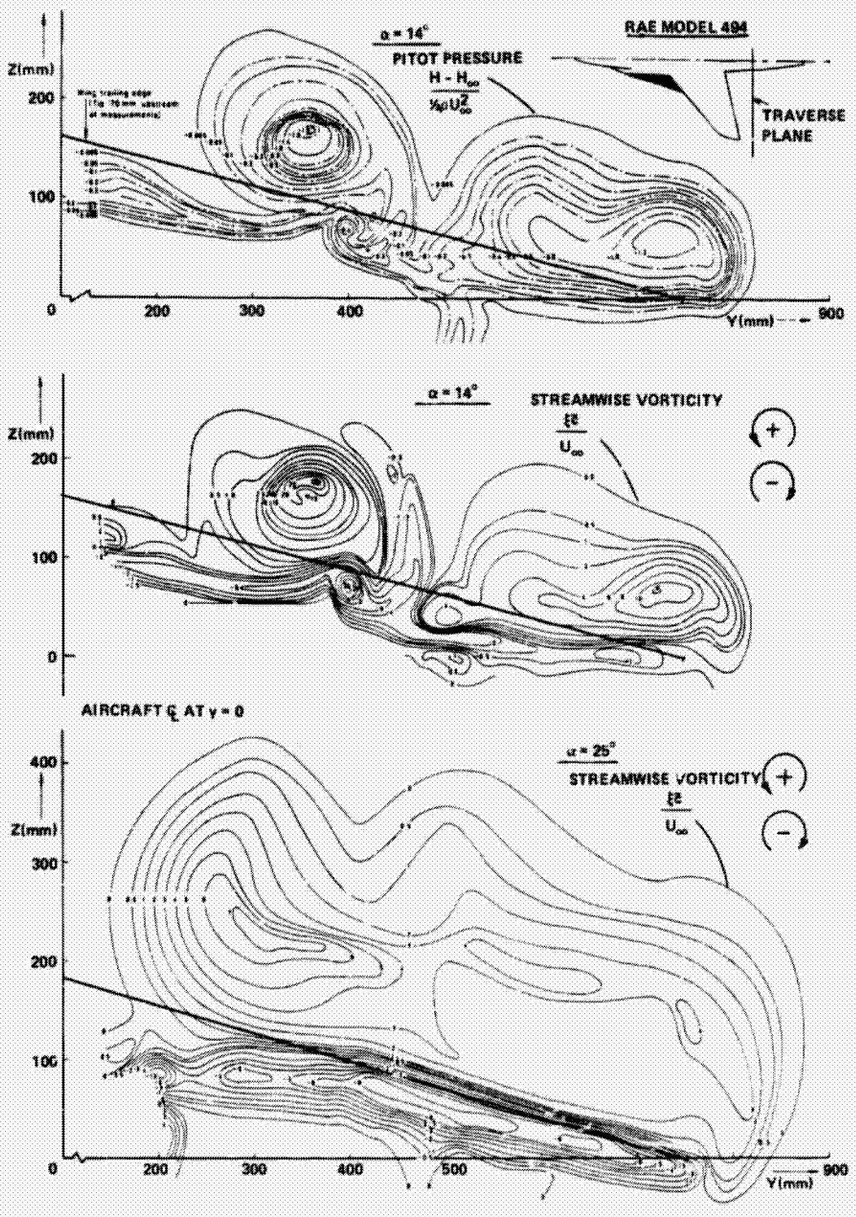

Fig. 207 Flow field behind a straked configuration at high angle of attack (Moss 1978).

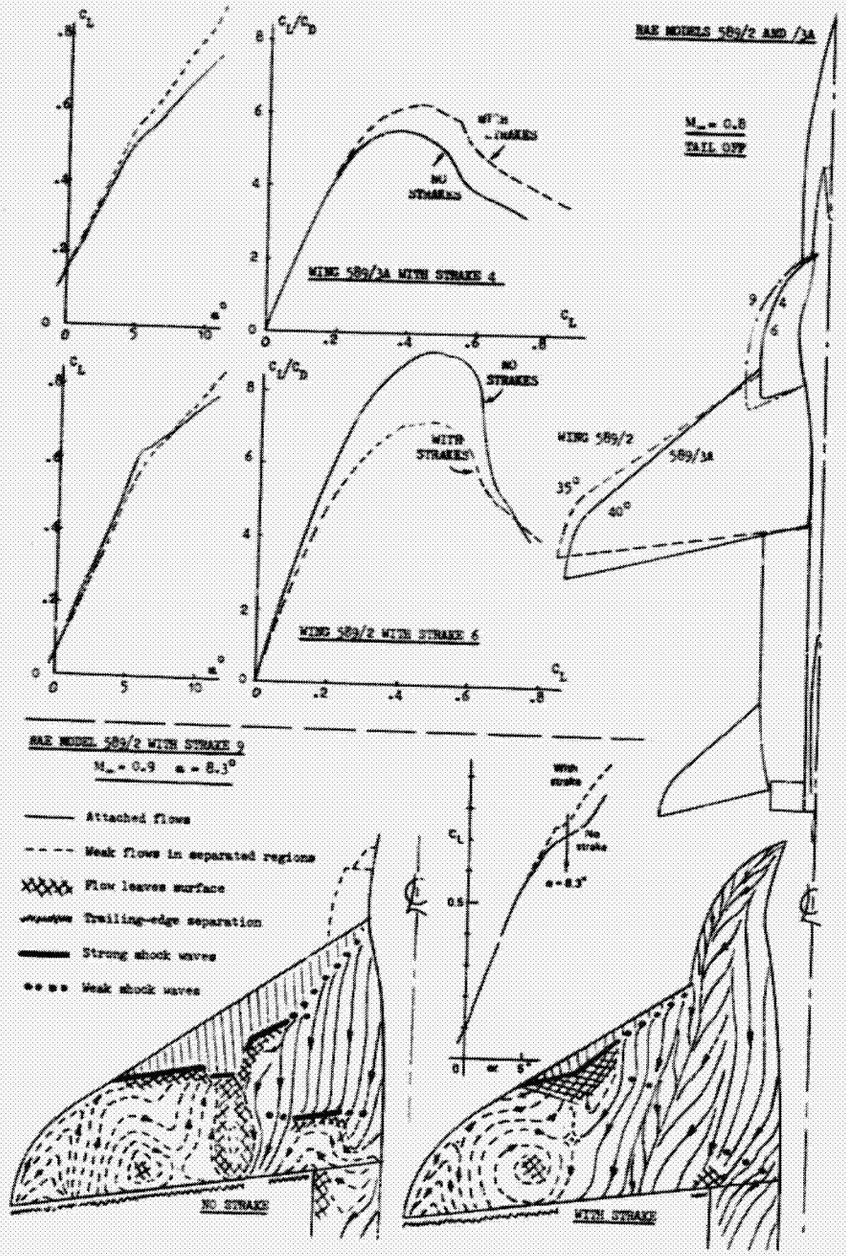

Fig. 208 Effect of strakes on wing performance at high speeds (Moss 1978).

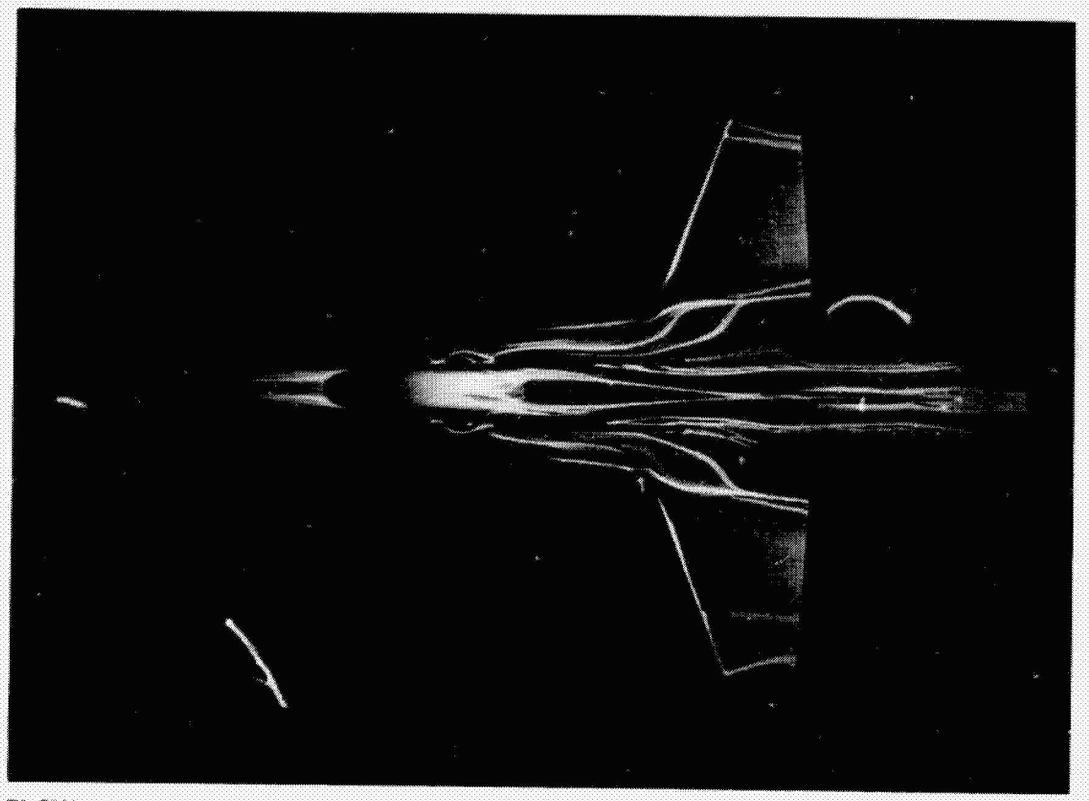

Fig. 209 Oil-flow pattern on fighter aircraft with long strakes and twin fins at angle of attack in subsonic flow (E. R. Beeman 1977: personal communication).

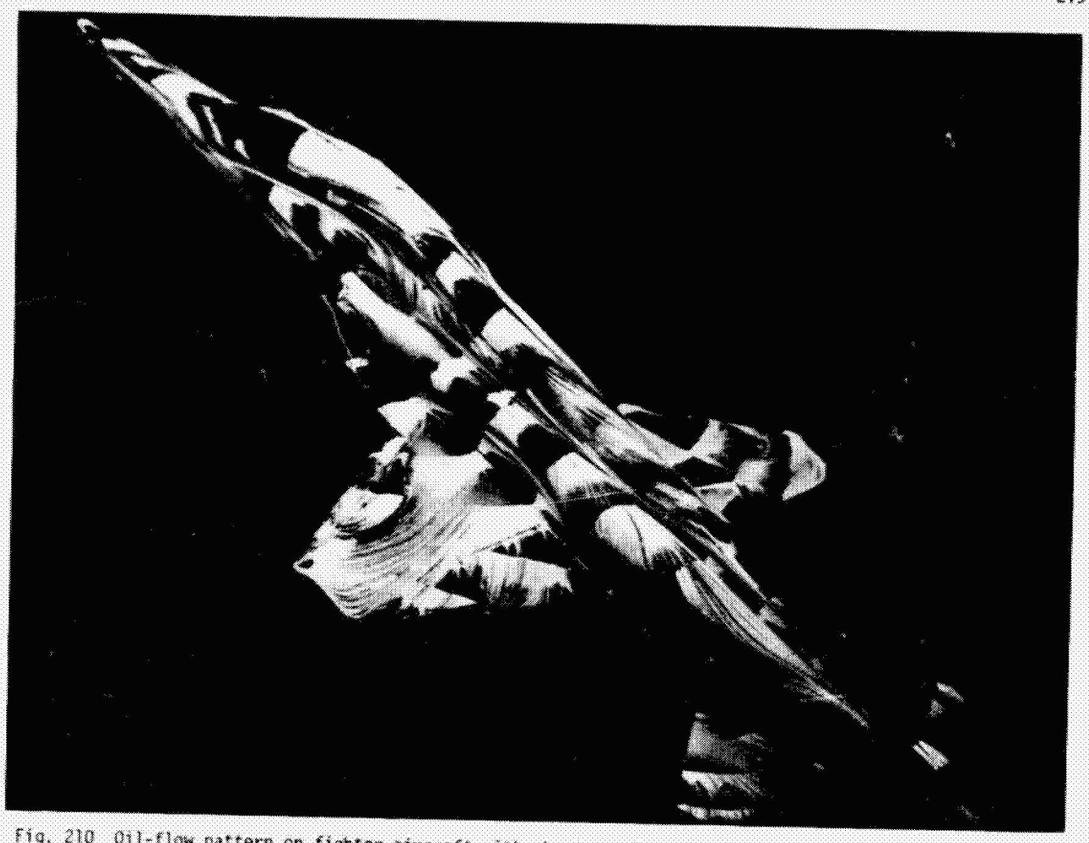

Fig. 210 Oil-flow pattern on fighter aircraft with short strakes and single fin at angle of attack with L.E. and T.E. flaps deflected in low-speed flow (E. R. Beeman 1977: personal communication).

Fig. 211 Breakdown of strake vortices over wing of fighter aircraft at high angle of attack (Erickson 1979).